2016

Comb-Like Acrylic-Based Polymer Latexes Containing Nano-Sized Crystalline or Liquid Crystalline Domains

Comb-Like Acrylic-Based Polymer Latexes Containing Nano-Sized Crystalline or Liquid Crystalline Domains

Ehsan Mehravar

2016

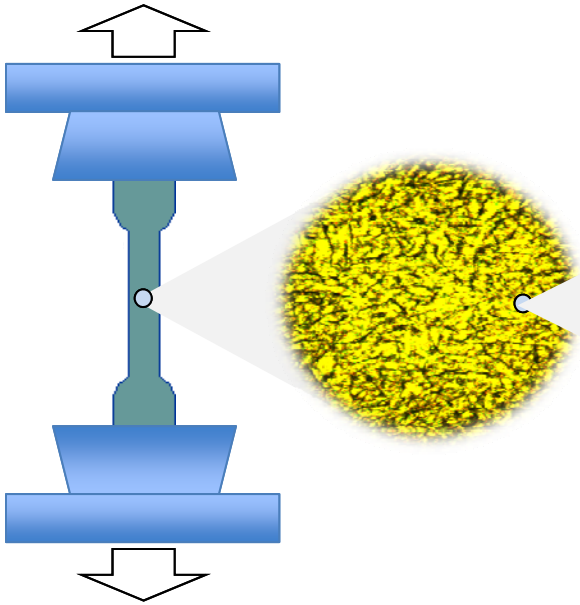

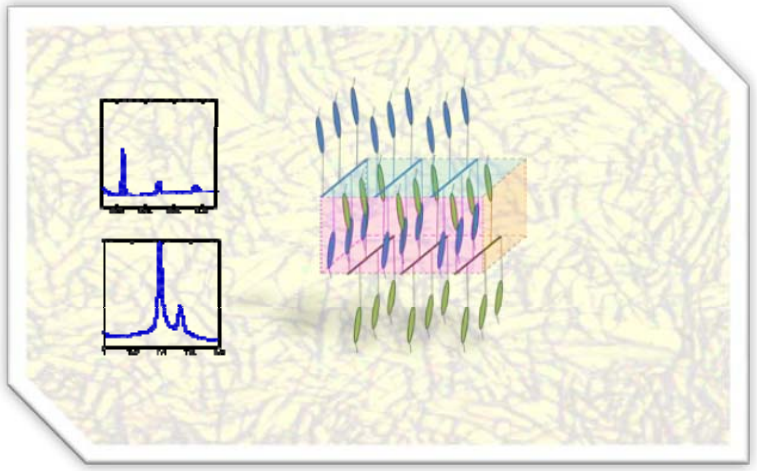

Chemical Engineering Group
Applied Chemistry Department
University of the Basque Country

Ehsan Mehravar

Universidad del País Vasco Euskal Herriko Unibertsitatea

POLYMAT

Comb-Like Acrylic-Based Polymer Latexes Containing Nano-Sized Crystalline or Liquid Crystalline Domains

Ehsan Mehravar

Supervised by: J. M. Asua and J. R. Leiza

Chemical Engineering Group
University of the Basque Country UPV/EHU
Donostia-San Sebastián
(2016)

(cc)2016 EHSAN MEHRAVAR (cc by-nc-nd 4.0)

To My Parents,

To Samane

Acknowledgments

I would like to express my sincere gratitude to my supervisors, Prof. José M. Asua and Prof. Jose R. Leiza for their guidance, support, supervision and patience. This dissertation would never have been accomplished without their encouragement and their valuable ideas. I must say that I was lucky that I had the opportunity to work under their supervision.

Special thanks to all the professors of the Chemical Engineering Group, Professors María Paulis, Maria J. Barandiaran, Jose C. de la Cal, Radmila Tomovska, David Mecerreyes, Alejandro Müller and Jacqueline Forcada for the great scientific discussions and for encouraging me during these years. I would like to show my gratitude to Ines who always helped me for all the paperwork and problems during these years. I cannot find words to express my gratitude to you Ines. Thank you very much. Onintza I appreciate your help during these years.

I would like to thanks the Industrial Liason Program for the Polymerization in dispersed media for their financial support and their great ideas and discussions in ILP meetings.

I would like to show my gratitude to Dr. Bernd Reck for his hospitality, support and his interest in my work during the time I spent in BASF. I would like to thank many people in BASF company specially Dr. Frank Pirrung for technical support in miniemulsification process, Dr. Joost Leswin for technical support in formulating paints, Dr. Michael A. Gross and Dr. Jörg-Alexander Dimmer for technical support in adhesive formulations; Ms. Christina Laue for assistance in synthesizing the latexes, Ms. Melanie Hook for assistance in studying the adhesive properties and Mr. Steffen Weber for assistance in paint preparation and studying the paint properties.

I would like to express my gratitude to people in Materials Physic Center (CFM): Prof. Aranxe Arbe and Dr. Amaia Iturrospe for X-Ray measurements, data analysis and discussions; Prof. Angel Alegria and Mr. Gerardo Martinez for dielectric measurements and data analysis.

I would like to thank Prof. Antxon Santamaria and Dr. Mercedes Fernandes for technical support and discussions in DMTA analysis. Special thanks to Dr. Gracia Patricia Leal, for TEM and SEM analysis and to Dr. Mariano Barrado Meléndez and Maria T. Miranda for TEM analysis. To Dr. Jose I. Mirando and Dr. Iñaki Santos for their kind help with the NMR analysis. And to Dr. Alba Gonzales for water vapor transmission rate and oxygen permeability analysis.

I would like to express my gratitude to Prof. Mikel Gaztelumendi, Dr. Jon Urquijo, Dr. Nora Arambura and Itziar Otaegi from Polymer Technology Group for sample preparation and tensile test measurement at high temperature. And I would like to thanks Dr. Loli Martin from Engineering Faculty for helping me in polarized optical microscopy analysis.

I would like to extend thanks to my colleagues that I met in Polymat. It was a pleasure knowing you all. Ali and Shaghayegh, lovely couple, thank you for your support and friendship. Amaia, Miren, Patx, Wendy, Freddy, Karim, Alejandro, Edurne, Paula, Pablo, Juliana, Julieta, muchas gracias por todo. Monica, Audrey and Maitane, wish you all the best in your life and in being perfect mothers.

Ana B, Ana M, Ziortza, Jone and Joseba, I had a great time in Prague with you. Fernando, Nick, Alex, Julie, Nerea, It´s been a pleasure knowing you all, thanks for the good memories that we shared.

Sevilay and Mehmet, perfect Turkish couple, we had a great time together, thanks for the delicious meatball. Gordana, thanks for the good moments that we shared, wish you, Miki and Goran happiness in your life.

My Italian colleagues, Stefano, Francesca and Massimo, it was a pleasure knowing you. grazie di tutto e in bocca al lupo ☺. Noushin, wish you all the best in

your life. Jessica and Elodie the girls who make the best cookies and pizza, bon courage. Alicia, I enjoed you company during PRE conference in Munich (near Munich in fact). Iñaki and Aitor, it was a pleasure knowing you guys. Veronica, good luck with your paints. Sil, Syrung, Adrian and Bertha, wish you all the best and good luck in your thesis. Aintzane, Garbiñe, Haritz, Daniele, Isabel, Guilia, Iñaki, Ana sanchez, Guiomar, Nerea, Alex, Leire, Andere and Amaury, It´s been a pleasure knowing you all.

I would like to thank all my family for their support during the whole educational years specially my father who always encourage me to continue my education and my beloved mother who always support me with her endless kindness and love.

And finally, Samane, the love of my life, I was fortunate to have you here in the last two years. Without your support I would never been able to overcome all the problems in theses years. Thank you for your help, encouragement, happiness and love.

Content

Chapter 1. Introduction

Conventional (meth)acrylate polymer latexes have been widely used for coatings, adhesives, paper and textile finishes, cement additives and other applications [1-6]. These polymers exhibit useful properties such as adhesion to relatively polar substrates (steel, aluminum, tin, glass and wood) [6,7], durability, weather resistance [6], flexibility in composition and glass transition temperature (T_g) [8], and compatibility with many polar polymers [9] and inorganic components [10-13]. However, since these polymers are generally amorphous, they cannot compete in demanding applications where polymers with some degree of crystallinity performed well; e.g., they do not exhibit good mechanical properties (toughness) and they are inferior to olefins in terms of water resistance, barrier properties and durability. Therefore, there is a need of polymer compositions which provide better mechanical and barrier properties, adhesion to polar and non-polar substrates, water and weather resistances and durability.

Crystalline and liquid crystalline domains are known to impart improved mechanical [14-33] and barrier [30,34-41] properties of polymers; therefore, the

introduction of crystalline and/or liquid crystalline domains in amorphous (meth)acrylate polymer matrix may be a good solution for the above mentioned purpose.

1.1. Incorporation of Crystalline Domains into Amorphous (Meth)acrylate Polymers

1.1.1. Olefin Polymers

The first methods to incorporate crystalline domains to the amorphous (meth)acrylate polymers included physically mixing (meth)acrylate polymers and olefin polymers. Since these polymers are generally not compatible, the resulting blends have poor physical properties. Although improving compatibility of these two phases by using compatibilizers has been reported [42,43], generally this method has not been successful. Epoxy containing ethylene / (meth)acrylate copolymers can be crosslinked by using any crosslinker known in the epoxy chemistry such as secondary and tertiary amines [44]. So far these agents appear to be rather ineffective.

Another method is the copolymerization of (meth)acrylate and olefin monomers. Pepe et al. [45] reported an improvement of the barrier properties of amorphous waterborne wood coatings by copolymerizing ethylene and vinyl acetate

monomers. Copolymerization of olefins and polar monomers (other than vinyl acetate [46]) is difficult because of the widely different reactivity ratios (e.g., for acrylate–ethylene copolymerization, $r_{acrylate} = 13.94$; $r_{ethylene} = 0.01$). Nevertheless, the copolymerization of non-polar olefins with polar (meth)acrylates has been achieved by using metal catalysts [47-51], but this results in an average of the properties of each homopolymer rather than in enhanced properties. Moreover, the copolymerization of olefins and (meth)acrylate monomers prevents adjacent polyolefin chains packing into the crystal lattice.

1.1.2. Poly (n-alkyl) (Meth)acrylates

Another method to introduce crystalline domains in amorphous (meth)acrylate polymers is using crystallizable long-side chain $(CH_2)_{n>10}$ n-alkyl (meth)acrylate monomers**.** These monomers are able to copolymerize with short chain monomers.

Parker et al. [52] used synthetic wax monomers to incorporate crystalline domains into the meth(acrylate) polymers. Synthetic wax monomers are monomers obtained by transesterification of (meth)acrylate esters and high molecular weight ($C_{20} - C_{300}$) alcohols [53]. The polymers produced with these monomers have an amorphous backbone, and the side alkyl chains can crystallize. Performing reactions in solution polymerization, aqueous suspension polymerization, and aqueous

dispersion polymerization processes, they showed that polymers with crystalline domains had potential applications as adhesives, wood coatings and textile coatings; however, no detailed study on the performance of semicrystalline polymers was reported.

n-alkyl (meth)acrylate monomers with relatively long side chains $(CH_2)_n$ ($10 \leq n \leq 22$) are commercially available. The copolymerizing long side chain alkyl acrylates with short chain alkyl (meth)acrylates or other non-crystallizable monomers has been scarcely reported [54-57]. In most cases, bulk and solution batch copolymerizations were carried out and although some patents have been published [58-60] little is known about the synthesis of waterborne latex particles containing these crystalline domains in particular for coating applications. Agirre et al. [61] synthesized waterborne semicrystalline temperature-responsive pressure sensitive adhesives. The crystalline polymer fraction was produced in situ within the particles by miniemulsion polymerization of a non-branched long chain acrylate. They observed a temperature-responsive behavior by incorporation of crystalline domains in amorphous pressure sensitive adhesives. Moreover, the authors reported that with the right distribution and concentration of crystalline polymers a simultaneous increase in both shear resistance and peel strength was observed. Popadyuk et al. [62] studied thermoresponsive latexes for fragrance encapsulation and release. Zhang et al.

[63] prepared poly(perfluoroalkyl acrylate-co-stearyl acrylate) copolymers by miniemulsion polymerization and the copolymer was precipitated with ethanol and dissolved in tetrahydrofuran to form films. The reasons for using this environmentally unfriendly procedure to obtain films were not discussed, but diffraction scanning calorimetry data showed that the latexes were not film-forming at room temperature. Jasinski et al. [64] synthesized poly(thioether ester) nanolatex containing crystalline domains. The authors reported that the crystalline domains were efficient barrier to water penetration and improved the poly-(thioether ester) latex hydrolytic stability. A similar procedure [65] has been used to prepare dual-stimuli-responsive nanocarriers sensitive to both oxidation and hydrolysis.

1.1.2.1. Crystallinity and Properties of Poly (n-alkyl) (Meth)acrylates

The properties of poly (n-alkyl) (meth)acrylates have been of continuing interest since they were first investigated in the 1940's by Rehberg et al. [66]. Unlike conventional crystalline polymers whose backbone crystallizes, in this case, the long n-alkyl side chains of poly(n-alkyl) (meth)acrylates crystallizes [55,56,67,68]. The melting–crystallization transition of the long side chains, which occurs at the melting temperature (T_m) and can be controlled by side-chain length, causes significant changes in the physical properties of the polymer [57,67,69-74]. The longer the side-

chain length (n) of the polymer, the more side chain carbons are able to crystallize which increases the energy required to melt the polymer (ΔH_f) as well as the crystallite size distribution, which in turn influences T_m and its breadth.

Wide angle X-Ray scattering (WAXS) studies of poly (n-alkyl) (meth)acrylates showed that the n-alkyl side chains formed hexagonal crystalline lattice [75]. Figure 1.1 is a schematic taken from Reference 75 illustrating the hexagonal packing structure for the comb-shaped polymer.

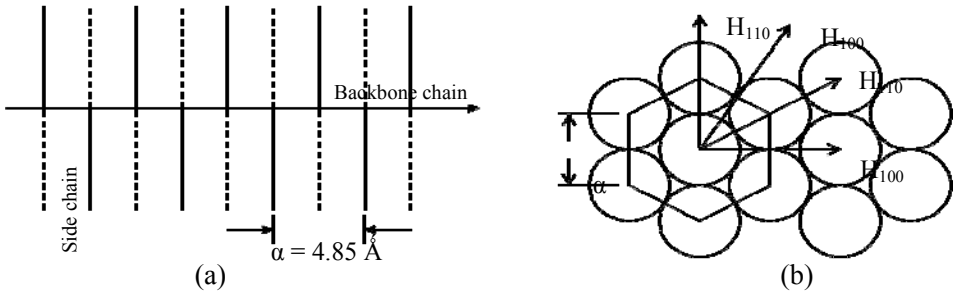

Fig. 1.1. The schematic of hexagonal packing structure for comb-shaped polymers. The side chains extending from the main chain in an all-trans conformation is illustrated in 1.1a where solid side-chain lines denote side chains extending from main chain and dashed side chains are those from other neighboring main chains alternating into the packing structure. α, the distances between side chains, calculated from $\alpha = \frac{2d_{100}}{\sqrt{3}}$, d_{100} is Bragg space. This diagram was taken from Reference 75.

The small angle X-Ray scattering (SAXS) studies by Plate et al. [75] and Hsieh et al. [76] suggested end to end packing and interdigitating packing formations for poly (n-alkyl) acrylates (PA). These two packing formations coexist for PA (Figure 1.2).

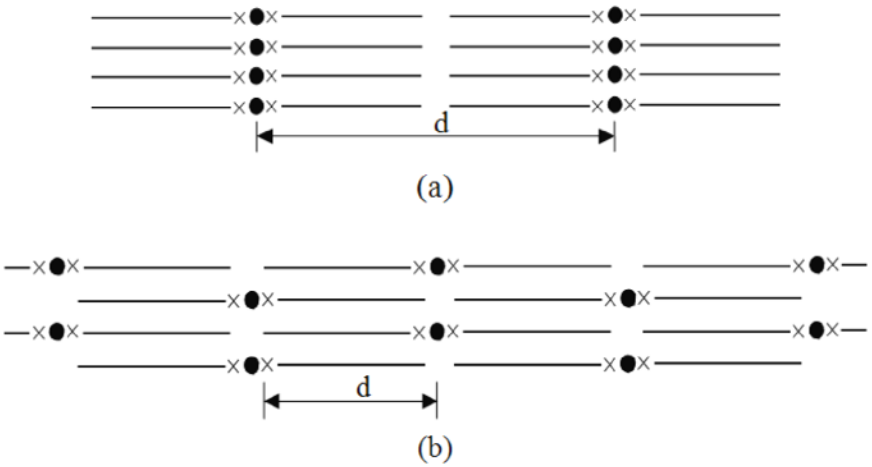

Fig. 1.2. The two side-chain packing formations revealed by SAXS include interdigitating packing (a) and end-to-end side-chain packing (b) for PA [74,75]. (X) attachment budge; (●) Main chain.

Plate et al. [75] observed striking differences in the diffraction patterns between PA and poly(n-alkyl) methacrylates (PMA). In the case of PMA they proposed that the disordered packing of the end groups of side chains occurs because of the increased bulkiness of the main chain and they proposed the one-layered

lamellar structure for these polymers (Figure 1.3 (a)). Later, Hsieh et al. [76] proposed a new structural model for the PMA, where the side chain crystallites are formed by intercalating side chains pointing in opposite directions (Figure 1.3 (b)). The more flexible main chain of PA allows a closer packing of the side chains leading to a higher crystallinity of these polymers with respect to PMA. Therefore, in this study we will use long side chain acrylates to introduce crystalline domains into the amorphous (meth)acrylate polymers.

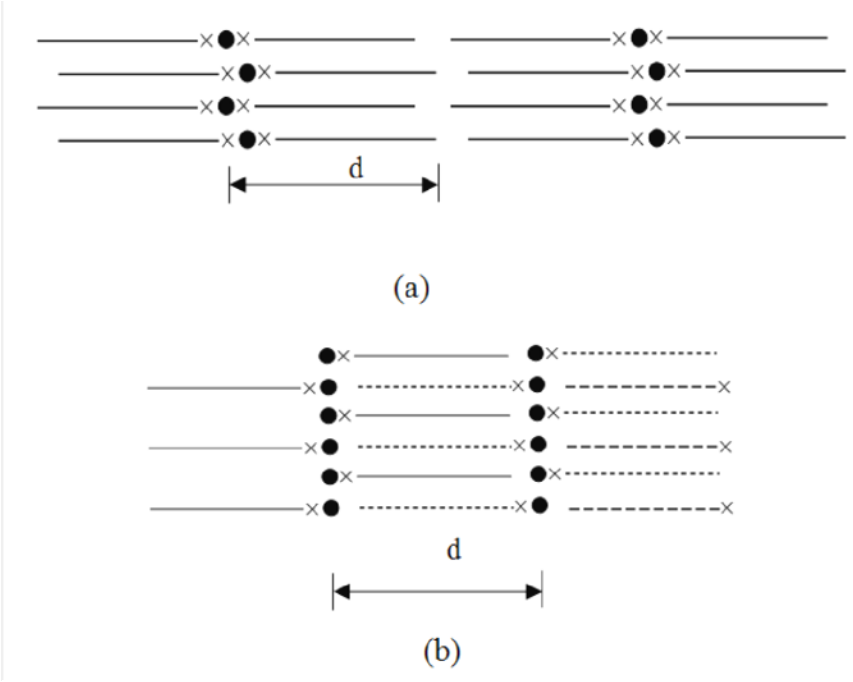

Fig. 1.3. Model proposed for PMA by (a) Plate et al. [75] and (b) Hsieh et al. [76] (intercalating side chains model). (X) attachment budge; (●) Main chain.

In addition to structural studies, the thermal characteristics, crystallinity and transport properties of these polymers have been widely studied [54-56,66-68,70-74,77]. Rehberg et al. [66] studied the thermal transitions of comb-like polymers with different side chain length. The thermal transitions of PAs and PMAs with different side chain lengths are plotted in Figure 1.4. They found that the glass transition temperature (T_g) dropped as the side chain increased up to 8-10 carbon atoms and that crystallinity appeared for side chains reaching a certain critical value of n >11. Moreover, it can be seen that, for the same side chain length the higher flexibility of backbone in PAs led to the lower T_g and higher packing and crystallinity in comparison with PMAs.

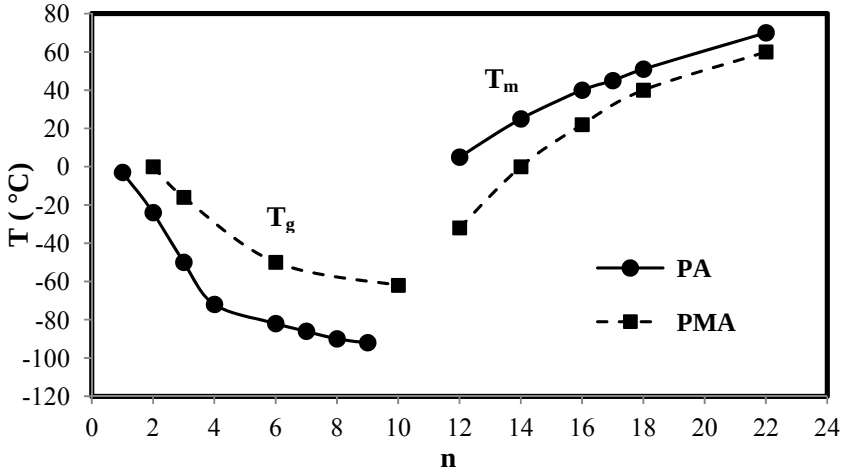

Fig. 1.4. The glass transition and melting temperatures versus side-chain length (n) reported from Rehberg et al. [66].

1.2. Incorporation of Liquid Crystalline Domains into Amorphous Polymers

1.2.1 Liquid Crystals

Liquid crystals (LCs) are highly anisotropic fluids that exist between the disorder of the isotropic liquid phase and the neatly arranged lattices of crystals [78]. This state of aggregation refers to a mesomorphic structure or a mesophase, where the term “mesophase” originated from the Greek word “meso” which means “in between”. Compared to isotropic liquids, LCs align in a higher state of order, as shown in Figure 1.5. On the other hand, LCs have a higher intermolecular and intramolecular mobility than the solid crystals. Therefore, they have several degrees of freedom of molecular rotation, translation, oscillation and intramolecular conformational change [79]. This unusual phase behavior has attracted the interest of both theoretical and experimental researchers.

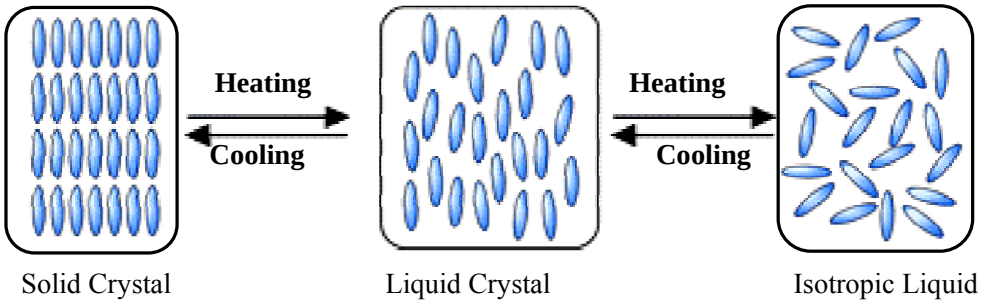

Fig. 1.5. Placement of the liquid crystal phase within the general scheme of the common phase of matter; the 'sticks' represent molecules.

1.2.2. Classification of Liquid Crystals

LCs are often classified as thermotropic and lyotropic (Figure 1.6). The phase transitions of thermotropic LCs depend on temperature, while those of lyotropic LCs depend on both temperature and concentration. Lyotropic LCs aggregate to form hollow spheres, column or laminar structures, with properties depending on the solvent. They do not have commercial applications.

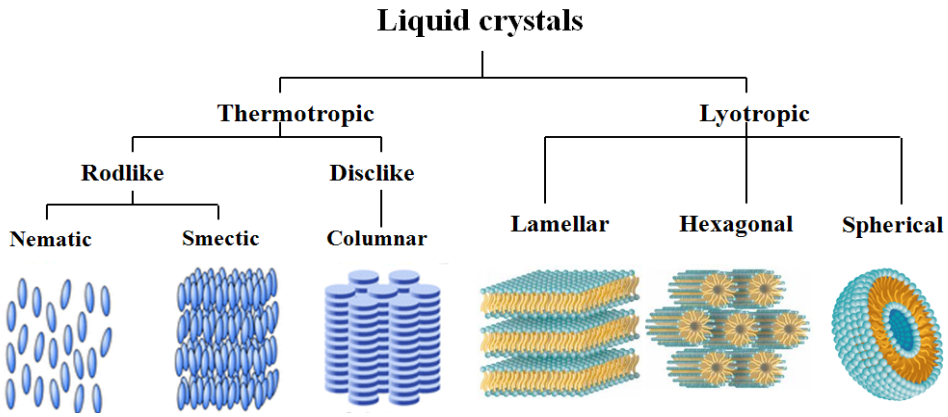

Fig. 1.6. Classification of liquid crystals.

1.2.1.1. Thermotropic Liquid Cryatls

The thermotropic liquid crystals the transitions between mesophases are brought about by thermal processes (heating or cooling). When the temperature is decreased there is a step-wise increase in the order of the material that goes from the isotropic phase to crystalline, the intermediate phases being liquid crystals (Figure 1.7). The degree of orientation order and the specific type of order depend on the chemical structure, molecular arrangement and external factors such as temperature, pressure and force fields. Therefore, a system may exhibit polymorphism with different liquid crystalline phases. According to the level of order, thermotropic LCs

broadly classified into two main types: nematic and smectic phases which, in turn, are further subdivided as shown in Figure 1.7.

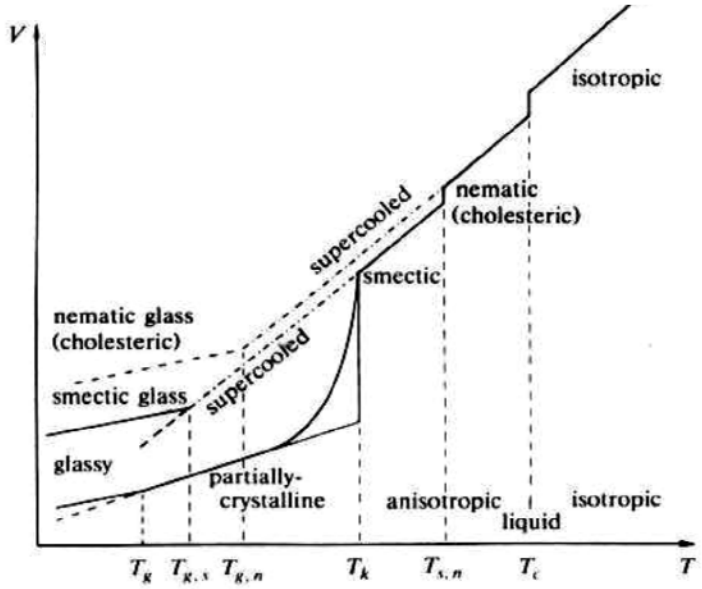

Fig. 1.7. Phase transition diagram of various first-order transitions in LCs and liquid ccrystalline polymers [80].

1.2.1.1.1. Nematic Phase

The nematic phase is the simplest and the most common mesophase observed in LCs. The term “nematic” has its origins in Greek word meaning “thread” which describes the appearance of this mesomorphic phase. In the nematic phase, the

particles have an overall direction of orientation but the positions of the individual particles are still random (Figure 1.8). In fact, the nematic order is not perfect and there can be considerable fluctuation about the average molecule orientation, which is described by a unit vector called the director, denoted by **n**.

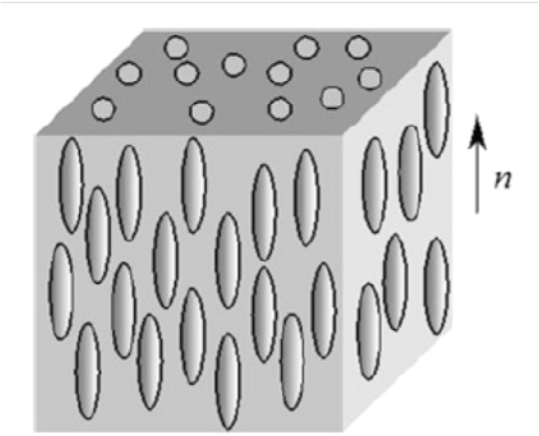

Fig. 1.8. Schematic representation of liquid crystalline molecules aligned in the nematic phase.

The nematic phase can be characterized by X-Ray diffraction (XRD) with a diffuse peak around 20°, which roughly represents the average distance between the molecules. However, it is hard to distinguish a nematic phase from an isotropic melt or an amorphous solid through XRD. Polarized Light Microscopy (PLM) that enables

the characterization of the liquid crystalline textures, is an easy and useful method to identify the nematic phase.

1.2.1.1.2. Smectic Phase

Smectic liquid crystalline phases are named because their basic layer structure gives them a soapy feel, which is described by the Greek word "smegma". There are several variants of smectic LCs and they have been characterized based on their order and symmetry. In smectic phase, the rod-shaped molecules form a set of parallel planes of regular spacing. The two most common variants of smectic phases are smectic **A** and smectic **C** (Figure 1.9(a) and (b)). Smectic **A** phase is the least ordered of all smectic phases and the director lies along the layer normal. In smectic **C**, the director of each layer is inclined at an angle β to the layer normal, this angle being identical for all layers. Contrary to the smectic **A** and **C** phases, the rest of the smectic phases show some positional order within the layer, depending on the type of phase. There are several possibilities for smectic phase in the case of tilted structures, depending on the direction of the tilted and the positional ordering: smectic **B**, **E**, **I**, **F**, **G**, **J** and **M** phase [81]. For example, in smectics **B** centers of mass of molecules in layers are located at points of the hexagonal lattice and the director is perpendicular to layers (Figure 1.9(c)) and quasi-hexagonal arrangement of centers of mass of molecules in layers is typical for smectics **E** (Figure 1.9(d)). The common feature of

all smectics phases is their layered structures, which can be easily identified by XRD at low angle, 2θ below 10°.

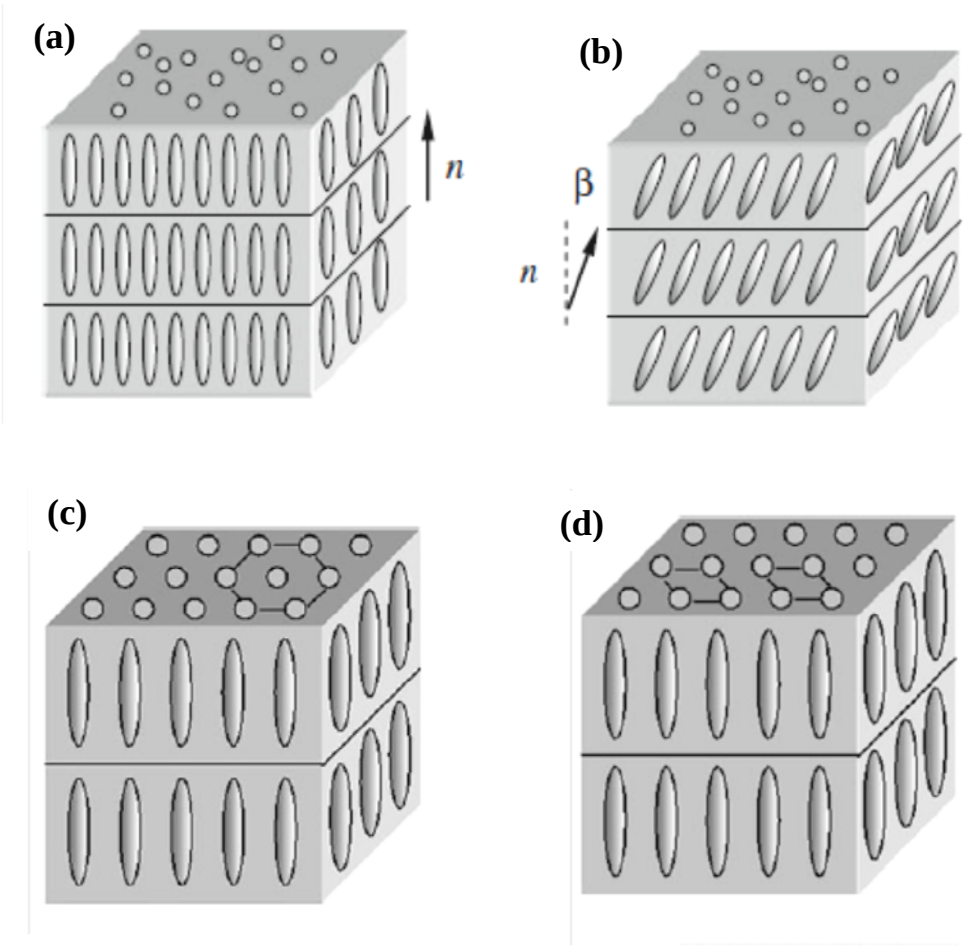

Fig. 1.9. Schematic representations of liquid crystalline molecules aligned in (a) smectic **A**, (b) smectic **C,** (c) smectic **B** and (d) smectic **E** phases.

1.2.2. Liquid Crystalline Polymers

Liquid crystalline polymers (LCPs) are a class of materials that combine the properties of polymers with those of LCs. These "hybrids" show the same mesophases characteristic of ordinary LCs, yet retain many of the useful and versatile properties of polymers. For normal flexible polymers to display LC characteristics, rod-like or disk-like elements (mesogens) must be incorporated into their chains. The architectures of LCPs may vary (as shown in Figure 1.10) and can be as a first approximation classified into two groups: main-chain (MCLCPs) and side-chain liquid crystalline polymers (SCLCPs). MCLCPs are formed when the mesogens are part of the main-chain of a polymer. Conversely, SCLCPs are formed when the mesogens are connected as side-chains to the polymer by a flexible "bridge" (spacer). Other LCPs are combined-LCPs, which are a hybrid between main-chain and side-chain LCPs, liquid crystal blends, liquid crystal networks and liquid crystal elastomers (liquid crystal polymers could be cross-linked to form elastomers, their most interesting property is the ability to change their shape reversibly after the application of a certain external stimulus [82]).

As mentioned before, for MCLCPs, the mesogens are introduced directly into the polymer backbones. These stiff regions along the main-chain allow the polymer to orientate in a manner similar to ordinary LC and thus display liquid crystallinity.

These mesophases include naphthalene, stilbene and related structures as well as traditional phenylene groups [83]. There are two distinct groups of MCLCPs according to differentiated by the manner in which the stiff regions are formed. In the first group, the mesogenic units formed the polymer backbone and only the functional groups of monomer units separate them. In the second group, the mesogenic units are inked with flexible spacers and the spacers provide independent movement to themesogens, which facilitates proper alignment.

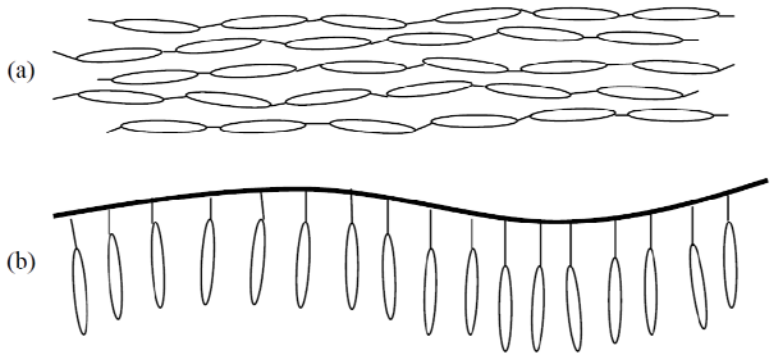

Fig. 1.10. The architectures of liquid crystalline polymer: (a) main-chain liquid crystalline polymers and (b) side-chain liquid crystalline polymers

1.2.2.1. Side Chain Liquid Crystal Polymers

In SCLCPs, the mesogenic groups are laterally attached to the polymeric chain by a flexible spacer unit. The major difference observed between main chain and side

chain LCPs is that the mesogenic group has a greater mobility in the side-chain LCPs. In this study, we will focus on side chain liquid crystalline monomers and polymers.

SCLCPs have considerable application potential in many fields such as optical data storage; optic, electro-optic, and nonlinear optic devices; and photomechanical applications [84-87].

Finkelmann et al. [88,89] pioneered the synthesis of SCLCPs, materials which combine the anisotropy of liquid crystalline mesogens with the mechanical properties of polymers. Although there were some earlier attempts [89], they succeeded in decoupling the motions of the polymer main chain from those of the mesogen, which allows the side chain moieties to build up long range ordering. They were able to synthesize polymers with nematic, smectic and cholesteric phases via free radical polymerization of methacryloyl type monomers [90]. Generally, a SCLCPs comprises three distinct structural units: a polymer backbone, a mesogenic group and flexible alkyl spacer (inserted between main chain and mesogenic side groups). SCLCPs (end-on SCLCPs) with mesogenic group directly attached to the polymer backbone without any flexible spacer have been reported, but they contain a flexible alkyl tail. The nature of the polymer backbone and mesogenic groups, and the length of flexible spacer and tail largely affect the properties of SCLCPs [86,87, 90-98]. The flexible spacer decouples the interaction of the side chain and the polymer backbone, which

disrupted the ordered packing of the side mesogens [88,99]. On the other hand, the alkyl tail induces fluidity to the side chain and plays a very important role in the formation of LC phase structure for the SCLCPs without spacer. The effects of spacer and tail length on the mesomorphisem behavior of different types of SCLCPs have been studied in literature [86,87,91,93,98,100]. Craig et al. [86] have systematically studied the influence of flexible spacer length from 3 to 12 on the self-organization of a series of methacrylate SCLCPs containing biphenyl mesogenic group in the side chain. They pointed out that the mesomorphism behavior of polymers depended on the spacer length; namely, propyl member showed only a smectic **E** phase, and butyl member showed exclusively a nematic and a smectic **C** phase; the pentyl, hexyl, and heptyl members formed a smectic **E** and a smectic **A** phase, whereas, octyl, nonyl, decyl, undecyl and dodecyl homologues members exhibited a smectic **B** and a smectic **A** phase below clearing temperature. However, the complete characterization of molecular packing of the side chain and the phase structures of polymers by using XRD methods for these polymers was not reported. Recently, Ni et al. [100] have reported the synthesis and characterization of a series of end-on methacrylate SCLCPs based on the biphenyl mesogen without the flexible spacer. The results indicated that polymers formed a smectic phase and the length of alkyl tails played an important role in the phase behavior and the side chain molecular packing of the polymers. In addition, the end-on SCLCPs exhibited higher glass transition

temperatures in comparison with the SCLCPs synthesized with flexible spacers and without alkyl tail (comparison References 86 and 100). In another study, Yu et al. [101] reported the effect of spacer and tail length on the phase structures and transitions of a series of biphenyl containing polyacetylenes SCLCPs. It has been reported that for the shorter spacers, the (semi)rigid polymer backbone and mesogenic group in the side chain tightly coupled together. 5 methylene units spacer decouple this effect and longer spacers led to more gauche conformations and promoted the formation of liquid crystals with higher order.

In almost all studies, the LCPs were synthesized by solution homopolymerization of side chain liquid crystalline monomers using low concentration (solvent/monomer = 7-10 wt/wt) and oil soluble thermal initiators. In most cases, the polymer yield was limited to 60-70 wt% and in some cases, polymers with low molecular weight were obtained. Furthermore, polymer properties may lay within the molecular weight dependent regime [87,102]. However, little is known about the polymerization of these monomers in aqueous media. Vennes et al. [103] synthesized colloidal particles of nematic and smectic liquid-crystalline acrylate polymers with different particles sizes (0.5 and 2.5 μm) and polydispersity by dispersion polymerization. They observed that the nematic director of the mesogens

within the colloidal particles could be rotated due to the photochemical trans-cis-isomerization of the azobenzene chromophores.

1.2.3. Polymer Composites Containing Liquid Crystalline Domains

The incorporation of LCs and LCPs into the polymer matrix using various processing techniques such as thermal processing (extrusion, injection molding and blow molding) [24,26,32,35,36,37], solvent casting [33,104] and polymerization [16,105] has been reported. There is plenty of evidences that LCs and LCPs improve the barrier properties of polymers [30,35-37,39,105]. Reinforcement of polymers with LCPs led to an increase of both elastic modulus and ultimate strength and to a decrease of the ultimate tensile strain [21,22,24-26,30,32,106]. Processing conditions and compatibility between LCPs and polymer matrix strongly affected the barrier and mechanical properties of polymer composites [21,26,30,32,107].

In addition, liquid crystalline domains have been incorporated to amorphous solvent-borne coatings [14,15,17,18,19,29]. Thus, Chen et al. [14,15,17,19] and Athawale et al. [29] synthesized liquid crystalline (meth)acrylic copolymers coatings by grafting p-hydroxybenzoic acid to the COOH-functional side chain of the (meth)acrylic copolymers. The same procedure was used by Chiang et al. [18] to

synthesize liquid crystalline alkyd resins. In both cases the coatings containing liquid crystalline domains showed better adhesion to substrates and chemical resistance; higher toughness, hardness and impact resistance; and lower polymer solution viscosity. Solvent borne coatings are under the scrutiny of environmental agencies and are being replaced by waterborne coatings.

1.3. Objective

This thesis focus on both coating and adhesive applications of waterborne (meth)acrylic-based copolymer latexes containing crystalline domains and liquid crystalline polymers.

The main objective of this thesis in the coating part is toughening the soft (meth)acrylic-based latex particles via introducing crystalline and liquid crystals domains within the waterborne latex particles. It is expected that the presence of these domains in the coating latex particles and finally in the polymer film will improve the mechanical properties of the polymer films (Figure 1.11).

The propose of this study in the adhesive application part is improving the adhesive properties of amorphous (meth)acrylic based pressure sensitive adhesive via introducing crystalline domains in the waterborne pressure sensitive adhesive.

In addition, the presence of the hydrophobic crystalline and liquid crystalline domains is expected to improve the water resistance and barrier properties of the polymer films.

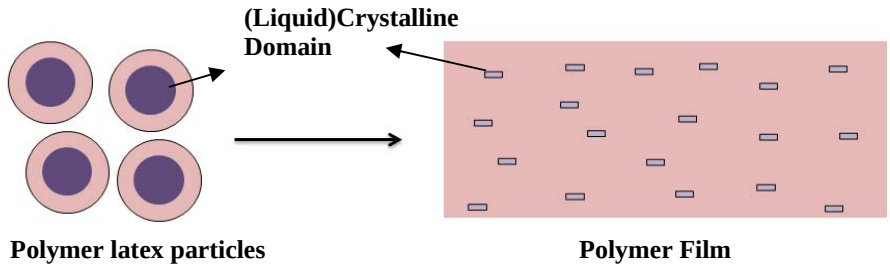

Fig. 1.11. Schematic view of a polymer particles and polymer film containing crystalline and liquid crystalline domains.

To introduce these hard and tough domains two approaches will be considered:

- Using crystallizable n-alkyl $(CH_2)_{10+}$─CH_3 side-chains of the polymer backbone via copolymerization of monomers having long side chains with conventional (meth)acrylate monomers (comb-like crystalline polymers).
- Using side chain LCPs formed by polymerization of monomers with rod-like mesogenic groups. Mesogenic monomers yielding side-chain LCPs seem to be more suitable for free radical polymerization.

Because the monomers containing crystallizable side chains and mesogenic groups can be highly hydrophobic and therefore insoluble in water, miniemulsion polymerization has been selected to incorporate these compounds in the main polymeric matrix [108,109].

1.4. Outline of the thesis

In **Chapter 2,** the synthesis, characterization and performance of waterborne (meth)acrylic dispersions containing crystalline domains for coating applications are investigated. Octadecyl acrylate (commercially known as stearyl acrylate, SA) with 18 methylene units is used to introduce the hydrophobic and crystalline domains to the amorphous short chain (meth)acrylate latex particles. This monomer is the longest side chain acrylate monomer with high purity which is commercially available. Methyl methacrylate (MMA), n-butyl acrylate (BA) and acrylic acid (AA) were the short monomers used in this work. The effect of the polymerization strategy and comonomer composition on the polymer architecture, crystallinity, and particle and film morphologies was investigated. Moreover, the effect of crystalline and hydrophobic domains on the properties (mechanical and barrier properties as well as on the water sensitivity) of polymer films cast from the latexes was investigated.

In **Chapter 3,** the synthesis and characterization of a series of methacrylate side chain liquid crystalline monomers (n-MLCM, n is the number of methylene group in the spacer) able to undergo free radical polymerization was carried out. These monomers were polymerized in miniemulsion. The thermal characterization, phase behaviors and the molecular packing of polymers were investigated by a combination of techniques including differential scanning calorimetry, polarized light microscopy as well as small and wide angle X-ray scattering.

In **Chapter 4,** the synthesis, characterization and performance of waterborne (meth)acrylic dispersions containing liquid crystalline domains for coating applications are presented. The n-MLCMs monomers synthesized in Chapter 3 were used to introduce the liquid crystalline domains to the amourphous short chain (meth)acrylate latex particles. MMA, BA and AA as short monomers are used in this work. The effect of the comonomer composition and the spacer length of the monomers on the polymer liquid crystallinity and on the properties (mechanical and barrier properties as well as on the water sensitivity) of polymer films formed from the latexes were investigated.

In **Chapter 5,** the performance of the semicrystalline latex particles containing poly(SA) domains in coating formulations was studied. Therefore, they were used as binders in paint formulation and the main properties of the paints studied and

compared with the properties of a commercial paint. In addition, the synthesis, characterization and performance of semicrystalline waterborne pressure sensitive adhesives containing poly(SA) domains were discussed. Moreover, the effect of the incorporation of the crystalline and hydrophobic domains of poly(SA) on the adhesive properties of films were investigated.

In **Chapter 6,** the most relevant conclusions of this thesis are presented.

1.5. References

[1] Ohama, Y., 1995. *Handbook of polymer-modified concrete and mortars: properties and process technology*. William Andrew.

[2] Urban, D. and Takamura, K., 2002. *Polymer dispersions and their industrial applications*. Wiley-VCH.

[3] Dunn, D.J., 2003. *Adhesives and Sealants: Technology, Applications and Markets*. iSmithers Rapra Publishing.

[4] Tracton, A.A. ed., 2005. *Coatings technology handbook*. CRC press.

[5] Aggarwal, L.K., Thapliyal, P.C. and Karade, S.R. *Constr Build Mater*, 2007, 21, 379-383.

[6] Ebnesajjad, S. and Landrock, A.H., 2014. *Adhesives technology handbook*. William Andrew.

[7] Petrie, E., 2000. *Handbook of Adhesive and Sealants*. McGraw-Hill.

[8] Fernández-García, M., Cuervo-Rodriguez, R. and Madruga, E.L. *J Polym Sci, Polym Phys*, 1999, 37, 2512-20.

[9] Irfan, M.H., 2012. *Chemistry and technology of thermosetting polymers in construction applications*. Springer Science & Business Media.

[10] Ramos-Fernández, J.M., Guillem, C., Lopez-Buendía, A., Paulis, M. and Asua, J.M. *Prog Org Coat*, 2011, 72, 438-442.

[11] Reyes, Y., Peruzzo, P.J., Fernández, M., Paulis, M. and Leiza, J.R. *Langmuir*, 2013, 29, 9849-9856.

[12] Aguirre, M., Salazar-Sandoval, E.J., Johansson, M., Ahniyaz, A., Paulis, M. and Leiza, J.R. *J Mater Chem*, 2014, 2, 20280-20287.

[13] González, E., Bonnefond, A., Barrado, M., Barrasa, A.M.C., Asua, J.M. and Leiza, J.R. *Chem. Eng. J*, 2015, 281, 209-217.

[14] Chen, D.S. and Jones, F.N. *J Polym Sci A1*, 1987, 25, 1109-1125.

[15] Chen, D.S. and Jones, F.N. *J Appl Polym Sci*, 1988, 36, 141-163.

[16] Smith, G.W. and Vaz, N.A. *Liq Cryst*, 1988, 3, 543-571.

[17] Chen, D.S. and Jones, F.N. *J Appl Polym Sci*, 1989, 37, 1063-1078.

[18] Chiang, W.Y. and Yan, C.S. *J Appl Polym Sci*, 1992, 46, 1279-1290.

[19] Jones, F.N., Chen, D.S., Dimian, A.F. and Wang, D., North Dakota State University, 1993, U.S. Patent 5,218,045.

[20] Landel, R.F. and Nielsen, L.E., 1993. *Mechanical properties of polymers and composites*. CRC Press

[21] Turek, D.E. and Simon, G.P. *Polymer*, 1993, 34, 2750-2762.

[22] Ogata, N., Tanaka, T., Ogihara, T., Yoshida, K., Kondou, Y., Hayashi, K. and Yoshida, N. *J Appl Polym Sci,* 1993, 48, 383-391.

[23] Kennedy, M.A., Peacock, A.J. and Mandelkern, L. *Macromolecules*, 1994, 27, 5297-5310.

[24] Lin, Q. and Yee, A.F. *Polymer*, 1994, 35, 3463-3469.

[25] Lin, Q. and Yee, A.F. *Polym Composites*, 1994, 15, 156-162.

[26] O'Donnell, H.J. and Baird, D.G. *Polymer*, 1995, 36, 3113-3126.

[27] Perego, G., Cella, G.D. and Bastioli, C. *J Appl Polym Sci,* 1996; 59: 37-43.

[28] Ramkumar, D.S. and Bhattacharya, M. *J Mater Sci,* 1997, 32, 2565-2572.

[29]Athawale, V.D. and Bailkeri, R.S. *Liq Cryst*, 2000, 27, 1021-1027.

[30] Trongsatitkul, T., Aht-Ong, D. and Chinsirikul, W. *Macromol Sy*, 2004, 216, 265-280.

[31] Renouf-Glauser, A.C., Rose, J., Farrar, D.F. and Cameron, R.E. *Biomaterials*, 2005, 26, 5771-5782.

[32] Kalkar, A.K., Deshpande, A.A. and Kulkarni, M.J. *J Appl Polym Sci,* 2007, 106, 34-45.

[33] Jang, K.S., Johnson, J.C., Hegmann, T., Hegmann, E. and Korley, L.T. *Liq Cryst*, 2014, 41, 1473-1482.

[34] Paul, D.R. and Yampol'skii, Y.P., 1993. *Polymeric gas separation membranes*. CRC press.

[35] Flodberg, G., Hellman, A., Hedenqvist, M.S., Sadiku, E.R. and Gedde, U.W. *Polym Eng Sci*, 2000, 40, 1969-1978.

[36] Flodberg, G., Höjvall, L., Hedenqvist, M.S., Sadiku, E.R. and Gedde, U.W. *Int J Polym Mater*, 2001, 49, 157-177.

[37] Flodberg, G., Hedenqvist, M.S. and Gedde, U.W. *Polym Eng Sci,* 2003, 43, 1044-1057.

[38] Drieskens, M., Peeters, R., Mullens, J., Franco, D., Lemstra, P.J. and Hristova-Bogaerds, D.G. *J Polym Sci Pol Phys,* 2009, 47, 2247-2258.

[39] Kanehashi, S., Kusakabe, A., Sato, S. and Nagai, K. *J Mater Sci*, 2010, 365, 40-51.

[40] Guinault, A., Sollogoub, C., Ducruet, V. and Domenek, S. *Eur Polym J*, 2012, 48, 779-788.

[41] Comyn, J. ed., 2012. *Polymer permeability*. Springer Science & Business Media.

[42] Patel, R., Monsanto Company, 1985, U.S. Patent 4,555,546.

[43] Deyrup, E.J. and Tam, C.C., EI Du Pont de Nemours, 1988, U.S. Patent 4,758,629.

[44] Wolfe Jr, J.R., EI Du Pont de Nemours, 1988, U.S. Patent 4,782,110.

[45] Pepe, F.R., Hegedus, C.R. and Rabasco, J.J., *Air Products Polymers, LP, 2006,* U.S. Patent 7,029,725.

[46] Dieterich D, Uhling, K. Ullmann's Encyclopedia of Industrial Chemistry, 2002, Wiley-VCH Verlag GmbH, Weinheim, 6th ed.

[47] Mecking, S., Johnson, L.K., Wang, L. and Brookhart, M. *J Am Chem Soc,* 1998, 120, 888-899.

[48] Soula, R., Saillard, B., Spitz, R., Claverie, J., Llaurro, M.F. and Monnet, C. *Macromolecules,* 2002, 35, 1513-1523.

[49] Rünzi, T., Fröhlich, D. and Mecking, S. *J Am Chem Soc*, 2010, 132, 17690-17691.

[50] Bouilhac, C., Rünzi, T. and Mecking, S. *Macromolecules,* 2010, 43, 39-64.

[51] Sauca, S.N., Agirre, A., Even, R.C. and Asua, J.M. *Eur Polym J*, 2012, *48*, 1212-1217.

[52] Parker, H. Y; Merritt, R. F; Fu, Z; Ibbitson, S. A; Gore, R. H; and Wolfersberger, M. A. H. 2003, U. S. Patent 6,552,147.

[53] Schlaefer, F.W. and Gross, A.W., *Rohm And Haas Company*, *1996,* U.S. Patent 5,856,611.

[54] Jordan, E.F., Artymyshyn, B., Speca, A. and Wrigley, A.N. *J Polym Sci Polym Chem*, 1971, 9, 3349-3365.

[55] Jordan, E.F. *J Polym Sci Polym Chem,* 1971, 9, 3367-3378.

[56] Jordan, E.F., Riser, G.R., Artymyshyn, B., Pensabene, J.W. and Wrigley, A.N. *J Polym Sci Polym Chem,* 1972, 10, 1657-1679.

[57] O'Leary, K. and Paul, D.R. 2006, *Polymer*, 47, 1245-1258.

[58] Stewart, R.F., Landec Corporation, 1995, U. S. Pat: 5,387,450.

[59] Stewart, R.F., Balachander, N., Bitler, S.P., Phan, L. and Yoon, V.Y., Landec Corporation, 2003, U.S. Patent 6,540,984.

[60] Geurts, J., Schellekens, MAJ., Nabuurs, T., Overbeek, G.C, 2009. PCT Int. Appl, WO 2009016239 A1 20090205.

[61] Agirre, A., Heras-Alarcón, C.D.L., Wang, T., Keddie, J.L. and Asua, J.M. *ACS Appl Mater Interfaces*, 2010, 2, 443-451.
[62] Popadyuk, N., Popadyuk, A., Kohut, A. and Voronov, A. *Int J Cosmetic Sci,* 2015.

[63] Zhang, Q., Wang, Q., Jiang, J., Zhan, X. and Chen, F.. Langmuir, 2015, 31, 4752-4760.

[64] Jasinski, F., Lobry, E., Tarablsi, B., Chemtob, A., Croutxé-Barghorn, C., Le Nouen, D. and Criqui, A. *ACS Macro Letters*, 2014, 3, 958-962.

[65] Jasinski, F., Rannée, A., Schweitzer, J., Fischer, D., Lobry, E., Croutxé-Barghorn, C., Schmutz, M., Le Nouen, D., Criqui, A. and Chemtob, A. *Macromolecules*, 2016, 49, 1143−1153

[66] Rehberg, C.E. and Fisher, C.H. *J Am Chem Soc*, 1944, 66, 1203-1207.

[67] Jordan, E.F., Feldeisen, D.W. and Wrigley, A.N. *J Polym Sci Polym Chem*, 1971, 9, 1835-1852.

[68] Jordan, E.F. *J Polym Sci Polym Chem*, 1972, 10, 3347-3366.

[69] Greenberg, S.A. and Alfrey, T. *J Am Chem Soc*, 1954. 76, 6280-6285.

[70] Mogri, Z. and D. R. Paul. *Polymer*, 2000, 42, 2531-2542.

[71] Mogri, Z. and D. R. Paul. *Polymer*, 2001, 42, 7765-7780.

[72] O'Leary, K. and Paul, D.R. *Polymer*, 2004, 45, 6575-6585.

[73] O'Leary, K. 2005**,** Physical Properties of Poly (n-alkyl acrylate) Copolymers. PhD Thesis, The University of Texas at Austin.

[74] O'Leary, K. and Paul, D.R. *Polymer*, 2006, 47, 1226-1244.

[75] Plate, N.A. and Shibaev, V.P. *Macromol Rev*, 1974, 8, 117-253.

[76] Hsieh, H.W.S., Post, B. and Morawetz, H. *J Polym Sci Pol Phys,* 1976, 14, 1241-1255.

[77] Plate, N.A.F. and Shibaev, V.P., 2012. *Comb-shaped polymers and liquid crystals*. Springer Science & Business Media.

[78] Chandrasekhar, S., 1992*, Liquid Crystals, Second edition*, Cambridge University Press.

[79] Collyer, A.A. ed., 2012. *Liquid crystal polymers: from structures to applications* (Vol. 1). Springer Science & Business Media.

[80] Sperling, L.H., 2005. *Introduction to physical polymer science*. John Wiley & Sons.

[81] Baumgärtel, H., Franck, E.U., Grünbein, W. and Stegemeyer, H. 1994, *Topics in Physical Chemistry,* Steinkopff Darmstadt Springer.

[82] Ohm, C., Brehmer, M. and Zentel, R., 2012. *Liquid Crystal Elastomers: Materials and Applications*. Springer Berlin Heidelberg.

[83] Nishihara, Y. ed., 2012. *Applied cross-coupling reactions* (Vol. 80). Springer Science & Business Media.

[84] McArdle, C.B., 1990. *Side chain liquid crystal polymers*. Springer Science & Business Media.

[85] Imrie, C.T., Karasz, F.E. and Attard, G.S. *Macromolecules*, 1992, 25, 1278-1283.

[86] Craig, A.A. and Imrie, C.T. *Macromolecules*, 1995**,** *28,* 3617-3624.

[84] Cook, A.G., Inkster, R.T., Martinez-Felipe, A., Ribes-Greus, A., Hamley, I.W. and Imrie, C.T. *Eur Polym J*, 2012**,** 48, 821-829.

[88] Finkelmann, H., Ringsdorf, H. and Wendorff, J.H. *Makromol Chem,* 1978, 179, 273-276.

[89] Finkelmann, H., Ringsdorf, H., Siol, W. and Wendorff, J.H. *Makromol Chem*, 1978, 179, 829-832.

[90] Finkelmann, H., Happ, M., Portugal, M. and Ringsdorf, H. *Makromol Chem* 1978, 179, 2541-2544.

[91] Wang, D., Ye, G., Zhu, Y. and Wang, X. *Macromolecules*, 2009**,** 42, 2651-2657.

[92] Han, M., Kidowaki, M., Ichimura, K., Ramanujam, P.S. and Hvilsted, S. *Macromolecules*, 2001**,** 34, 4256-4262.

[93] Freiberg, S., Lagugné-Labarthet, F., Rochon, P. and Natansohn, A. *Macromolecules*, 2003**,** *36*, 2680-2688.

[94] Tang, X., Gao, L., Fan, X. and Zhou, Q. *J Polym Sci A1*, 2007**,** *45*, 5190-5198.

[95] Zheng, Z., Su, Z., Wang, L., Xu, J., Zhang, Q. and Yang, J. *Eur Polym J*, 2007, 43, 2738-2744.

[96] Ganicz, T. and Stańczyk, W**.** *Materials*, 2009**,** 2, 95-128.

[97] Isayama, J., Nagano, S. and Seki, T. *Macromolecules*, 2010**,** 43, 4105-4112

[98] Chen, S., Ling, A. and Zhang, H.L. *J Polym Sci A1*, 2013**,** 51, 2759-2768.

[99] Finkelmann, H. and Rehage, G., 1984. Liquid crystal side chain polymers. In *Liquid Crystal Polymers II/III* (pp. 99-172). Springer Berlin Heidelberg.

[100] Ni, B., Liao, J., Chen, S. and Zhang, H.L. *RSC Advances*, 2015**,** 5, 9035-9043.

[101] Yu, Z.Q., Li, T.T., Zhang, Z., Liu, J.H., Yuan, W.Z., Lam, J.W., Yang, S., Chen, E.Q. and Tang, B.Z. *Macromolecules*, 2015**,** 48, 2886-2893.

[102] Nakano, T., Hasegawa, T. and Okamoto, Y. *Macromolecules*, 1993**,** 26, 5494-5502.

[103] Vennes, M. and Zentel, R. *Macromol Chem Physic*, 2004**,** *205*, 2303-2311.

[104] Li, G., Yin, J., Li, B., Zhuang, G., Yang, Y. and Nicolais, L. *Polym Eng Sci*, 1995, 35, 658-665.

[105] Kajiyama, T., Nagata, Y., Washizu, S. and Takayanagi, M. *J Membrane Sci*, 1982, 11, 39-52.

[106] Brostow, W. ed., 2013. *Mechanical and thermophysical properties of polymer liquid crystals* (Vol. 3). Springer Science & Business Media.

[107] Datta, A. and Baird, D.G. *Polymer*, 1995, 36, 505-514.

[108] Asua, J.M. *Prog Polym Sci*, 2002, 27, 1283-1346.

[109] Asua, J.M. *Prog Polym Sci*, 2014, 39, 1797-1826.

Chapter 2. Acrylic-Based Polymer Latexes Containing Nano-Sized Crystalline Domains Formed by Comb-Like Polymers

2.1. Introduction

Waterborne (meth)acrylic based latexes commonly obtained by emulsion polymerization are used in applications such as coatings, adhesives, and cement additives [1-6]. Most of these applications involve the formation of a film from the polymeric dispersion. Generally, these polymers are amorphous and they have inferior mechanical properties (toughness), water resistance, barrier properties and durability as compared with polyolefins.

The presence of crystalline domains in the amorphous (meth)acrylic copolymer latexes may be beneficial as they may improve the mechanical properties of these soft polymers. Moreover, these crystalline domains may enhance the barrier properties and water resistance of the films, which are critical characteristics in some applications such as paints, in particular for exterior uses, and other protective coatings.

As mentioned in Chapter 1, a way to introduce crystalline domains in amorphous (meth)acrylic polymers is using long-side chain (CH2)n>10 n-alkyl (meth)acrylate monomers. Unlike conventional crystalline polymers whose backbone crystallizes, in this case, the long n-alkyl side chains of poly(n-alkyl (meth)acrylates) crystallizes [7-10].

In this chapter, the synthesis of waterborne (meth)acrylate dispersions containing crystalline domains for coating applications was investigated. A key requirement for these materials is their ability to form coherent films at room temperature. Therefore, the particles should contain both amorphous phase with the adequate glass transition temperature (T_g) and crystalline domains. The crystalline domains were produced in situ by polymerization of a long-side chain acrylate (LCA) monomer. The degree of crystallinity was controlled by copolymerization of LCA monomer with short-side chain (meth)acrylate (SC(M)A) monomers. The copolymerization of the SC(M)A monomer mixture was adjusted to control the T_g of the amorphous phase. Octadecyl acrylate (commercially known as stearyl acrylate, SA) as long acrylate and methyl methacrylate (MMA), n-butyl acrylate (BA) and acrylic acid (AA) as short monomers were used. Since, SA is highly hydrophobic and therefore insoluble in water, miniemulsion polymerization has been selected to synthesize these waterborne (meth)acrylic-based latex particles [11-13]. For this

process, SA in addition to form crystalline domains, plays the role of costabilizer, which has the additional benefit of avoiding the use of a non-reactive costabilizer (e.g. hexadecane) that remains in the product after polymerization increasing its volatile organic compounds content. The effect of the polymerization strategy and comonomer composition on the crystallinity, polymer architecture, and particle and film morphologies was investigated.

In addition, for the first time, the effect of crystalline and hydrophobic domains on the properties (mechanical and barrier properties as well as on the water sensitivity) of polymer latexes for coating applications was investigated.

2.2. Experimental Section

2.2.1. Materials

Technical grade monomers, methyl methacrylate (MMA, Quimidroga), n-butyl acrylate (BA, Quimidroga) and acrylic acid (AA, Aldrich) as SC(M)A monomers, as well as stearyl acrylate (SA, Aldrich) as LCA monomer were used without purification. Potassium persulfate (KPS) as water soluble radical initiator, sodium dodecyl sulfate (SDS) as anionic surfactant and sodium bicarbonate ($NaHCO_3$) as both buffer and to control the miniemulsion viscosity by reducing the electrostatic

interactions among droplets were supplied by Aldrich and used as received. Deionized water was used as polymerization media.

2.2.2. Experimental design

Table 2.1 summarizes the experimental design in which both the comonomer composition and the polymerization strategy were varied. The comonomer composition were from SA/SC(M)A = 0/100 to SA/SC(M)A = 40/60 wt/wt. The SA amount was limited in order to be able to form films at room temperature. A homopolymerization of SA was carried out to determine the heat of polymerization.

The latexes obtained without SA were used as reference to study the effect of incorporating crystalline domains in the particles. As SA is water insoluble, all the latexes containing this monomer were synthesized by miniemulsion polymerization. Series A (homopolymerization of SA) was carried out in batch. The strategies used for the preparation of the SA/SC(M)A copolymers are summarized in Scheme 2.1. In Series B and C the latexes were prepared by first homopolymerizing a substantial part of SA (60% conversion) and then the mixture of SC(M)A monomers was added either as a shot (Series B of experiments, Runs 4B-7B) or fed to the reactor during 3 h under starved conditions (Series C of experiments, Runs 4C-7C). In these series, an amorphous copolymer of SA/SC(M)A is expected to be formed in the second stage of

the process. In Series D, SA was completely polymerized (100 % conversion) in batch miniemulsion polymerization, and then the mixture of SC(M)A monomers was fed to the reactor during 3 h and copolymerized in the presence of poly(stearyl acrylate) (poly(SA)) homopolymer (Series D of experiments, Runs 4D-6D). The reference latexes, 1E and 2E, that did not contained SA, were synthesized by batch and semibatch emulsion polymerization.

Table 2.1. Summary of the synthesized copolymer latexes with different monomer composition and polymerization strategies.

	Series A	**Series B**	**Series C**	**Series D**	**Series E**	**SA/SC(M)A[a] (wt/wt)**
Miniemulsion polymerization	1A	---	---	---		100/0
	---	4B	4C	4D		40/60
	---	5B	5C	5D		30/70
	---	6B	6C	6D		20/80
	---	7B	7C	---		10/90
Emulsion polymerization	Batch				1E	0/100
	Semibatch				2E	0/100

[a] SC(M)A: MMA/BA/AA=49/49/2 wt%.

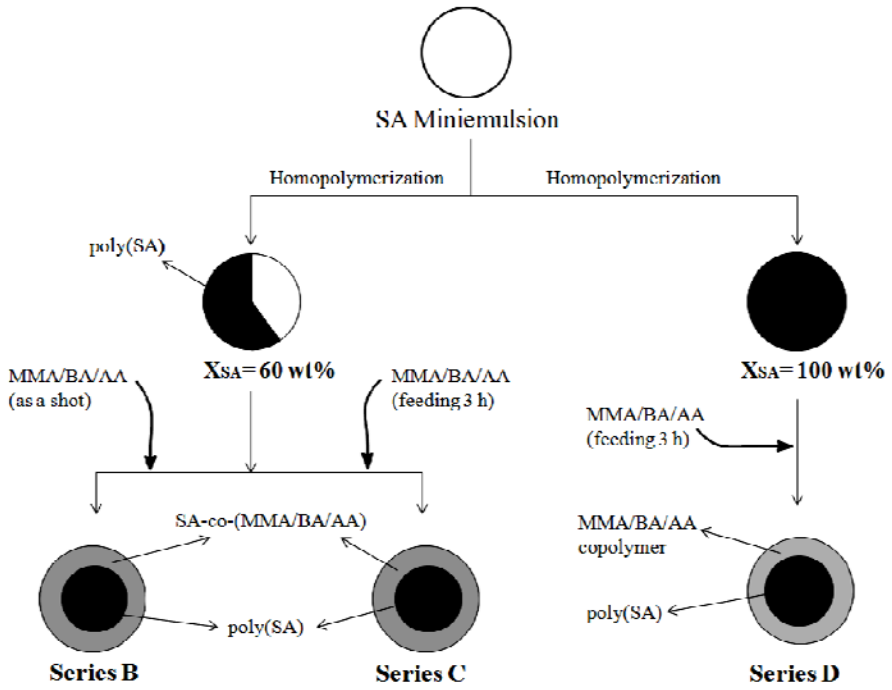

Scheme 2.1. Schematic representation of the synthesis of the SA-co-SC(M)A latexes.

2.2.3. Miniemulsion Polymerization

For the preparation of SA miniemulsion, SDS (1 wt% based on all monomers) and $NaHCO_3$ (0.16 wt% based on all monomers) were added to the total amount of deionized water. The mixture was kept at 40 ºC under magnetic agitation (700 rpm) for 20 minutes to produce a homogeneous solution. Due to the physical characteristics of SA monomer (solid at room temperature), to facilitate the dispersion of this monomer in the aqueous phase and have a more homogeneous

miniemulsion, melted SA monomer was added to the aqueous phase and mixed for 20 minutes at 40 °C. It is worth pointing out, that short chain monomers cannot be added at this stage because this will preclude the formation of poly(SA) crystalline domains. These coarse emulsions were sonicated by using a Brandson Sonifier 450 (amplitude 70% and 50% duty cycle) over 15 minutes under magnetic stirring and in an ice bath to avoid overheating.

In Series B and C, 60 % of SA should be polymerized before adding the SC(M)A monomers. In practice, this requires a fast and reliable method to monitor the conversion of SA. Reaction calorimetry meets these requirements [14-17]. Therefore, the reactions were carried out in a commercial calorimetric reactor (RTCal™, Mettler-Toledo). RTCal™ is a novel and leading edge technology that provides easy access to heat flow data online in real time without calibrations [18]. RTCal™ is equipped with a 1L glass jacket reactor vessel, an anchor impeller, platinum resistance thermometer, a nitrogen inlet and a sampling tube.

The SA monomer conversion was calculated on-line using the following expression:

$$X_{SA}(\mathrm{t}) = \frac{\int_0^{\mathrm{t}} \mathrm{Q_r(t)dt}}{\int_0^{\infty} \mathrm{Q_r(t)dt}} = \frac{\int_0^{\mathrm{t}} \mathrm{Q_r(t)dt}}{\Delta \mathrm{H_P}.\mathrm{M_0}} \qquad (2.1)$$

Where $Q_r(t)$ is the generated heat, ΔH_P is SA homopolymerization enthalpy (ΔH_P = -67.5 kJ/mol, measured in the RTCal calorimeter in Run 1A and determining conversion by ^{1}H NMR) and M_0 is the initial amount of SA.

In Series B, C and D the SA miniemulsion was transferred to the calorimetric reactor, purged with nitrogen and heated to the reaction temperature (70 ºC). Then, the initiator (0.5 wt% based on SA monomer) solution was added as a shot and the SA homopolymerization was started. Once the desired SA monomer conversion was reached (X_{SA} = 60 wt% in Series B and C, X_{SA} = 100 wt% in Series D), and additional initiator solution (0.5 wt% based on MMA+BA+AA monomer) was added as a shot and then the SC(M)A monomers were added to the reactor as neat monomers in one shot (Series B) or fed during 3 h (Series C, D). The copolymerizations were continued for 4 h.

Emulsion copolymerizations of SC(M)A monomers were carried out in batch and semibatch. In semibatch, the reactor was charged with the aqueous phase containing SDS (1 wt% based on all monomers) and $NaHCO_3$ (0.16 wt% based on all monomers), purged with nitrogen and heated to the reaction temperature (70 ºC). Then, the initiator (0.5 wt% based on all monomers) solution was added as a shot and the mixture of SC(M)A monomers was fed to the reactor during 3 h.

The organic phase content in all miniemulsion and emulsion polymerizations was 45 wt%.

2.2.4. Characterization

Global and Instantaneous Conversions. In the case of series D as well as in the emulsion polymerizations, samples withdrawn from the reactor were analyzed gravimetrically to calculate the instantaneous conversion (based on the total amount of monomer fed up to the sampling time). Because of physical characteristic of SA monomer (not volatile), in series B and C a combination of gravimetry and ^{1}H NMR analysis was used to measure monomer conversion in second step of polymerization.

Monomer droplet and particle sizes were measured by dynamic light scattering in a Zetasizer Nano Z (Malvern Instruments). The samples were prepared by dilution of the latex in distilled water. The values given are z-average values obtained through cumulants analysis. The equipment was operated at 20 °C and the values reported were the average of two repeated measurements.

Gel fraction is defined as the fraction of polymer that is not soluble in a good solvent (tetrahydrofuran, THF, in this case) and the **swelling degree** is inversely related with the crosslinking density of the gel. The gel fraction and swelling degree were measured by Soxhlet extraction, using THF as the solvent. A glass fiber square

pad was impregnated with latex (a few drops) and dried overnight. The extraction was carried out for 24 h under reflux conditions (about 70 °C). The gel remained in the glass fiber and it was weight in wet conditions (w_s) and after drying in the oven at 60ºC (w_g), whereas the sol polymer was recovered from the THF solution. The fraction of gel and swelling degree were calculated as follows:

$$\text{gel}(\%) = \frac{w_g}{w_p} \times 100 \qquad (2.2)$$

$$\text{Swelling degree} = \frac{w_s}{w_g} \qquad (2.3)$$

Where w_g is the weight of insoluble fraction of sample (dried sample), w_s is the weight of the swollen gel after 24 hours extraction and w_p is the weight of whole polymer sample.

The **Molecular Weight Distribution** of the soluble fraction was determined by gel permeation chromatography (GPC) at 35 °C. The GPC instrument consisted of an injector, a pump (Waters 510), three columns in series (Styragel HR2, HR4, and HR6), and a differential refractometer (Waters 2410) as detector. To measure the MWD of the samples, the sol part obtained after Soxhlet extraction (see Gel Fraction section) was concentrated and then directly analyzed by GPC. The flow rate of THF through the columns was 1 mL min-1, and samples were filtered before injection into

the GPC (filter pore size = 0.45 μm, Albert). Polystyrene (PS) standards were used to calibrate the equipment and the reported molar masses are reported to PS.

Thermal characterization. The melting temperature (T_m), the heat of fusion (ΔH_f) and the glass transition temperature (T_g) were determined by differential scanning calorimetry (DSC, Q1000, TA Instruments). The films cast at 23 °C from the final latexes. The scanning cycles consisted of first cooling to -50 °C at 10 °C/min, then heating from -50 to 120 °C at 10 °C/min, cooling again from 120 to -50 °C at 10 °C/min, and then heating to 120 °C at a rate of 10 °C/min. The first heating run is a better representative of the film cast at 23 °C. This heating run allows greater phase separation and hence in the second run the transitions are often better defined. The crystallinity of the polymers, X_c, was calculated as $\Delta H_f/\Delta H_{f0}$, where ΔH_f is the observed calorimetric heat of fusion of existing crystals and ΔHf_0 is the heat of fusion for the 100% crystalline phase that has been reported to be 219.5 J/g [9,19,20].

The **morphology** of latex particles and films was studied by means of transmission and scanning electron microscopy (TEM and SEM). TEM analysis was carried out with a TecnaiTM G2 20 Twin device at 200 kV (FEI Electron Microscopes). The latexes were diluted with deionized water (0.05 wt%) placed on copper grids covered with Formvar R and dried at ambient temperature. The films were cryosectioned with a Leica EMUC6 cryoultramicrotome at 30 °C below the T_g

of the sample, with a Diatome 45° diamond knife, and the observations were made in the microscope described above. Scanning Electron Microscopy (SEM, Hitachi S 4800) was used to evaluate the coalescence of particles in fractured surfaces of films cast at 23 and 60 °C; images were obtained at 15 kV from gold coated samples.

The **transparency** of the polymer films were measured using a UV-2550PC UV/Vis spectrophotometer (Shimadzu). Therefore, the transmission spectra in the 300 to 800 nm wavelength range were measured. The thickness of the polymer films was 700 μm.

Mechanical properties of the films were determined by tensile tests according to the ASTM D882 standard test. The films with the thickness of 700 μm were dried in Teflon molds at 60 °C for one week to obtain films without defects (some latexes did not form good films at 23 °C) and the measurements were carried out in a Stable Micro System TA HD Plus Texture Analyzer by using a 5 kN load cell under controlled conditions (23 °C and 55% of humidity). The test speed was 0.42 mm sec^{-1}. The results reported were the average of 5-10 repeated measurements and the reproducibility was good.

To study the water **sensitivity** of the films, the liquid water uptake and static contact angle to water were measured. 700-800 μm thick films were cast from the

latexes in Teflon molds under both controlled environment (23°C and 55% humidity) and at 60 °C for one week.

For water uptake, the films were weighed (m_0) and immersed in distilled water at room temperature (23-25 °C). Then, they were removed at given times, dried with paper, weighed (m_t) and placed again in distilled water. The water uptake was calculated as:

$$\text{Water uptake}(\%) = \frac{m_t - m_0}{m_0} \times 100 \qquad (2.4)$$

The reported data for each film is the average of 3 samples and the reproducibility of the measurements was good.

Static contact angle (CA) measurements of films were performed by the sessile drop method with distilled water, using a goniometer OCA 20 with a high-performance image processing system (Data Physics Instruments GmbH), in air under controlled environment (23°C and 55% humidity). The data presented are the average of 20-30 readings. In order to remove the surfactant, the films were immersed in distilled water for one night and then dried for one week at ambient temperature.

Water vapor transmission experiments were carried out using a gravimetric cell. The films were cast from the latexes in Teflon molds and dried under both

controlled environment (23°C and 55% humidity) and at 60 °C for one week. The thickness of the films was 250-300 μm. The films were placed in the upper part of a cell filled with water. The cell was well-sealed, so that the water could only escape by permeating through the film, and it was placed on a balance within a temperature-controlled chamber (25°C) to measure the loss of weight during time. The permeability to water was calculated from the slope of the weight loss (water loss) versus time plot, as follows [21,22]:

$$WVTR = \frac{\text{m. } f_{\text{thickness}}}{A(a_{\text{int}} - a_{\text{ext}})} \qquad (2.5)$$

Where m is the slope of the curve, $f_{thickness}$ is the film thickness, A is the area of contact between the film and water vapor (2.54 cm^2), a_{int} is the water vapor activity in the headspace of the cell (considered to be 1) and a_{ext} is the water vapor activity in the chamber (measured using a thermohygrometer). Aramendia et al. [23] and Okubo et al. [24] observed that permeability depended on the orientation of the film with respect to the water in the gravimetery cell. They observed that for the latexes stabilized by using conventional surfactants, the water vapor permeability of the films when air-film side was facing the water was substantially higher than when the substrate-film side faced the water in the gravimetery cell. In this work, the

measurements were carried out placing the film-substrate side of the film facing the water and the weight loss of water was recorded every 30 sec for 5 hours.

Oxygen permeability measurements were carried out using a MOCON OX-TRAN Model 2/21 gas permeability tester (USA) in accordance with ASTM standard D3985 and ISO 15105-1,2. The films were cast at 60 °C with the thickness of 150-250 μm. The films were sealed between a chamber containing oxygen and an oxygen free chamber. A coulometric sensor measured the oxygen transmitted through the film. The permeability of O_2 through the copolymer films was tested at 760 mm Hg, 0 % of relative humidity and 23 °C. Oxygen permeability data were reported in Barrers ($1\text{Barrer} = \frac{10^{-10}\text{cm}^3\ \text{STP cm}}{\text{cm}^2\ \text{s cmHg}}$).

2.3. Results and Discussion

The SA miniemulsion droplet and the final particle sizes of the latexes are given in Table 2.2. It can be seen that in Series B, C and D the sizes of the SA miniemulsion droplets were almost the same even though the miniemulsions were prepared with different surfactant/SA ratios. Therefore, it can be concluded that, under the conditions used in these experiments the limiting factor in the miniemulsification of SA monomer is not the surfactant concentration, but the energy used in the miniemulsification process that controlled the droplet break up [25,26]. It

is worth mentioning that the SA miniemulsions were prepared by using a sonifier in the above mentioned conditions and no attempt was done to control the SA miniemulsion droplet size and droplet size distribution in this study. Table 2.2 includes the theoretical values of the final latexes in Series B, C and D assuming that there was not coagulation and secondary nucleation. Comparison with the measured sizes of the final latexes shows that secondary nucleation occurred and that the extent of this process decreased as the fraction of SA in the formulation increased. The reason was the low ratio of seed particles surface area to volume of water (low solids content and number of particles at the beginning of second step of polymerization) and hence the oligoradicals in the aqueous phase were able to grow without being captured by the existing particles. The second reason is that the rate of growth of the oligoradicals increases with the monomer concentration in the aqueous phase which increased as the fraction of SC(M)A in the formulation increased. This effect seems to be less important as the differences between Series B (shot addition of SC(M)A) and C (continuous feeding) were not significant despite the significant differences in monomer conversion (Figure 2.1). The presence of small amorphous particles (white particles) in the TEM micrographs of latex 6D is an evidence of occuring secondary nucleation during second step of polymerization (Figure 2.2). Moreover, these micrographs show that the particles containing poly(SA) domains had core-shell morphology with the dark poly(SA) domains in the core.

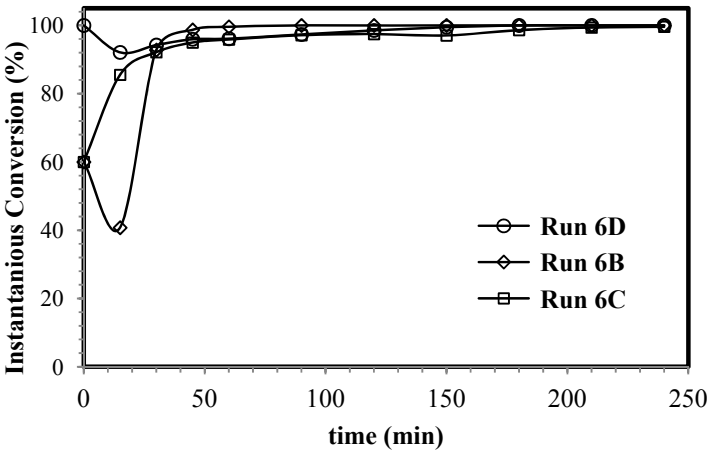

Fig. 2.1. Instantaneous monomer conversions (second step of polymerization) of Runs 6B, 6C and 6D.

Table 2.2. Droplet and particle sizes of miniemulsion droplets and particles (Runs in Table 2.1).

Run	SA/SC(M)A[a] (wt/wt)	SDS/SA monomer (wt%)	Droplet size (SA miniemulsion) (nm)	Final Particle size (nm)	Theoretical Particle size[b] (nm)
batch miniemulsion					
1A	100/0	1	190	197	190
batch miniemulsion of SA (60% conversion) + shot of SC(M)A monomers					
4B	40/60	2.5	140	169	190
5B	30/70	3.3	137	141	204
6B	20/80	5	138	133	236
7B	10/90	10	136	126	293
batch miniemulsion of SA (60% conversion) + 3 h addition of SC(M)A monomers					
4C	40/60	2.5	139	167	188
5C	30/70	3.3	137	155	204
6C	20/80	5.0	145	145	248
7C	10/90	10	138	120	297
batch miniemulsion of SA (100% conversion) + 3 h addition of SC(M)A monomers					
4D	40/60	2.5	150	161	204
5D	30/70	3.3	138	150	206
6D	20/80	5.0	142	142	243
emulsion copolymerization					
Batch (1E)	0/100	-------	-------	81	-------
Semibatch (2E)	0/100	-------	-------	67	-------

[a] SC(M)A: MMA/BA/AA=49/49/2 wt%. [b] without secondary nucleation and coagulations.

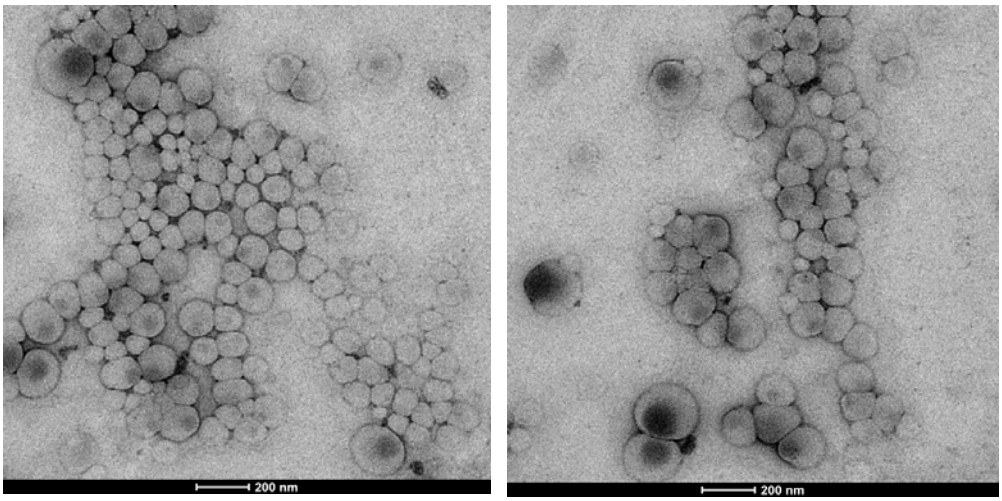

Fig. 2.2. The TEM micrograph of synthesized latex in Run 6D.

The monomer ratio and copolymerization strategies affected copolymer microstructure. In this work, the polymer architecture was characterized in terms of the gel fraction, the swelling ratio and the sol molecular weights. First, it has to be pointed out that no gel content was detected in the latexes obtained by emulsion polymerization of SC(M)A monomers (Runs 1E and 2E). The lack of gel for these runs was due to the presence of MMA in the formulations [27,28]. Gel is formed by the combination of intermolecular chain transfer to polymer (that leads to long chain branches in the polymer) and termination by combination of branched growing radicals (leading to network formation and eventually gel polymer). Because hydrogen abstraction occurs in acrylate units [29,30], the increase of MMA units in

the copolymer chains reduces the option of having branched radicals [28]. Furthermore, the reactivity ratio of MMA is higher than that of the acrylates, and hence, the radicals are predominantly in MMA units, whose activity for hydrogen abstraction is significantly lower than that of the acrylate radicals. In the same vein, MMA radicals terminate by disproportionation, which also reduces the probability of having cross-linking branched chains and, hence, gel polymer formation. On the other hand, Figure 2.3 shows that gel was formed in the presence of SA and that the gel content increased with SA content in Series B, C and D. In addition, the gel fractions were ordered as Series D > Series B > Series C. The gel fraction in latex 1A, i.e. in a fully converted SA homopolymer; was 48 wt%. Therefore, this should be the gel fraction of the SA homopolymer formed in the first stage of Series D where a 100% conversion of SA was reached. In Series B and C, the gel fraction of SA homopolymer formed in the first stage (60% conversion) was most likely lower because in batch polymerization of acrylic monomers, the gel is formed during the last parts of the process [31,32]. The difference in the gel content of the SA homopolymer is the first reason for the higher gel content in Series D as compared with Series B and C. However, simple calculations show that the gel of SA homopolymer is not enough to account for the gel fractions reported in Figure 2.3. For example, for latex 6D, the gel of the SA homopolymer represented only 9.6 % in the final latex whereas a 40 % of gel was measured. Therefore, the majority of the

final gel was formed by the polymer produced in the second stage from SC(M)A monomers. Considering that no gel was observed in Runs 1E and 2E carried out in the absence of Poly(SA), it can be concluded that the gel formed in the second stage of Series B, C and D was formed by grafting of the second stage monomers on the preformed poly(SA), presumably through hydrogen abstraction (transfer to polymer). Note that NMR cannot be used to prove the grafting reaction because the quaternary carbons produced after the intermolecular chain transfer reaction are below the detection limit of the ^{13}C NMR equipment which is around 0.5% and because the quaternary carbons of the MMA unit hinder their observation [28]. The higher amount of poly(SA) in Series D as compared to Series B and C, led to a higher final gel. In addition, analysis of the data within Series D shows that the amount of gel produced during the second stage increases with the fraction of SA in the formulation. Again the reason is that the higher the concentration of poly(SA) the more likely the transfer to polymer. Moreover, Figure 2.3 shows that for the same monomer composition, the gel content in Series B is higher than in Series C. When the mixture of SC(M)A monomers was added to the reactor as a shot (Series B) the copolymer formed at the beginning was richer in MMA and at the end of the reaction, the monomer mixture was rich in acrylates. Therefore, transfer to polymer increased because of the higher polymer concentration and the relative abundance of secondary acrylate radicals. In addition, termination occurred mainly by combination. This led

to long chains grafted on poly(SA) that increased the gel fraction. On the other hand, in Series C, as the mixture of SC(M)A monomers was fed to the reactor under starved conditions, MMA is distributed among the whole process which lowered radical activity for hydrogen abstraction and increased the termination by disproportionation. Both reduced the probability of having long chains and, hence, the increase in gel was lower.

To demonstrate that polymer gels were chemically crosslinked (grafted), swelling measurement of poly(SA) homopolymer (Run 1A) and representative copolymers (Runs 4B,4C and 4D) have been carried out using THF as solvent and the results are given in Table 2.3. Swelling is inversely related to the crosslinking density of the polymer. The swelling value obtained for these polymers were between 15 and 20, clearly indicating that these polymers were mildly crosslinked.

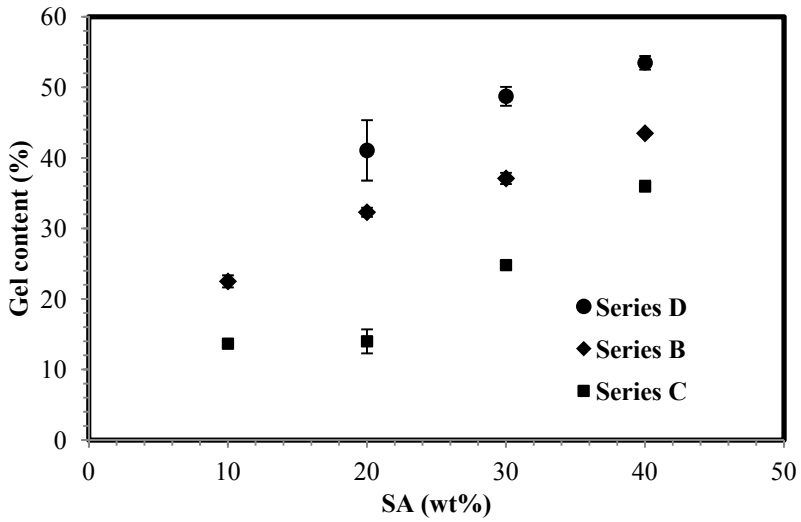

Fig. 2.3. The evolution of gel fraction for the synthesized SA/SC(M)A copolymers in Series B, C and D of experiments.

The weight-average molecular weight and the dispersity (Đ) for the soluble part (see gel fraction part) of the copolymers is presented in Table 2.3. As can be seen, the average molecular weights of the sol copolymers of latexes with highest gel fraction (Series D) is lower than for the latexes with lower gel fraction (Series C and B). Moreover, the presence of all SC(M)A monomers at the beginning of second stage of polymerization in Series B led to higher propagation to termination rate ratio and consequently higher average molecular weights of the sol copolymers in Series B than in Series C. The same can be said for the differences in average molecular weights of the synthesized SC(M)A copolymers in semibatch and batch emulsion systems.

Table 2.3. The weight-average molecular weight and the dispersity (Đ) for the soluble part and the swelling degree of the copolymers synthesized in miniemulsion and emulsion systems.

Run	SA/SC(M)A[a] (wt/wt)	Mw, Soluble Part (g/mol)	Đ	Swelling degree
batch miniemulsion				
1A	100/0	548000	4.9	15.8 ± 0.8
batch miniemulsion of SA (60% conversion) + shot of SC(M)A monomers				
4B	40/60	960000	4.3	19 ± 0.2
5B	30/70	984000	3.2	
6B	20/80	1083000	3.4	
7B	10/90	1221000	2.9	
batch miniemulsion of SA (60% conversion) + 3 h addition of SC(M)A monomers				
4C	40/60	679000	3.8	15.3 ± 2
5C	30/70	637000	3.9	
6C	20/80	640000	3.6	
7C	10/90	693000	3.8	
batch miniemulsion of SA (100% conversion) + 3 h addition of SC(M)A monomers				
4D	40/60	445000	4.6	20 ± 1
5D	30/70	492000	3.5	
6D	20/80	119000	4.4	
emulsion copolymerization				
Batch (1E)	0/100	904000	2.8	0
Semibatch (2E)	0/100	542000	2.6	0

[a] SC(M)A monomers: MMA/BA/AA=49/49/2 wt%.

For these systems there was no substantial difference between the DSC scans observed in the first and second runs. Figure 2.4(a) presents the second run DSC scans of the SA homopolymer (Run 1A) together with the copolymers synthesized in Series B (For better observation of T_g, the DSC scans of the Series B copolymers re-scaled and are shown in Figure 2.4(b)). The DSC of poly(SA) shows an endothermic peak at 51 °C due to the melting of poly(SA) crystalline domains. The DSC traces of the copolymers contain one endothermic peak corresponding to pure poly(SA) and hence decreasing with its content; and a second order transition, which has been assigned as a glass transition.

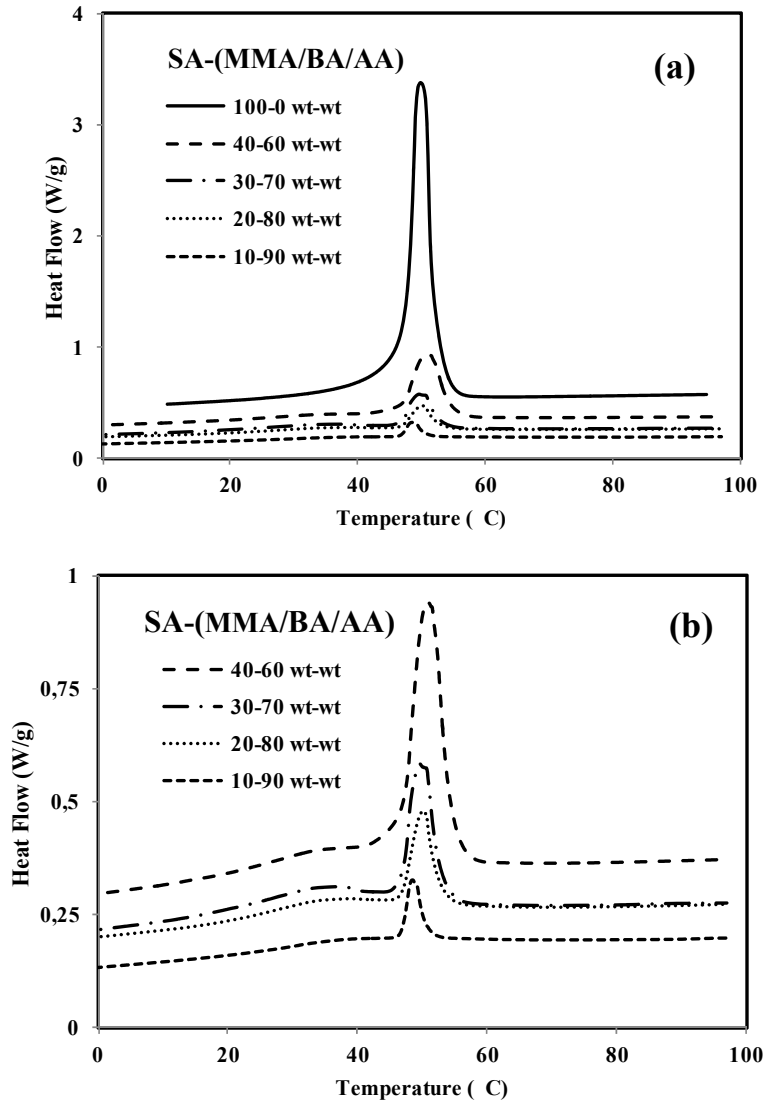

Fig. 2.4. (a) Second heating DSC scans for the SA homopolymer (Run 1A) and synthesized copolymers of SA/SC(M)A with different monomer composition (Series B in Table 2.1). (b) The re-scaled second heating DSC scans for the synthesized copolymers in Series B. (Exo Down)

Melting temperature, heat of fusion, crystallinity degree and the glass transition temperature of all the latexes are given in Table 2.4. This table also includes the crystallinity (X_C^*) estimated assuming the only source of crystallinity is the 41.5 % of the poly(SA) homopolymer produced in the first stage, and that this crystallinity is not modified in the second stage. The heat of fusion ΔH_f, of poly(SA) (Run 1A) is 91 J/g, which leads to crystallinity degree of 41.5 % that is very close to the SA homopolymer synthesized in bulk polymerization [9]. Jordan and coworkers [9] considered that the crystallinity degree was an indication of the number of methylene groups in the side chain which take part in crystallization, n_{cryst}. They estimated that the n_{cryst} for poly(SA) was about 9; and considered that the rest of methylene groups in the side chain (close to the polymer backbone) and also the backbone of poly(SA) remained in amorphous state.

Table 2.4 shows that in each series of experiments, heat of fusion and therefore the crystallinity degrees of the copolymers increased as the SA comonomer concentration increased. For Series D, Xc and Xc^* are almost identical namely the crystalline domains of the final latexes were formed in the first stage and grafting on poly(SA) that occurred in the second stage did not affect the crystals. For Series B and C, Xc and Xc^* did not coincide, showing that new crystalline domains were formed in the runs carried out with the highest SA/SC(M)A ratio (40/60, Runs 4B and

4C), likely due to the formation of poly(SA) chains/blocks by polymerization of the remaining 40 % SA. The amount of new crystalline domains was higher for Series C (semicontinuous addition of SC(M)A monomers) than for Series B (shot addition) because the fraction of SA in the monomer mixture was higher. For low SA/SC(M)A ratios (Runs 6B, 7B, 6C, 7C) $Xc < Xc^{*}$, which seems to indicate that grafting reduced the crystallinity. However, the accuracy of the measurements at this level of crystallinity makes uncertain this hypothesis.

Table 2.4. Composition, crystallinity properties and glass transition temperature for synthesized copolymers.

Run	SA/SC(M)A[a] (wt/wt)	Crystallinity properties				T_g (^{0}C)
		T_m (^{0}C)	ΔH_f (J/g)	Xc[b] (%)	X_C* (%)	
batch miniemulsion						
1A	100/0	51	91.0	41.5	41.5	-116
batch miniemulsion of SA (60% conversion) + Shot of SC(M)A monomers						
4B	40/60	51	26.0	11.8	10.0	20.5
5B	30/70	50	12.6	5.7	7.5	19.6
6B	20/80	50	9.2	4.2	5.0	27.5
7B	10/90	49	3.0	1.7	2.5	31.0
batch miniemulsion of SA (60% conversion) + 3 h addition of SC(M)A monomers						
4C	40/60	50	28.4	12.9	10.0	12.7
5C	30/70	50	16.8	7.7	7.5	13.7
6C	20/80	49	10.1	4.6	5.0	13.0
7C	10/90	49	5.2	2.3	2.5	13.0
batch miniemulsion of SA (100% conversion) + 3 h addition of SC(M)A monomers						
4D	40/60	52	36.0	16.4	16.6	14.0
5D	30/70	51	27.0	12.3	12.5	14.0
6D	20/80	50	18.0	8.2	8.3	15.3
emulsion copolymerization						
Batch (1E)	0/100	----	----	----	----	36.0
Semibatch (2E)	0/100	----	----	----	----	17.8

[a]SC(M)A monomers: MMA/BA/AA=49/49/2 wt%. [b] referred to the whole polymer.

The T_g of the copolymers is affected by the process (Table 2.4). Latexes 1E and 2E obtained by batch and semibatch emulsion polymerization provide a good base for comparison. Latex 2E has a T_g = 17.8 °C, which agrees well with a homogeneous copolymer of composition (MMA/BA/AA= 49/49/2 wt/wt). The high T_g observed for 1E (T_g= 36 °C) corresponded to the MMA rich copolymer formed at the beginning of the process due to the high reactivity ratio of MMA. The T_g of the BA rich copolymer was not observed. For Series D, where the second stage monomers were fed in a semicontinuous fashion, the T_g of the copolymer was slightly lower than for latex 2E, perhaps due to the contribution of the poly (SA-graft-SC(M)A) formed during the second stage of the process, because of the low T_g of the amorphous domains of poly(SA).

In Series C, the second stage was also carried out in a semicontinuous fashion, in this case in the presence of residual SA (40% of the initial one). In this series, a SA rich polymer expected to be formed at the beginning of the second stage, but later a MMA/BA/AA copolymer with some SA units that slightly reduced the T_g was formed.

In Series B, the second stage was carried out in batch and similar to the case of Run 1E a MMA rich was formed at the beginning. This is the T_g observed. This T_g

decreases with the fraction of SA present in the second stage because this resulted in a higher incorporation of SA units to the MMA rich polymer.

Figure 2.5 presents the effect of the polymerization strategy on particle morphology. It can be seen that the particles present a core-shell morphology with the poly(SA) in the core. Usually, conventional amorphous (meth)acrylates are rather transparent to the electron beams; therefore, the dark areas were due to the contribution of the poly(SA) domains. Figure 2.5 is in agreement with the polymerization procedure results. Latex 5D presents a higher proportion of dark zones and the differences between latexes 5B and 5C are not evident.

Figure 2.6 shows the TEM figures of cross-sections of the films cast from latexes 5B, 5C and 5D. It can be seen that in all cases, the poly(SA) was well dispersed in the film and that the poly(SA) domains were more clearly defined in the 5D film, likely because in this case the poor compatibilization between the poly(SA) formed in the first stage and the SC(M)A formed in the second one, whereas in the case of 5B and 5C 40% of the SA copolymerized with the SC(M)A monomers. The differences are even clearer in the case of the films cast at 60 °C, i.e., above the melting temperature of the poly(SA), where the presence of large domains of poly(SA) proves the occurrence of phase separation and coalescence during film formation. Phase separation and coalescence have been reported during film

formation from alkyd acrylics hybrid latexes [33]. Using a mathematical model to analyze the experimental results, the authors concluded that the compatibility between the phases had a greater influence than the morphology of the particles in determining the film structure. Here, better compatibility of poly(SA) (from first stage) and the amorphous copolymer of SA/SC(M)A (formed in the second stage) in Series B and C led to lower phase separation and coalescence of poly(SA) domains than the Series D even for the films cast at 60 °C.

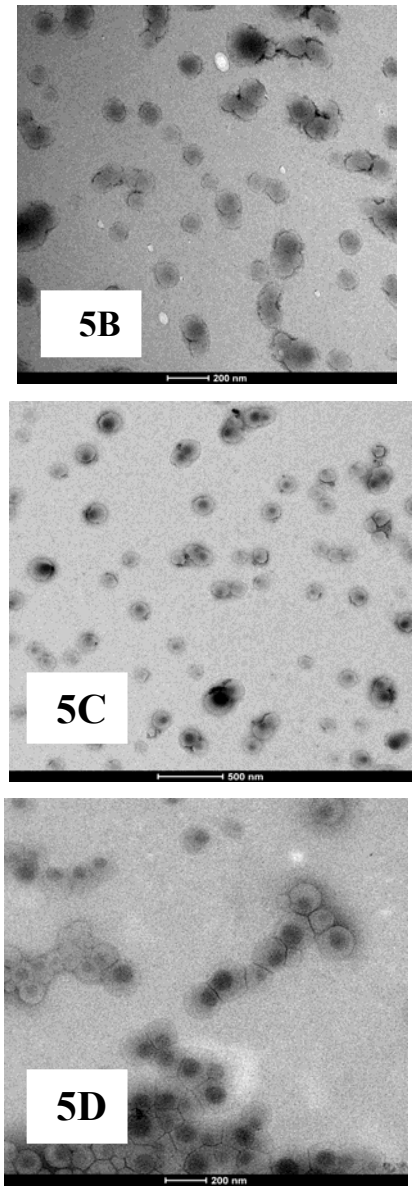

Fig. 2.5. Effect of the polymerization strategy on particle morphology for SA/SC(M)A= 30/70 (wt/wt).

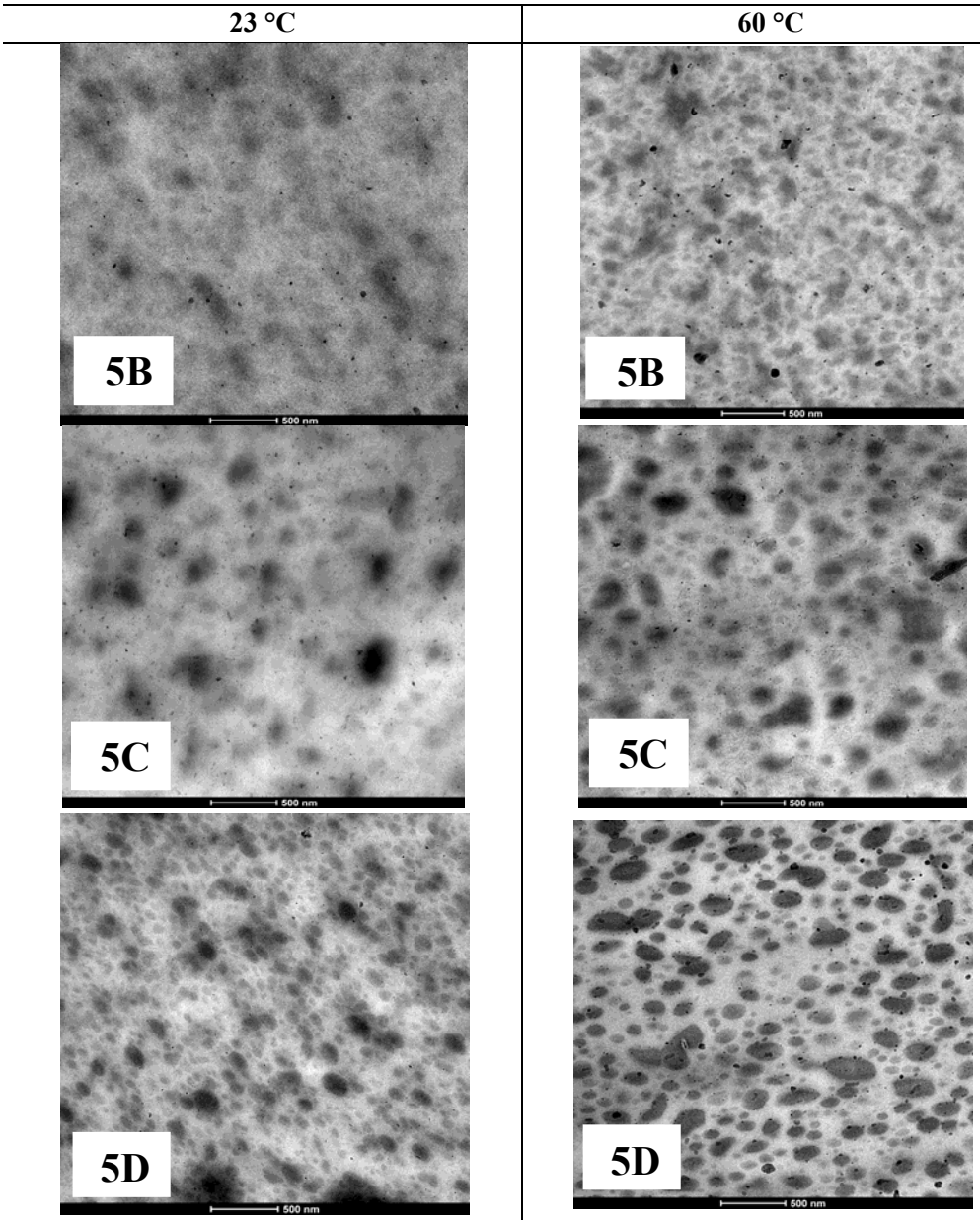

Fig. 2.6. TEM micrographs of cross-section of films cast at 23 °C (left) and 60 °C (right) from the latexes 5B, 5C and 5D.

Further information about the structure of the films can be obtained from the SEM images of the fractured surfaces of the films cast at 23 °C and 60 °C from those latexes (Figure 2.7). In the films cast at 23 °C with latex 5D, hard domains of poly(SA) are evident showing a poor adhesion with the poly(SC(M)A). On the other hand, the presence of amorphous SA/SC(M)A copolymer with low T_g in the latexes synthesized in series B and C improve the coalescence of the particles, and the compatibilizing effect of SA/SC(M)A copolymer reduce the phase separation. Furthermore, the rather homogeneous structure of copolymer matrix in Series C led to better coalescence of particles and formation of a smoother film in comparison with Series B. The SEM micrographs of fractured surfaces of the films cast at 60 °C show that the particles coalesced very well during film formation and since the casting temperature is higher than the melting temperature of poly(SA), the poly(SA) hard domains that were formed after cooling were better integrated in the films.

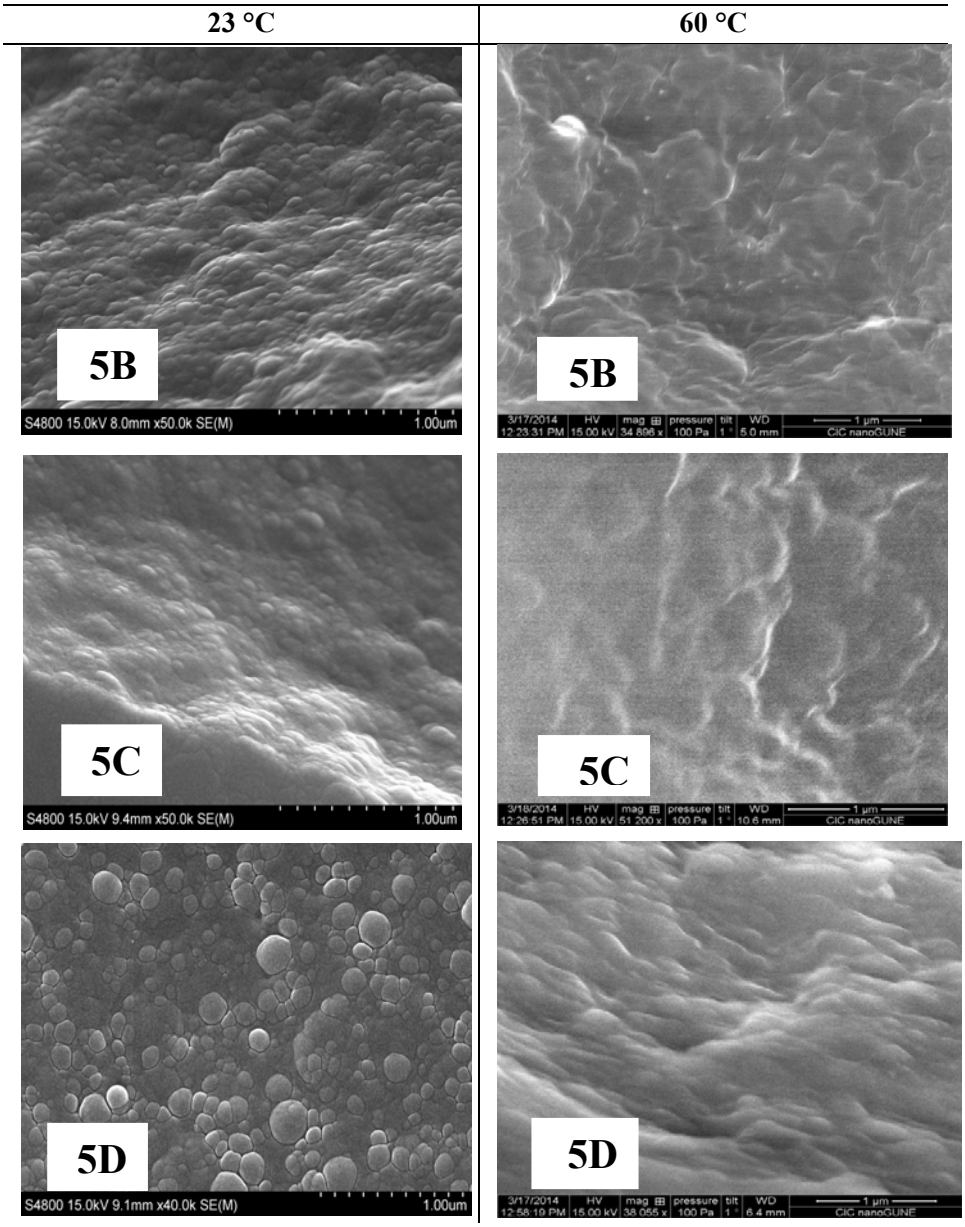

Fig. 2.7. SEM micrographs of fractured surfaces of films cast at 23 °C (left) and 60 °C (right) from the latexes 5B, 5C and 5D.

The differences in particle and film morphologies of the copolymers synthesized in different strategies led to films with different transparency. Figure 2.8 shows the UV–vis spectroscopy of the films cast at 60 °C from the latexes 5B, 5C and 5D. It can be seen that transmittance agrees well with the TEM micrographs of the cross-section of the films (Figure 2.6, right), namely, it decreased with phase separation. In addition, Figure 2.9 shows that the casting temperature affected the film transparency. It can be observed that the film cast at 60 °C from latex 5D was more opaque than the one cast at 23 °C, likely due to the stronger phase separation and coalescence of poly(SA) domains when the film was formed above the melting temperature of poly(SA).

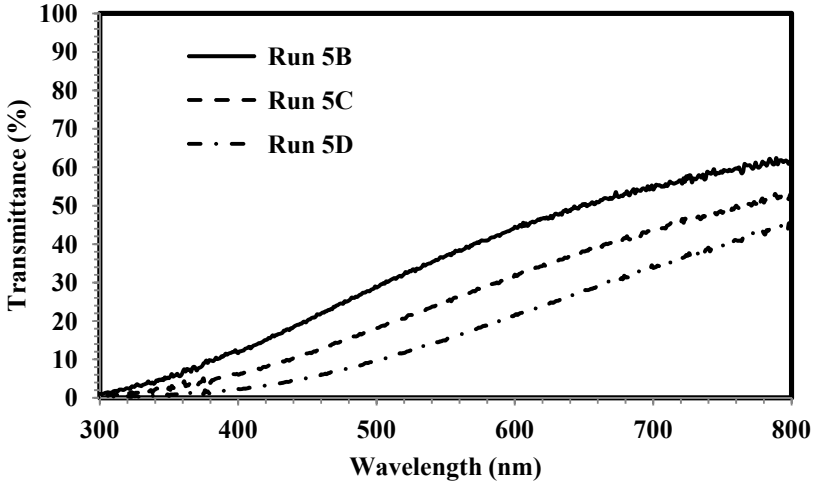

Fig. 2.8. Transmittance of films cast at 60 °C from the latexes 5B, 5C and 5D.

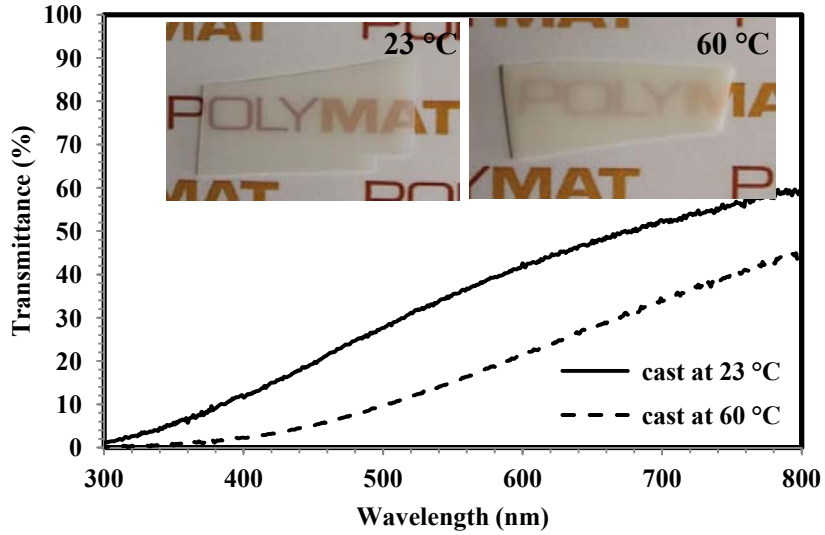

Fig. 2.9. Transmittance of films cast at 23 and 60 °C from latex 5D. Insert: photo images of films.

The mechanical properties of the films cast from Series B, C and D of latexes as well as those of the amorphous copolymers (1E and 2E latexes) are summarized in Table 2.5. Figure 2.10 shows the stress-strain curves for Series B and Run 1E. It can be seen that in Series B, Young's modulus (the slope obtained at low strains), yield stress, toughness (the area under the curve, which is energy per unit volume that the polymer absorb before fracturing) and ultimate strength decreased and the elongation at break point increased when the content of SA in the latex increased from 0 to 30 wt%. The latex with 40 wt% SA did not follow this trend. Moreover, with increasing

SA content from 0 to 20 wt%, the strain softening of the films decreased and for the films with 30 and 40 wt% of SA the strain softening disappeared. To find the reasons for these observations, the structure and the properties of different constituents of the films must be considered.

Table 2.5. Mechanical properties of the films.

Run	SA/SC(M)A[a] (wt/wt)	Young´s Modulus $\times 10^{-2}$ (MPa)	Yield Stress (MPa)	Toughness $\times 10^{-6}$ ($J \cdot m^{-3}$)	Elongation @Break $\times 10^{-2}$ (%)	Ultimate Strength (MPa)
batch miniemulsion of SA (60% conversion) + Shot of SC(M)A monomers						
4B	40/60	1.02±0.03	4.60±0.44	12.31±0.93	2.00±0.09	8.14±0.61
5B	30/70	0.63±0.08	2.59±0.12	18.60±1.69	3.51±0.21	8.23±0.45
6B	20/80	1.17±0.11	3.35±0.32	22.26±1.21	3.35±0.17	9.79±.41
7B	10/90	1.79±0.17	5.67±0.72	26.86±1.92	3.24±0.25	12.38±0.46
batch miniemulsion of SA (60% conversion) + 3 h addition of SC(M)A monomers						
4C	40/60	0.27±0.02	1.35±0.11	13.86±1.61	3.12±0.27	6.46±0.31
5C	30/70	0.18±0.03	0.76±0.08	19.17±1.26	4.10±0.22	7.67±0.52
6C	20/80	0.23±0.01	0.87±0.03	21.62±2.18	4.66±0.23	7.66±0.61
7C	10/90	0.21±0.02	0.91±0.10	24.17±1.63	4.97±0.17	9.94±0.39
batch miniemulsion of SA (100% conversion) + 3 h addition of SC(M)A monomers						
4D	40/60	1.31±0.11	4.34±0.29	22.17±1.74	2.46±0.18	12.96±0.93
5D	30/70	0.99±0.16	2.99±0.37	28.64±2.12	3.38±0.34	13.55±0.84
6D	20/80	0.75±0.04	1.91±0.24	27.38±1.42	3.83±0.21	12.30±0.87
emulsion copolymerization						
Batch (1E)	0/100	2.46±0.16	7.58±0.11	20.27±1.30	2.32±0.20	12.95±0.65
Semibatch (2E)	0/100	0.32±0.08	0.98±0.10	17.53±1.48	4.37±0.31	7.25±0.50

[a] SC(M)A: MMA/BA/AA=49/49/2 wt%.

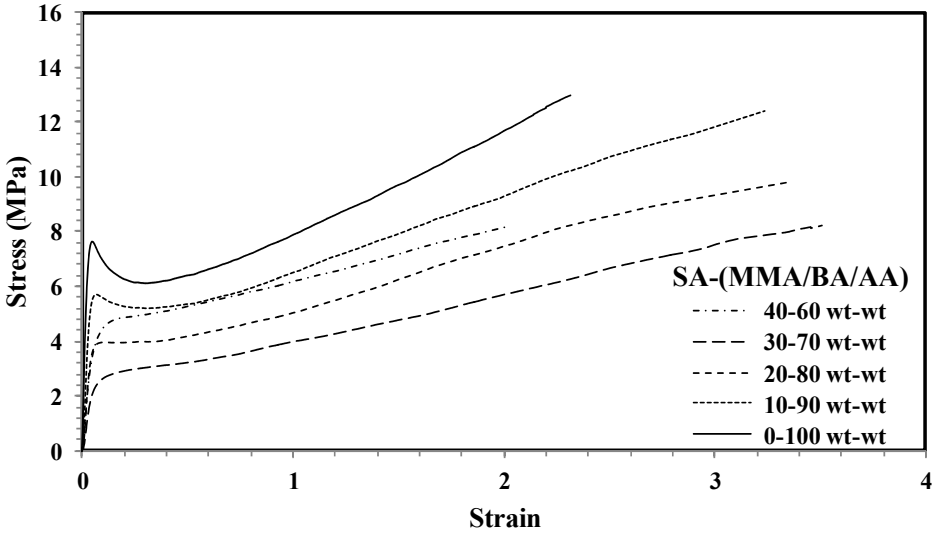

Fig. 2.10. The stress-strain behavior of copolymers obtained from Series B as well as Run 1E.

Table 2.4 shows that the majority of poly(SA) homopolymer (Run 1A) was an amorphous polymer. The combination of DSC, dynamical mechanical thermal analysis (DMTA) and dielectric measurements was used to study the amorphous phase and transition temperatures of poly(SA). The details of the experiments are given in Appendix I. It was found that the T_g of poly(SA) is about -116 ºC which is in a good agreement with the predicted T_g for amorphous state of poly(SA) in the literature (-111 ºC) [7].

This means that the presence of poly(SA) homopolymer in the film had two counteracting effects. In one part, the crystalline domains reinforced the mechanical properties, and on the other hand, the amorphous part had a plasticizing effect. In the region of 10 – 30 wt% content, the plasticizing effect was predominant as it is also observed by the decrease of the T_g as the SA content increased. However, at 40 wt%, the crystalline fraction was high enough to overcome the effect of the amorphous domains.

Table 2.5 shows that the effect of SA content on the mechanical properties of the latexes in Series C was not as prominent as observed in Series B. However, with increasing SA content and crystallinity, the elongation at break, toughness and ultimate strength decreased (see Table 2.5). Moreover, the comparison of the mechanical properties of Series C with Run 2E showed that the Young´s modulus and the yield stress of the latexes with 10 - 30 wt% SA were lower than those of Run 2E. However, the ultimate strength and the toughness were higher than Run 2E.

It is worth mentioning that in the semicrystalline latexes of Series B and C, the amount of both crystalline domains and amorphous domains of poly(SA) and SA/SC(M)A copolymer increased with SA content. Thus, in these series (10 – 30 wt% SA) the effect of crystallinity was compensated by the plasticizing effect of the

amorphous material. At higher SA content (latexes 4C and 4B) the higher crystallinity overcame the effect of the amorphous domains.

The stress-strain behavior of the films from latexes in Series D and latex 2E is presented in Figure 2.11. This figure and the mechanical properties given in Table 2.5 show that with increasing SA composition (and hence crystallinity), the Young's modulus and the yield stress of the copolymers increased; however, the elongation at break point decreased. Moreover, the ultimate strength for these semicrystalline latexes was independent of their composition and this value was substantially higher than that of the blank SC(M)A copolymer sample. In comparison with the amorphous SC(M)A copolymer (Run 2E), the semicrystalline copolymers in Series D showed higher toughness overcoming one of the weaknesses of conventional (meth)acrylate polymers.

In Series D, the SA was completely polymerized first and then the SC(M)A monomers were polymerized in semicontinuous. Therefore, the final latexes contained crystalline and amorphous poly(SA), amorphous SC(M)A copolymer and some grafted copolymer (see gel fraction part). Figure 2.14 shows that the crystalline domains of poly(SA) improved the mechanical properties of the amorphous copolymer.

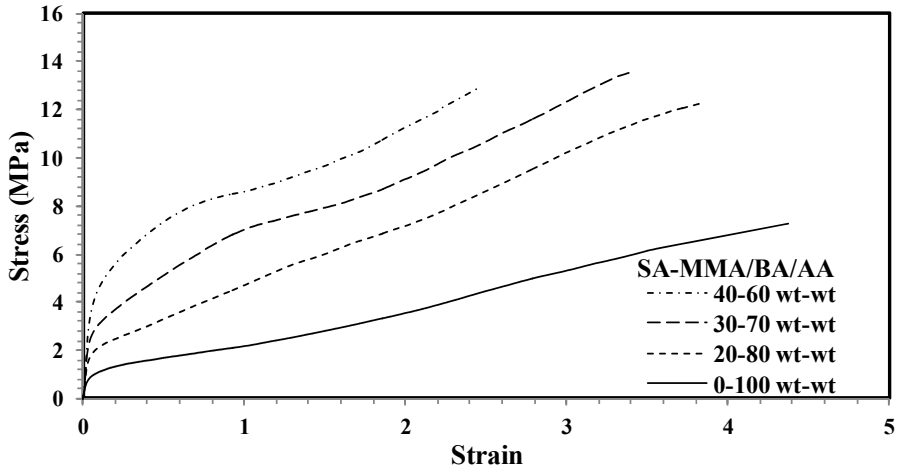

Fig. 2.11. The stress-strain behavior of copolymers obtained from Series D as well as Run 2E.

The stress-strain behavior of the films of the same monomer composition (SA/SC(M)A =40-60 wt/wt) synthesized using different strategies (Runs 4B, 4C and 4D) is presented in Figure 2.12. This figure shows that the Young's modulus, yield stress and ultimate strength of the latexes synthesized in Series B were higher than in Series C. However, the elongation at break in Series C was larger than in Series B. Since the main difference in the synthesis of these latexes is the way in which the SC(M)A monomers were added to the reactor (as a shot for Series B and feeding in Series C), the differences in mechanical properties can be attributed to the differences in the copolymer structures. As discussed before the T_g of the synthesized copolymers

in Series B is higher than the Series C. In addition, the gel fraction of the copolymers in Series B was higher than in Series C (Figure 2.3). Therefore, the reinforcing effect of both the higher T_g and the higher gel fraction in Series B were responsible for the higher Young´s modulus, yield stress and the ultimate strength of Series B (as compared with Series C). The same can be said for the differences in mechanical properties of the SC(M)A copolymers synthesized in batch and semibatch emulsion polymerization (Runs 1E and 2E).

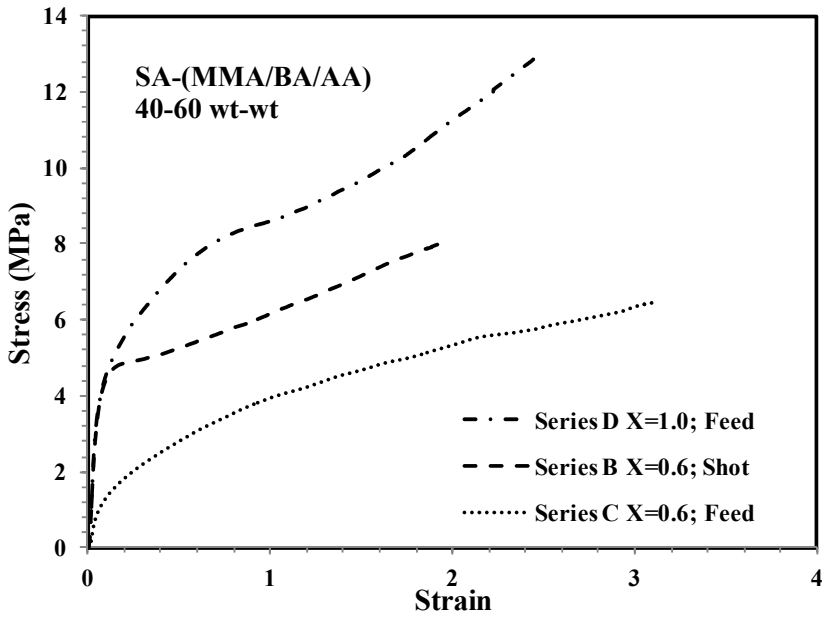

Fig. 2.12. The stress-strain behavior of the latexes synthesized with the same monomer composition in Series B, C and D of experiments (Runs 4B, 4C and 4D).

In addition, Figure 2.12 shows that the mechanical properties of the latexes in Series D are higher than those in Series B and C. The lower mechanical properties of the films in Series B and C can be related to lower crystallinity (see Table 2.4) and also to the presence of amorphous poly(SA) and SA/SC(M)A copolymers in the polymer matrix. These amorphous polymers led to a decrease of the T_g and the mechanical properties. These results indicate that the introduction of poly(SA) crystalline domains to amorphous (meth)acrylate copolymer matrix improve mechanical properties; conversely, the presence of the amorphous SA/SC(M)A copolymer and the amorphous part of poly(SA) lower the mechanical properties. Moreover, the higher gel fraction of Series D latexes (see Figure 2.3) could be also a reason for showing higher mechanical properties.

Figure 2.13 presents the results of the liquid water uptake measurements for the films cast at 23 °C (Figure 2.13(a)) and at 60 °C (Figure 2.13(b)) from the latexes synthesized in Series D as well as from Run 1E. At both casting temperatures, the liquid water uptake of the semicrystalline films was lower than that of the fully amorphous film. On the other hand, the liquid water uptake for the films cast at 60 °C decreased with increasing crystallinity and hydrophobic monomer content. The crystalline domains of poly(SA) acted as a barrier for water and reduced the kinetics of water uptake in the films. Moreover, with increasing SA concentration, the acrylic

acid content and water sensitivity of polymer films decreased. The liquid water uptake of the films cast at 23 °C did not continuously decrease with crystallinity and hydrophobic monomer concentration. The deviation of Run 4D is attributed to the irregularities of the film that formed blisters that swelled with water (Figure 2.14(a)). These irregularities were not present in the other films of the Series D cast at 23 °C and in those cast at 60 °C (see Figure 14(b) for the film cast from the same latex at 60 °C). Moreover, for the latexes able to form good films at 23 °C (Runs 5D, 6D and 2E) there was no significant effect of the casting temperature on the water uptake.

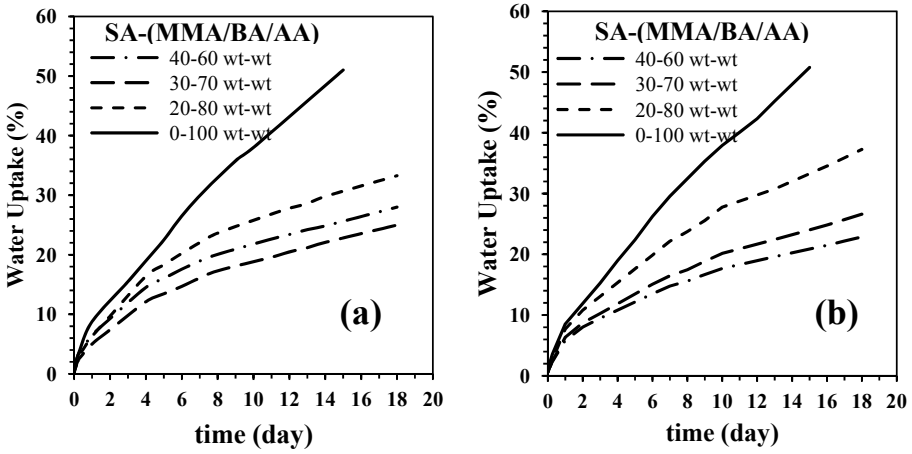

Fig. 2.13. Liquid water uptake measurement of the films cast at (a) 23 °C and (b) 60 °C from the latexes in Series D and the latex 2E.

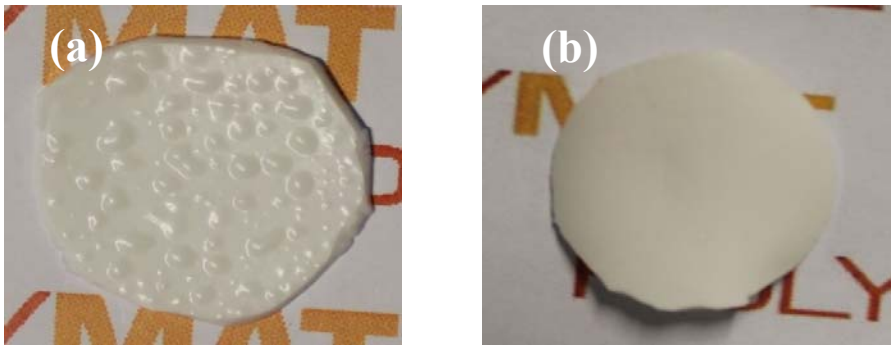

Fig. 2.14. The substrate-film interface photo after 18 days immersing in distilled water for the film cast at (a) 23 °C and (b) 60 °C from the latex 4D.

The liquid water uptake measurements of the films cast at 60 °C from latexes obtained by different strategies with the same monomer composition (SA/SC(M)A = 40/60 wt/wt; Runs 4B, 4C and 4D) and Run 2E are presented in Figure 2.15. This figure shows that the liquid water uptake of semicrystalline copolymers was lower than that of the amorphous copolymer of SC(M)A. Moreover, the liquid water uptake of the semicrystalline copolymer ranges as Run 4C > Run 4D > Run 4B. This indicates that for this system, water uptake is affected by both the amorphous and the crystalline phases. The higher the T_g of the amorphous phase (lower free volume) and the higher the crystalline fraction the lower the water uptake. Run 4D has a higher crystallinity and slightly harder amorphous phase than Run 4C and therefore a lower water uptake. On the other hand, as compared with Run 4D, the higher T_g of the amorphous phase of Run 4B compensated the lower crystallinity and presented a lower water uptake. The effect of the T_g of the amorphous phase on water uptake has

been reported for other systems. Thus, Agarwal et al. [34] demonstrated that water absorption of soft acrylic-based latex films decreased with T_g; and Mudge et al. [35] improved the water resistance of poly(vinyl acetate) adhesives by introducing higher T_g poly(methyl methacrylate).

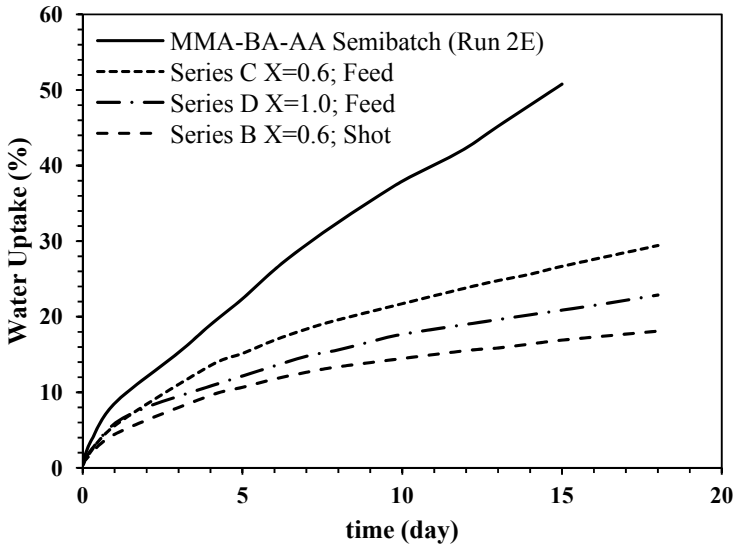

Fig. 2.15. The liquid water uptake measurement of the films cast at 60 °C from the latexes synthesized in Runs 4B, 4C and 4D as well as Run 2E.

Table 2.6 presents the water vapor transmission rates (WVTR) of the films cast at 23 and 60 °C from the latexes synthesized in Series D and in Run 2E. The results show that for both temperatures, the WVTRs of semicrystalline copolymers in Series D were lower than that of the amorphous copolymer of SC(M)A in Run 2E; and that

the water vapor permeability decreased with increasing SA content. With increasing SA content, the film became more hydrophobic and therefore the diffusion of water vapor decreased. Moreover, the crystalline domains of poly(SA) acted as a barrier for water vapor and increase the tortuosity of the diffusion path reducing the diffusion rate. In addition, as the SA content increased, the acrylic acid content decreased, which lowered the water sensitivity of the films [36,37].

Table 2.6. Results of the water vapor transmission rate (WVTR) of films obtained from the latexes.

Run	**SA/SC(M)A[a] (wt-wt)**	**Xc[b] (%)**	**WVTR (g.mm/m^2.day)**
		Cast film at **23 °C**	
2E	0-100	0.00	11.6±1.8
6D	20-80	8.22	9.1±0.7
5D	30-70	12.30	7.4±1.0
4D	40-60	16.40	6.7±0.9
		Cast film at **60 °C**	
2E	0-100	0.00	10.0±1.0
6D	20-80	8.28	6.9±0.4
5D	30-70	12.40	5.4±0.9
4D	40-60	16.40	4.7±0.8

[a] SC(M)A: MMA/BA/AA=49/49/2 wt%. [b] referred to the whole polymer.

For the films with the same monomer composition, the WVTR in films cast at 60 °C was lower than those cast at 23 °C, although the crystallinity of films cast at 23

and 60 °C was almost the same (Table 2.6). The main reason for the lower permeability of the films cast at 60 °C is the better coalescence of the particles containing poly(SA) domains during film formation. This was shown in Figure 2.7 that presents the SEM micrographs of the fractured surface of films cast at 23 and 60 °C from the latexs synthesized in different strategies. It can be seen the hard crystal domains are evident for the film cast at 23 °C (< T_m of poly(SA)), whereas at 60 °C (> T_m of poly(SA)) a much smother surface is was observed, which indicates a better coalescence of the hard crystal domains.

Table 2.7 shows the WVTR and the oxygen permeability of the films cast at 60 °C from the latexes synthesized in Series B, C and D with the same monomer composition (SA/SC(M)A=40/60 wt/wt (Runs 4B, 4C and 4D)). This table also includes the permeability values for the amorphous copolymer film from Run 2E and for a polypropylene (PP, supplied by Repsol, Spain) film processed at 200 °C for comparison purpose. These results clearly show that the permeability to water and oxygen of Series D is lower than for Series B and C. This shows the improving effect of crystallinity on the barrier properties of these films. An interesting point is that the permeability to oxygen for the amorphous copolymer of SC(M)A (Run 2E) is lower than that of the semicrystalline copolymers synthesized in Series B and C with 40 wt% SA (Runs 4B and 4C). This behavior is due to the structure of the copolymers.

Generally, polymer structures that have poor water vapor barrier properties show good gas barrier properties [38]. Highly polar polymers such as those containing hydroxyl or carboxylic groups are good gas barriers, but do not perform well to prevent permeation of water vapor. On the other hand, non-polar polymers such as polyethylene and propylene are excellent water barriers, but poor gas barriers [38,39]. Therefore, the higher concentration of acrylic acid in the amorphous SC(M)A copolymers results in a lower oxygen permeability and a high WVTR. On the other hand, the presence of aliphatic-like long-side chain of SA in the amorphous SA/SC(M)A copolymer in Run 4B and 4C led to a higher oxygen permeability.

Table 2.7. Results of the water vapor transmission rate (WVTR) and oxygen permeability of films cast at 60 °C.

Run	SA/SC(M)A[a] (wt-wt)	Xc[b] (%)	WVTR (g.mm/m^2.day)	Oxygen permeability (barrer)
		Cast at **60 °C**		
2E	0-100	0.00	10.0±1	2.28±0.26
4B	40-60	11.87	6.4±0.9	3.73±0.00
4C	40-60	12.98	6.7±0.0	2.66±0.06
4D	40-60	16.40	4.7±1.1	1.97±0.00
		Polypropylene sample processed at **200 °C**		
PP	------	50.00	2.6±1.0	2.03±0.08

[a] SC(M)Ac: MMA/BA/AA=49/49/2 wt%. [b] referred to the whole polymer.

The static contact angles of the air-film and substrate-film interfaces of the films cast at 60 °C from the latexes in Series D and Run 2E are given in Table 2.8.

Moreover, the contact angles of films cast at 60 °C from Runs 4B and 4C are included. It can be seen that the contact angles increased with the content of the most hydrophobic monomer (SA) and that crystallinity had no effect on the contact angle. On the other hand, the contact angles of the substrate-film interface were higher than those of the air-film interface.

Table 2.8. The static contact angle values of air-film and substrate-film interfaces of the films cast at 60°C from the copolymer latexes (after washing with water).

Run	SA/SC(M)Ac[a] (wt-wt)	film at 60 °C	
		Air-film	Substrate-film
2E	0-100	79 ± 2 °	88 ± 3 °
6D	20-80	85 ± 3 °	96 ± 3 °
5D	30-70	88 ± 3 °	100 ± 2 °
4D	40-60	92 ± 3 °	102 ± 3 °
4B	40-60	90 ± 4 °	101 ± 3 °
4C	40-60	92 ± 3 °	103 ± 2 °

[a]SC(M)A: MMA/BA/AA=49/49/2 wt%.

Figure 2.16 presents the SEM micrographs of the air-film and substrate-film interfaces for the film cast from latex 4D. It can be seen that the air-film interface (a) was much smoother than the substrate-film interface (b). Figure 2.17, that presents the SEM micrographs of the different regions across the film, shows that the film

varied from relative smooth near the air-film interface to a rougher topology near the substrate-film interface. This suggests that the large and more hydrophobic particles (SA-rich) sedimented accumulating at the bottom of the film, whereas the small particles containing SA and the ones that did not contain SA accumulated at the air-film interface. This resulted in an anisotropic film that was more hydrophobic at the substrate-film interface.

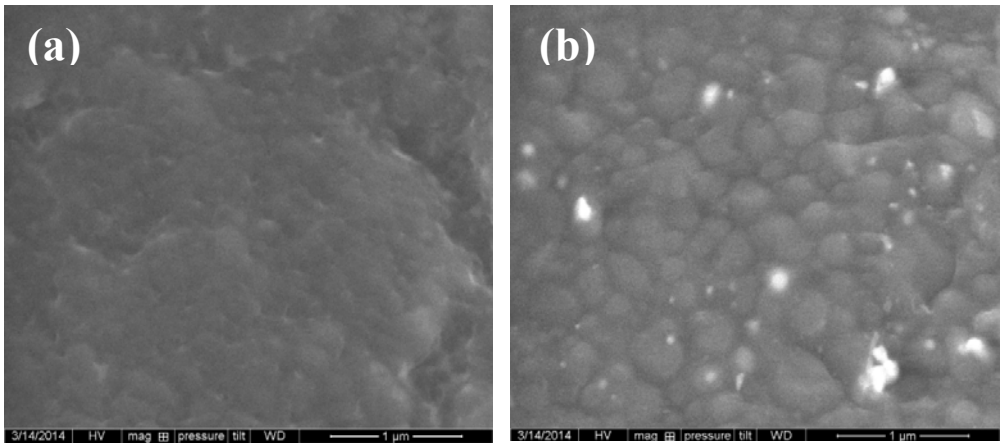

Fig. 2.16. The SEM micrograph of (a) air-film and (b) substrate-film interfaces of the film cast at 60 °C from the latex synthesized in Run 4D.

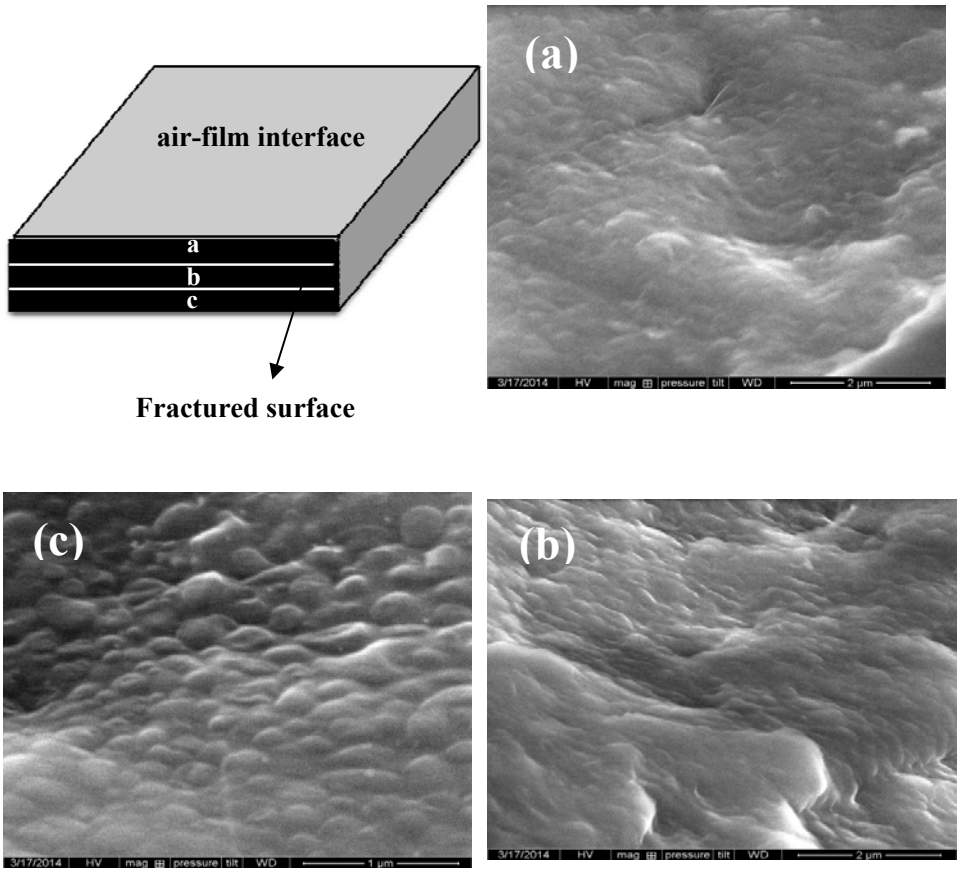

Fig. 2.17. SEM micrographs of different regions of fractured surface of the film cast at 60°C from the latex synthesized in Run 4D.

2.4. Conclusions

Semicrystalline, waterborne polymer latexes have been synthesized by using different strategies in 2-step miniemulsion polymerizations. The first step consisted in the homopolymerization of stearyl acrylate (SA), which led to formation of crystalline domains. Homopolymerization of SA also led to the formation of very low T_g amorphous polymer. The degree of crystallinity was controlled by the conversion of SA achieved in the first step (60% in Series B and C, and 100% in Series D) and by the way in which the short side chain (meth)acrylates (a mixture of methyl methacrylate, n-butyl acrylate and acrylic acid) were fed in the second step (shot for Series B and semicontinuously for 3 h for Series C and D).

It was found that some secondary nucleation occurred during the second step and that the extent of this process decreased as the fraction of SA in the formulation increased. For Series D, the crystalline domains were formed during the first step and the crystals were not modified during the second step of the process. For Series B and C, crystallinity increased during the second step for the highest concentration of SA (40%) and decreased for lower fractions. Crystallinity was higher in Series C than in Series B because the concentration of SA at the beginning of the second stage was higher. In all cases, crystallinity increased with the SA content of the formulation and was maximum for Series D.

Gel (polymer insoluble in THF) was formed both during the homopolymerization of SA in the first step (following the classical mechanism for acrylate monomers) as well as during the copolymerization in the second stage (by grafting the second stage monomers on the amorphous part of the poly(SA)). The amount of gel produced in the second stage increased with the fraction of SA in the formulation and it was higher in Series D than in Series B and C.

The TEM micrographs of the particles showed a core-shell morphology with the crystalline poly(SA) forming the dark core. Series D presented a higher proportion of dark zones in agreement with the higher crystalline content. All the latexes yielded good films at room temperature with the crystalline domains well dispersed in the film. SEM micrographs of the fractured surfaces of the films showed better compatibility between crystalline and the amorphous phases in the case of Series B and C than for Series D. TEM images showed no proof of aggregation of crystalline domains during film formation at room temperature, but substantial coalescence occurred casting the films at 60 °C (i.e. above the melting temperature of poly(SA). Transparency of the films decreased with the size and number of crystalline domains and was the lowest for Series D cast at 60 °C.

The performance of waterborne polymer latexes containing nano-sized crystalline domains also was studied. Comparison with the performance offered by

regular latexes, namely latexes devoid of crystalline domains, showed that mechanical and barrier properties as well as the resistance to water improved with the incorporation of the crystalline domains.

On the other hands, the performance of the latexes containing SA was affected in a complex way by the interplay between the amorphous and crystalline parts. Although in some cases, the increase of SA content led to better mechanical properties, the counteracting effect of the amorphous and crystalline fractions led in other cases to a decrease of the Young´s modulus and the yield stress.

In addition, the mechanical properties of the latexes improved with the T_g of the polymer produced in the second step that depended on the feeding strategy of short chain (meth)acrylates ($T_{g\ shot} > T_{g\ continuous\ feeding}$).

The effect of the T_g of the second step polymer was even more accused on water uptake where it overcame the effect of crystallinity.

Water vapor permeability decreased as the SA content increased and it was affected by the quality of the film that depended on the casting temperature; the higher this temperature the better film and the lower water vapor permeability. For the same overall composition, oxygen permeability decreased with the crystalline fraction.

It was found that stratification of polymer particle during film formation led to anisotropic films showing higher water contact angles at the substrate-film interface than for the air-film interface. In both interfaces water contact angles were only affected by the SA content, namely, they were independent of the polymerization strategy.

2.5. References

[1] Ohama, Y., 1995. *Handbook of polymer-modified concrete and mortars: properties and process technology*. William Andrew.

[2] Urban, D. and Takamura, K., 2002. *Polymer dispersions and their industrial applications*. Wiley-VCH.

[3] Dunn, D.J., 2003. *Adhesives and Sealants: Technology, Applications and Markets*. iSmithers Rapra Publishing.

[4] Tracton, A.A. ed., 2005. *Coatings technology handbook*. CRC press.

[5] Aggarwal, L.K., Thapliyal, P.C. and Karade, S.R. *Constr Build Mater*, 2007, 21, 379-383.

[6] Ebnesajjad, S. and Landrock, A.H., 2014. *Adhesives technology handbook*. William Andrew.

[7] Jordan, E.F. *J Polym Sci Polym Chem,* 1971, 9, 3367-3378.

[8] Jordan, E.F., Riser, G.R., Artymyshyn, B., Pensabene, J.W. and Wrigley, A.N. *J Polym Sci Polym Chem,* 1972, 10, 1657-1679.

[9] Jordan, E.F., Feldeisen, D.W. and Wrigley, A.N. *J Polym Sci Polym Chem*, 1971, 9, 1835-1852.

[10] Jordan, E.F. *J Polym Sci Polym Chem*, 1972, 10, 3347-3366.

[11] Ugelstad, J., El-Aasser, M.S. and Vanderhoff, J.W. *J Polym Sci, Polym Lett*, 1973, 11, 503-513.

[12] Asua, J.M. *Prog Polym Sci*, 2002, 27, 1283-1346.

[13] Asua, J.M. *Prog Polym Sci*, 2014, 39, 1797-1826.

[14] Gugliotta, L.M., Arotcarena, M., Leiza, J.R. and Asua, J.M. *Polymer*, 1995, 36, 2019-1023.

[15] de Buruaga, I.S., Echevarria, A., Armitage, P.D., De la Cal, J.C., Leiza, J.R. and Asua, J.M. *AIChE J*, 1997, 43, 1069-1081.

[16] Elizalde, O., Azpeitia, M., Reis, M.M., Asua, J.M. and Leiza, J.R. *Ind Eng Chem Res,* 2005, 44, 7200-7207.

[17] Agirre, A., Heras-Alarcón, C.D.L., Wang, T., Keddie, J.L. and Asua, J.M. *ACS Appl Mater Interfaces*, 2010, 2, 443–451.

[18] World News. *J Lab Autom,* 2007, 12, A14-A43.

[19] Zhu, X., Gu, Y., Chen, G., Cheng, Z. and Lu, J. *J Appl Polym Sci*, 2004, 93, 1539-1545.

[20] Broadhurst., MG. *Res Natl Bur Stand A Phys Chem,* 1962, 66A, 241-249.

[21] Miguel, O., Fernandez-Berridi, M.J. and Iruin, J.J. *J Appl Polym Sci*. 1997, 64, 1849-1859.

[22] Aramendia, E., Barandiaran, M.J., Grade, J., Blease, T. and Asua, J.M. *Langmuir*, 2005, 21, 1428-1435.

[23] Aramendia, E., Barandiaran, M.J., Grade, J., Blease, T. and Asua, J.M. Improving Latex Performance by Using Polymerizable Surfactants. in Daniels, E., Sudol, E.D. and El-Aasser, M.S. Editors, ACS Symp. Ser. 801, 168 (2002)

[24] Okubo, M., Takeya, T., Tsutsumi, Y., Kadooka, T. and Matsumoto, T. *J Polym Sci Polym Chem*, 1981, 19, 1-8.

[25] Manea, M., Chemtob, A., Paulis, M., de la Cal, J.C., Barandiaran, M.J. and Asua, J.M. *AIChE J*, 2008, 54, 289–297.

[26] López, A., Chemtob, A., Milton, J.L., Manea, M., Paulis, M., Barandiaran, M.J., Theisinger, S., Landfester, K., Hergeth, W.D., Udagama, R. and McKenna, T. *Ind Eng Chem Res*, 2008, 47, 6289-6297.

[27] Elizalde, O., Arzamendi, G., Leiza, J.R. and Asua, J.M. *Ind Eng Chem Res*, 2004, 43, 7401-7409.

[28] González, I., Asua, J.M. and Leiza, J.R. Polymer, 2007, 48, 2542–2547.

[29] Plessis, C., Arzamendi, G., Leiza, J.R., Schoonbrood, H.A., Charmot, D. and Asua, J.M. *Ind Eng Chem Res,* 2001, 40, 3883-3894.

[30] Plessis, C., Arzamendi, G., Leiza, J.R., Schoonbrood, H.A., Charmot, D. and Asua, J.M. *Macromolecules*, 2001, 34, 5147–5157.

[31] Arzamendi, G. and Asua, J.M. *Macromolecules*, 1995, 28, 7479-7490.

[32] Yadav, A.K., Barandiaran, M.J. and de la Cal, J.C. *Macromol React Eng*, 2014, 8, 467-475.

[33] Goikoetxea, M., Reyes, Y., Carolina, M., Minari, R.J., Beristain, I., Paulis, M., Barandiaran, M.J., Keddie, J.L. and Asua, J.M. *Polymer*, 2012, 53, 1098-1108.

[34] Agarwal, N. and Farris, R.J. *J Appl Polym Sci*, 1999, 72, 1407-1419.

[35] Mudge, P.R. and Hespe, G., National Starch and Chemical Investment Holding Corporation, 1995. U.S. Patent 5,439,960.

[36] Athawale, V.D. and Rathi, S.C. *J Appl Polym Sci*, 1996, 59, 1243-1247.

[37] Reyes-Mercado, Y., Vázquez, F., Rodríguez-Gómez, F.J. and Duda, Y. *Colloid Polym Sci*, 2008, 286, 603-609.

[38] Comyn, J. ed., 2012. *Polymer permeability*. Springer Science & Business Media.

[39] Jia, L. and Xu, J. *Polym J,* 1991, 23, 417-425.

Chapter 3. Synthesis and Phase Behavior of Side-Chain Liquid-Crystalline Polymers Containing Biphenyl Mesogens with Different Spacer Lengths

3.1. Introduction

As mentioned in Chapter 1, side chain liquid crystalline polymers (SCLCPs) have considerable application potential in many fields such as optical data storage; optic, electro-optic, and nonlinear optic devices; and photomechanical applications [1-4].

Generally, a side-chain liquid-crystal polymer comprises three distinct structural units: a polymer backbone, a mesogenic group and flexible alkyl spacer (inserted between main chain and mesogenic side groups). However, another type of SCLCPs (end-on SCLCPs) has been reported where mesogenic group directly attached to the polymer backbone without any flexible spacer, but they contain a

flexible alkyl tail. Therefore, the flexible alkyl tail can be considered as the forth structural units of the SCLCPs. Figure 3.1 presents the different architectures of the SCLCPs containing rod-like mesogenic group and flexible spacer and tail. The nature of the polymer backbone and mesogenic groups, and the length of flexible spacer and tail largely affect the properties of SCLCPs [3,4,5-13]. The flexible spacer decouples the interaction of the side chain and the polymer backbone, which disrupted the ordered packing of the side mesogens [14,15]. On the other hand, the alkyl tail induces fluidity to the side chain and plays a very important role in the formation of LC phase structure for the SCLCPs without spacer. The effects of mesogenic group, spacer and tail length, and the polymer backbone on the mesomorphisem behavior of different types of SCLCPs have been studied in literature [3,5,7,10,16,17]. However, the studying phase behavior and molecular packing of these polymers by using X-ray analyses as more reliable and modern techniques is scarce [18-23].

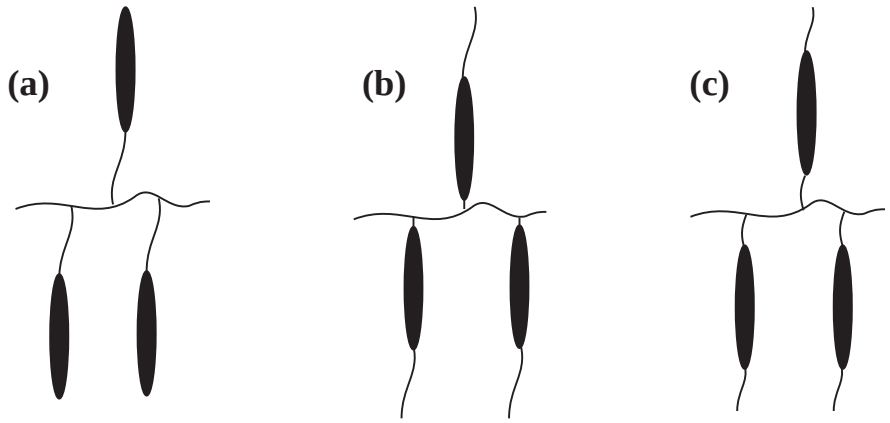

Fig. 3.1. The architectures of rod-like SCLCPs containing (a)alkyl spacer, (b) alkyl tail and (c) alkyl spacer and tail.

In almost all studies, the LCPs were synthesized by solution homopolymerization of side chain liquid crystalline monomers using low concentration (solvent/monomer = 7-10 wt/wt) and oil soluble thermal initiators. In most cases, the polymer yield was limited to 60-70 wt% and in some cases, polymers with low molecular weight were obtained, whose properties may lay within the molecular weight dependent regime [4,24]. However, little is known about the polymerization of these monomers in aqueous media. Vennes et al. [25] synthesized colloidal particles of nematic and smectic liquid-crystalline acrylate polymers with different particles sizes (0.5 and 2.5 μm) and polydispersity by dispersion polymerization. They observed that the nematic director of the mesogens within the

colloidal particles could be rotated due to the photochemical trans-cis-isomerization of the azobenzene chromophores.

In this chapter, monomers (Ethyl 4'-((n-(methacryloyloxy)alkyl)oxy)-[1,1'-biphenyl]-4-carboxylate, n=3,4,5,6, see Scheme 3.1) able to form SCLCPs were synthesized first. Then, the synthesis and characterization of a series of polymethacrylate side-chain liquid-crystalline polymers bearing biphenyl mesogen with different spacer lengths and a fixed tail, (n-PMLCM; with n = 3, 4, 5, 6, see Scheme 3.1) was investigated. The n-PMLCMs were synthesized by miniemulsion radical homopolymerization in aqueous media. Full monomer conversion and high molecular weight (M_n of ~ 10^5 g/mol) polymers with high thermal stability were obtained. Moreover, the liquid crystal behavior, the molecular packing of the side chain and the phase structures of the polymers were studied by the combination of differencial scanning calorimeter (DSC), polarized light microscopy (PLM) and particularly small-angle X-ray diffraction (SAXS) and wide-angle X-ray diffraction (WAXD) methods. All polymers show mesomorphism behavior and present Smectic ↔ Smectic ↔ Isotropic Liquid transitions with increasing temperature.

3.2. Experimental Section

3.2.1. Materials

4′-Hydroxy-4-biphenylcarboxylic acid (1, Scheme 3.1) was purchased from Discovery Fine Chemicals Ltd. Dibromoalkane, potassium carbonate, potassium bicarbonate and methacrylic acid (MAA) were purchased from Aldrich and used without further purification. Potassium persulfate (KPS, Aldrich) as water soluble radical initiator and alkyldiphenyloxide disulfonate (Dowfax^{TM} 2A1, The Dow Chemical Company) as anionic surfactant were used as received.

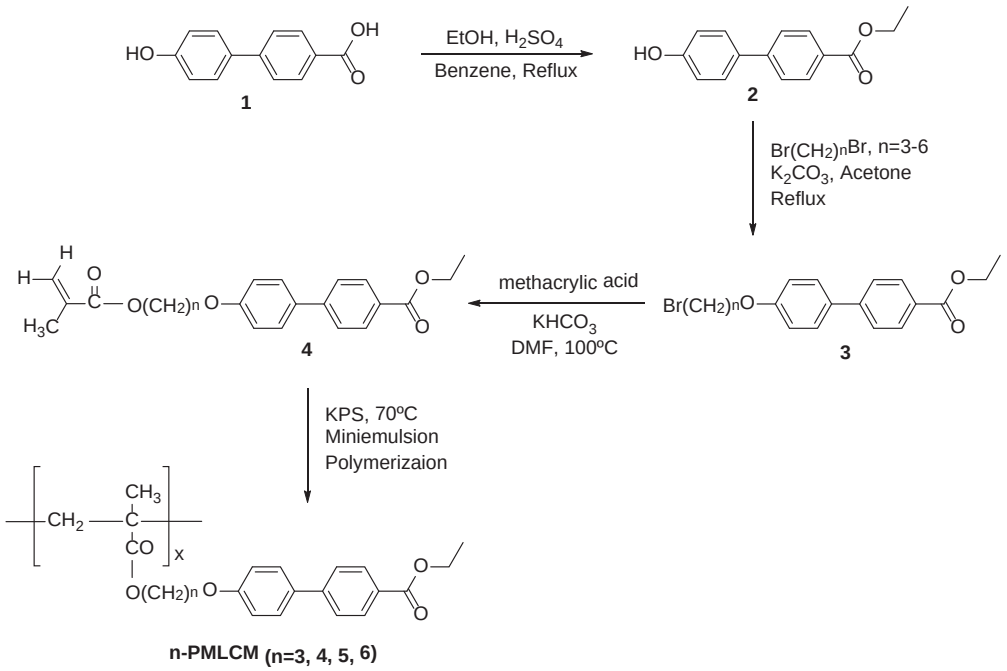

Scheme 3.1. Synthetic route used to prepare the n-MLCM monomers and n-PMLCM polymers.

3.2.2 Measurements

^{1}H NMR measurements were performed on Bruker AVANCE-400 and 500 MHz spectrometers using $CDCl_3$ as solvent.

The molecular weight distribution and the average molecular weights were determined by gel permeation chromatography (GPC). Polystyrene (PS) standards were used to calibrate the equipment and the reported molar masses are referred to PS.

The thermal stability of polymers were measured by Thermal Gravimetric Analysis (TGA) on a TGA Q 500 (TA) instrument at a heating rate of 10 °C min^{-1} from ambient temperature to 700 °C in nitrogen atmosphere.

The thermal characterization of polymers and monomers were carried out by DSC using a Q1000, TA Instruments. The samples were heated from 25 to 230 °C (25 to 120 °C for monomers, to avoid thermal polymerization), maintained at 230 °C for 3 min, cooled to -50°C, maintained at - 50 °C for 3 min and finally reheated to 230 °C (120 °C for monomers). The heating and cooling rate was 10 °C min^{-1} in all cases and the measurements were carried out under nitrogen atmosphere.

The identification of the liquid-crystalline phases was performed by polarized light microscopy (PLM) using a Nikon ECLIPSE E600 optical microscope equipped with a Mettler-Toledo hot stage (FP82HT). Clear characteristic optical textures that allowed phase assignments were obtained by cooling the polymer at either 0.2 or 0.3

°C min^{-1} from about 10 °C above the clearing temperature to ambient temperature. The PLM is described in detail in Appendix II.

Small-angle X-ray scattering (SAXS) experiments were conducted in a Rigaku 3-pinhole PSAXS-L equipment operating at 45 kV and 0.88 mA. The MicroMax-002+ X-Ray Generator System is composed by microfocus which sealed tube source module and integrated X-Ray generator unit which produces Cu Kα transition photons of wavelength $\lambda = 0.1542$ nm. The flight path and the sample chamber in this equipment are under vacuum. The scattered X-Rays are detected on a two-dimensional multiwire X-Ray Detector (Gabriel design, 2D-200X). This gas-filled proportional type detector offers a 200 mm diameter active area with ca. 200 micron resolution. After radial integration, the scattered intensities were obtained as a function of momentum transfer $q= 4\pi\lambda^{-1}\sin\theta$. Reciprocal space calibration was done using silver behenate as standard. The sample to detector distance was 0.5 m, covering a q-range between 0.05 $Å^{-1}$ and 0.90 $Å^{-1}$. The measurements as a function of temperature were performed by means of a Linkam Scientific Intruments THMS600 temperature controller. This setup allows measurements in the range from -196 to 600 °C with a temperature stability of ±0.1 °C. The measuring time was 30 min at each temperature.

Wide-angle X-ray scattering (WAXS) measurements were performed on a Bruker D8 Advance diffractometer working in parallel beam geometry. With the help of a Göbel mirror, the originally divergent incident X-ray beam from line focus X-ray tube (Cu, operating at 40 kV and 40 mA) is transformed into an intense and parallel beam that is free of Kβ radiation. The parallel beam optic required in the secondary beam path is achieved by an equatorial axial Soller slit of 0.2 °. The linear detector LYNXEYE used presents an active area of 14.4 mm × 16 mm. Measurements were performed in reflection varying the scattering angle 2θ from 5-30 ° with a step of 0.05 °. The time employed was 5 s/point. The sample powders were placed in an Anton Paar TTK 450 low-temperature chamber under vacuum conditions allowing variations of sample temperature from -193 to 450°C with 1 °C resolution.

3.2.3. Synthesis and characterization of monomers

For the state of simplicity and clarity, the ethyl 4'-((n-(methacryloyloxy)alkyl)oxy)-[1,1'-biphenyl]-4-carboxylate monomers will be named n-MLCM and the corresponding polymers will be named n-PMLCM (n is the number of the methylene units in the alkyl spacers). The n-MLCM and n-PMLCM series were prepared according to the synthetic route shown in Scheme 3.1. The synthetic details of 6-MLCM as representative monomer are reported here.

The *ethyl-4-(4-hydroxy)phenyl Benzoate* (**2**, Scheme 3.1) was prepared according to the method described by Trollsås et al. [26]. Thus, the solution of 4′-hydroxy-4-biphenylcarboxylic acid (**1**) (10 g, 46.65 mmol) in 100 ml of ethanol (99.99%) and 100 ml of benzene containing a catalytic amount of H_2SO_4 was refluxed for 24 h. The reaction mixture was cooled and poured into distilled water, and then extracted twice with CH_2Cl_2. The organic phase was separated and washed with distilled water, dried with Na_2SO_4, filtered, and evaporated. The yellow-white powder was dissolved in $CHCl_3$, where unreacted **1** precipitated. The $CHCl_3$ solution was filtered and evaporated resulting in a white crystalline powder, yield 9.49 g (84%). ^{1}H NMR ($CDCl_3$, 400 MHz) δ 1.43 (t, 3H,-CH_2CH_3), 4.42 (q, 2H,-CH_2CH_3), 6.96 (d, 2H,3′-H and 5′-H), 7.54 (d, 2H, 2′-H and 6′-H), 7.64 (d, 2H, 2-H and 6-H), 8.11 (d, 2H, 3-H and 5-H).

The *ethyl 4'-((6-bromohexyl)oxy)-[1,1'-biphenyl]-4-carboxylate* (**3**) and the ethyl 4'-((6-(methacryloyloxy)hexyl)oxy)-[1,1'-biphenyl]-4-carboxylate (**4**) (n-MLCM monomers) were synthesized by modifying the preparation methods for ω-(4'-methoxybiphenyl-4-yloxy)alkyl methacrylatels liquid crystalline monomers reported in the literatures [3,23]. Therefore, the mixture of **2** (8.33 g, 34.38 mmol), 1,6-dibromohexane (83.81 g, 344 mmol) and potassium carbonate (34.23 g, 258.3 mmol) were refluxed with stirring in acetone (380 ml) for 24 h. The reaction mixture

was filtered hot, the residue washed with acetone, and the acetone removed by rotating evaporation. Light petroleum or hexane (40-60 °C) was added to the concentrated organic extracts and the resulting precipitate collected and dried. The crude product was recrystallised from ethanol with hot filtration to ensure the complete removal of the dimeric side-product. Yield 8.816 g (64.1%). ^{1}H NMR ($(CD_3)_2CO$, 400 MHz) δ 1.27-1.45 (m, 5H, -CH_2CH_3, $O(CH_2)_3CH_2(CH_2)_2Br$), 1.57 (t, 2H,-$O(CH_2)_2CH_2$), 1.85 (t, 2H, -OCH_2CH_2), 1.93 (t, 2H, -CH_2CH_2Br), 3.55 (t, 2H, -CH_2Br), 4.1 (t, 2H, -OCH_2), 4.38 (q, 2H,-CH_2CH_3) , 7.08 (d, 2H, 3′-H and 5′-H), 7.7 (d, 2H, 2′-H and 6′-H), 7.78(t, 2H, 2-H, and 6-H), 8.08 (d, 2H, 3-H, and 5-H).

Ethyl 4'-((6-(methacryloyloxy)hexyl)oxy)-[1,1'-biphenyl]-4-carboxylate (**4**)**.** Methacrylic acid (2.242 g, 27.91 mmol), was reacted with potassium hydrogen carbonate (3.189 g, 31.85 mmol) at room temperature for 5 min to form potassium methacrylate. The solution of **3** (8.816 g, 22.03 mmol) and hydroquinone (0.063 g, 2.203 mmol) in N,N'- dimethylformamide (120 ml) was added to potassium methacrylate salt and the resulting mixture was stirred at 100 °C for 24 h. The reaction mixture was allowed to cool and was poured into water (ca. 1000 ml). The resulting precipitate was filtered, dried and dissolved in dichloromethane. The organic solution was washed with 5% aqueous sodium hydroxide and then water. The solvent evaporated and the solid monomer filtered and washed with water. The crude

product was recrystallized from ethanol. Yield: 7.48 g (83%). ^{1}H NMR ($CDCl_3$, 400 MHz) δ 1.44 (t, 3H, -CH_2CH_3), 1.54 (m, 4H, O$(CH_2)_2$ CH_2C*H*2), 1.77 (m, 2H, -CH_2CH_2OC(O)), 1.86 (m, 2H,-OCH_2CH_2), 1.98 (s, 3H, -C(CH_3)=CH_2), 4.04 (t, 2H, -CH_2OC(O)), 4.2 (t, 2H, -OCH_2), 4.42 (q, 2H,-CH_2CH_3), 5.58 (s, 1H, CH_2=C- cis), 6.13 (s, 1H, CH_2=C- trans), 7.01 (d, 2H, 3′-H and 5′-H), 7.59 (d, 2H, 2′-H and 6′-H), 7.64 (d, 2H, 2-H, and 6-H), 8.11 (d, 2H, 3-H, and 5-H).

3-MLCM: White solid; yield 90%. ^{1}H NMR ($CDCl_3$, 400 MHz) δ (ppm): 1.45 (t, 3H, -CH_2CH_3), 1.99 (s, 3H, -C(CH_3)=CH_2), 2.24 (m, 2H, ,-C(O)OCH_2CH_2), 4.17 (t, 2H, -CH_2OC(O)), 4.28 (t, 2H, -OCH_2), 4.43 (m, 2H,-CH_2CH_3), 5.61 (s, 1H, CH_2=C- cis), 6.16 (s, 1H, CH_2=C- trans), 7.03 (d, 2H, 3′-H and 5′-H), 7.6 (d, 2H, 2′-H and 6′-H), 7.65 (t, 2H, 2-H, and 6-H), 8.12 (d, 2H, 3-H, and 5-H).

4-MLCM: White solid; yield 94%. ^{1}H NMR ($CDCl_3$, 400 MHz) δ (ppm): 1.45 (t, 3H, -CH_2CH_3), 1.59 (s, 2H, - CH_2CH_2OC(O)), 1.97 (d, 5H,-OCH_2CH_2, -C(CH_3)=CH_2), 4.1 (s, 2H, -CH_2OC(O)), 4.29 (s, 2H, -OCH_2), 4.44 (dd, 2H,-CH_2CH_3), 5.6 (s, 1H, CH_2=C- cis), 6.15 (m, 1H, CH_2=C- trans), 7.02 (d, 2H, 3′-H and 5′-H), 7.6 (d, 2H, 2′-H and 6′-H), 7.65 (t, 2H, 2-H, and 6-H), 8.12 (d, 2H, 3-H, and 5-H).

5-MLCM: White solid; yield 97%. ^{1}H NMR ($CDCl_3$, 400 MHz) δ (ppm): 1.45 (t, 3H, -CH_2CH_3), 1.63 (m, 4H, O$(CH_2)_2$ CH_2), 1.81 (m, 2H,-CH_2CH_2OC(O)), 1.9 (m,

2H, -OCH$_2$C*H*$_2$), 1.99 (s, 3H, -C(C*H*$_3$)=CH$_2$), 4.07 (t, 2H, -C*H*$_2$OC(O)), 4.23 (t, 2H, -OC*H*$_2$), 4.43 (q, 2H,-C*H*$_2$CH$_3$), 5.6 (d, 1H, CH$_2$=C- cis), 6.15 (m, 1H, CH$_2$=C- trans), 7.02 (d, 2H, 3′-H and 5′-H), 7.6 (d, 2H, 2′-H and 6′-H), 7.65 (t, 2H, 2-H, and 6-H), 8.12 (d, 2H, 3-H, and 5-H).

In all monomers, the chemical shifts and peak integrations of all protons were in excellent agreement with its expected structure. The ^{1}H NMR spectra of 6MLCM is shown in Figure 3.2.

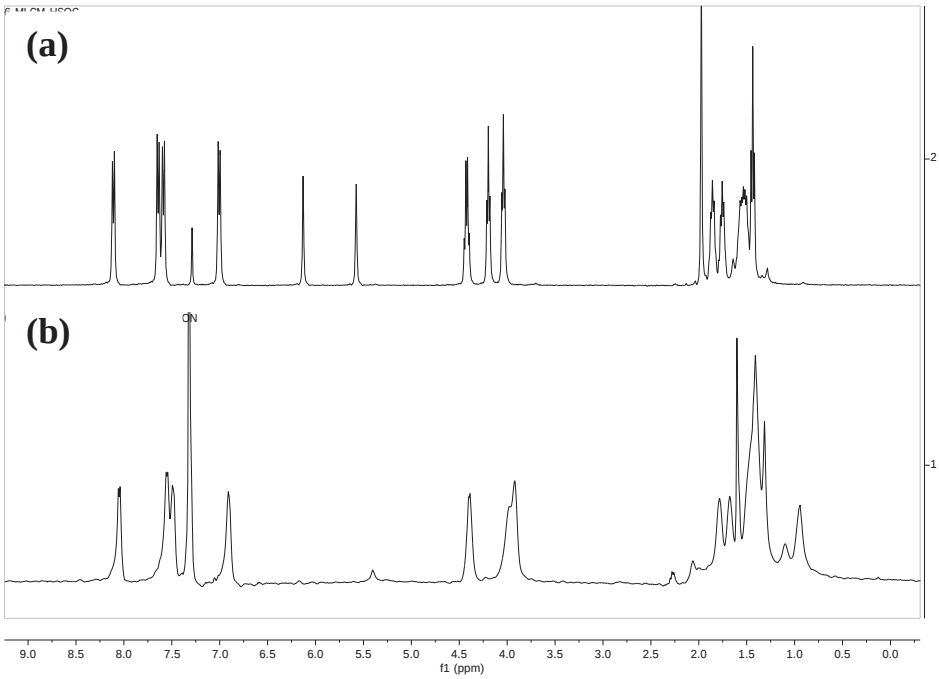

Fig. 3.2. ^{1}H NMR spectrum of (a) 6-MLCM and (b) 6-PMLCM.

The thermal properties of the monomers were examined by DSC. Figure 3.3 shows the second heating DSC scans of n-MLCMs (n= 3, 4, 5, 6) at a rate of 10°C min^{-1} under nitrogen atmosphere after eliminating the thermal history. All the monomers showed a single endothermic melting peak. Above the melting point, the samples were isotropic. It can be seen that the melting point of monomers decreases with increasing spacer length, probably due to the plasticization effect of the long alkyl spacers [27]. No further phase structural studies of those monomers were performed due to their easy thermal polymerization.

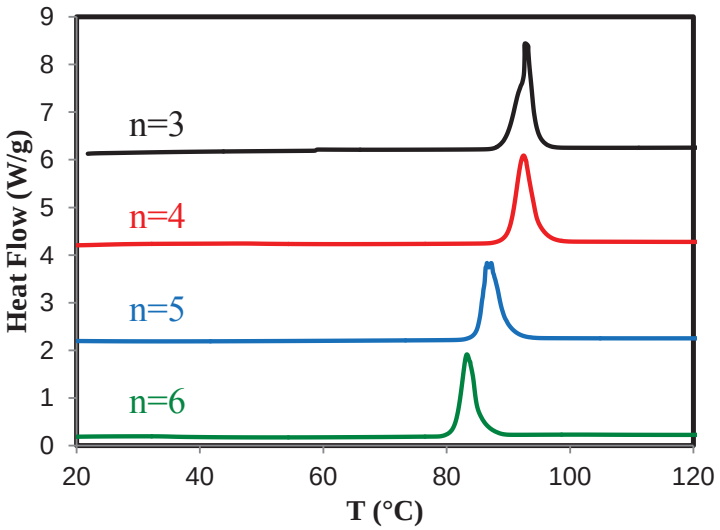

Fig. 3.3. DSC curves of n-MLCMs during the second heating scan at a rate of 10 °C min^{-1} under nitrogen atmosphere. For clarity, 6 W/g was added to the scan of the sample n=3; 4 W/g to that of sample n=4 and 2 W/g was added to the scan of the sample n=5.

3.2.4. Synthesis and characterization of polymers

n-PMLCMs were obtained by both solution and miniemulsion radical polymerization. The solution homopolymerization of n-MLCMs led to low molar mass (M_n of ~ 10^3-10^4 g/mol) polymers with 60-70 wt% yield. Therefore, in this study the n-PMLCMs were synthesized by miniemulsion radical polymerization. This polymerization technique led to full monomer conversion and high molar mass (M_n of ~ 10^5 g/mol) polymers. The formulation of miniemulsion radical polymerization of n-MLCMs (Scheme 3.2) is given in Table 3.1. At ambient temperature the n-MLCMs are solid crystals and their melting points are above 80 °C. Therefore, in order to emulsify them, the n-MLCMs were dissolved in chloroform and this solution was added to the aqueous phase containing emulsifier (Dowfax 2A1) and mixed for 10 minutes. The coarse emulsions were sonicated by using a Hielscher Sonifier (UIS250v, amplitude 100 and energy pulsed at 1 Hz) over 10 minutes in an ice bath to avoid overheating. The miniemulsion of n-MLCMs was transferred to a 50 ml flask, purged with nitrogen, and heated to 70 °C under magnetic agitation. Then, an aqueous solution of initiator (KPS, 1 wt% based on monomer) was added as a shot and the polymerization proceeded for 3 h. Afterwards, the chloroform was removed completely by rotatry evaporation. Full monomer conversion was achieved as shown by the ^{1}H NMR spectra of final polymers (disappearance of the peaks associated with

the alkene protons at 5.6 and 6.1 ppm in the ^{1}H NMR spectra of n-PMLCM). As a representative example, the ^{1}H NMR spectra of 6-PMLCM is shown in Figure 3.2). The absorption peaks of n-PMLCMs were broad and consistent with the expected polymer structure. The final particle diameter was around 70-75 nm.

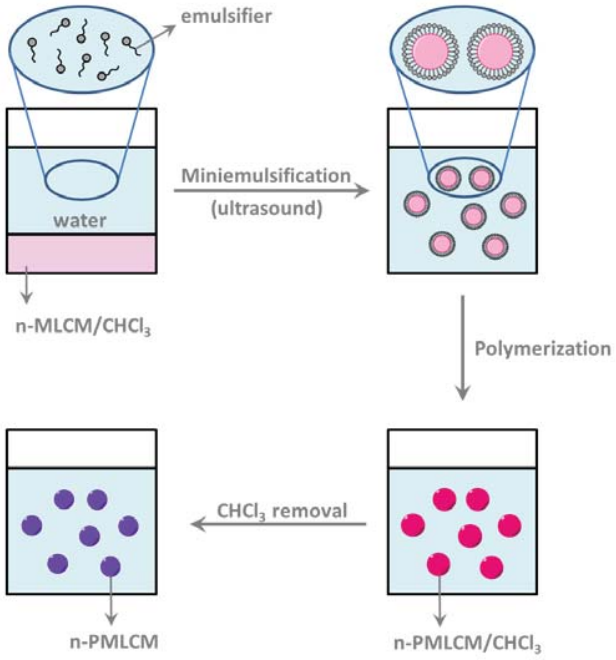

Scheme 3.2. Miniemulsification and miniemulsion polymerization of n-MLCMs.

Table 3.1. Formulation used to synthesize n-PMLCMs in miniemulsion polymerization

Component	**Amount (g)**
n-MLCM	1
Chloroform	3
Dowfax 2A1	0.14*
Water	22.23
KPS	0.01**

* 3.5 wt% based on organic phase. ** 1 wt% based on monomer.

The number and weight average molecular weights of the part of these polymers soluble in THF are given in Table 3.2. These high molecular weights ensured that the thermal properties of the polymers lay outside the molecular weight dependent regime [4,28].

Table 3.2. The average molecular weights and dispersity of n-PMLCMs.

n-PMLCM	**n**			
	3	**4**	**5**	**6**
M_w (g/mol)	278,000	373,000	519,000	256,000
M_n (g/mol)	100,000	172,000	216,000	100,000
M_w/M_n	2.78	2.17	2.40	2.56

3.2.4.1. Phase Transitions and Phase Structures of the Polymers

For the characterization of the thermal behavior, phase transitions and phase structure in bulk, the n-PMLCMs were first purified, removing emulsifier and initiator. The n-PMLCMs were dissolved in THF, precipitated into a large amount of methanol, and filtered. The resulting solid was dried at 40 °C under vacuum for 48 h. The thermal stabilities of the polymers were investigated by TGA in nitrogen atmosphere (Figure 3.4). All the polymers showed very good thermal stability, and the temperatures at 5% weight loss (T_d) under nitrogen were about 280 °C measured at a rate of 10 °C min^{-1} (see Table 3.3).

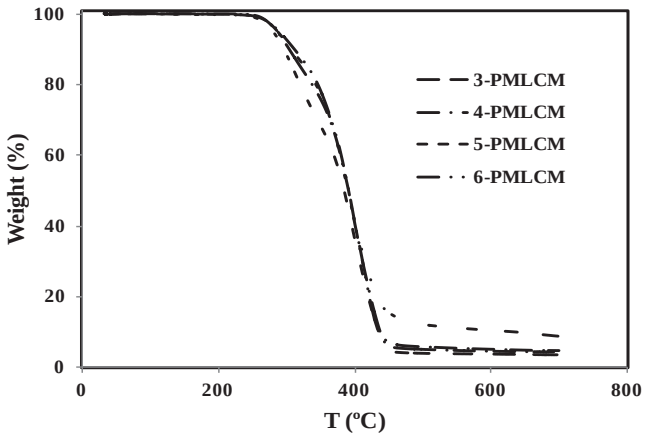

Fig. 3.4. TGA curves of n-PMLCMs at a rate of 10 °C min^{-1} under nitrogen atmosphere.

3.2.4.1.1. DSC Analysis

Figure 3.5 shows the first cooling and second heating DSC curves of n-PMLCM (n= 3, 4, 5, 6) at a rate of 10 °C min^{-1} under nitrogen atmosphere after eliminating the thermal history. Upon cooling, two exothermic processes are detected, that we will denote as I (melting, at lower temperatures) and II (clearing, at higher temperatures). The heating DSC traces contain two endothermic peaks located about 3-8 degrees above those observed on cooling, suggesting that they correspond to the same underlying phenomena and therefore they were also denoted as I and II. The results of 5-PMLCM and 6-PMLCM also reveal a weak second-order-like transition that could be assigned to a glass transition. This feature could not be resolved in the samples with n=3 and n=4. The thermal characteristics of all the polymers are listed in Table 3.3 and represented in Figure 3.6 as function of the number of methylene units in the spacer group. A clear odd-even effect can be seen in the values of the transition temperatures and the associated entropies.

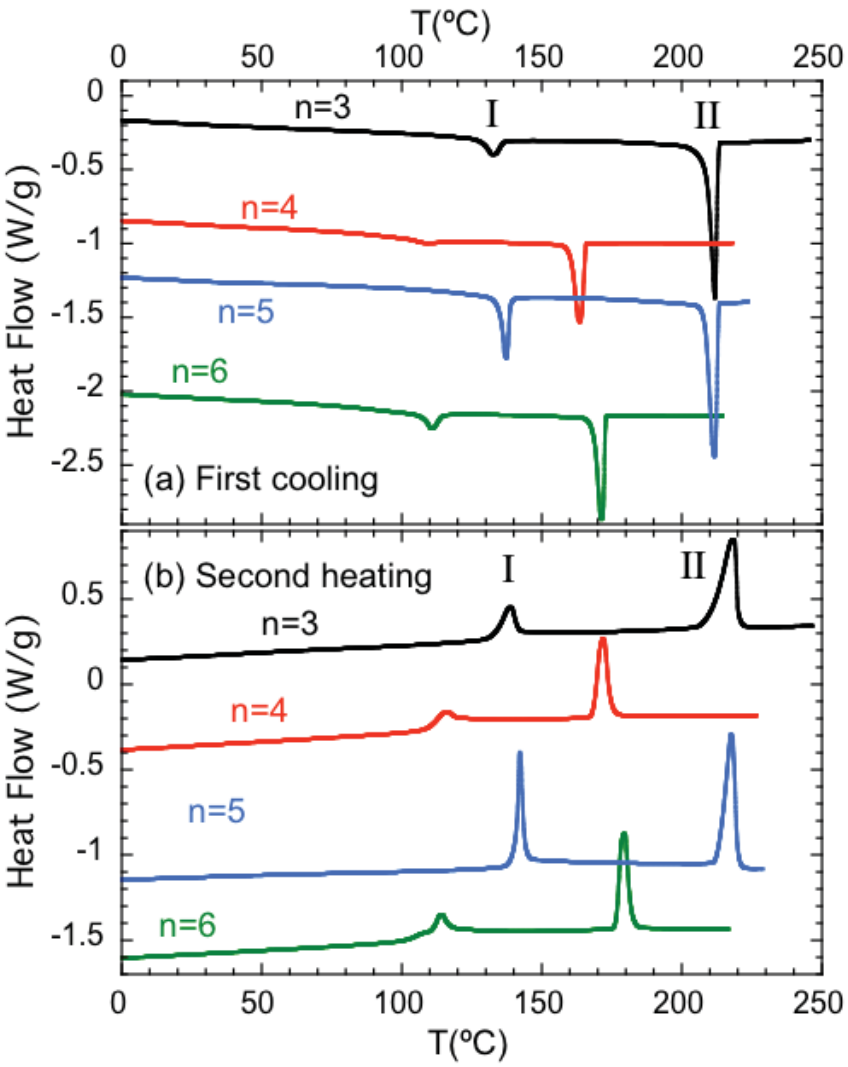

Fig. 3.5. DSC curves of n-PMLCMs during the first cooling (a) and second heating scan (b) at a rate of 10 °C.min^{-1} under nitrogen atmosphere. For clarity, 0.6 W/g was added to the scan of the sample n=4; 1.2 W/g to that of sample n=5 and 1.6 W/g was added to the scan of the sample n=6. (Exo Down)

Table 3.3. Thermal properties of the n-PMLCMs. Results obtained from the first cooling DSC scan are denoted with the subscript 'c', and from the second heating, with subscript 'h'.

n	$T_{I,c}$[a] (°C)	$T_{II,c}$[b] (°C)	$T_{I,h}$[a] (°C)	$T_{II,h}$[b] (°C)	$\Delta H_{I,h}$ (kJ/mol)	$\Delta H_{II,h}$ (kJ/mol)	$\Delta S_{I,h}/R$	$\Delta S_{II,h}/R$	T_g (°C)	T_d[c] (°C)
3	133	212	138	218	2.14	7.60	0.63	1.86	---	289
4	~ 109	165	115	172	1.01	4.48	0.34	1.21	---	285
5	137	212	142	218	4.30	7.94	1.24	1.94	92	280
6	111	171	114	179	1.92	5.31	0.60	1.41	82	288

[a] Smectic – Smectic and [b]Smectic – Isotropic transitions, as identified by PLM and XR [c] the temperatures at 5% weight loss of the samples in TGA.

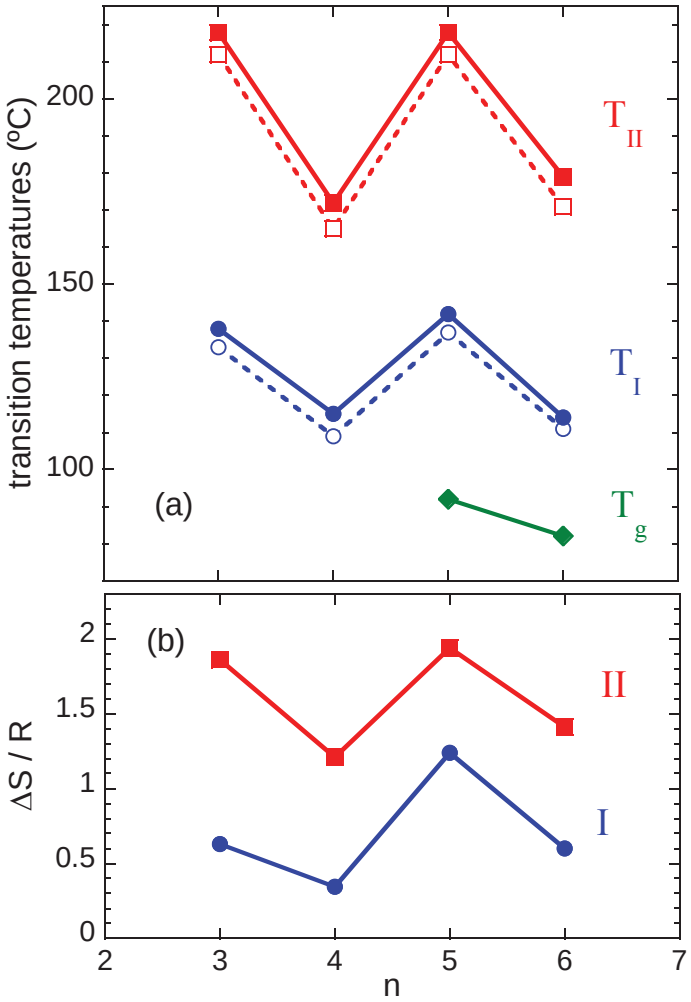

Fig. 3.6. Transition temperatures (a) and entropies (b) associated with the thermal transitions (I: circles; II: squares; glass: diamonds) as function of the number of methylene units in the spacer. Solid lines represent values obtained from the second heating scan and dashed lines to the first cooling scan. The transition temperatures and entropies of poly[ω-(4´-methoxybiphenyl-4-yloxy)alkyl methacrylate]s in reference 3 extracted from second heating scans are plotted with cross symbols and dot lines for comparison purpose.

3.2.4.1.2. Polarized Light Microscope Characterization

Polarized light microscope (PLM) equipped with a hot stage is an useful tool for the study of the morphology of LC and PLCs. Figure 3.7 shows the PLM images of n-PMLCMs, which were obtained from the sample cooled from isotropic melt by using very low cooling rate (0.2 °C min^{-1}). PLM revealed that when the 3-PMLCM and 6-PMLCM were cooled from the isotropic phase, a smectic needle like texture was formed (Figure 3.7(a,g)). These results point to the formation of a smectic **A** (Sm**A**) phase below T_{II}. On further cooling, poorly focal-conic texture developed (Figure 3.7(b,h)). The assignment of an isotropic to Sm**A** phase transition to the process at T_{II} for these polymers is also supported by the measured entropy change associated with the transition (see Table 3.3), which is comparable to that seen for other types of side-chain liquid-crystal polymers [16,29]. When the lower-temperature transition T_I was passed, no detectable change in the optical textures was observed.

The PLM of 5-PMLCM showed a bâtonnets structure when the sample was cooled from the isotropic state (Figure 3.7(e)). On further cooling the bâtonnets coalesced, and a defined focal conic fan texture was exhibited (Figure 3.7(f)). This can be assigned to a Sm**A** phase (Figure 3.7(e)). No detectable change in the optical texture was observed on further cooling and passing the lower-temperature transition.

The 4-PMLCM sample showed completely different PLM textures. When this sample was cooled from above T_{II}, a granular texture was formed (see Figures 3.7(c) and (d)) which was also assigned to an isotropic to Sm**A** phase transition at T_{II} [16]. Also, no detectable change in the optical texture was resolved on further cooling and passing the lower-temperature transition T_I for 4-PMLCM.

PLM was thus able to detect and identify the phase transition (Sm**A** to isotropic liquid) for the higher transition temperature T_{II} for n-PMLCM with n = 3, 5 and 6. However, the kind of transition below T_{II} for the 4-PMLCM sample as well as the structural changes accompanying the lower transition temperature for all polymers could not be resolved by this technique.

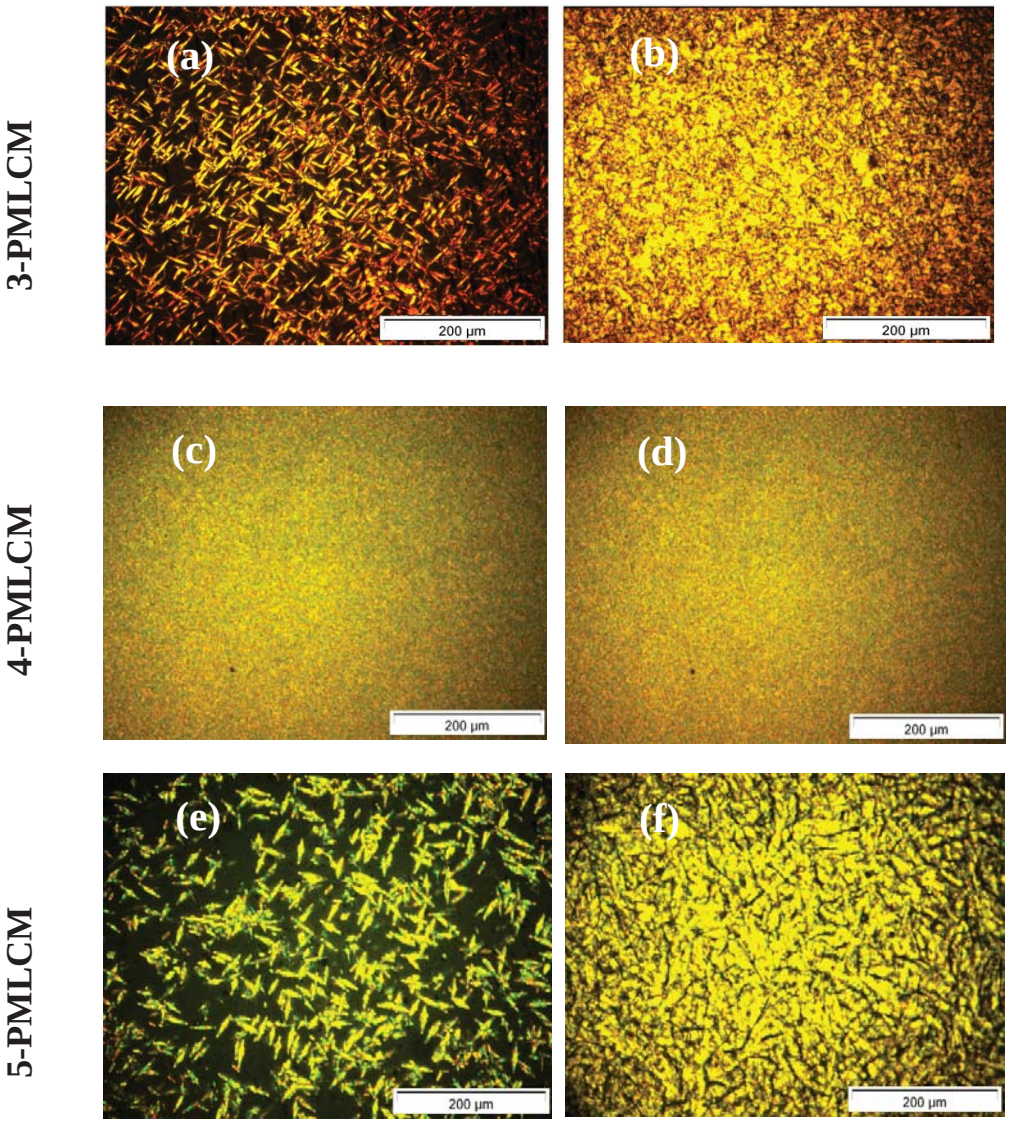
3-PMLCM
4-PMLCM
5-PMLCM
(a)
(b)
(c)
(d)
(e)
(f)
200 µm

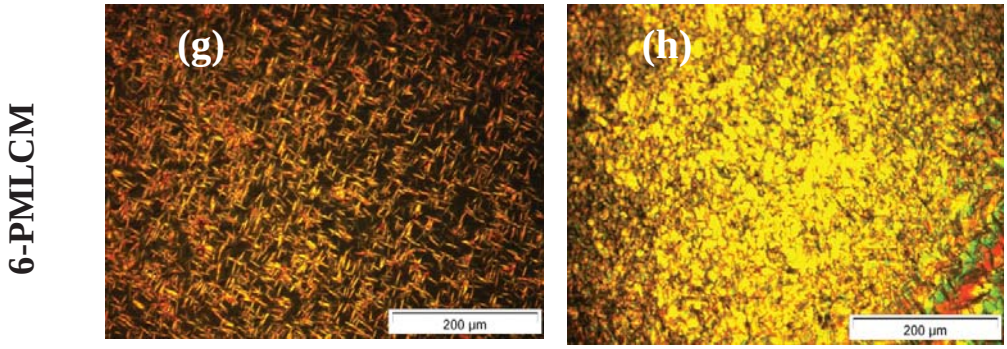

Fig. 3.7. PLM images of the texture of: 3-PMLCM at (a) 211 °C and (b) 184 °C; 4-PMLCM at (c) 164 °C and (d) 142 °C; 5-PMLCM at (e) 211 °C and (f) 162 °C; 6-PMLCM at (g) 196 °C and (h) 174 °C. Note that the PLM images at 50 °C were indistinguishable from those shown in (b), (d), (f) and (h).

3.2.4.1.3. X-Ray Characterization

Trying to resolve the structural details at nanoscopic/atomic scale, SAXS and WAXS experiments were performed. These techniques can provide useful information concerning molecular arrangement, mode of packing, and type of order in a mesophase of polymer liquid crystals [13,18-21,23]. In the experiments, the samples were heated up to 20 °C above the T_{II} and then cooled at -10 °C min^{-1}, collecting patterns at different temperatures down to 30 ºC.

Figure 3.8 shows data recorded by the two diffraction instruments at three representative temperatures: above T_{II} (red dashed-dotted line), between T_I and T_{II}

(green dotted line) and below T_I (blue continuous line). For all systems, the revealed structural features are qualitatively similar:

(i) Above T_{II}, the patterns do not show sharp diffraction peaks, but very broad maxima. This feature qualifies the phase above T_{II} as a typical liquid-like state (isotropic liquid phase) characterized by a main peak appears centered at about 1.2 – 1.3 $Å^{-1}$ (denoted as Q^*, see Figure 3.8(a)). Broad peaks can also be resolved at lower Q-values, in the region of about 0.5 $Å^{-1}$ and even around 0.25 $Å^{-1}$, but their intensities are very weak.

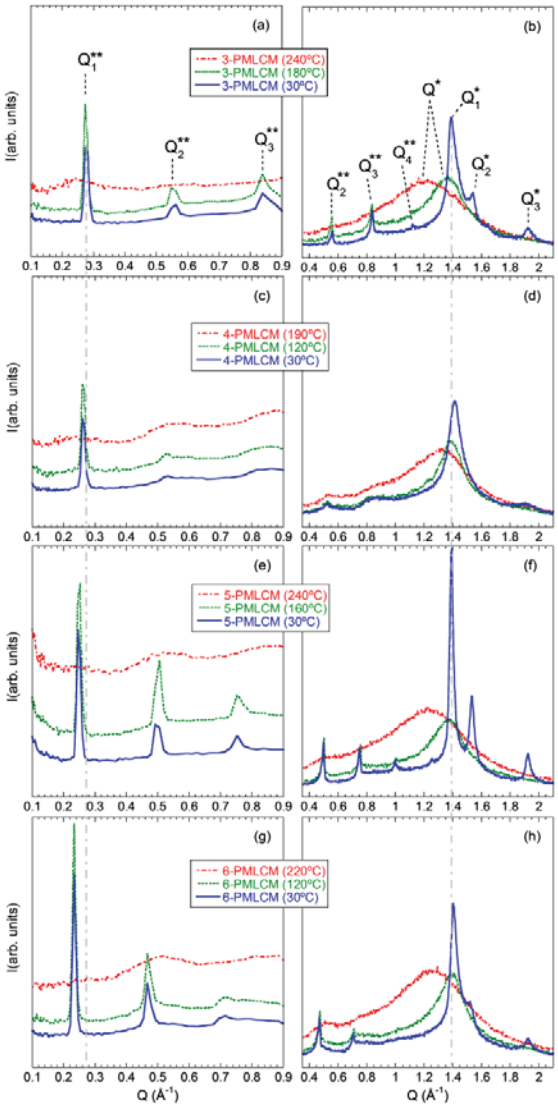

Fig. 3.8. XR-results at the temperatures indicated. (a) and (b): 3-PMLCM; (c) and (d): 4-PMLCM; (e) and (f): 5-PMLCM; (g) and (h): 6-PMLCM. Panels on the left: SAXS results; panels on the right: WAXS results. Grey dashed-dotted vertical lines mark the positions of Q1** and Q1* for the 3-PMLCM sample.

(ii) Cooling the system below T_{II}, sharp peaks appear at low scattering angles, below Q ~1Å^{-1}. Particularly noteworthy is the emergence of a first intense peak centered in the region 0.2…0.3Å^{-1} which we will call Q_1^{**} (Figure 3.8(a)). The positions of the less intense peaks in the SAXS region denoted as Q_2^{**}, Q_3^{**}, etc are multiple values of that of Q_1^{**} (see Figures 3.9 and 3.10) suggesting an underlying layered structure characterized by a periodicity $D = 2\pi/Q_1^{**}$ [13,18] (see Table 3.4). The peaks characterizing this long-period layered structure are very narrow. Recalling that the peak width δ can be related to the domain size ζ of the ordered domain via the Debye-Scherrer equation $\zeta = 2\pi/\delta$, values of the order of 40-60 nm are deduced for the domain size (see Table 3.4). This means that the lamellar order extends over ≈ 20 parallel layers. An analysis of the patterns by means of the software 'Scatter' [30] led to the intimation of the lateral extension of the layers, which was of the order of 1μm. For a given sample, the features of the peaks characterizing this kind of ordering –width, intensity and position– are independent of temperature, as can directly be seen in the patterns of Figure 3.8 and in more detail in Figure 3.11 for the sample with n=5. Figures 3.12 and 3.13, as well as 3.14 and 3.15 displaying the temperature dependence of the positions of the different identified maxima also corroborate this observation. This implies that, once this long-range lamellar order is established in the samples, the layered structure is completely insensitive to temperature changes, even across the low-temperature transition T_I.

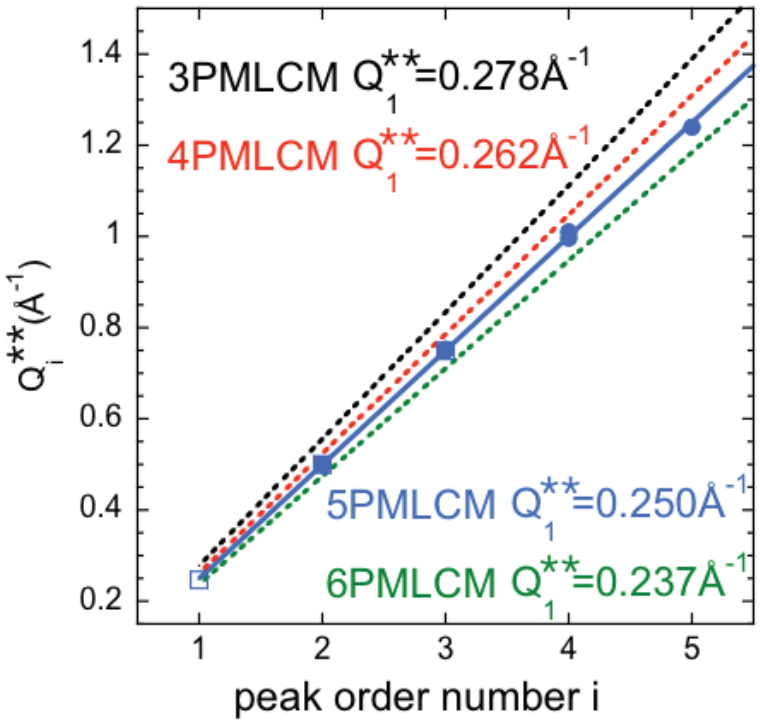

Fig. 3.9. Position of the maxima attributed to the long-range order periodicity as function of the assigned reflection order index obtained for the 5-PMLCM sample. Results from SAXS are represented by squares and results from WAXS by circles. The continuous blue line is a linear regression fit $Q_i^{**}= i*Q_i^{**}$ with the value $Q_i^{**}=0.250Å^{-1}$. Dotted lines represent the fits corresponding to the other samples investigated with the color code indicated in the figure.

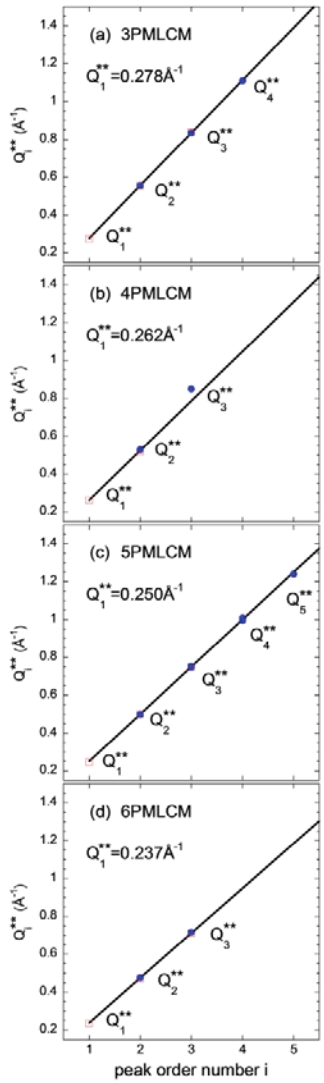

Fig. 3.10. Position of the maxima attributed to the long-range order periodicity as function of the assigned reflection order index obtained for: (a) 3-PMLCM; (b) 4-PMLCM; (c) 5- PMLCM; (d) 6- PMLCM. Results from SAXS are represented by squares and results from WAXS by circles. Continuous lines are linear regression fits $Q_i^{**}= i*Q_1^{**}$ with the value indicated Q_1^{**}-values.

Table 3.4. D-spacing and domain size(ζ), maximum length of the monomers .

Sample	**D (Å)**[a]	**maximum length(Å)**[b]	**ζ (nm)**[a]
3-PMLCM	22.7±0.35	22.7	440±50
4-PMLCM	23.9±0.45	23.8	390±50
5-PMLCM	25.2±0.30	25.3	600±50
6-PMLCM	26.7±0.45	26.2	410±50

[a] Obtained from the scatter fits of SAXS results; [b] calculated from ChemBio 3D;

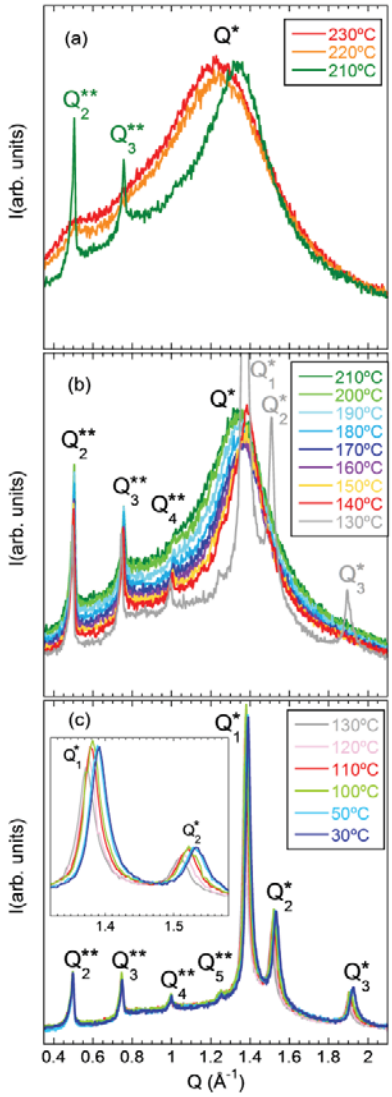

Fig. 3.11. Temperature evolution of WAXS-results 5-PMLCM: (a) isotropic phase and highest temperature investigated below T_{II}; (b) between T_{II} and highest temperature investigated below T_I; (c) below T_I. Insert in (c) is a magnification of the Q-range $1.32 \leq Q \leq 1.58$ Å^{-1}.

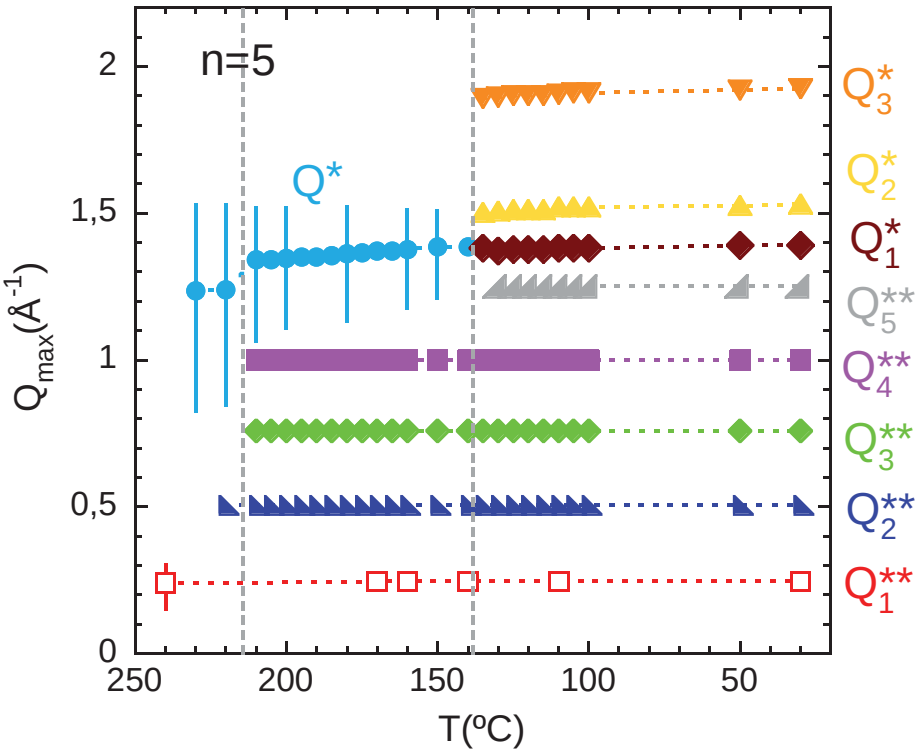

Fig. 3.12. Temperature dependence of the positions of the different peaks identified in the XR-patterns (empty symbols: SAXS; filled symbols: WAXS) of 5-PMLCM sample. For the peaks centered at Q_1** and Q* and selected temperatures, the vertical lines represent the width of the peak at its half maximum. Note that for the peak at Q_1**, at temperatures below T_{II} this width is of the order of the size of the point, and therefore cannot be resolved in the plot.

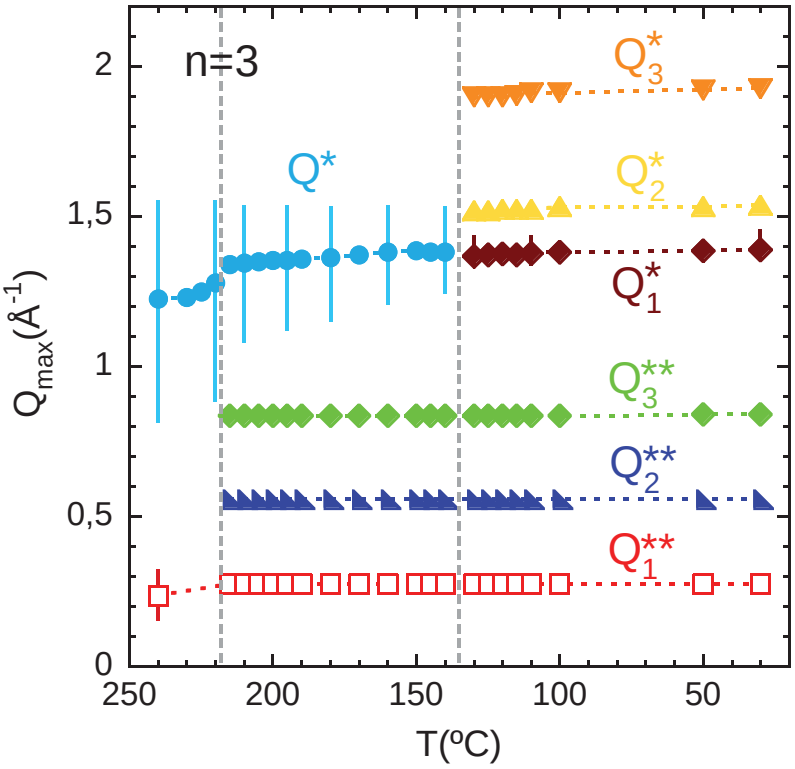

Fig. 3.13. Temperature dependence of the positions of the different peaks identified in the XR-patterns (empty symbols: SAXS; filled symbols: WAXS) of the high-molecular weight 3-PMLCM sample. For the peaks centered at Q_1** and Q_1* and selected temperatures, the lines represent the width of the peak at its half maximum. Note that for the peak at Q_1**, at temperatures below the clearing point this width is of the order of the size of the point, and therefore cannot be resolved in the plot.

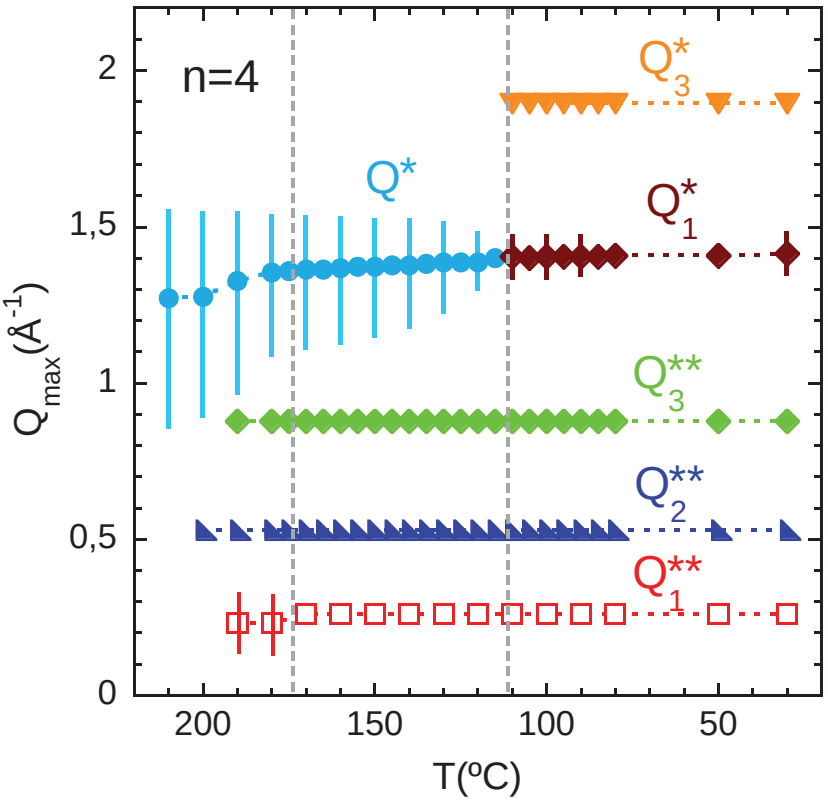

Fig. 3.14. Temperature dependence of the positions of the different peaks identified in the XR-patterns (empty symbols: SAXS; filled symbols: WAXS) of the high-molecular weight 4-PMLCM sample. For the peaks centered at Q_1** and Q_1* and selected temperatures, the lines represent the width of the peak at its half maximum. Note that for the peak at Q_1**, at temperatures below the clearing point this width is of the order of the size of the point, and therefore cannot be resolved in the plot.

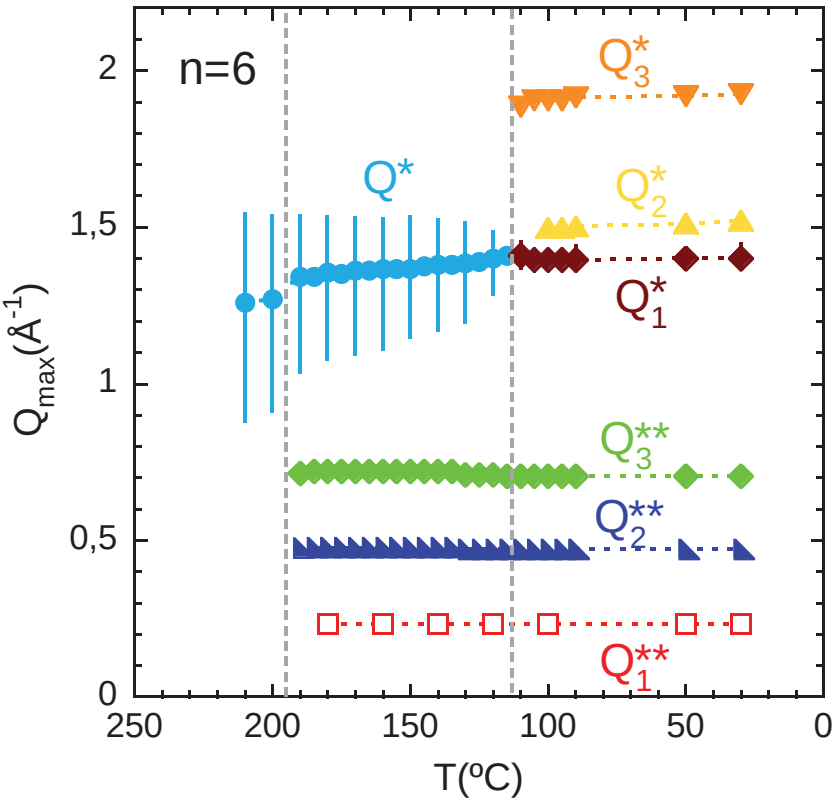

Fig. 3.15. Temperature dependence of the positions of the different peaks identified in the XR-patterns (empty symbols: SAXS; filled symbols: WAXS) of the high-molecular weight 6-PMLCM sample. For the peaks centered at Q_1** and Q_1* and selected temperatures, the lines represent the width of the peak at its half maximum. Note that for the peak at Q_1**, at temperatures below the clearing point this width is of the order of the size of the point, and therefore cannot be resolved in the plot.

(iii) The appearance of long-range lamellar order below T_{II} is accompanied by a pronounced narrowing and shift toward higher Q-values of the main peak observed in the WAXS region (position denoted as Q^*, Figure 3.8). In the temperature region between T_I and T_{II}, this peak is still quite broad, pointing to a certain degree of short-range order better defined than in the isotropic phase but still typical of a liquid-like system. This signature of ordering could be attributed to the establishment of an orientational order of the mesogenic units below T_{II}, and the peak would be associated with the two-dimensional liquid-like intermesogenic organization within the layers [17]. Thus, between T_I and T_{II} the structure of the samples is liquid-crystalline and the lamellar order with large period corresponds to a Sm**A** phase. T_{II} can thus be identified as a Sm**A** ↔ isotropic transition.

(iv) Further cooling of the system below T_I leads to the emergence of three sharp peaks in the WAXS region $Q < 2Å^{-1}$ for the samples with n=3, 5 and 6 (denoted as Q_1^*, Q_2^*, Q_3^*, Figure 3.8), indicative for a higher degree of ordering than that characterizing the Sm**A** phase found at higher temperatures. Contrarily to the SAXS peaks related to the long-period lamellar order, the positions of the peaks Q_i^* depend on temperature (Figures 3.11(c), 3.12 and 3.13, 3.14 and 3.15). These peaks can be attributed to the development of

long-range order in the mesogenic organization, i.e., would be related with the emergence of a 2D-crystalline structure within the lamellar layers. In particular, the peaks can be assigned to the (110), (200) and (210) reflections corresponding to the side-chain packing with a smectic **E (**Sm**E)** structure [22,23,31]. T_I can thus be identified as a Sm**E** ↔ Sm**A** transition. We note that, as in conventional crystalline polymers, an underlying broad feature can be observed in the XR-patterns also below T_I, indicating the coexistence of ordered regions with amorphous portions of the material.

(v) In a given phase, the positions of the WAXS peaks are very similar for all the samples. This can be well appreciated in Figure 3.16, where the values of the associated characteristic length d_i defined as $d_i=2\pi/Q_i^*$ (calculated for i=1,2 in the highly ordered smectic phase and also for the peak Q* above T_I) are displayed as function of temperature for the four samples investigated. We note the discontinuous behavior of the characteristic distances across both the transitions, reflecting underlying first-order transitions. The occurrence of a melting process during heating and the involvement of nucleation and growth processes in the transitions during cooling would also explain the differences observed in the values of T_I and T_{II} by DSC for the two experimental conditions.

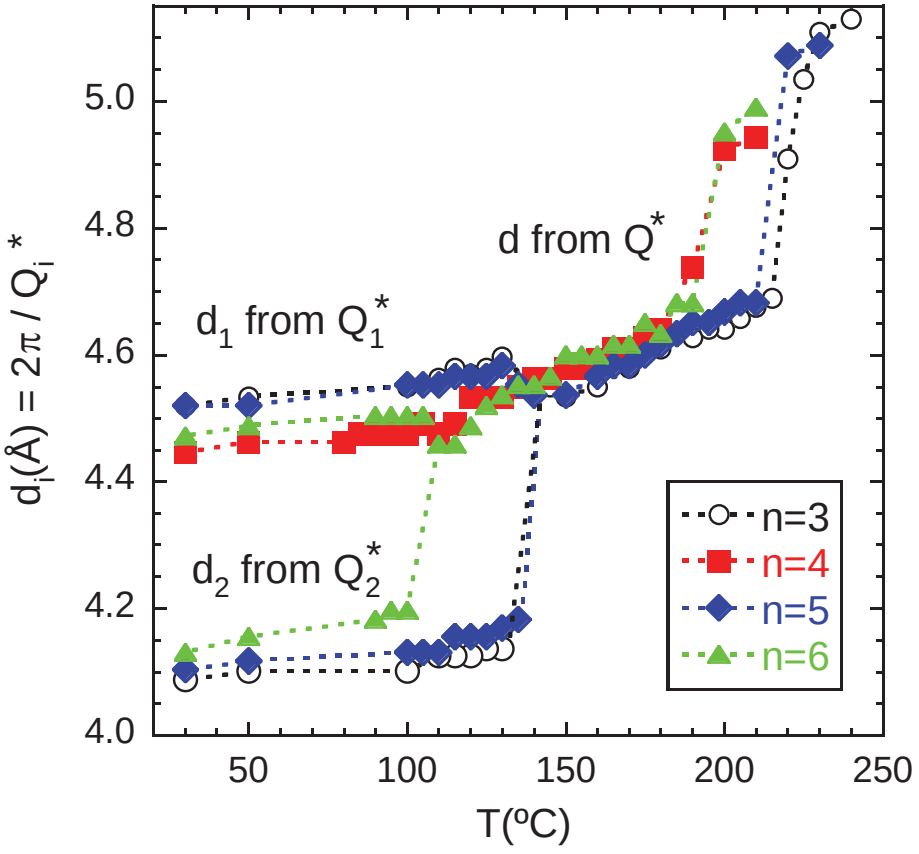

Fig. 3.16. Temperature dependence of the characteristic lengths defined as $d_i = 2\pi/Q_i^*$ characteristic for the ordering within the lamellae, for the different samples investigated.

Once the origins of the transitions and the general common structural features of all the samples have been identified, we can now discern the following differences depending on the length of the mesogen:

(i) The position of the first peak Q_1^{**} increasingly shifts toward lower values with increasing length of the spacer. This can be observed at first sight in Figure 3.8, from the difference in the first peak centers for $n \geq 4$ with respect to the vertical line marking the peak position for n=3. The positions of the corresponding higher-order reflections Q_2^{**}, Q_3^{**}, etc vary accordingly. These observations reflect an increase in the lamellar periodicity D with the mesogen length (Table 3.4). This dependence is represented in Figure 3.17.

(ii) The ordering features are more marked in the samples with odd number of methylene carbons in the spacer group than those where n is even. In particular, for n=4 the level of ordering seems to be rather low, while for n=5 the extreme narrowing of the main WAXS peak allows resolving even the 5^{th} order reflection of the lamellar structure (Figures 3.8(f) and 3.11(c)). This observation also applies to the perfection of the lamellar structure. As can be appreciated in Table 3.4, the lamellar domains are larger for odd n than for even n. Increasing n though, the differences seem to become less manifest.

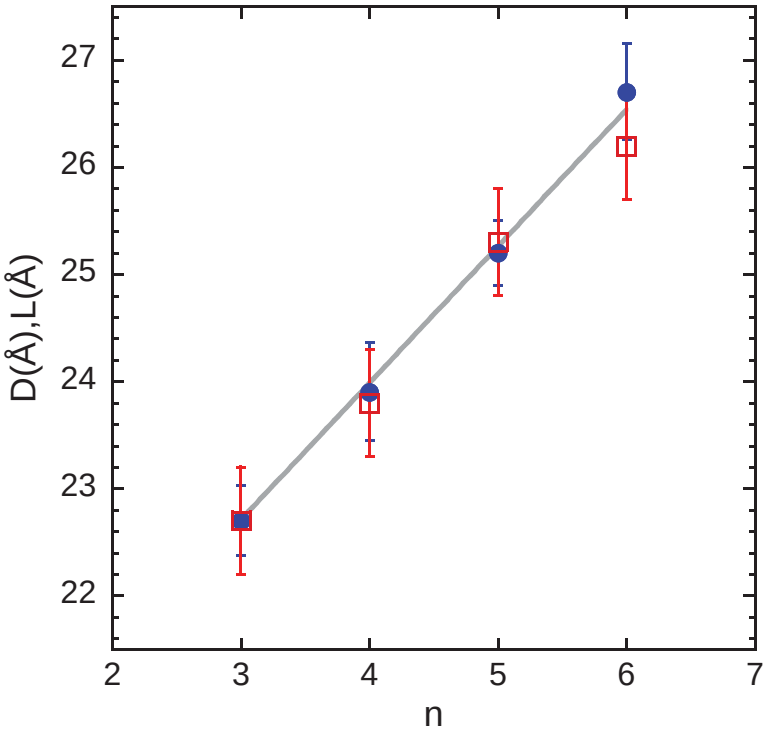

Fig. 3.17. Lamellar periodicity D (filled circles) as a function of the number of methylene units in the spacer. For comparison, the characteristic maximum length of the monomer L is also represented as empty squares.

(iii) In Figure 3.16, the even-odd effect on the transition temperatures identified by DSC becomes evident. Looking in detail, we could also discern an even-odd effect on the d_1–values and a slight increase of d_2 with increasing value of n. However, the differences are lower than 1.5%.

Next we attempt to interpret the XRD results in terms of molecular parameters. First of all, we note the monotonic behavior of the interlamellar spacing D with increasing spacer group length (see Figure 3.17). Within the uncertainties, we can describe this behavior as:

$$D(Å) = 18.9 + n\ell\cos(\theta/2) \qquad (3.1)$$

with ℓ=1.54Å the C-C bond length and θ=68º the bond angle in an alkane chain. This means that the lamellar thickness can be simply explained by the increase of the length of the spacer. The observed D-values are actually in excellent agreement with the estimated length L of the projection of the monomer on the direction perpendicular to the main-chain plane, when it adopts its most extended conformation (see Table 3.4 and Figure 3.17). The L-values have been obtained by means of the program ChemBio3D Ultra (version 15.1.0.144), simulating the chemical structures of the monomers in their all-trans conformation (see Figure 3.18). Thus, it seems that this maximum length is the key parameter determining the period in the lamellar

crystalline structure. From Figure 3.18 we can also deduce that, especially for odd n-values, the mesogens are practically perpendicular to the plane defined by the backbone atoms. Taking also into account the predominantly syndiotactic stereochemistry of the polymers (see Figure 3.19 and Table 3.5), we propose as a plausible scenario an arrangement where the main chains would be laying on parallel planes between which the side groups would be placed in a fully interdigitated way.

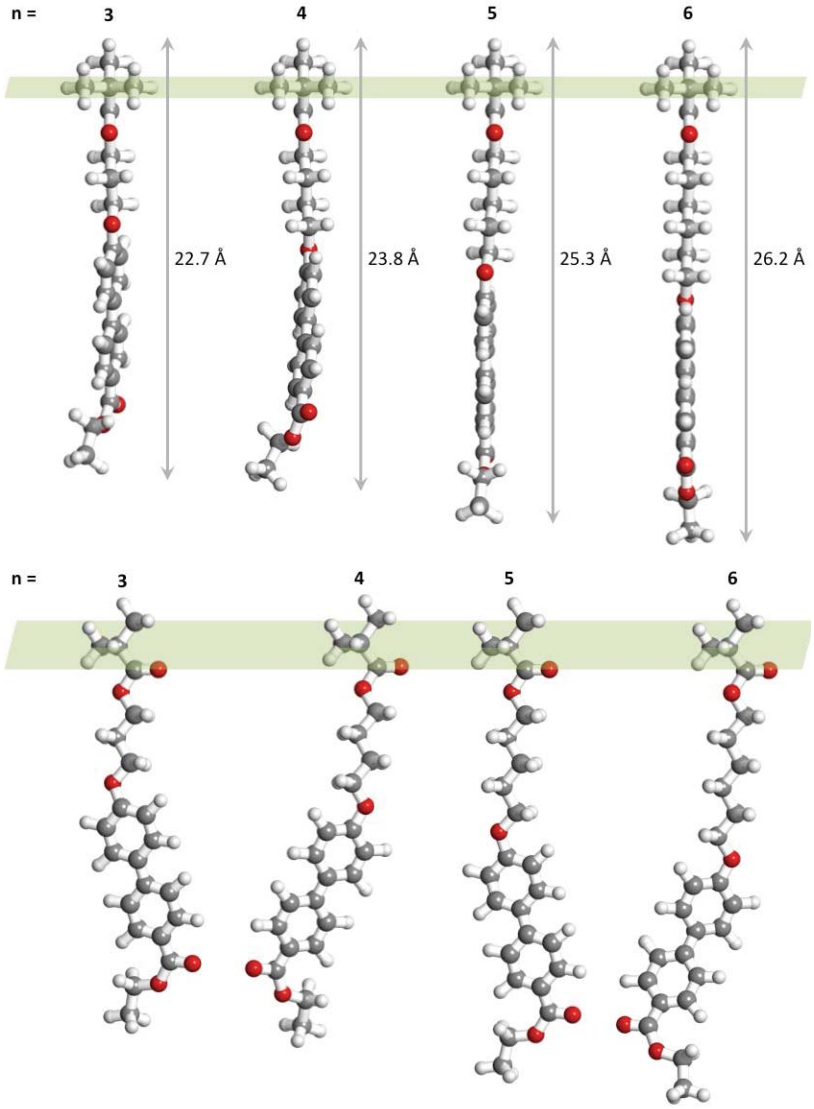

Fig. 3.18. Monomers in all-trans conformation of the spacer group as obtained with the ChemBio3D Ultra program. Upper panel: main chain parallel to the plane of the paper; lower panel: main-chain perpendicular to the plane of the paper.

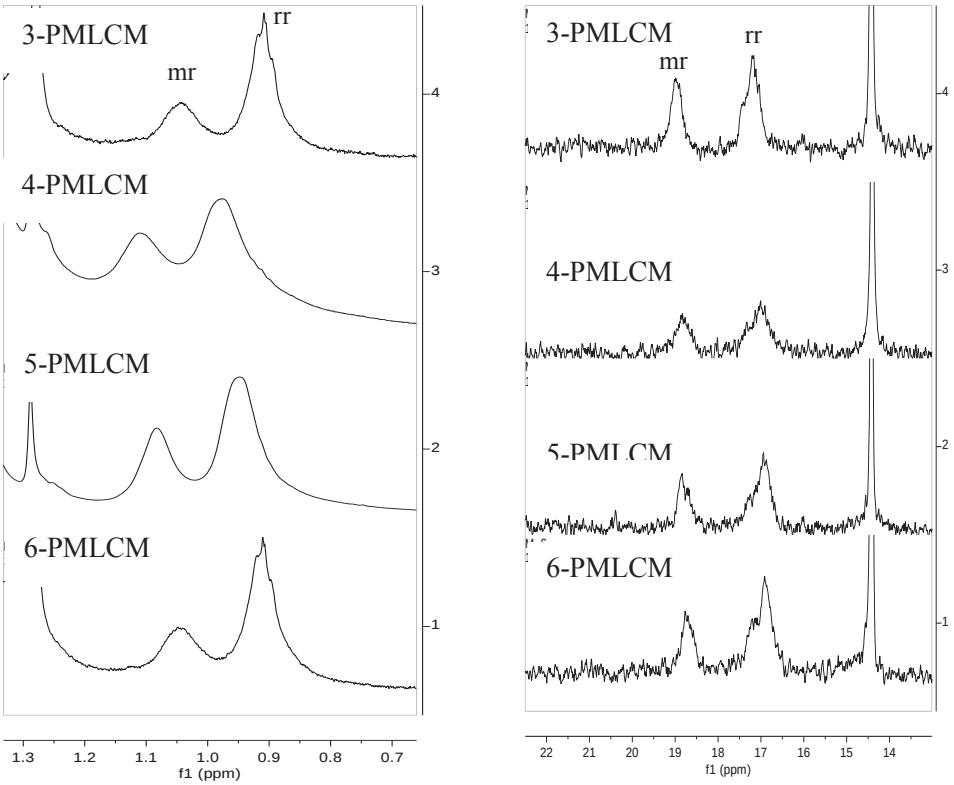

Fig. 3.19. Region of ^{1}H NMR ($CDCl_3$, 500 MHz) spectrum (left) and ^{13}C NMR ($CDCl_3$, 500 MHz) spectrum (right) for n-PMLCMs showing the peaks associated with the methyl protons.

Table 3.5. Tacticities[a] of n-PMLCMs

sample	mm	mr	rr
3-PMLCM	0.00	0.38	0.62
4-PMLCM	0.00	0.46	0.54
5-PMLCM	0.00	0.30	0.70
6-PMLCM	0.00	0.39	0.61

[a]mass fraction of isotactic (mm), heterotactic (mr) and syndiotactic (rr). the reported values are the average of tacticities calculated from ^{1}H NMR and ^{13}C NMR spectrums.

On the other hand, the values of Q_1^*, Q_2^*, Q_3^* of 3, 5 and 6-PMLCM at room temperature (i. e., below T_I) coincide, within the experimental uncertainties, with those expected for a two-dimensional orthorrombic unit cell with dimensions a=8.1Å and b=5.4Å, as it was proposed in reference 31 for the mesogens packing in a series of poly(silynemethylene)s. Table 3.6 shows the comparison between the d-spacings deduced from our WAXS experiments (including two more higher order reflections measured for the 5-PMLCM sample in an extended Q-range, see Fig. 3.20) and those calculated assuming such a structure [31]. On the basis of this agreement, the consideration of the above arguments and taking into account the predominantly syndiotactic character of the samples (n=3, 5 and 6, see Table 3.5), the following tentative picture for the molecular arrangement of n-PMLCM below T_I is proposed): Regardless of the spacer length, the polymers organize themselves leading to single-layer arrangements of the mesogens. To observe an increase of D (inter-layer distance) as that dictated by Eq. (1), the side-groups on both sides of the backbone

should be interpenetrated. Main chains lye in planes in an alternated fashion. We may identify the b-lattice parameter (b=5.4Å) with the distance between two alternated side groups along the chain backbone (which, in the syndiotactic sequence, would be directly facing each other). This assignment is supported by the similarity of this characteristic length with the average distance between a main-chain carbon and its fourth neighbor along the backbone in all-trans conformation obtained for PMMA (80% syndiotactic) from MD-simulations (4.8Å) [32]. Conversely, the lattice parameter a=8.1Å would be determined by the distance between two facing side-groups belonging to nearest neighbor chains which backbones lye in the same plane. To produce this kind of structure, we note that the spacer should be in all-trans conformation. In the Sm**A** and isotropic states, the main broad peak centered at Q* shall be originated from correlations between pairs of atoms belonging to neighboring side groups, arising from monomers of the same chain and also from monomers of different chains.

Table 3.6. Measured d-spacing (in Å) for n-PMLCMs and calculated on the basis of an orthorhombic unit cell (a=8.14Å, b=5.42Å) for the index indicated.

	n=3	**n=4**	**n=5**	**n=6**	**calc.**	**hkl**
$\mathbf{d_1}$	4.52	4.45	4.52	4.47	4.51	110
$\mathbf{d_2}$	4.09		4.11	4.12	4.07	200
$\mathbf{d_3}$	3.27	3.31	3.27	3.27	3.25	210
$\mathbf{d_4}$			2.56		2.57	120
$\mathbf{d_5}$			2.43		2.43	310

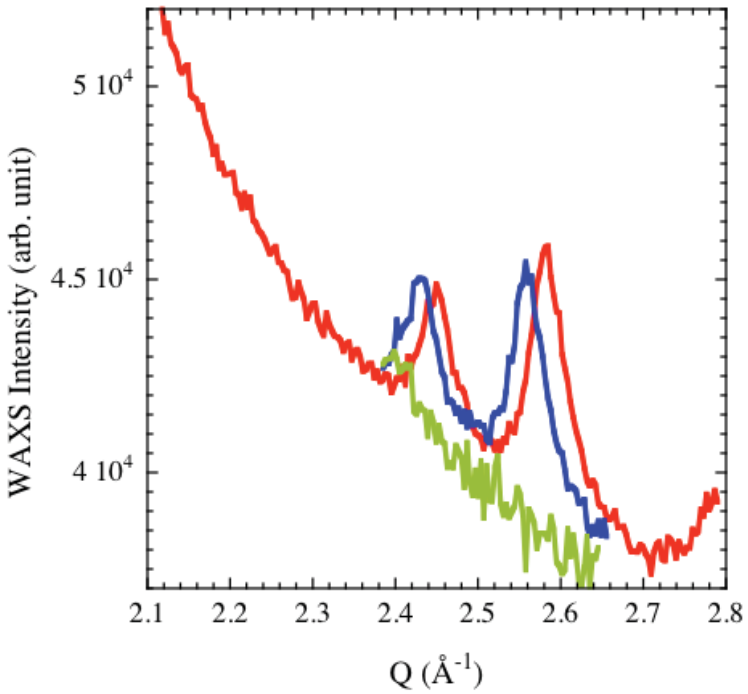

Fig. 3.20. WAXS pattern on 5-PMLCM at 30ºC (red), 115ºC (blue) and 150ºC (green).

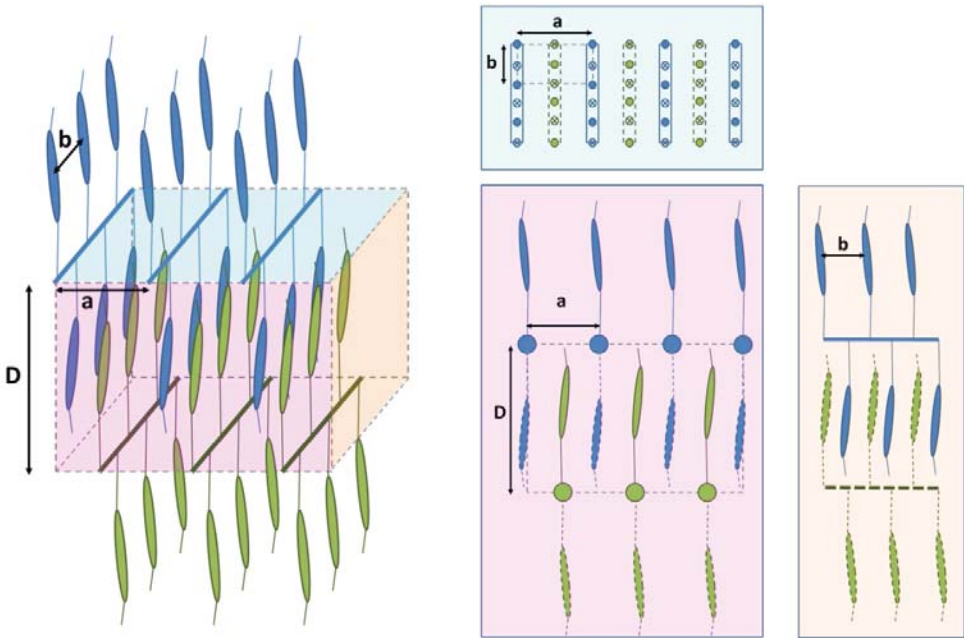

Fig. 3.21. Possible single layer 3D arrangement and the corresponding 2D projections (blue: top projection, pink: front projection, and orange: side projection) of n-PMLCM. The drawing has been scaled to roughly represent the case n=5.

3.3. Discussion

Based on DSC, PLM and SAXS and WAXS results, all polymers show mesomorphism behavior and present Sm**E** (Sm**E** or Sm**C** for 4-PMLCM) ↔ Smectic **A** ↔ Isotropic Liquid transitions with increasing temperature. The dependence of the transition temperatures as well as the entropy changes associated with the melting and clearing transitions (expressed as the dimensionless quantity ΔS/R) exhibit a distinct

odd-even effect with the number of carbon atoms in the spacer, n. The odd members exhibit the higher values of these quantities. These odd–even effects are most often attributed to the alternation in the average shape of the side-chain and its effect on the relative orientation of the mesogenic groups on varying the parity of the spacer [2]. It is widely reported in the literature that for spacers with the even numbers of methylene units, the mesogenic group is constrained to lie at some angle with respect to the polymer backbone whereas for odd-members the mesogenic unit is orthogonal with respect to the backbone. The odd-membered spacers can therefore pack more efficiently and resulting in higher transition temperatures, and also for the odd-membered spacers the liquid crystalline environment selects conformations giving rise to a greater conformational component in the overall entropy [2]. This view is supported by quantum chemistry as well as neutron scattering studies on other polymethacrylate based side chain liquid crystal polymers [2,33].

The even/odd distinct behavior has also an impact on the structural properties. In the particular samples here investigated, the simulations of the monomer units point to more pronounced tilts of the mesogens in the even members (see Fig.3.18). This effect is more marked for n=4 than for n=6. The high flexibility imparted by the longer alkyl spacer of 6-PMLCM would allow easily accommodating the mesogens in the highly ordered arrangement of a Sm**E** structure, as that above proposed (Fig

3.21). On the contrary, we could expect that ordering would be more difficult for the shorter 4-PMLCM mesogens. In fact, the granular PLM images and the much broader peaks of the patterns exhibited by this sample reflecting a less developed ordering. The difficulty for packing of 4-PMLCM also translates in the absence of the peak at Q_2*. We note the rather different tacticity of this sample (the syndiotactic fraction of 4-PMLCM is lower than the 3, 5 and 6-PMLCM, Fig. 3.19 and Table 3.5). This is another ingredient preventing a regular organization in a Sm**E**-like structure as that clearly found for the other samples. In the case of 4-PMLCM, the layered structure of mesogens is clearly evidenced by the SAXS peaks, but a discrimination between Sm**C** and Sm**E** for the low temperature phase cannot be made on the basis of our results.

We note that the orthorrombic cell with dimensions a≈8Å, b≈5.4Å within the layers seems to be recurrent for biphenyl-based mesogens, being found in many systems with different nature of the backbone and independently of the presence of a long tail. This kind of arrangement has been reported for liquid-crystal formers like poly(silynemethylene)s [31], polyacetylenes [23], side-chain liquid crystalline/ amorphous diblock copolymers [34], and even for poly(2,5-bis{[6-(4-butoxy-4′-oxybiphenyl) hexyl]oxycarbonyl}styrene) (a combined main-chain/side-chain LC polymer) [22]. Biphenyl mesogenic groups seem to crystallize –if possible– in

structures close to that achieved by biphenyl molecules. For biphenyl molecules, a monoclinic lattice with a=8.12Å, b=5.63Å and β=95.1º was reported in reference 35; similar values are also found in references 36 and 37. In biphenyl crystals, four biphenyl molecules arrange parallel to each other, surrounding a molecule in the center of the unit cell. A similar optimized geometry to that adopted by the individual molecules seems to be taken by the mesogenic units in the polymeric system. However, we note that in the polymeric liquid crystals with long spacers, the space between parallel biphenyl moieties would not be occupied by another biphenyl unit, but mainly by the alkyl segment of the spacer (see Figure 3.21).

Regarding the effect of the tail on the phase behavior of the polymers, we can compare our results with those reported for poly[ω-(4′-methoxybiphenyl-4-yloxy)alkyl methacrylate]s [3], where the tail is just a methoxy (OMe) moiety. The main differences are the following: (i) the values of T_{II} were systematically lower for those polymers than the ones found in this work (see Figure 3.22, the T_I, T_{II}, T_g and ΔS/R of poly[ω-(4´-methoxybiphenyl-4-yloxy)alkyl methacrylate]s with 3, 4, 5 and 6 methylene units in the spacer from reference 3 are plotted) leading to a much narrower Sm**A** phase region; (ii) two transitions could in fact not be resolved for the sample with n=3 carbons in the spacer and a direct isotropic - Sm**E** transition was reported; (iii) for the n=4 polymer, a nematic phase was found instead of the Sm**A**.

The lower values of the T_{II} transitions could be attributed to the lower molar mass of those samples (about 29000 g/mol). We recall that with the polymerization method used in this work we can deliver samples with high enough molar mass to reach the region of molar mass independent properties, as it is the case of the here reported systems. To clarify this point, we also synthesized by solutuin polymerization samples with $M_n \approx 10000$ g/mol, i.e., even lower molar mass as those reported in reference 3. Though the T_{II} values decrease with respect to the high-molar mass counterparts (Fig. 3.22), they are still well above those reported for the OMe-tail polymers. This indicates that the longer tails impart a high stability to the Sm**A** phases. On the other hand, we observe that in the low-molar mass samples synthesized by us the mesogenic structural ordering within the lamellae is more developed (see Figure 3.23), but the lamellar structure is less perfect than in the high-molar mass systems (see Figure 3.24). However, the presence of smectic phases below T_{II} is evidenced by sharp (though less intense) peaks for all the members, including n=3 and n=4. In particular, the sample with n=4 still shows smectic A phase between T_I and T_{II}. These findings point to a facilitation of the ordering by the presence of tails in the mesogens. These flexible moieties allow a better accommodation of the biphenyls in the lowest energy configuration. Being less

voluminous than rings, they can more easily fill the sparse free volume left close to the chain backbones.

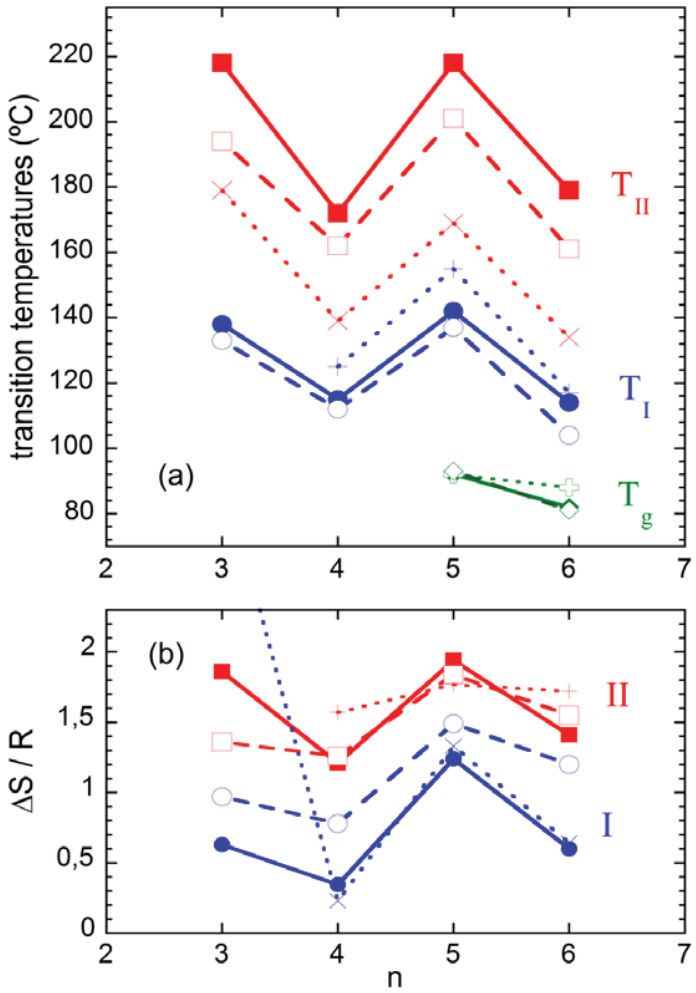

Fig. 3.22. Transition temperatures (a) and entropies (b) associated with the thermal transitions of high molar mass n-PMLCMs (solid symbols), low molar mass n-PMLCMs (empty symbols) and poly[ω-(4′-methoxybiphenyl-4-yloxy)alkyl methacrylate]s in reference 3 (cross symbols) for comparison purpose as function of the number of methylene units in the spacer. The thermal transitions were extracted from second heating scans.

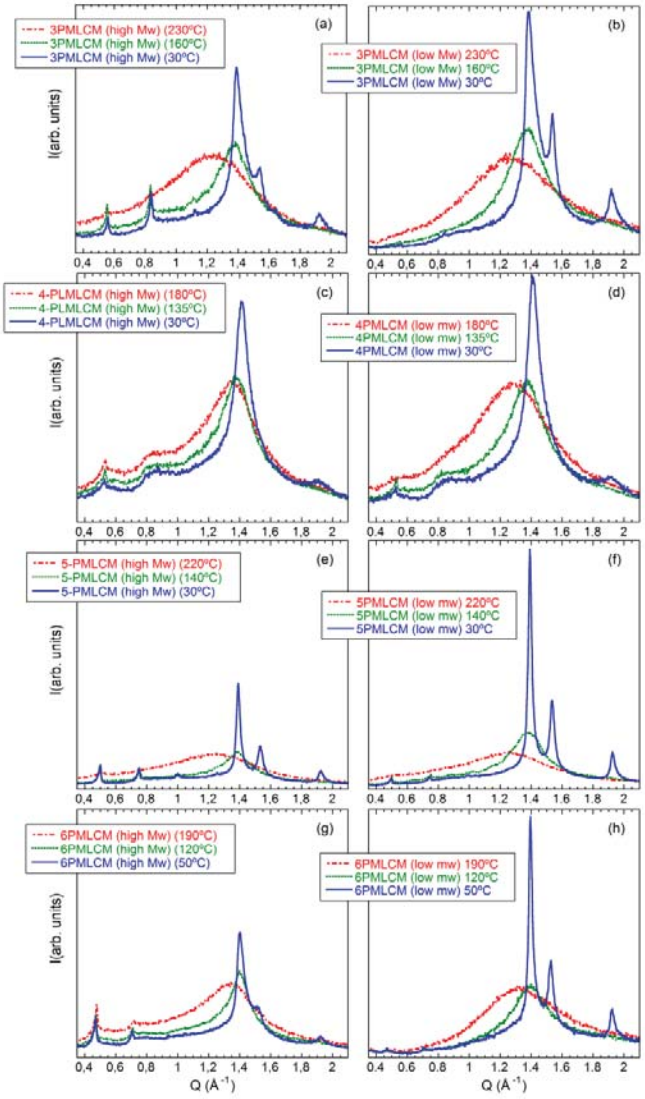

Fig. 3.23. WAXS-results at the temperatures indicated. (a) and (b): 3-PMLCM; (c) and (d): 4-PMLCM; (e) and (f): 5-PMLCM; (g) and (h): 6-PMLCM. Panels on the left: high molar mass samples; panels on the right: low molar mass samples.

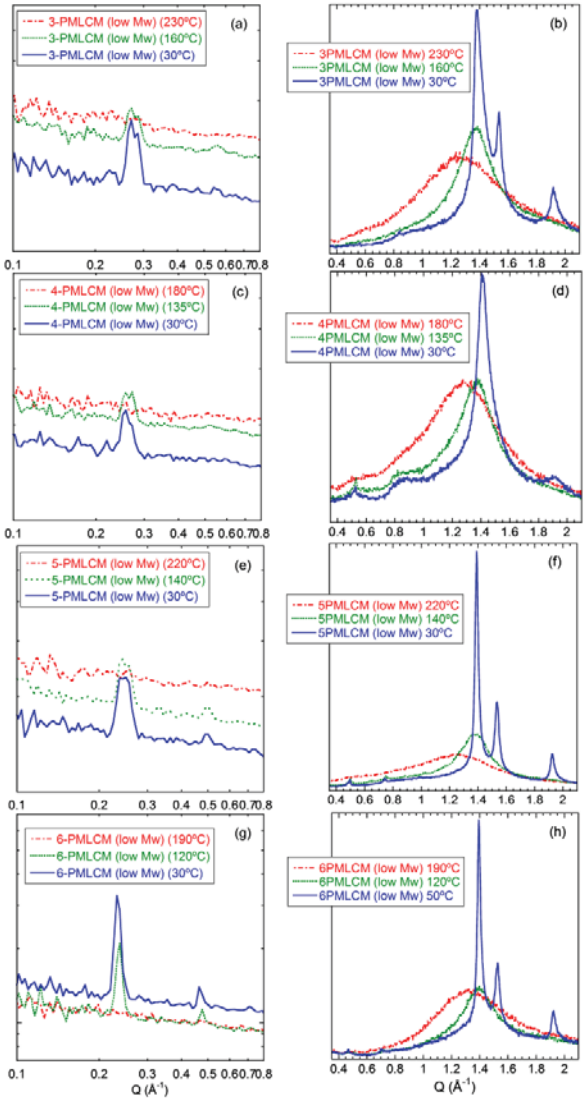

Fig. 3.24. XR-results at the temperatures indicated. (a) and (b): 3-PMLCM; (c) and (d): 4-PMLCM; (e) and (f): 5-PMLCM; (g) and (h): 6-PMLCM, for low molar mass samples. Panels on the left: SAXS results; panels on the right: WAXS results.

Finally, we comment that in the isotropic phase reminiscences of the lamellar structure are found as broad peaks in the low-Q range. These reveal underlying scattering length density fluctuations with characteristic distances broadly distributed around those dictated by the liquid crystalline order. An estimation of the domain size in this case would lead to $\zeta \approx 2D$, pointing to an actual frustration of the long-range order. It is also noteworthy that the presence of broad low-Q peaks characteristic for a nano-structuration has been reported for a wide variety of poly(methacrylates) with side groups of different nature, ranging from simple alkyl groups [38-41] to more complex moieties including heterocycles [42]. In fact, coarse-grained molecular dynamics simulations on comb-like polymers [43] have demonstrated that the emergence of nano-domains rich in either main chains or side groups is a natural entropic consequence of this kind of chain architecture. Obviously, the rigidity of the mesogenic side groups in the samples investigated in this work strongly promotes that nano-segregation and imposes a high degree of perfection in the periodicity of the nano-domains.

3.4. Conclusions

We have successfully synthesized a series of methacrylate side-chain liquid crystal polymers (n-PMLCMs, n=3, 4, 5, 6) in aqueous media by free radical miniemulsion polymerization. The molecular characterizations of the polymers were performed with ^{1}H NMR, GPC and TGA. Full monomer conversion and high molar mass (M_n ~10^5 g/mol) polymers with high thermal stability were obtained.

The phase behavior was investigated by a combination of DSC, PLM, SAXS and WAXS. The thermal characterization of the polymers exhibited that the melting and the clearing temperatures show a regular odd-even effect as the length and parity of the spacer is varied, with the odd members exhibiting the higher values. The entropy change associated with the melting and clearing transitions exhibit a similar dependence on n. This behavior may be rationalized by considering the change in the average shape of the side chain as the parity of the spacer is varied.

The combination of PLM and X-Ray studies revealed mesomorphic liquid crystalline behavior with a monolayer structure for polymers. Moreover, it was observed that the structural properties of the polymers depended on the parity of the spacer. The liquid crystal phase transition of n-PMLCMs follows the sequence of Smectic **E** (Sm**E** or Sm**C** for 4-PMLCM) ↔ Smectic **A** ↔ Isotropic Liquid. The

results showed lower level of ordering for 4-PMLCM in comparison with other members while the maximum level of ordering obtained for 5-PMLCM.

The thermal and mesomorphic behaviors of the n-PMLCMs have also been compared to other polymers containing the same mesogenic unit but different alkyl tail. It was observed that the alkyl tail play an important role in thermal and mesomorphic properties of studied polymers. The polymers containing longer tail showed higher thermal transitions and level of ordering. Longer tails facilitate the ordering of the mesogens and allow more efficient packing around the backbones, imparting high stability to the smectic phases formed.

3.5. References

[1] McArdle, C.B., 1990. *Side chain liquid crystal polymers*. Springer Science & Business Media.

[2] Imrie, C.T., Karasz, F.E. and Attard, G.S. *Macromolecules*, 1992, 25, 1278-1283.

[3] Craig, A.A. and Imrie, C.T. *J. Mater. Chem*, 1994**,** 4, 1705-1714.

[4] Cook, A.G., Inkster, R.T., Martinez-Felipe, A., Ribes-Greus, A., Hamley, I.W. and Imrie, C.T. *Eur Polym J*, 2012**,** 48, 821-829.

[5] Finkelmann, H., Happ, M., Portugal, M. and Ringsdorf, H. *Makromol Chem* 1978, 179, 2541-2544.

[6] Han, M., Kidowaki, M., Ichimura, K., Ramanujam, P.S. and Hvilsted, S. *Macromolecules*, 2001**,** 34, 4256-4262.

[7] Freiberg, S., Lagugné-Labarthet, F., Rochon, P. and Natansohn, A. *Macromolecules*, 2003**,** *36*, 2680-2688.

[8] Tang, X., Gao, L., Fan, X. and Zhou, Q. *J Polym Sci A1*, 2007**,** *45*, 5190-5198.

[9] Zheng, Z., Su, Z., Wang, L., Xu, J., Zhang, Q. and Yang, J. *Eur Polym J*, 2007, 43, 2738-2744.

[10] Wang, D., Ye, G., Zhu, Y. and Wang, X. *Macromolecules*, 2009**,** 42, 2651-2657.

[11] Ganicz, T. and Stańczyk, W**.** *Materials*, 2009**,** 2, 95-128.

[12] Isayama, J., Nagano, S. and Seki, T. *Macromolecules*, 2010**,** 43, 4105-4112

[13] Chen, S., Ling, A. and Zhang, H.L. *J Polym Sci A1*, 2013**,** 51, 2759-2768.

[14] Finkelmann, H. and Rehage, G., 1984. Liquid crystal side chain polymers. In *Liquid Crystal Polymers II/III* (pp. 99-172). Springer Berlin Heidelberg.

[15] Finkelmann, H., Ringsdorf, H. and Wendorff, J.H. *Makromol Chem,* 1978, 179, 273-276.

[16] Chen, S., Ling, A. and Zhang, H.L. *J Polym Sci A1*, 2013**,** 51, 2759-2768.

[17] Ni, B., Liao, J., Chen, S. and Zhang, H.L. *RSC Advances*, 2015**,** 5, 9035-9043.

[18] Chen, X., Tenneti, K.K., Li, C.Y., Bai, Y., Wan, X., Fan, X., Zhou, Q.F., Rong, L. and Hsiao, B.S. *Macromolecules*, 2007, 40, 840-848.

[19] Zhu, X.Q., Liu, J.H., Liu, Y.X. and Chen, E.Q. *Polymer*, 2008, 49*,* 3103-3110.

[20] Li, X., Wen, R., Zhang, Y., Zhu, L., Zhang, B. and Zhang, H. *J Mater Chem*, 2009, 19, 236-245.

[21] Li, Z., Zhang, Y., Zhu, L., Shen, T. and Zhang, H. *Polymer Chemistry*, 2010, 1, 1501-1511.

[22] Xie, H.L., Jie, C.K., Yu, Z.Q., Liu, X.B., Zhang, H.L., Shen, Z., Chen, E.Q. and Zhou, Q.F. *J Am Chem Soc*, 2010, 132, 8071-8080.

[23] Yu, Z.Q., Li, T.T., Zhang, Z., Liu, J.H., Yuan, W.Z., Lam, J.W., Yang, S., Chen, E.Q. and Tang, B.Z. *Macromolecules*, 2015**,** 48, 2886-2893.

[24] Han, M., Kidowaki, M., Ichimura, K., Ramanujam, P.S. and Hvilsted, S. *Macromolecules*, 2001**,** 34, 4256-4262.

[25] Vennes, M. and Zentel, R. *Macromol Chem Physic*, 2004**,** *205*, 2303-2311.

[26] Trollsås, M., Sahlen, F., Gedde, U.W., Hult, A., Hermann, D., Rudquist, P., Komitov, L., Lagerwall, S.T., Stebler, B., Lindström, J. and Rydlund, O. *Macromolecules*, 1996, *29*, 2590-2598.

[27] Lam, J.W., Kong, X., Dong, Y., Cheuk, K.K., Xu, K. and Tang, B.Z. *Macromolecules*, 2000, *33*, 5027-5040.

[28] Imrie, C.T., Karasz, F.E. and Attard, G.S. *J Macromolr Sci A*, 1994, *31,* 1221-1232.

[29] Imrie, C.T., Karasz, F.E. and Attard, G.S. *Macromolecules*, 1993, 26, 3803-3810.

[30] Förster, S., Apostol, L. and Bras, W. *J Appl Crystallogr*, 2010, 43, 639-646.

[31] Park, S.Y., Zhang, T., Interrante, L.V. and Farmer, B.L. *Macromolecules*, 2002**,** *35*, 2776-2783.

[32] Genix, A.C., Arbe, A., Alvarez, F., Colmenero, J., Schweika, W. and Richter, D. *Macromolecules*, 2006, *39*, 3947-3958.

[33] Hamley, I.W., Fairclough, J.P.A., King, S.M., Pedersen, J.S., Richardson, R.M., Imrie, C.T. and Graig, A.A. *Liq cryst*, 1997, *22,* 679-684.

[34] Al-Hussein, M., de Jeu, W.H., Vranichar, L., Pispas, S., Hadjichristidis, N., Itoh, T. and Watanabe, J. *Macromolecules*, 2004**,** *37,* 6401-6407.

[35] Wyckoff, R.W. *Crystal Structures*, 2nd ed., J. Wiley: New York, 1971; Vol. 6, Part 2.

[36] Charbonneau, G.T. and Delugeard, Y. *Acta Cryst,* 1977, *B33*, 1586-1588.

[37] Puschnig, P., Ambrosch-Draxl, C., Heimel, G., Zojer, E., Resel, R., Leising, G., Kriechbaum, M. and Graupner, W. *Synthetic Metals,* 2001, *116*, 327-331.

[38] Beiner, M. and Huth, H. *Nat mater*, 2003, 2, 595-599.

[39] Arbe, A., Genix, A.C., Colmenero, J., Richter, D. and Fouquet, P. *Soft Matter*, 2008, 4, 1792-1795.

[40] Beiner, M. *MacromoL rapid comm*, 2001, 22, 869-895.

[41] Arbe, A., Genix, A.C., Arrese-Igor, S., Colmenero, J. and Richter, D. *Macromolecules*, 2010,*43,* 3107-3119.

[42] Tejero, R., Arbe, A., Fernández-García, M. and López, D. *Macromolecules*, 2015, *48*, 7180-7193.

[43] Moreno, A.J., Arbe, A. and Colmenero, J. *Macromolecules*, 2011, 44, 1695-1706.

Chapter4. Acrylic-Based Composite Latexes Containing Liquid Crystalline Domains

4.1. Introduction

It has been shown in Chapter 2 that the mechanical properties, water resistance and barrier properties of conventional (meth)acrylate based latexes can be improved by incorporating crystalline domains in an amorphous (meth)acrylic polymer matrix formed by crystallization of the lateral alkyl chains of long-side chain n-alkyl acrylate. The long-side chain n-alkyl acrylate domains were introduced into the polymer particles via miniemulsion polymerization. However, the temperature range of applications is relatively narrow as the melting point of the crystalline domains was only 50 °C. A way to expand this temperature range is to incorporate liquid crystalline polymers (LCPs) within the polymer particles.

LCPs have been studied widely in the literature [1-5] and their incorporation into the polymer matrix using various processing techniques such as thermal processing (extrusion, injection molding and blow molding) [6,7,8,9,10,11], solvent casting [12,13] and polymerization [14,15] has been reported. There is plenty of

evidence that LCs and LCPs improve the barrier properties of polymers [9-11,15-17]. Reinforcement of polymers with LCPs led to an increase of both elastic modulus and ultimate strength and to a decrease of the ultimate tensile strain [6-8,16,18-21]. Processing conditions and compatibility between LCPs and polymer matrix strongly affected the barrier and mechanical properties of polymer composites [7,8,16,18,22].

Liquid crystalline domains have also been incorporated to solvent-borne coatings [3,4,23-26]. Thus, Chen et al. [3,4,23,25] and Athawale et al. [26] synthesized liquid crystalline (meth)acrylic copolymers coatings by grafting p-hydroxybenzoic acid to the COOH- containing (meth)acrylic copolymers. The same procedure was used by Chiang et al. [24] to synthesize liquid crystalline alkyd resins. In both cases, the coatings containing liquid crystalline domains showed better adhesion to substrates and chemical resistance; higher toughness hardness and impact resistance; and lower polymer solution viscosity. Solvent borne coatings are under the scrutiny of environmental agencies and are being replaced by waterborne coatings.

In this work, for the first time, the synthesis, characterization and performance of waterborne polymer dispersions containing liquid crystalline domains is reported. The liquid crystalline domains were produced by polymerization of side chain liquid crystalline monomers. The amorphous polymer matrix was produced by copolymerization of short side chain (meth)acrylate (SC(M)A) monomers with a

composition leading to a glass transition temperature appropriate for coating applications. Methacrylate side chain liquid crystalline monomers (n-MLCM) containing biphenyl mesogen with different spacer lengths and a fixed tail, [Ethyl 4'-((n-(methacryloyloxy)alkyl)oxy)-[1,1'-biphenyl]-4-carboxylate]s (n-MLCM; with n = 3, 4, 5, 6, see Scheme 4.1) were used. The synthesis and homopolymerization of these monomers that leads to a polymeric liquid crystal has been reported in Chapter 3. Since the n-MLCMs are hydrophobic monomers, miniemulsion polymerization has been selected to synthesize these waterborne semicrystalline latexes. In addition, as these monomers are solids with high melting temperature (Tm > 80 °C) they were dissolved in $CHCL_3$ prior miniemulsification. The effect of comonomer composition and n-MLCM spacer length on the liquid crystallinity and polymer architecture was studied. Moreover, the effect of liquid crystalline domains on the mechanical and barrier properties as well as on the water sensitivity of the films cast from the composite latexes was investigated.

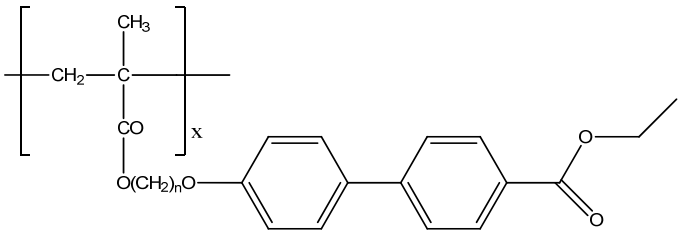

Poly (n-MLCM) n= 3, 4, 5, 6

Scheme 4.1. Structure of n-MLCM homopolymers.

4.2. Experimental section

4.2.1. Materials

Technical grade monomers, methyl methacrylate (MMA, Quimidroga), n-butyl acrylate (BA, Quimidroga) and acrylic acid (AA, Aldrich) as short side chain (meth)acrylate SC(M)A monomers were used as received. A series of methacrylate side chain liquid crystalline monomer (n-MLCM (n= 3-6)) were synthesized as described in Chapter 3. Potassium persulfate (KPS, Aldrich) as water soluble radical initiator and alkyldiphenyloxide disulfonate (Dowfax^{TM} 2A1, The Dow Chemical Company) as anionic surfactant were used as received. Deionized water was used as polymerization media.

4.2.2. Synthesis of the composite latexes

A 2-step miniemulsion polymerization was used to synthesize the composite latexes containing the liquid crystalline polymers (Scheme 4.2). In the first step, the polymer liquid crystal was formed by miniemulsion homopolymerization of n-MLCM. It is worth pointing out that short chain monomers cannot be added at this stage because this will preclude the formation of liquid crystalline domains. A solution of n-MLCMs in chloroform was added to the aqueous phase containing

Dowfax 2A1 (3 wt% based on all monomers) and mixed under mechanical agitation for 10 minutes. The coarse emulsion was sonicated by using a Hielscher Sonifier (UIS250v, amplitude 100 and energy pulsed at 1 Hz) over 10 minutes in an ice bath to avoid overheating. The n-MLCM miniemulsion was purged with nitrogen and the miniemulsion homopolymerization was carried out in batch by using KPS (1 wt% based on n-MLCM) at 70 °C for 3 h in a 50 ml flask immersed in an oil bath and equipped with a magnetic stirrer. Afterwards, the chloroform was removed completely by rotary evaporation. The second step was carried out in a Miniplant M100 setup (Chemspeed Technologies) in 100 ml stainless steel reactors equipped with reflux condenser, nitrogen inlet and a stainless steel anchor-type stirrer (200 rpm were used in the polymerizations). The poly(n-MLCM) latex produced in the first step was transferred to the reactor, purged with nitrogen and heated to the reaction temperature (70 °C). Then, the aqueous solution of initiator (KPS, 1 wt% based on SC(M)A monomers) was added as a shot and the mixture of SC(M)A monomers was fed to the reactor under starved conditions during 3 h. The reactions continued for 1 h more in batch.

To study the effect of the polymer liquid crystal domains on the properties of synthesized latexes, two series of experiments were designed. In Series A, 6-MLCM (crystalline monomer with 6 CH_2 units in the spacer) was used and the ratio of poly(6-MLCM) / poly(SC(M)A) was varied (20/80 and 30/70). This series also

includes the homopolymer of 6-MLCM as a reference. In Series B, the ratio poly(n-MLCM) / poly(SC(M)A was 20/80 and the length of the spacer was varied (3,4,5 and 6). The formulations used in these experiments are summarized in Table 4.1.

In addition, a latex devoid of liquid crystalline domains was synthesized by semibatch emulsion copolymerization and was used as reference to study the effect of incorporating liquid crystalline domains in the particles. For the emulsion polymer, the reactor was charged with the aqueous phase containing Dowfax^{TM} 2A1 (3 wt% based on monomers), purged with nitrogen and heated to the reaction temperature (70 °C). Then, the initiator (KPS, 1 wt% based on monomers) solution was added as a shot and the mixture of SC(M)A monomers was fed to the reactor during 3 h. After that, the system was allowed to react for 1 h in batch (Run C in Table 4.1).

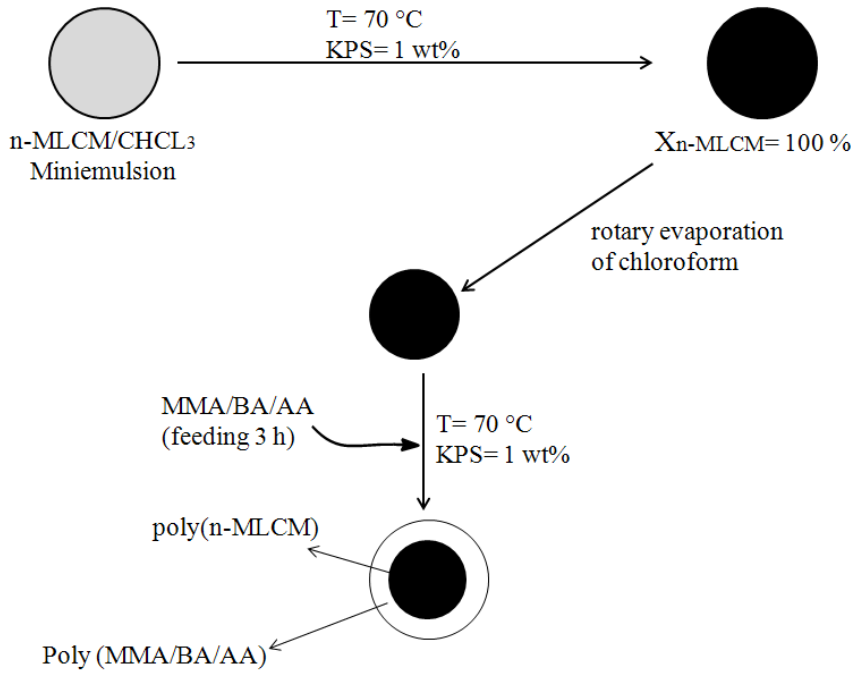

Scheme 4.2. Schematic representation of the synthesis of the n-MLCM/SC(M)A copolymer latexes.

Table 4.1. Formulation used to synthesize n-MLCM/SC(M)A copolymer latexes

	Run	n-MLCM		$CHCL_3$ (g)	SC(M)A[a] (g)	Dowfax 2A1 (g)	n-MLCM/ SC(M)A (wt/wt)
		n	(g)				
Miniemulsion polymerization	**Series A (6-MLCM/SC(M)A)**						
	A-6-100[b]	6	1.0	3	0	0.140[e]	100/0
	A-6-30[c]	6	1.5	3	3.5	0.150	30/70
	A-6-20[c]	6	1.5	3	6	0.225	20/80
	Series B (n-MLCM/SC(M)A)						
	B-5-20[c]	5	1.5	3	6	0.225	20/80
	B-4-20[c]	4	1.5	3	6	0.225	20/80
	B-3-20[c]	3	1.5	3	6	0.225	20/80
Emulsion polymerization	C[c]	----	0	0	7.5	0.225	0/100

[a]SC(M)A: MMA/BA/AA=49/49/2 wt%. [b]solids content=5 wt%. [c]solids content=15.7 wt%. [e]3.5wt% based on (6-MLCM+$CHCL_3$).

4.2.3. Characterization

Monomer droplet and polymer particle sizes were measured by dynamic light scattering (DLS) using a Zetasizer Nano Series (Malvern Instruments Ltd.). The values given are z-average values obtained through cumulants analysis. The equipment was operated at 20 °C and the values reported were the average of two repeated measurements.

Only a fraction of the poly(n-MLCM) was soluble in tetrahydrofuran (THF). The **Molecular Weight Distribution** (MWD) of the soluble fraction was determined by gel permeation chromatography (GPC) at 35 °C. The GPC instrument consisted of an injector, a pump (Waters 510), three columns in series (Styragel HR2, HR4, and HR6), and a differential refractometer (Waters 2410) as detector. To measure the MWD of the samples, the sol part obtained after Soxhlet extraction was dissolved in THF and analyzed by GPC. The flow rate of THF through the columns was 1 mL min^{-1}, and samples were filtered before injection into the GPC (filter pore size = 0.45 μm, Albert). Polystyrene (PS) standards were used to calibrate the equipment and the reported molar masses are referred to PS.

Thermal characterization. The melting (T_m) and clearing (T_c) temperatures, the corresponding enthalpies and the glass transition temperature (T_g) were determined by differential scanning calorimetry (DSC, Q1000, TA Instruments) of films cast at 23 °C from the final latexes. The scanning cycles consisted of first cooling to -50 °C at 10 °C min^{-1}, then heating from -50 to 230 °C at 10 °C min^{-1}, cooling again from 230 to -50 °C at 10 °C min^{-1}, and then heating to 230 °C at a rate of 10 °C min^{-1}. It is worth mentioning that poly(n-MLCM)s has a very good thermal stability (5% weight loss at 280 °C measured by TGA at a rate of 10 °C min^{-1}under nitrogen atmosphere, see Chapter 3).

The **morphology** of latex particles and films was studied by means of transmission electron microscopy (TEM). TEM analysis was carried out with a TecnaiTM G2 20 Twin device at 200 kV (FEI Electron Microscopes). The latexes were diluted with deionized water (0.05 wt%) placed on copper grids covered with Formvar R and dried at ambient temperature. The films were cryosectioned with a Leica EMUC6 cryoultramicrotome at 30 °C below the T_g of the sample, with a Diatome 45° diamond knife.

Mechanical properties of the films were determined by tensile test measurements according to the ASTM D882 standard test. The films dried at 23 °C for one week. Also, the samples molded at 200 °C by using hot press equipment (200 bar pressure) and a Teflon mold with standard dimensions to obtain samples without defects. The thickness of the films and samples was 700 μm and the measurements were carried out in a Stable Micro System TA HD Plus Texture Analyzer under both controlled conditions (23 °C and 55% of humidity) and 60 °C. The test speed was 0.42 $mm.sec^{-1}$. The results reported were the average of 4-5 repeated measurements and the reproducibility was good. It is worth mentioning that the liquid crystallinity and thermal characteristic of the copolymer processed at 200 °C was the same of the films cast at 23 °C.

To study the **water sensitivity** of the films, the liquid water uptake was measured and to study the **barrier property,** water vapor transmission experiments were carried out using a gravimetric cell. The films were prepared as described above for the tensile test with the thickness of 250-300 μm. The tests were described in detail in Chapter 2.

4.3. Results and discussion

The droplet diameter of n-MLCM/chloroform miniemulsion and the particle diameters of the poly(n-MLCM) latexes (after removing chloroform) as well as the final diameter of the composite particles are given in Table 4.2. This table also includes the theoretical particle diameter of the final latexes assuming that there were neither coagulation nor secondary nucleation. Comparison with the actual sizes of the final latexes shows that substantial secondary nucleation occurred and that the extent of this process decreased as the fraction of n-MLCM in the formulation increased. The reason was that for the same final solids content, the number of poly(n-MLCM) particles at the beginning of the second step increased with the fraction of n-MLCM in the formulation. Consequently the probability of capturing the oligoradicals in the aqueous phase increased lowering the extend of secondary nucleation. The presence of small amorphous particles (white particles) in the TEM micrographs of latex A-6-2 is an evidence of the secondary nucleation during the second step of the

polymerization (Figure 4.1). The micrographs in this figure show that the composite particles had core-shell morphology with the dark poly(n-MLCM) domains in the core. Table 4.2 also shows that all the samples had similar sol molecular weights.

Table 4.2. Droplet and particle sizes of miniemulsion droplets and particles as well as the average molecular weight and dispersity for the soluble part of n-MLCM/SC(M)A composite latexes (Runs in Table 1)

Run	SA/SC(M)A[a] (wt/wt)	Miniemulsion droplet size (nm)	PLC seeds particle diameter[b] (nm)	Composite particle diameter (nm)	Theoretical Particle diameter (nm)	Mw, Soluble Part (g/mol)	Đ
Series A (6-PMLCM/SC(M)A)							
A-6-100	100/0	105	84	---	---	256400	2.6
A-6-30	30/70	125	110	130	164	246000	3.0
A-6-20	20/80	150	107	115	182	315000	3.6
Series B (n-PMLCM/SC(M)A)							
B-5-20	20/80	146	105	133	179	222000	3.7
B-4-20	20/80	150	103	110	172	338000	4.1
B-3-20	20/80	155	94	126	160	386000	3.3
C	0/100	---	---	45	---	286000	2.8

[a] SC(M)A: MMA/BA/AA=49/49/2 wt%. [b] after removing choloroform.

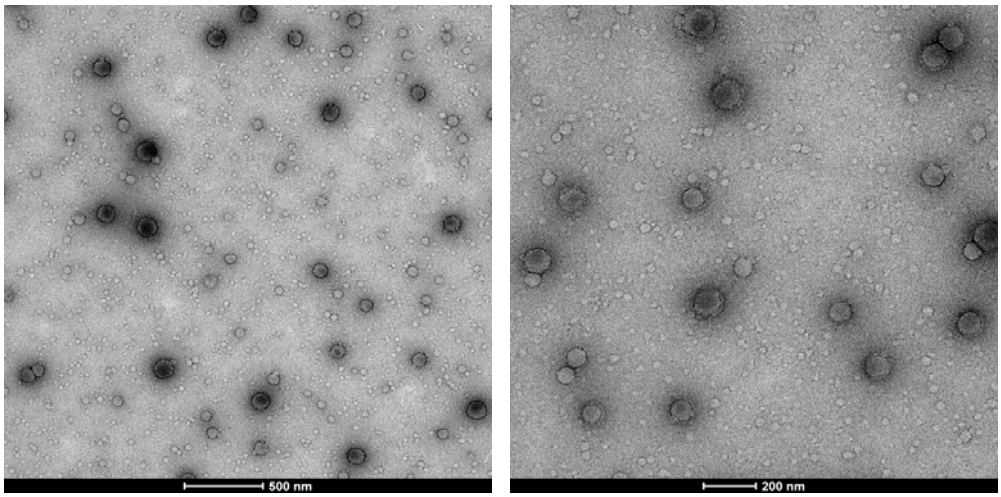

Fig.4.1. The TEM micrographs of latex A-6-20.

The second heating DSC scans of the synthesized copolymers in Series A and B are plotted in Figures 4.2 and 4.3, respectively, and the thermal characteristics of these samples are listed in Table 4.3.

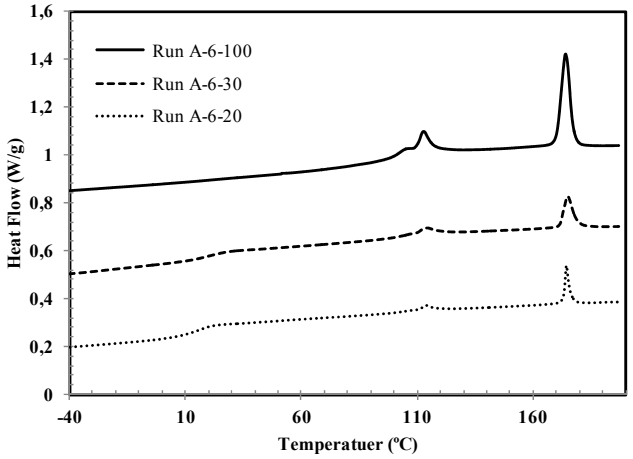

Fig. 4.2. The DSC scans obtained on the second heating of 6-MLCM/SC(M)A composite latexes (Series A in Table 1); For clarity, 0.7 W/g was added to the scan of the sample A-6-100 and 0.3 W/g to that of sample A-6-30 (Exo Down).

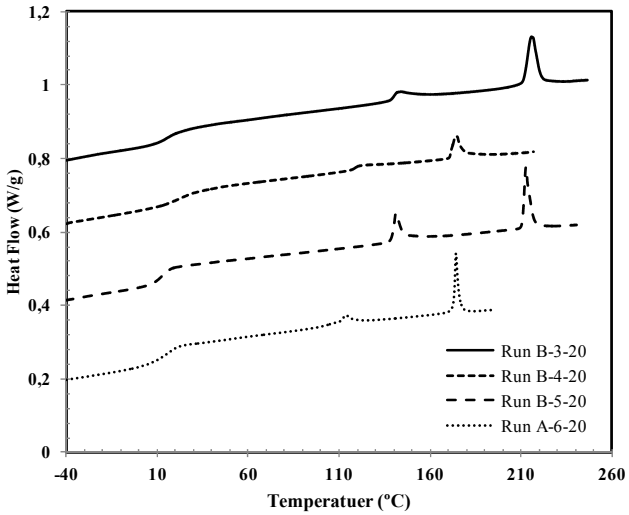

Fig. 4.3. The DSC scans obtained on the second heating of n-MLCM/SC(M)A=20-80 wt% composite latexes (Series B and Run A-6-20 in Table 1); For clarity, 0.65 W/g was added to the scan of the sample B-3-20; 0.45 W/g to the scan of sample B-4-20 and 0.25 W/g to that of sample B-5-20 (Exo Down).

Table 4.3. Thermal properties of n-MLCM/SC(M)A composite latexes

Run	n-MLCM/SC(M)A[a] (wt/wt)	T_g (°C)	T_{SS}[b] (°C)	T_{SI}[c] (°C)	ΔH_{SS} (J/g)	ΔH_{SI} (J/g)
Series A (6-PMLCM/SC(M)A)						
A-6-100	100/0	80	113	174	5.240	12.99
A-6-30	30/70	19	113	174	1.002	3.91
A-6-20	20/80	15	113	174	0.552	2.44
Series B (n-PMLCM/SC(M)A)						
B-5-20	20/80	14	141	213	1.740	3.48
B-4-20	20/80	19	117	173	0.161	1.91
B-3-20	20/80	15	142	215	0.850	4.88
C	0/100	15	---	---	---	---

[a] SC(M)A: MMA/BA/AA=49/49/2 wt%; [b]Smectic **E** (Smectic **E** or **C** for poly(4-MLCM))-Smectic **A** transition; [c]Smectic **A** - Isotropic transition.

It can be seen that the DSC traces of all latexes contained two endothermic peaks that corresponded to the melting (lower temperature peak) and clearing (higher temperature peak) transitions of poly(n-MLCM). In Chapter 3 the melting transition has been attributed to smectic **E** (Smectic **E** or **C** for poly(4-MLCM)) to smectic **A** phase transition and the clearing peak corresponding to smectic **A** to isotropic liquid phase transition. In addition, it has been reported in Chapter 3 that the melting and clearing transitions of poly(n-MLCM) showed an odd-even effect (in both melting and

clearing temperature as well as in the corresponding enthalpy changes) with spacer length, with the odd members exhibiting the higher values. These effects are also clear in the composite latexes.

Moreover, the DSC scans of composite latexes showed a second-order transition, due to the glass transition of the amorphous copolymer of SC(M)A.

WAXS of the composite film cast at 23 °C from composite latexes in Series A are presented in Figure 4.4. It can be seen that all of the five sharp peaks with 2θ angle ranging from 5 ° to 30 ° displayed in the Run A-6-100 (poly(6-MLCM)) can be observed in the composite films which indicates that the liquid crystalline domainswere not perturbed by the in amorphous SC(M)A copolymer matrix. Moreover, the intensity of the WAXS peaks increased with poly(6-MLCM) ratio.

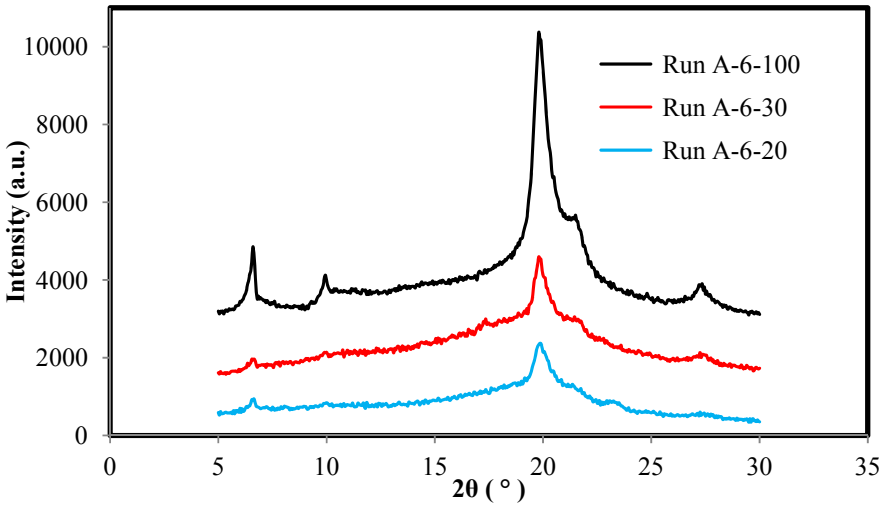

Fig. 4.4. WAXS curves of composite films from Series A latexes at 30 °C.

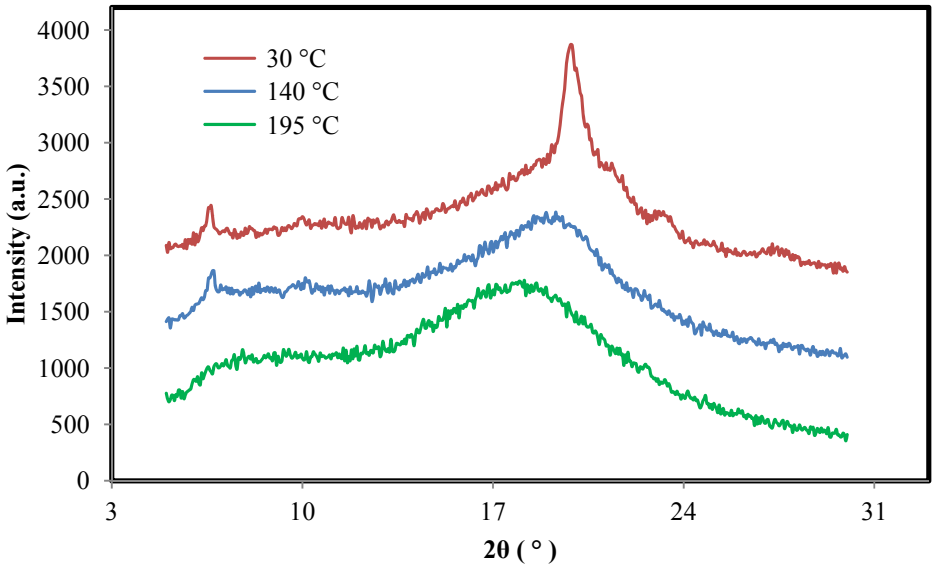

Fig. 4.5. Temperature evolution of WAXS-results of casted film from A-6-20 composite latex.

Figure 4.5 shows data recorded for the A-6-20 composite film at three representative temperatures: above clearing transition (at 195 °C), between melting and clearing transitions (at 140 °C), and below melting transition (at 30 °C).

Below the melting transition, the scattering peaks at low angle region, which indicate the layer structure of liquid crystalline domains, and the high angle diffractions, which indicate the high degree of ordering inside the layers (smectic **E**) are completely clear. When the temperature was increased above the melting temperature, the diffraction peak in the high angle region broadens to be a scattering halo and on the other hand, the low angle diffraction behavior did not change. This means that the above the melting temperature the liquid crystalline domains still preserved their layered structure but there was not special orientation inside the layers (smectic **A**). When the temperature exceeded the clearing transition (195 °C), the scattering halo in the high angle region continually broadened and slightly shifted to lower angle. Meanwhile, the diffractions in the low angle region completely disappeared. The two amorphous halos observed in both low and high angle region indicate an isotropic melt composite.

The polarized light microscopy of the film cast from the A-6-20 composite latex above and below the clearing transition temperature are shown in Figure 4.6. As can be seen, the sample is in isotropic liquid state above clearing temperature (black texture). At 140 °C, below the clearing transition, the formation of liquid crystalline domains was detected. This texture remained unchanged when the sample was cooled to room temperature.

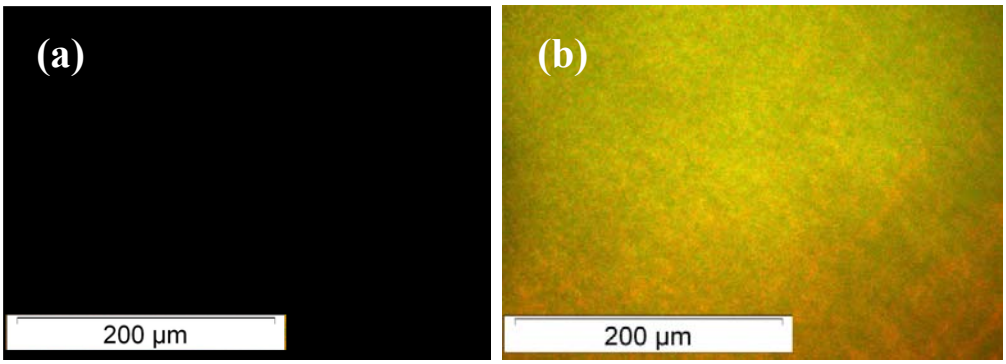

Fig.4.6. The PLM texture of the A-6-20 composite film at (a) 195 °C and (b) 140 °C. Note that the PLM image at room temperature was the same as that shown in (b).

The TEM micrographs of the cross-sections of the film cast at 23 ºC from A-6-30 latex and the same film after being processed at 200 ºC are shown in Figure 4.7. It can be seen that in the film cast at 23 ºC, the poly(6-MLCM) domains (dark phase in

the micrographs) were well dispersed in the film without any indication of aggregation between them (coagulation was not possible because the high melting temperature of this polymer (Table 4.3)). When the film was processes at 200 ºC (above the melting and clearing temperatures of poly(6-MLCM)), migration and coalescence of the poly(6-MLCM) nuclei led to the formation large clusters that where homogenously distributed in the film. The extensive phase separation suggests that poly(6-MLCM) and the SC(M)A copolymer were incompatible.

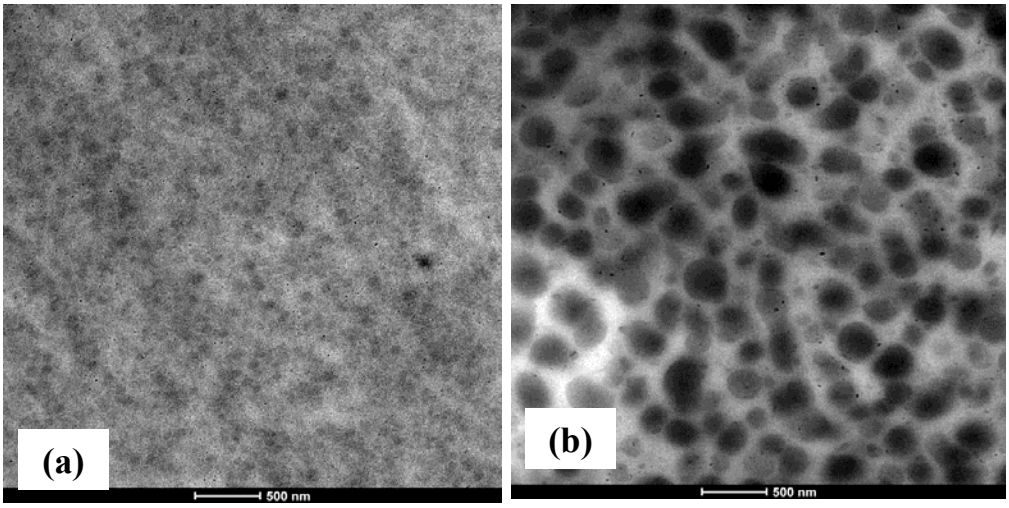

Fig. 4.7. The TEM micrographs of the cross-section of (a) the cast film at 23 ºC (b) the processed film at 200 ºC from Run A-6-30 latex.

The stress-strain behavior of the films cast from composite latexes in Series A at 23 °C and also the samples molded at 200 °C are shown in Figure 4.8 This figure also includes the amorphous latex C. It is worth mentioning that the homopolymers of n-MLCMs were highly crystalline and they did not form film at room temperature and that the homopolymers processed at 200 °C were highly brittle. It can be seen that for the films cast at 23 °C (Figure 4.8(a)), the Young's modulus (the slope obtained at low strains) and the yield stress of the films increased with the poly(6-MLCM) content whereas the elongation at break point decreased. The ultimate strength of the films was almost the same. The effect of liquid crystalline domains on the mechanical properties of the films is more prominent for the samples processes at 200 °C. As can be seen the Young's modulus, yield stress and the ultimate strength of the composites increased and the elongation at break point decreased with increasing poly(6-MLCM) content (Figure 4.8(b)). Moreover, the comparison of the tensile properties of the cast films cast at 23 °C and 200 °C show that the mechanical properties of composite samples processed at 200 °C was better than those of the films cast at 23 °C. The lower mechanical properties of the films cast at 23 °C were attributed to the defects in the film. The stress-strain behavior of the film cast at 23 °C and the sample processed at 200 °C for the latex C is almost the same. The mechanical properties of the composites in Series A as well as the amorphous copolymer (latex C) processed at 200 °C are summarized in Table 4.4. It can be seen that the liquid crystalline domains

of poly(6-MLCM) substantially reinforced the mechanical properties of amorphous copolymers of SC(M)A and that the maximum toughness was observed for a 20% of poly(6-MLCM).

Table 4.4. Mechanical properties of composite latexes.

Run	SA/SC(M)A[a] (wt/wt)	Young´s Modulus $\times 10^{-2}$ (MPa)	Yield Stress (MPa)	Toughness $\times 10^{-6}$ ($J \cdot m^{-3}$)	Elongation @ Break $\times 10^{-2}$ (%)	Ultimate Strength (MPa)
Series A (6-PMLCM/SC(M)A)						
A-6-100	100/0	---	---	---	---	---
A-6-30	30/70	2.71±0.32	8.20±1.12	15.03±0.95	1.28±0.07	15.45±0.83
A-6-20	20/80	0.64±0.14	2.28±0.13	33.59±1.92	4.25±0.43	14.00±0.64
Series B (n-PMLCM/SC(M)A)						
B-5-20	20/80	1.14±0.09	5.21±0.2	30.70±2.11	3.45±0.17	12.60±1.02
B-4-20	20/80	1.70±0.12	6.30±0.22	31.64±1.62	2.97±0.15	14.52±1.23
B-3-20	20/80	1.83±0.19	8.75±0.15	25.59±2.36	2.12±0.21	14.20±0.53
C	0/100	0.33±0.07	0.84±0.16	17.53±1.48	6.44±0.57	8.40±0.61

[a] SC(M)A: MMA/BA/AA=49/49/2 wt%.

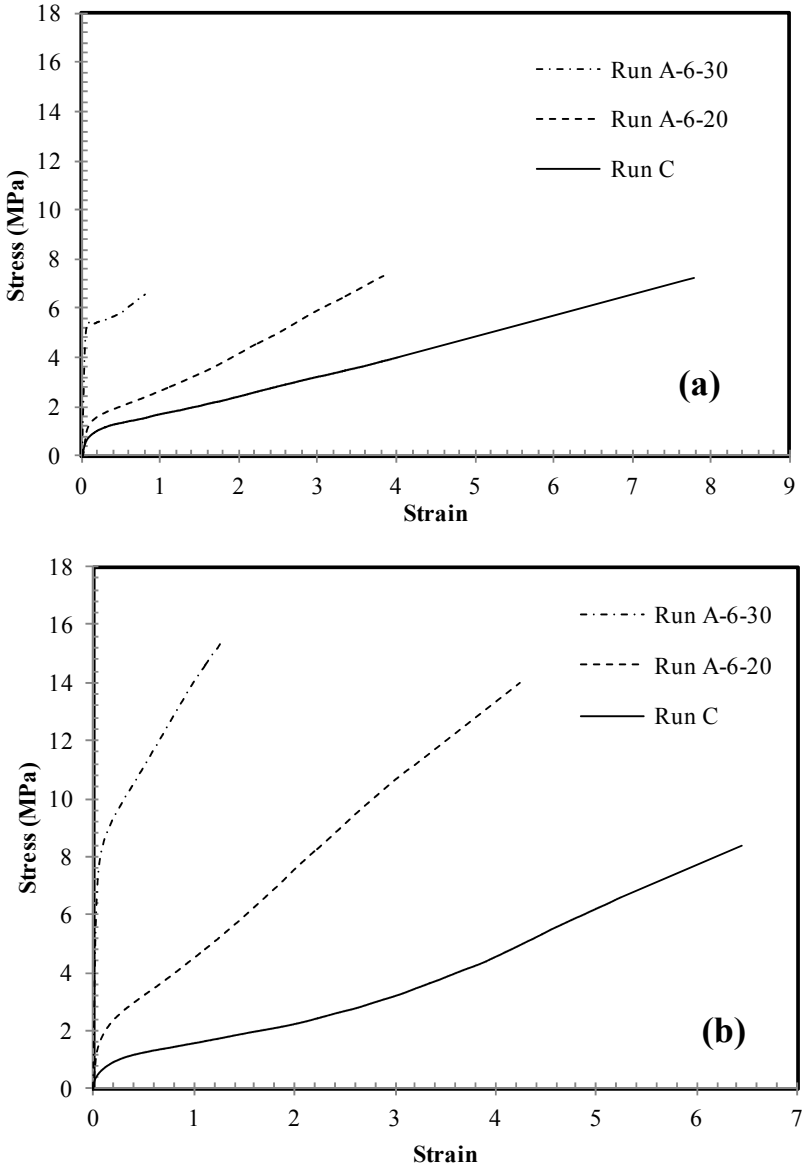

Fig. 4.8. The stress-strain behavior of the films (a) cast at 23 °C and (b) processed at 200 °C from composite latexes in Series A, Run C is included as a reference.

Figure 4.9 presents the stress-strain behavior of the composite samples with the same poly(n-MLCM)/poly(SC(M)A) ratio (20/80 wt/wt) and different lengths of the spacer. The sample containing only SC(M)A is included as reference. The mechanical properties are given in Table 4.4. It is remarkable the strong effect of the length of the spacer on the mechanical properties of the composite films. The longer the spacer the lower the Young´s modulus and the yield stress, but the higher the elongation at break and the toughness. No clear effect of the length of spacer on the ultimate strength was observed.

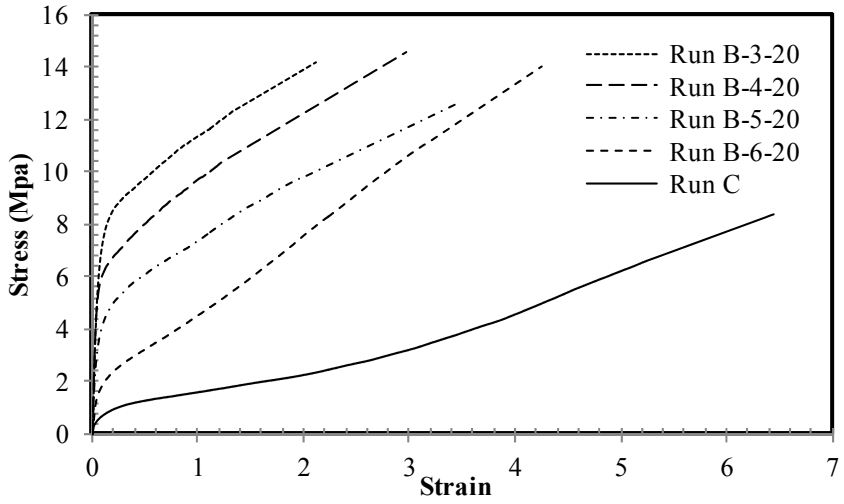

Fig. 4.9. The stress-strain behavior of the films processed at 200 °C from the composite latexes obtained from Series B and Run A-6-20, Run C is included as a reference.

The differences should be related to the microstructure of the poly(n-MLCM). The structure and phase transition behavior of n-MLCM homopolymers were studied comprehensively by combination of DSC, polarized light microscopy, and small and wide angle X-ray scattering measurements in Chapter 3. The results, which are imparted by the X-ray scattering results of the composite latexes presented in this chapter suggested that at room temperature, homopolymers of n-MLCM had a monolayer smectic **E** (Smectic **E** or **C** for poly(4-MLCM)) crystal structure. In smectic **E**, the molecules are arranged into a orthorrombic structure within the layer and in smectic **C**, the director of each layed is inclined to the layer normal [27]. The graphical layered structures of poly(n-MLCM) is shown in Figure 4.10. The polymer backbone, the flexible spacer and the terminal tail of the monomer units remain in amorphous state and the mesogenic groups formed a highly ordered structure. The highly ordered structure of mesogenic groups is rigid and reinforced the mechanical properties. On the other hand, the flexible spacers and the terminal tails had a plasticizing effect. Therefore, the poly(n-MLCM) domains can be considered as a composite formed by chemically linked hard and soft subdomains and the longer the spacer the less rigid is the domain leading to lower Young´s modulus and higher elongation at break of the whole composite. This is a new two-scale multicomposite that has more degrees of freedom to fine tune the mechanical properties of the films.

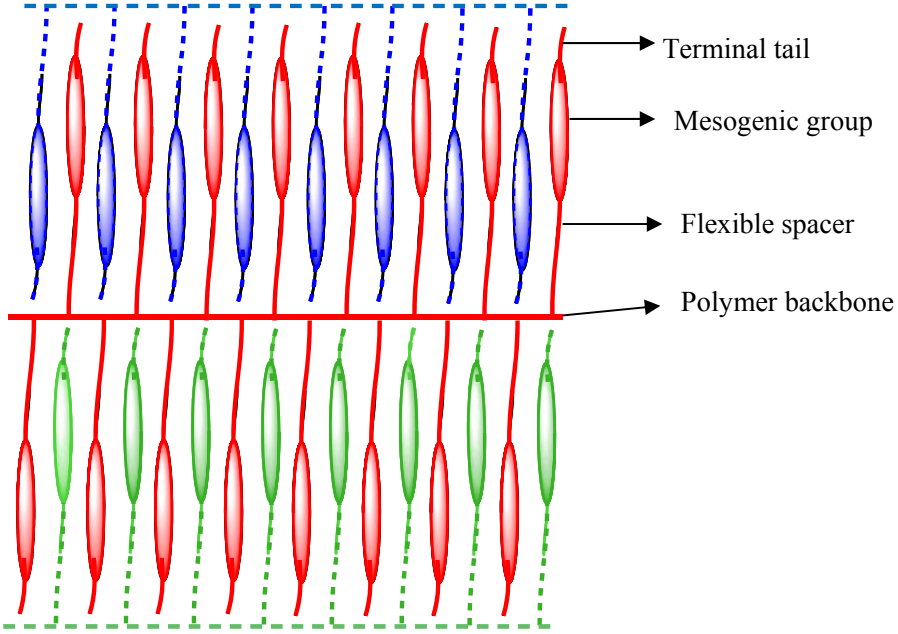

Fig. 4.10. The proposed smectic liquid crystalline structure of poly(n-MLCM) based on the XR-study (Chapter 3). The mesogenic group and continuous lines (red color) mean that the represented moiety is in a plane toward the reader, while moieties displayed by ellipses and dashed lines (in blue and green) lye on a plane behind. Different colors also correspond to different chains.

Table 4.5 presents the water vapor transmission rates (WVTR) of the films processed at 200 °C from the n-MLCM/SC(M)A=20/80 composite latexes (the amorphous Run C is included as a reference). The results show that the WVTRs of the films containing n-MLCMs was substantially lower than that of the amorphous copolymer of SC(M)A (Run C). The liquid crystalline domains of poly(n-MLCM)

acted as a barrier for water vapor and increase the tortuosity of the diffusion path reducing the diffusion rate. Moreover, for the samples containing n-MLCMs, the acrylic acid content is lower, which lowered the water sensitivity of the films in comparison with the amorphous copolymer in Run C [28].

Table 4.5. Results of the water vapor transmission rate (WVTR) of the films processed at 200 °C.

Run	**n-MLCM/SC(M)A**[a] **(wt/wt)**	**WVTR ($g.mm/m^2.day$)**
A-6-20	20/80	8.9 ± 0.7
B-5-20	20/80	9.0 ± 0.8
B-4-20	20/80	7.7 ± 0.5
B-3-20	20/80	8.2 ± 0.6
C	0/100	15.2 ± 2.6

[a] SC(M)A: MMA/BA/AA=49/49/2 wt%.

Figure 4.11 presents the results of the liquid water uptake measurements for the both films cast at 23 °C and the films processed at 200 °C from the n-MLCM/SC(M)A latexes. It can be seen that the liquid water uptake of the films containing liquid crystalline domains was substantially lower than that of the fully amorphous film for the both 23 °C and 200 °C. Moreover, the water uptake of the films containing poly(n-MLCM) showed a plateau after 2-3 days immersed in water, but the water uptake of the amourphous SC(M)A copolymer continuously increased

for the whole period in which it was monitored (10-11 days). In addition, it can be seen that the water uptake seemed to increase with the length of the spacer likely due to the plasticizing effect of the spacer. On the other hand, the comparison of the liquid water uptake of the films cast at 23 °C and the films processed at 200 °C shows that the water uptake of the films processed at 200 °C is lower than that of the films cast at 23 °C. The main reason for the lower water uptake of the films processed at 200 °C can be attributed to the better particle coalescence and high film quality.

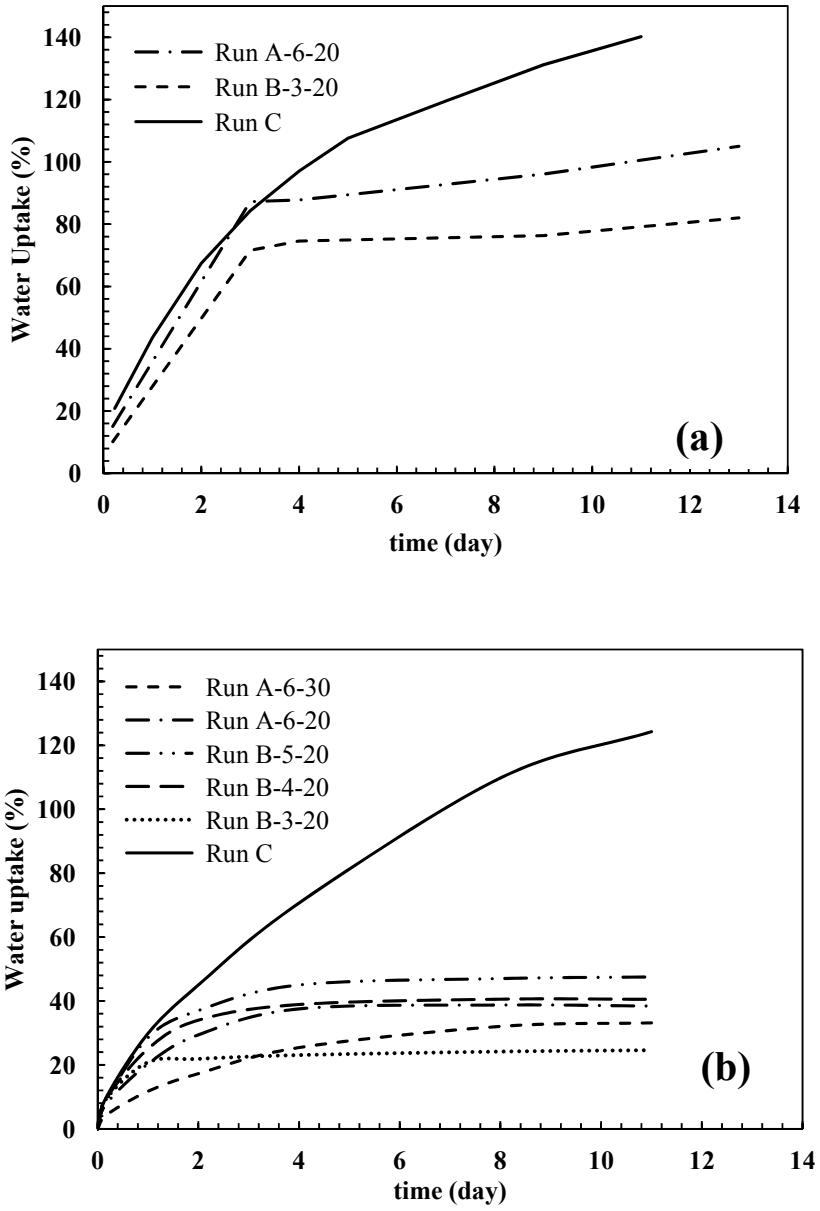

Fig. 4.11. The liquid water uptake measurement of the (a) films cast at 23 °C and (b) the films processed at 200 °C.

4.4. Comparison crystalline and liquid crystalline polymers

It has been shown that the incorporation of crystalline domains of poly(stearyl acrylate) (poly(SA)) in an amorphous (meth)acrylate polymer matrix improved the mechanical and barrier properties, and water sensitivity of amorphous (meth)acrylate polymers. However, the temperature range of applications is expected to be limited to the melting point of the crystalline domains which is only 50 °C (Chapter 2). The incorporation of LCPs with higher melting point can expand the temperature range of application. In this part the performance of (meth)acrylate copolymer films containing poly(SA) or poly(6-MLCM) is compared.

Figure 4.12 presents the tensile properties at 23 °C and 55% relative humidity of the processed film at 200 °C from Run A-6-20 and the semicrystalline latex containing 20 wt% poly(SA) (latex 6D in Chapter 2). It is worth mentioning that for the comparison the film from latex 6D was also processed at 200 °C. It can be seen that at 23 °C the Young´s modulus and the yield stress of the film containing poly(SA) domains was slightly higher than those of the film containing poly(6-MLCM) whereas the ultimate strength, elongation at break and toughness of the film containing poly(6-MLCM) were slightly higher (Figure 4.12(a)). On the other hand, when the tensile tests were carried out at 60 °C (>T_m of poly(SA)) the film containing

poly(SA) showed liquid-like behavior and no elastic region was detected, whereas the film containing poly(6-MLCM) resisted against deformation and the mechanical properties were substantially higher than those of the film containing poly(SA). It is noticeable that the elongation at break of these two films when tested at 60 °C was higher than the height of the oven used for the tensile test and the samples did not fail in the ultimate point marked with (*) in the curves.

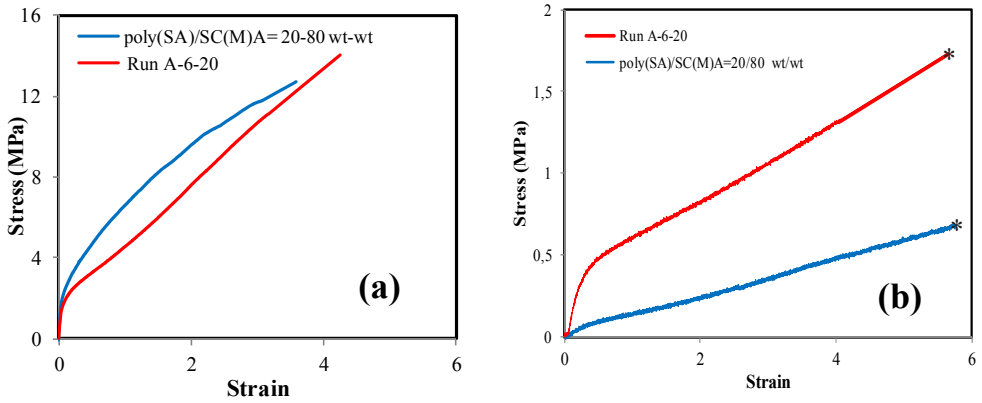

Fig. 4.12. The stress-strain behavior at (a) controlled condition (23 °C and 55% humidity), and (b) 60 °C, of the films processed at 200 °C from the latexes containing poly(SA) (Run 6D in Chapter 2) and poly(6-MLCM) (Run A-6-20).

The water uptake of films containing poly(SA) and poly(6-MLCM) are not directly comparable because these latexes were synthesized with different amounts of different surfactants. SDS (1 wt% based on monomer) and Dowfax 2A1 (3 wt% based on monomer) were used for poly(SA) and poly(6-MLCM) containing latexes,

respectively. The ratio of water uptake of the these films to the fully amorphous SC(M)A films with the same amount of surfactant can be a good estimation to evaluate the effect of these domains on the barrier and water sensivity of the films. The comparison results for the cast film at 23 °C from the latex A-6-20 and the latex 2D in Chapter 2 are summarized in Table 4.6. It can be seen that the water uptake of the film containing poly(SA) is slightly lower than the film containing poly(6-MLCM). Additionally, it is worth mentioning that the water uptake of the films containing liquid crystalline domains showed a plateau after 2-3 days immersed in water whereas the water uptake of the films containing poly(SA) continuously increased for the whole period in which it was monitored (20 days) (comparison of Figure 2.16 in Chapter 2 with Figure 4.11 in this Chapter).

Table 4.6. The comparison of water uptake of the films cast at 23 °C from the both latexes containing poly(SA) and poly(6-MLCM).

		Run A-6-20	**Run 6D**
Water uptake / water uptake $_{poly(SC(M)A)}$	4 days immersed	0.90	0.86
	9 days immersed	0.73	0.67

4.5. Conclusions

Waterborne polymer latexes containing liquid crystalline polymers (LCPs) have been synthesized by using 2-step miniemulsion polymerizations. In the first step, the seeds of LCPs were prepared by miniemulsion homopolymerization of a series of methacrylate side chain liquid crystalline monomers (n-MLCMs), which led to formation of liquid crystalline domains. The n-MLCMs contained a biphenyl mesogenic group, different spacer lengths, and a fixed tail in their side chain. The short side chain (meth)acrylates (SC(M)A (a mixture of methyl methacrylate (MMA), n-butyl acrylate (BA) and acrylic acid (AA), MMA/BA/AA=49/49/2 wt%) were fed semicontinuously for 3 h in the second step and copolymerized in the presence of n-MLCM homopolymer seeds. The effect of n-MLCM / SC(M)A ratio and the alkyl spacer lengths of n-MLCMs (n=3,4,5,6) on the properties of final latexes was investigated.

It was found that substantial secondary nucleation occurred during the second step of copolymerization in all experiments and the extent of this process decreased as the fraction of n-MLCM in the formulation increased. The combination of differential scanning calorimetry, polarized light microscopy and wide angle X-ray scattering showed that the LCPs were not perturbed by the amorphous polymer matrix. The LCPs showed mesomorphic behavior and their melting and clearing

transitions exhibit a distinct odd-even effect as the length and parity of the n-MLCM spacer was varied. The odd members exhibited the higher values.

The TEM micrographs of the particles showed a core-shell morphology with the liquid crystalline domains of n-MLCM homopolymer in the core. The TEM micrographs of the film cast at 23 °C showed a well dispersion of liquid crystalline domains in the film, but substantial coalescence of the LCPs occurred when the film was processed at 200 °C (i.e. above the melting temperature of poly(n-MLCM)).

It was observed that the presence of liquid crystalline domains reinforced the mechanical properties of amorphous SC(M)A copolymer. Moreover, the spacer of n-MLCMs had plasticizing effect on the n-MLCM/SC(M)A copolymer; the longer the spacer length, the higher the plasticizing effect.

The water vapor permeability and liquid water uptake of the copolymer films containing liquid crystalline domains were substantially lower than the fully amorphous copolymer of SC(M)A.

In addition, it was observed that the film preparation conditions strongly affected the mechanical, barrier and water resistance of the films. The mechanical and barrier properties as well as the water resistance of the films processed above the melting temperature of LCPs were higher than those of the films cast at 23 °C.

The comparison of the (meth)acrylate polymers containing both poly(stearyl acrylate) (poly(SA)) and poly(6-MLCM) showed that the mechanical properties of the films were almost the same when tested at 23 ° whereas the mechanical properties of the films containing poly(6-MLCM) was prominently higher than the films containing poly(SA) when the tensile tests were performed at 60 °C. Moreover, water uptake of the films containing poly(SA) was lower than the films containing poly(6-PMLCM).

4.6. References

[1] Finkelmann, H. and Rehage, G., 1984. Liquid crystal side chain polymers. In *Liquid Crystal Polymers II/III* (pp. 99-172). Springer Berlin Heidelberg.

[2] Finkelmann, H. *Angew Chem Int Edit*, 1987, *26,* 816-824.

[3] Hsu, C.S. *Prog polym sci*, 1997, *22,* 829-871.

[4] Wang, X. and Zhou, Q., 2004. *Liquid crystalline polymers*. World Scientific.

[5] Donald, A.M., Windle, A.H. and Hanna, S., 2006. *Liquid crystalline polymers*. Cambridge University Press.

[6] Lin, Q. and Yee, A.F. *Polymer*, 1994, 35, 3463-3469.

[7] O'Donnell, H.J. and Baird, D.G. *Polymer*, 1995, 36, 3113-3126.

[8] Kalkar, A.K., Deshpande, A.A. and Kulkarni, M.J. *J Appl Polym Sci,* 2007, 106, 34-45.

[9] Flodberg, G., Hellman, A., Hedenqvist, M.S., Sadiku, E.R. and Gedde, U.W. *Polym Eng Sci*, 2000, 40, 1969-1978.

[10] Flodberg, G., Höjvall, L., Hedenqvist, M.S., Sadiku, E.R. and Gedde, U.W. *Int J Polym Mater*, 2001, 49, 157-177.

[11] Flodberg, G., Hedenqvist, M.S. and Gedde, U.W. *Polym Eng Sci,* 2003, 43, 1044-1057.

[12] Jang, K.S., Johnson, J.C., Hegmann, T., Hegmann, E. and Korley, L.T. *Liq Cryst*, 2014, 41, 1473-1482.

[13] Li, G., Yin, J., Li, B., Zhuang, G., Yang, Y. and Nicolais, L. *Polym Eng Sci*, 1995, 35, 658-665.

[14] Smith, G.W. and Vaz, N.A. *Liq Cryst*, 1988, 3, 543-571.

[15] Kajiyama, T., Nagata, Y., Washizu, S. and Takayanagi, M. *J Membrane Sci*, 1982, 11, 39-52.

[16] Trongsatitkul, T., Aht-Ong, D. and Chinsirikul, W. *Macromol Sy*, 2004, 216, 265-280.

[17] Kanehashi, S., Kusakabe, A., Sato, S. and Nagai, K. *J Mater Sci*, 2010, 365, 40-51.

[18] Turek, D.E. and Simon, G.P. *Polymer*, 1993, 34, 2750-2762.
[19] Ogata, N., Tanaka, T., Ogihara, T., Yoshida, K., Kondou, Y., Hayashi, K. and Yoshida, N. *J Appl Polym Sci,* 1993, 48, 383-391.
[20] Lin, Q. and Yee, A.F. *Polym Composites*, 1994, 15, 156-162.

[21] Brostow, W. ed., 2013. *Mechanical and thermophysical properties of polymer liquid crystals* (Vol. 3). Springer Science & Business Media.

[22] Datta, A. and Baird, D.G. *Polymer*, 1995, 36, 505-514.

[23] Chen, D.S. and Jones, F.N. *J Appl Polym Sci*, 1989, 37, 1063-1078.

[24] Chiang, W.Y. and Yan, C.S. *J Appl Polym Sci*, 1992, 46, 1279-1290.

[25] Jones, F.N., Chen, D.S., Dimian, A.F. and Wang, D., North Dakota State University, 1993, U.S. Patent 5,218,045.

[26] Athawale, V.D. and Bailkeri, R.S. *Liq Cryst*, 2000, 27, 1021-1027.

[27] Ermakov, S., Nikolaev, V., Beletskii, A. and Eismont, O., 2016. *Liquid Crystals in Biotribology*. Springer.

[28] Reyes-Mercado, Y., Vázquez, F., Rodríguez-Gómez, F.J. and Duda, Y. *Colloid Polym Sci*, 2008, 286, 603-609.

Chapter 5. Performance of Waterborne Semicrystalline Latexes in Coating and Adhesive Applications

5.1. Introduction

The synthesis, characterization and properties of the waterborne (meth)acrylate dispersions containing crystalline domains for coating application have been reported in Chapter 2. In this chapter, the study was expanded to adhesive latexes and the performance of semicrystalline latexes in the both coating and adhesive applications are investigated.

This work was carried out at BASF SE, Ludwigshafen, Germany under the supervision of Dr. Bernd Reck using formulation slightly different from those used in Chapter 2. Therefore, the synthesis and characterization of the semicrystalline waterborne latexes used for the final applications is discussed briefly and then the study is focused on the evaluation of final applications of waterborne (meth)acrylate dispersions containing crystalline domains for both coating and adhesive applications.

The crystalline domains were produced in situ by polymerization of Octadecyl acrylate (commercially known as stearyl acrylate, SA). The composition of the SC(M)A monomer mixture was chosen for both coating and adhesive application. Methyl methacrylate (MMA), n-butyl acrylate (BA), acrylic acid (AA) and acrylamide (AM) were used as short monomers for coating application and 2-ethyl hexyl acrylate (2EHA), MMA and methacrylic acid (MAA) for adhesive application.

5.2. Experimental Section

5.2.1. Materials

Technical grade monomers, methyl methacrylate (MMA, BASF), n-butyl acrylate (BA, BASF), 2-ethylhexyl acrylate (2EHA, BASF), acrylamide (AM, BASF), methacrylic acid (MAA, BASF) and acrylic acid (AA, BASF), and stearyl acrylate (SA, Aldrich) were used without purification. Potassium persulfate (KPS, Fluka) as water soluble radical initiator, sodium bicarbonate ($NaHCO_3$, BASF) to control the miniemulsion viscosity by reducing the electrostatic interactions among droplets and Disponil FES32 (BASF) as anionic surfactants were used as received. Deionized water was used as polymerization media.

5.2.2. Experimental design

Tables 5.1-5.3 summarize the experimental design in which both the comonomer composition and the polymerization strategy were varied. The comonomer composition were from SA/SC(M)A = 0/100 to SA/SC(M)A = 40/60 wt/wt. The SC(M)A monomer composition in this study were MMA/BA/AA/AM= 49/49/1/1 wt% for coating application (Table 5.1) and 2EHA/MAA= 99/1 wt% (Table 5.2) and 2EHA/MMA/MAA= 84/15/1 wt% (Table 5.3) for adhesive application. The SA amount in copolymers was limited in order to be able to form films at room temperature for coating applications and tacky films for adhesive applications. Homopolymerization of SA was studied in Chapter 2 to prepare poly(stearyl acrylate) (poly(SA)) seeds which were used to synthesize SA/SC(M)A copolymers in seeded emulsion copolymerization. The latexes obtained without SA were used as reference to study the effect of incorporating crystalline domains in the particles. The SA was polymerized by miniemulsion polymerization in batch (Series A, Runs 1A and 1A´). The strategies used for the preparation of the SA/SC(M)A copolymers are summarized in Scheme 5.1. In Series C the latexes were prepared by first homopolymerizing a substantial part of SA (60% conversion) and then the pre-emulsion of SC(M)A monomers (SC(M)A monomers + water + surfactant) and initiator solution (KPS + water) were separately fed to the reactor during 3.5 h under

starved conditions (Series C of experiments, Runs 2C and 4C (Table 5.1), and Runs 2C″ and 3C″ (Table 5.3)). In this series, an amorphous copolymer of SA/SC(M)A is expected to be formed in the second stage of the process. In Series D, the seeds of poly(SA) (100 % conversion) were used as initial charge and then the pre-emulsion of SC(M)A monomers and initiator solution were fed to the reactor during 3.5 h in separated streams and copolymerization was carried out in the presence of poly(SA) homopolymer (Series D, Runs 1D-4D (Table 5.1), Runs 1D′-4D′ (Table 5.2) and 1D″-4D″ (Table 5.3)). The reference latexes, 1B, 1B′ and 1B″ that were devoid of SA, were synthesized in seeded semibatch emulsion polymerization by using polystyrene seeds (0.1 wt% based on monomer, particle diameter= 31 nm).

Blending also was used to prepare semicrystalline latexes for coating applications. Therefore, the amorphous SC(M)A copolymer latex (Run 1B) was mixed with poly(SA) latex (Run 1A) to obtain semicrystalline latexes with different copolymer composition and crystallinity (see Table 5.1).

Table 5.1. Summary of the synthesized copolymer latexes with different monomer composition and polymerization strategies (coating application).

	Series A	Series B	Series C	Series D	Blend[b]	SA/SC(M)A[a] (wt/wt)
Miniemulsion polymerization	1A	---	---	---	---	100/0
	---	---	4C	4D	Blend 4	40/60
	---	---	---	3D	---	30/70
	---	---	2C	2D	Blend 2	20/80
	---	---	---	1D	---	10/90
Emulsion polymerization	Semibatch seeded	1B	---	---	---	0/100

[a] SC(M)A: MMA/BA/AA/AM=49/49/1/1 wt%. [b] Blending Latex 1A and Latex 1B.

Table 5.2. Summary of the synthesized copolymer latexes with different monomer composition and polymerization strategies (adhesive application).

	Series A	Series B	Series C	Series D	SA/SC(M)A[a] (wt/wt)
Miniemulsion polymerization	1A´	---	---	---	100/0
	---	---	---	4D´	40/60
	---	---	---	3D´	30/70
	---	---	---	2D´	20/80
	---	---	---	1D´	10/90
Emulsion polymerization	Semibatch seeded	1B´	---	---	0/100

[a] SC(M)A: 2EHA/MAA=99/1 wt%.

Table 5.3. Summary of the synthesized copolymer latexes with different monomer composition and polymerization strategies (adhesive application).

	Series A	Series B	Series C	Series D	SA/SC(M)A[a] (wt/wt)
Miniemulsion polymerization	1A´	---	---	---	100/0
	---	---	---	4D″	40/60
	---	---	3C″	3D″	30/70
	---	---	2C″	2D″	20/80
	---	---	---	1D″	10/90
Emulsion polymerization	Semibatch seeded	1B″	---	---	0/100

[a] SC(M)A: 2EHA/MMA/MAA=84/15/1 wt%.

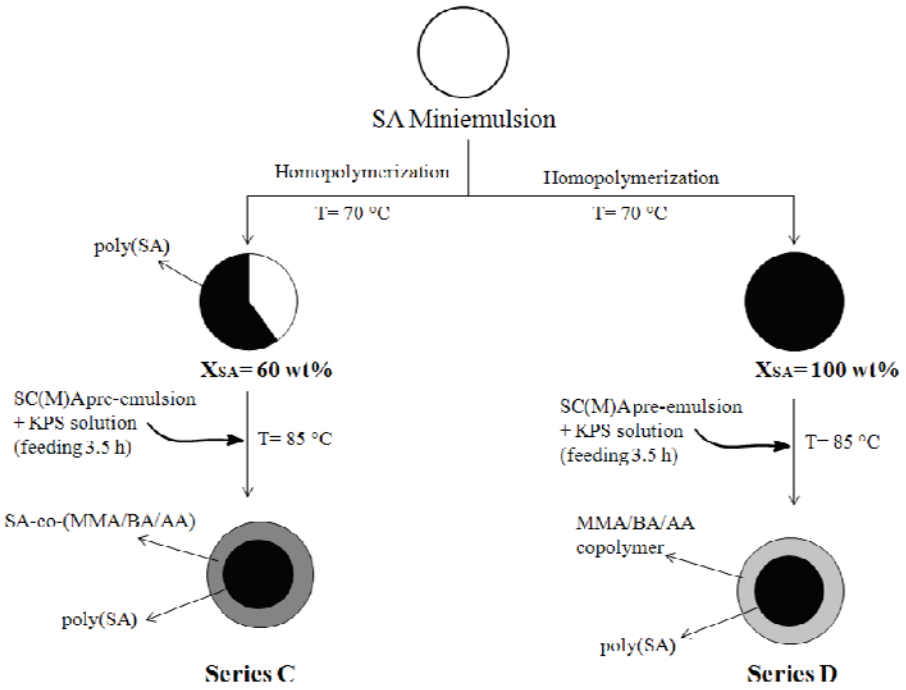

Scheme 5.1. Schematic representation of the synthesis of the SA-co-SC(M)A latexes.

5.2.3. SA miniemulsification and mini(emulsion) polymerization

For the preparation of SA miniemulsion, the SA pre-emulsions (the mixture of SA, $NaHCO_3$ (0.16 wt% based on SA), Disponil FES 32 and water) were prepared as described in Chapter 2. These coarse emulsions were sonicated by using a

Sonopuls HD 2070/2200 Sonifier (amplitude 100% and 100% duty cycle) over 20 minutes under magnetic stirring and in an ice bath to avoid overheating. Then, the miniemulsion was fed into a APV 2000 laboratory homogenizer, whose first valve was set to 600 bar and whose second valve was set to 60 bar. Two cycles were used to obtain stable and homogeneous SA miniemulsion.

In order to prepare stable SA miniemulsion and therefore poly(SA) miniemulsion latexes with desired droplet and particle sizes for coating and adhesive applications, different concentrations of Disponil FES 32 were used (see Table 5.4).

The miniemulsion and emulsion polymerizations were carried out in a 1L glass reactor vessel immersed in an oil bath and equipped with an anchor impeller, platinum resistance thermometer, condenser, two dosing systems, nitrogen inlet and sampling tube.

The poly(SA) seeds latexes (Series A) were synthesized in batch miniemulsion polymerization. Therefore, the SA miniemulsion was transferred to the reactor, purged with nitrogen and heated to the reaction temperature (70 ^{0}C). Then, the initiator (KPS, 0.5 wt% based on SA monomer) solution was added as a shot and the SA homopolymerization was carried out for 3 h.

The seeds of poly(SA) obtained in Series A were used in Series D to synthesize SA/SC(M)A copolymer latexes. Thus, the seeds of poly(SA) latex was transferred to the reactor as initial charge, purged with nitrogen and heated to the reaction temperature (85 ^{0}C). Then, the SC(M)A pre-emulsion (mixture of water, SC(M)A monomers and Disponi FES 32) and aqueous solution of initiator (0.5 wt% based on SC(M)A monomers) were fed to the reactor during 3.5 h in separated streams. Then, copolymerization was continued for 1 h.

In Series C, the SA miniemulsion was transferred to the reactor, purged with nitrogen and heated to the reaction temperature (70 ^{0}C). Then, the initiator solution (0.5 wt% KPS based on SA) solution was added as a shot and the SA homopolymerization was started. Once the desired SA monomer conversion was reached (X_{SA} = 60 wt%; at t ≈ 45 min after initiator injection), the SC(M)A pre-emulsion (mixture of water, SC(M)A monomers and Disponi FES 32) and the initiator solution (0.5 wt% based on SC(M)A monomers) were fed to the reactor during 3.5 h in separated streams. The copolymerization was continued for 1 h. Meantime, the reaction temperature increased to 85 ^{0}C after the first stage.

Seeded semicontinuous emulsion copolymerizations of SC(M)A monomers (Series B) were also carried out. The reactor was charged with the polystyrene seeds (particle diameter = 31 nm, 0.1 wt% based on monomer) and 20 wt% of water in the

formulation, purged with nitrogen and heated to the reaction temperature (85 ^{0}C). Then, the SC(M)A pre-emulsion (mixture of water, SC(M)A monomers and Disponi FES 32) and the initiator solution (0.5 wt% based on SC(M)A monomers) were fed to the reactor during 2.5 h in separated streams. Then copolymerization was continued for 1 h.

The organic phase content in all miniemulsion and emulsion polymerizations was 45 wt%.

5.2.4. Characterization

5.2.4.1. Characterization of copolymer latexes and films

Monomer droplet and particle sizes were measured by both dynamic light scattering (DLS) in a Zetasizer Nano Z (Malvern Instruments) and hydrodynamic chromatography (HDC) (Polymer Laboratories Particle Size Distribution Analyser (PL-PSDA)). The samples were prepared by dilution of the latex in distilled water. The values given from DLS are z-average values obtained through cumulants analysis and those from HDC are volume average.

Global and instantaneous monomer conversions were measured by the combination of gravimetry and ^{1}H NMR; the gel fraction and swelling degree were

measured by Soxhlet extraction, using THF as the solvent; the molecular weight distribution of the soluble fraction of polymers was determined by gel permeation chromatography (GPC); the thermal characterization of the polymer films were determined by differential scanning calorimetry (DSC); the morphology of latex particles and films was studied by means of transmission electron microscopy (TEM); the mechanical properties of the polymer films were determined by tensile tests. The detailed description of characterization methods is given in Chapter 2.

5.2.4.2. Characterization of Paints

The scrub resistance of the paints was determined by washability according to the ASTM D2486 standard test. The paint films (wet thickness = 180 μm) were applied to black plastic panels (Leneta, United States) and dried for one week at both 23 and 60 ºC. The coated panel was then scrubbed with a nylon bristle brush in an abrasive scrub medium (Leneta, United States) until the paint film was removed in three continuous thin lines across the shim. The number of back-and-forth strokes (cycles) required to remove the film over the shim is determined. The measurements were carried out in a Washability and Scrub Resistance Tester (Erichsen 494, Germany). The results reported were the average of 2-3 repeated measurements and the reproducibility was good.

Static contact angle (CA) measurements of the paint films were performed by the sessile drop method with distilled water, using a goniometer OCA 20 with a high-performance image processing system (Data Physics Instruments GmbH), in air under controlled environment (23°C and 55% humidity). The data presented are the average of 20-30 readings.

The hardness of the paint films were measured by pendulum hardness method according to ASTM D 4366. The pendulum hardness evaluates the hardness by measuring the damping time of an oscillation pendulum. The measurements provide information about the coating film resistance to dampen vibrations. The pendulum hardness of the paint films was tested by an Erichsen Pendulum Damping Tester, Model 299/300 (reference glass). The paint films (wet thickness = 250 μm) were applied to glass substrates and dried for one week at both 23 and 60 ºC. The paint films were tested under controlled environment (23°C and 55% humidity).

In term of visual appearance, gloss is one of the key features of paint. Gloss might vary from polymers to paints due to the incorporation of additives. The gloss of paints was measured with a BYK Micro-TRI-Gloss Meter at both 60 ° and 85 ° that are often used for semi-gloss and matte surfaces. The paint films were prepared in the same way as for the pendulum hardness test.

The rheology of the paints was measured using a MCR 102 rheometer (Anton Paar) with concentric cylinders geometry. This geometry is ideally suited for low viscosity fluids. Measurements were carried out at 25 °C by continuous increase of shear rate from 0.1 to 5000 s^{-1}.

5.2.4.3. Characterization of Adhesives

Adhesion Properties. The adhesive films used in the tests were formed by spreading the latex over a flame-treated polyethylene terephthalate (PET) sheet (29 μm thick) using a gap applicator with reservoir. The gap was adjustable in order to obtain films with the same thickness from the latexes with different solids content. The films were dried at both room temperature for 4 h and at 90 ºC (in a well ventilated oven) for 3 min.

The final dry film was around 55 μm thick. Finally, they were cut to make "tape strips" with the desired dimensions for each test. Peel resistance was determined by means of the 180° peel test [1]. In this test, a tape strip (4 cm × 2.5 cm) was applied to the stainless steel (SS) substrate using a given pressure (2 kg roller) to make the contact. The measurements were carried out after 20 minutes after the adhesive tape was attached to the substrate. The free end of the tape was clamped to the upper jaw of a Zwick/Roell tensile tester, which pulled the tape at an angle of

180° at a constant speed of 300 mm/min. The average force required to peel away the tape was recorded.

Shear resistance was assessed by the holding power shear test [2,3]. This test consisted of applying a standard area of tape (2.5 cm × 2.5 cm) on a stainless steel substrate under a load of 1 kg. The time to failure was recorded. The experiments were performed under different temperatures using a SAFT equipment (Sneep Industries).

To measure the tackiness of the adhesives, loop tack test were used. For performing the experiment, a PET film coated with the adhesive was folded to form a loop with the adhesive facing outwards. The ends of the loop were clamped for a distance of 10 mm into the top jaw of a Zwick/Roell testing machine leaving the loop hanging vertically downwards. The loop was positioned in contact with the surface (stainless steel, SS) at a speed of 300 mm/min till the obtaining of the full contact (2.5 cm x 2.5 cm) and then, the direction of the machine was immediately reversed and the separation between the loop and the substrate was carried out at 300 mm/min clam velocity [4,5]. The value of the loop tack was the maximum value of the peak and work of adhesion (the area under the peak) given by the equipment, averaged for two tests per latex. The type of detaching, adhesive (without any residue on the SS) or cohesive (with residues on the SS) was also recorded.

5.3. Results and discussions

5.3.1 SA miniemulsions and poly(SA) latexes

The summary of the SA miniemulsions and corresponding poly(SA) latexes with different solids content prepared by different concentrations of Disponil FES 32 are given in Table 5.4. It can be seen that the poly(SA) particle diameters are almost the same than those of the corresponding SA miniemulsion monomer droplets. Moreover, the droplet and particle diameters depended on the solids contents and the amount of surfactant used in miniemulsification process. Namely, with increasing surfactant concentration the droplet and final polymer particle diameters decreased. Moreover, the SA droplet and poly(SA) particle sizes increased with solids content.

In this study, the SA miniemulsion prepared with 35 % solids content and 2 wt% Disponil FES 32 (smaller particle size) was used to synthesize semicrystalline copolymer latexes for coating application and the one with 45 % solids content and 2 wt% Disponil FES 32 was used for adhesive application. The Disponil FES 32 concentration in the final coating latexes was 1.5 wt% and in the final adhesive latexes was 2 wt% based on the monomers. The final solids content of all latexes was 45 wt%.

Table 5.4. Summary of the poly(SA)latexes with different solids content obtained from different concentration of surfactant.

Surfactant	Chemical nature	[S] (wt%[a])	Solids content (wt%)	SA miniemulsion droplet diameter (nanosizer) (nm)	Poly(SA) particle diameter (nanosizer) (nm)
Disponil FES 32	Fatty alcohol ether sulfate + 4 EO[b], sodium salt	2	45	211	197 (170[c])
		2	35	187	175 (150[c])
		2	25	173	161
		3	45	195	170

[a]based on SA monomer; [b]EO: ethylene oxide; [c]measured by HDC.

5.3.2. Characterization and performance of semicrystalline acrylic based latexes for coating applications

The volume average particle diameter of the poly(SA) seeds and the Z average and volume average of final latexes for coating applications are given in Table 5.5. For the most of the latexes the HDC and DLS measurements are comparable. Moreover, it can be seen that in all series of experiments the final particle size decreased with increasing SA content. The reason was the increasing number of seed particles used as the SA content increased. Table 5.5 also includes the theoretical values of the final latexes in Series B, C and D assuming that there was neither coagulation nor secondary nucleation. Comparison with the actual sizes of the final latexes shows that secondary nucleation occurred during the second stage of polymerization in Runs 1B, 2C, 1D and 2D and that the extent of this process

decreased with increasing the number of seeds particles at the beginning of the second stage. The occurrence of secondary nucleation was comprehensively discussed in Chapter 2. The presence of small amorphous particles in the TEM micrographs of latex 2D (Figure 1) is an evidence of occurring secondary nucleation during the second stage of polymerization. Moreover, these micrographs show that the semicrystalline particles present a core-shell morphology with the dark poly(SA) domains in the core.

Table 5.5. Particle sizes of the latexes synthesized for coating application.

Run	SA/SC(M)A[a] (wt/wt)	Disponil FES32/ monomer (wt%)	Poly(SA) Particle size (HDC) (nm)	Final particle size (HDC) (nm)	Final Particle size (DLS) (nm)	Theoretical Particle size[b] (nm)
miniemulsion batch						
1A	100/0	2	150	150	175	----
seeds of poly(SA) (100% conversion) + 3.5 h addition of SC(M)A pre-emulsion and KPS solution						
4D	40/60	1.5	150	192	204	204
3D	30/70	1.5	150	206	215	224
2D	20/80	1.5	150	233	230	253
1D	10/90	1.5	150	279	260	323
batch miniemulsion of SA (60% conversion) + 3.5 h addition of SC(M)A pre-emulsion and KPS solution						
4C	40/60	1.5	150	190	202	204
2C	20/80	1.5	150	226	230	253
seeded emulsion copolymerization						
1B	0/100	1.5	31[c]	284	262	310

[a] SC(M)A: MMA/BA/AA/AM=49/49/1/1 wt%; [b] without secondary nucleation and coagulations; [c] Polystyrene seeds= 0.1 wt% based on monomer.

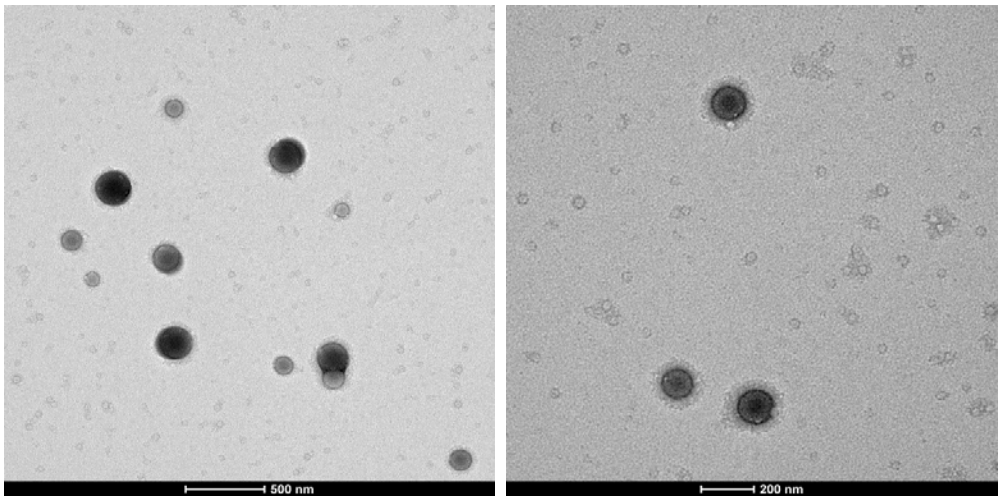

Fig. 5.1. The TEM micrograph of synthesized latex in Run 2D.

The monomer ratio and copolymerization strategies affected copolymer microstructure. The polymer architecture was characterized in terms of the gel fraction, the swelling ratio and the sol molecular weights. Figure 5.2 presents the gel fraction of the latexes synthesized for coating application (Runs in Table 5.1). The gel content in the latex obtained by seeded emulsion polymerizations of SC(M)A monomers (Run 1B) is 30 %. The same amount of gel also was measured in emulsion polymerization of SC(M)A carried out under the same conditions of Run 1B, but in the absence of seeds (the latex particle diameter = 250 nm). This amount of gel is in agreement with the results of Aguirreurreta et al [6] who recently reported 20-25 wt% gel content for latexes of MMA/BA/MAA=49.5/49.5/1 wt% synthesized

by seeded emulsion polymerization using SDS and Dowfax 2A1 as anionic surfactants. However, these amounts of gel are in conflict with other the results reported in Chapter 2, where no gel was detected in the emulsion polymerization of MMA/BA/AA=49/49/2 wt% (Run 2E, Table 2.1). They are also in conflict with other work that was carried out in our group. Gonzalez et al. [7] studied the effect of MMA composition on the gel polymer produced in the seeded semi-batch emulsion copolymerization of MMA/BA/MAA, reporting that the gel content decreased as the amount of MMA increased and the gel content for a 50/50 wt% MMA/BA copolymer at was negligible. This is puzzling because all these data were obtained in our lab using the same characterization procedure. A possible explanation is the effect of the particle size. The particles diameters were 67 nm (Chapter 2, no gel); 150 nm ([7], no gel); 250 nm (this chapter, gel) and ≥300 nm ([6], gel). A possible explanation is that for smaller particle sizes the number of radicals per article was small (0 – 1 system) and that termination occurred only between the short entry radicals and the long radicals in the particles. Under these circumstances, it is difficult to form gel. Therefore, the gel obtained from latex 1B most probably was due to the larger particle size (particle diameter = 260 nm) that led to a higher average number of radicals per particles, and consequently to the termination by combination of branched growing radicals.

In addition, Figure 5.2 shows that the overall gel fraction of latexes containing SA increased with the SA content in Series C and D. The gel fraction in latex 1A, i.e. in a fully converted SA homopolymer; was 76 wt%. A simple calculation shows that the gel content of the latexes in Series D is 10-12 wt% higher than the value expected by blending latexes 1B and 1A. Therefore, gel was produced during the second stage of this series. It is unlikely that this additional gel was formed by copolymerization of the short chain monomers because the size of the particles (and hence the average number of radicals per particle) decreased with the SA content. Most probably the second stage copolymers grafted on the poly(SA), presumably through hydrogen abstraction (transfer to polymer). On the other hand, Figure 5.2 shows that the gel fraction of the copolymers obtained in Series D were higher than those of Series C. The reason is the higher gel fraction of the SA homopolymer (100% conversion) used as initial charge in Series D. In Series C, the gel fraction of SA homopolymer formed in the first stage (60% conversion) should be likely lower because in batch polymerization of acrylic monomers, the gel is formed during the last parts of the process [8,9]. Moreover, the higher amount of poly(SA) at the beginning of second stage in Series D increased the probability of having chain transfer to polymer and higher final gel. The increase of the amount of gel produced during the second stage with the SA content in Series D was due to the more likely the intermolecular chain transfer to polymer. The swelling measurement carried out using THF as solvent and

given in Figure 5.2 show that swelling decreased with increasing gel content, namely the crosslinking density increased with the gel content.

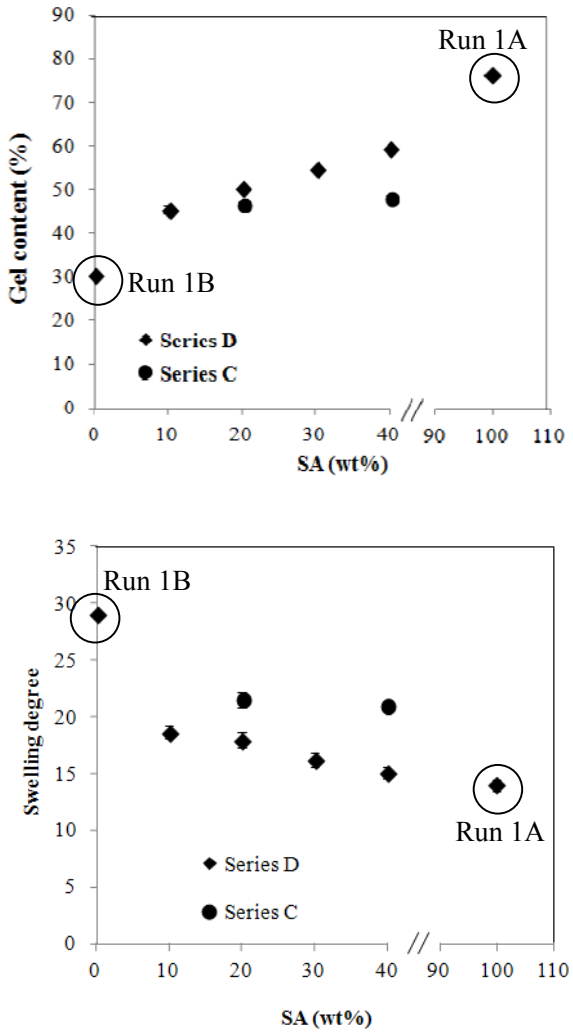

Fig. 5.2. The evolution of gel fraction and swelling ratio for the copolymers in Series A, B, C and D (coating application, Runs in Table 5.1).

The weight-average molecular weight and the dispersity (Đ) for the soluble part of the latexes synthesized for coating application is presented in Table 5.6. As can be seen, the average molecular weights of the sol copolymers of latexes in Series D (with higher gel fraction) are lower than the latexes with lower gel fraction (Series C and B). In addition, within Series D the sol molecular weight decreased with the gel content. The reason was that long polymer chains are preferently incorporated to the gel.

Table 5.6. The weight-average molecular weight and the dispersity (Đ) for the soluble part of the copolymers for coating applications (Runs in Table 5.1).

Run	SA/SC(M)A[a] (wt/wt)	Mw, Soluble Part (g/mol)	Đ
batch miniemulsion			
1A	100/0	368000	3.7
seeds of poly(SA) (100% conversion) + 3.5 h addition of SC(M)A pre-emulsion and KPS solution			
4D	40/60	219000	3.5
3D	30/70	240000	3.5
2D	20/80	257000	3.5
1D	10/90	304000	3.6
batch miniemulsion of SA (60% conversion) + 3.5 h addition of SC(M)A pre-emulsion and KPS solution			
4C	40/60	300000	4.1
2C	20/80	313000	3.7
seeded emulsion copolymerization			
1B	0/100	357000	4.1

[a] SC(M)A: MMA/BA/AA/AM=49/49/1/1 wt%.

Figure 5.3 presents the second DSC scans of the SA homopolymer (Run 1A) and copolymers synthesized in Series D (Runs 1D-4D, Table 5.1). The DSC of poly(SA) shows an endothermic peak at 51 °C and the DSC traces of the copolymers contain one endothermic peak corresponding to pure poly(SA) and hence decreasing with its content; and a second order transition, which has been assigned as a glass transition.

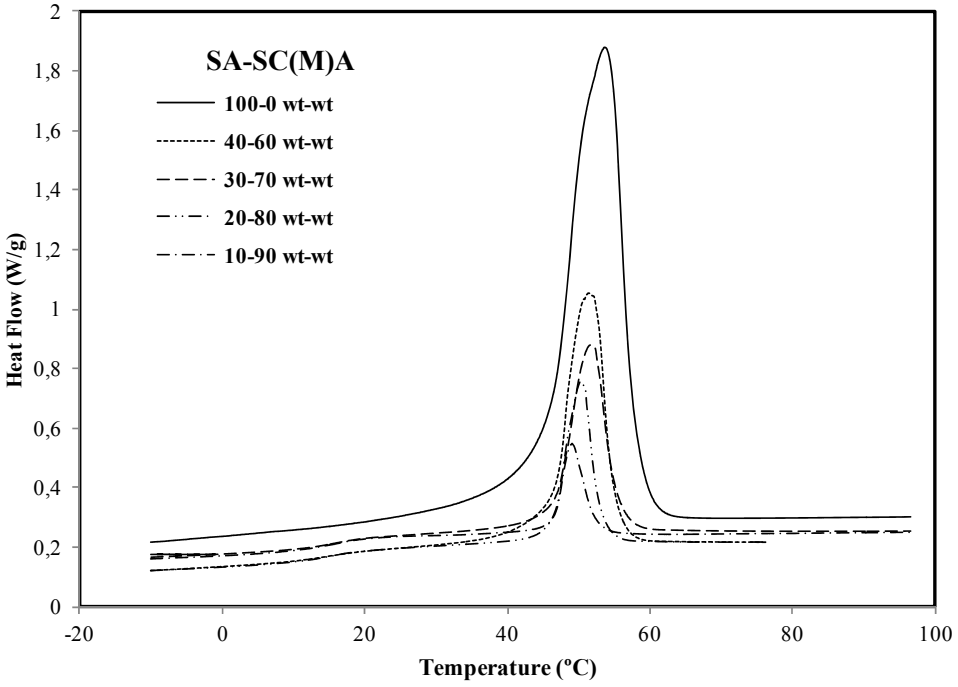

Fig. 5.3. Second heating DSC scans for the synthesized copolymers of SA/SC(M)A with different monomer composition (Series D in Table 5.1).

Melting temperature, heat of fusion, crystallinity degree and the glass transition temperature of the synthesized latexes as well as those of the blends for coating applications (Runs in Table 5.1) are given in Table 5.7. It can be seen that the crystallinity of the blends are the same of the synthesized latexes with the same monomer composition in Series D. The effect of polymerization strategy on the crystallinity and the T_g of cololymer latexes comprehensively discussed in chapter 2 and is not repeated here.

Table 5.7. Composition, crystallinity properties and glass transition temperature for copolymer latexes (coating application, Runs in Table 5.1).

Run	SA/SC(M)A[a] (wt/wt)	Crystallinity properties			T_g (^{0}C)
		T_m (^{0}C)	ΔH_f (J/g)	Xc[b] (%)	
batch miniemulsion					
1A	100/0	51	91.9	41.8	-116.0
seeds of poly(SA) (100% conversion) + 3.5 h addition of SC(M)A pre-emulsion and KPS solution					
4D	40/60	51	33.4	15.2	15.0
3D	30/70	51	23.5	10.7	16.1
2D	20/80	50	14.8	6.7	15.8
1D	10/90	49	7.5	3.4	16.9
batch miniemulsion of SA (60% conversion) + 3.5 h addition of SC(M)A pre-emulsion and KPS solution					
4C	40/60	51	21.3	9.7	13.8
2C	20/80	50	9.1	4.1	13.6
Seeded emulsion copolymerization					
1B	0/100	----	----	----	15.1
blending of 1A and 1B latexes					
Blend 4	40/60	51	23.5	10.7	15.0
Blend 2	20/80	51	14.9	6.7	15.0

[a]SC(M)A: MMA/BA/AA/AM=49/49/1/1 wt%; [b]referred to the whole polymer.

The mechanical properties of the films cast from Series C and D, as well as those of the amorphous SC(M)A copolymer (1B latex) and the blends (Blend 2 and Blend 4) are summarized in Table 5.8. Figure 5.4 shows the stress-strain curves for Series D and Run 1B. It can be seen that in Series D, Young's modulus (the slope obtained at low strains), yield stress, and ultimate strength increased and the elongation at break point decreased when the content of SA and crystallinity in the latex increased. Moreover, the Young's modulus and the yield stress of latex 1D (10 wt% of SA) is lower than those of the amorphous SC(M)A copolymer (Run 1B). The effect of crystallinity and copolymer composition on the mechanical properties of semicrystalline latexes was comprehensively discussed in Chapter 2 and is not repeated here.

Table 5.8. Mechanical properties of the films.

Run	SA/SC(M)A[a] (wt/wt)	Young´s Modulus $\times 10^{-2}$ (MPa)	Yield Stress (MPa)	Toughness $\times 10^{-6}$ ($J \cdot m^{-3}$)	Elongation @ Break $\times 10^{-2}$ (%)	Ultimate Strength (MPa)
seeds of poly(SA) (100% conversion) + 3.5 h addition of SC(M)A pre-emulsion and KPS solution						
4D	40/60	1.33±0.16	4.81±0.33	18.52±2.10	1.93±0.13	12.60±0.83
3D	30/70	0.99±0.12	1.40±0.16	20.24±1.72	2.70±0.20	11.75±1.2
2D	20/80	0.70±0.06	1.16±0.11	24.10±2.31	3.80±0.18	11.20±0.86
1D	10/90	0.31±0.04	0.35±0.07	22.79±2.20	4.19±0.31	11.01±1.02
batch miniemulsion of SA (60% conversion) + 3.5 h addition of SC(M)A pre-emulsion and KPS solution						
4C	40/60	0.47±0.03	3.39±0.18	12.59±1.40	2.02±0.20	8.30±0.4
2C	20/80	0.16±0.06	0.43±0.07	17.78±1.81	5.01±0.31	6.61±0.25
Seeded emulsion copolymerization						
1B	0/100	0.57±0.04	0.54±0.09	23.22±2.15	5.50±0.85	9.09±0.87
Blends from Run 1A and Run 1B latexes						
Blend4	40/60	0.97±0.05	4.65±0.31	13.30±1.27	2.03±0.34	7.83±0.65
Blen2	20/80	0.67±0.03	1.43±0.09	21.95±2.64	4.37±0.44	7.76±1.26

[a] SC(M)A: MMA/BA/AA/AM=49/49/1/1 wt%.

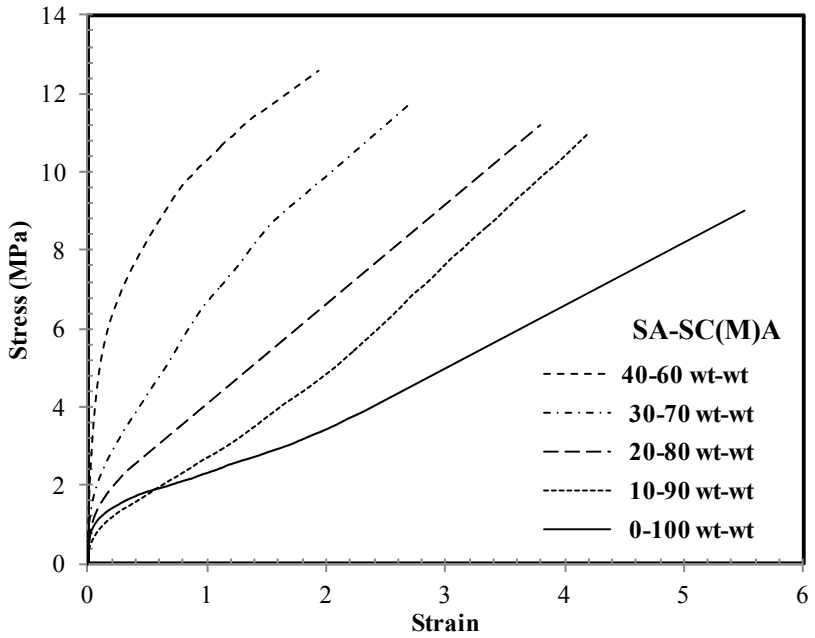

Fig. 5.4. The stress-strain behavior of copolymers obtained from Series D as well as Run 1B (Table 5.1).

The stress-strain behavior of the films of the same monomer composition (SA/SC(M)A =20-80 wt/wt) synthesized using different strategies (Runs 2C and 2D, Table 5.11) and also by blending the poly(SA) and SC(M)A latexes (Blends 2, Table 5.1) is presented in Figure 5.5. This figure shows that the mechanical properties of the latexes in Series D and blend sample were better than for Series C. The lower mechanical properties of the films in Series C can be related to lower crystallinity (see Table 5.7) and also to the presence of amorphous poly(SA) and SA/SC(M)A

copolymers in the polymer matrix. These amorphous polymers led to a decrease of the T_g and the mechanical properties. In addition, Figure 5.5 shows that the Young´s modulus, yield stress and elongation at break point of Blend 2 were higher than these of 2D. However, ultimate strength and strain hardening (the slope obtained in the plastic region) of 2D were higher. The difference in mechanical properties of Series D latexes and physically blended samples may be attributed to the grafting of SC(M)A copolymer on the poly(SA) homopolymer in Series D. The grafting of SC(M)A on the poly(SA) in Series D latexes resisted against deformation and increased the strain hardening and ultimate strength of copolymer films. Moreover, it must be considered that the samples were dried at 60 °C (above melting point of poly(SA)) and hence the phase separation between the poly(SA) and SC(M)A copolymer that has already been reported for the same copolymer systems in Chapter 2 could be worse in blend samples, where there is not grafting between poly(SA) and the SC(M) copolymer and this higher phase separation would be expected to affect the mechanical properties. Figure 5.6 presents the TEM micrographs of cross-section of the film cast at 60 ºC from latexes 2D and Blend 2. It can be seen that the phase separation between poly(SA) (black domains) and SC(M)A copolymer in Blend 2 was substantially higher than for latex 2D, which led to the heterogeneous distribution of bigger poly(SA) domains in the SC(M)A copolymer matrix.

These results indicate that the introduction of poly(SA) crystalline domains to amorphous (meth)acrylate copolymer matrix reinforced the mechanical properties (improved Young´s modulus, yield stress and ultimate strength). Conversely, the presence of the amorphous SA/SC(M)A copolymer and the amorphous part of poly(SA) lowered the mechanical properties.

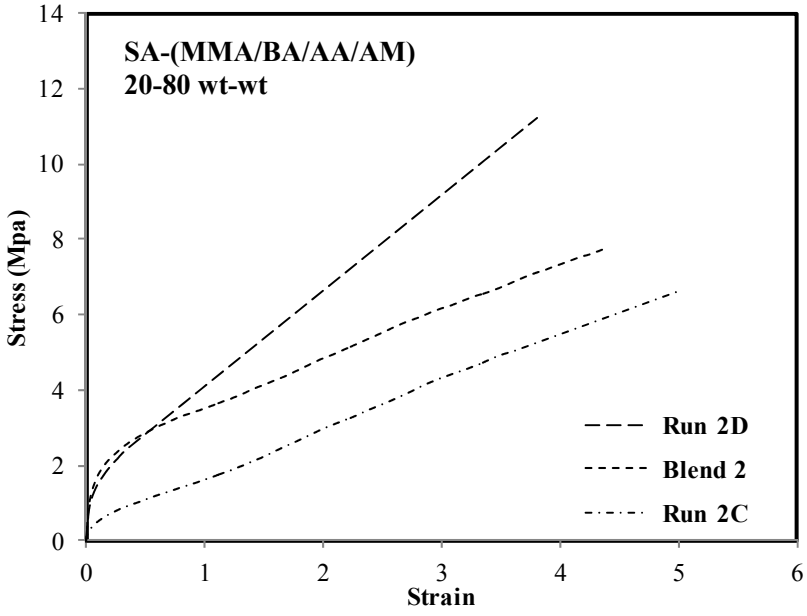

Fig.5.5. The stress-strain behavior of the latexes with the same monomer composition in Series C and D as well as blend sample (Runs 2C and 2D and Blend 2).

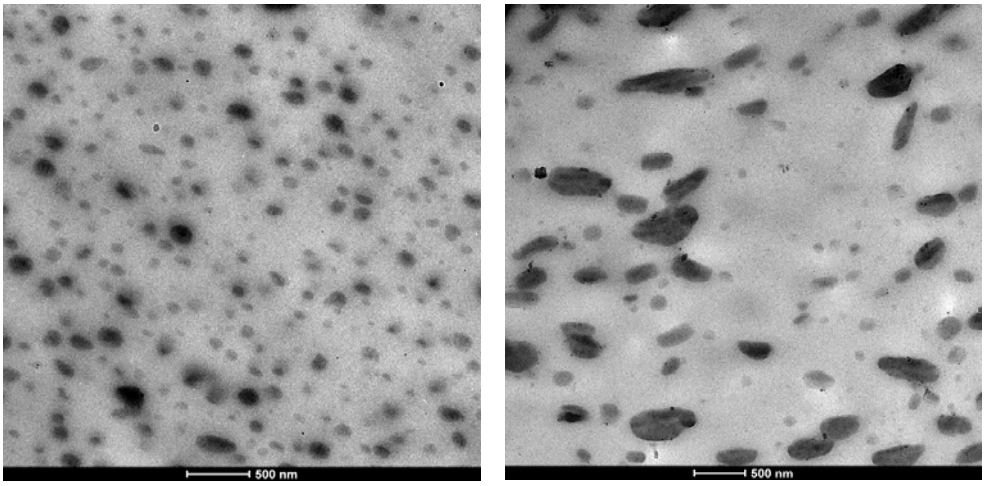

Fig. 5.6. TEM micrographs of cross-section of films cast at 60 ºC from the latexes 2D (left) and Blend 2 (right).

5.3.2.1. Incorporation of semicrystalline SA/SC(M)A copolymers as binders in paint formulations

Solventborne paints contain high levels of volatile organic compounds (VOC) and have been traditionally used on wood and metal surfaces, providing a high gloss finish but long drying times and strong odor [10]. In contrast, waterborne paints have faster drying times and lower level of VOCs. Because of government regulations the paint industry has dramatically reduced the environmental impact of paints by switching from solventborne to waterborne paints.

Generally, waterborne paint formulations contain polymer latexes as binders to hold the film together and supply coating integrity, pigments that provide the paint with color and covering power, thickeners that are viscosity modifiers to achieve a good pseudoplastic behavior, wetting agents and dispersants. Wetting agents are surfactants which reduce the surface tension of the coating facilitating substrate wetting and also aid pigment particles to be wet by the binder. Dispersants prevent flocculation of the pigment particles [10].

The polymer latex accounts for about the 50 % of the total weight and in large extent governs the properties of the coating. Therefore, the choice of the binder is of paramount importance. The use of conventional acrylic polymers as binders have been extensively exploited in paints because they provide the coating with good properties such as good exterior durability, UV stability, film clarity, and heat and alkali resistance [10]. The presence of crystalline domains in the polymer particles of binder may improve the barrier, water sensivity and mechanical properties of waterborne paints.

The objective of this part was focused on the use of the SA/SC(M)A copolymer latexes as binders in paint formulation.

5.3.2.1.1. Latexes used to formulate the paints

The latexes of Series B, C and D and also two blends from the latexes 1A and 1B (Runs in Table 5.1) were used to prepare the paints. A commercial standard latex (Acronal A754, BASF) for exterior paint applications was used for comparison purposes.

5.3.2.1.2. Preparation of waterborne paints

The waterborne paints were prepared by using a standard formulation for exterior coatings (RV 436 m. N40, BASF) in a two step process using the formulation in Table 5.10. First of all, the mill base (formulation in Table 5.9) was prepared by mixing the dispersant (Dispex AA 4140 NS, BASF), thickener (Natrosol 250 HR, BASF), defoamer (Foamaster MO 2134, BASF), freeze-thaw stabilizer (propylene glycol, butyl diglycol, both from BASF), coalescent agent (texanol, BASF) and water while stirring at about 400 rpm using a high speed disperser blade (DISPERMAT® LC30). The pigment (Kronos 2190 (TiO2), Kronos, Inc) and fillers (Omyacarb 5 GU (CaCO3), Omya; and Finntalc M15, Mondo Mineral, Inc) were then added slowly at 2000 rpm. Then, the mixing continued for 15 min. Finally, the polymer latex, the defoamer (Foamaster MO 2134, BASF) and the rheology modifier (Rheovis PE 1330, BASF) were incorporated to the mill base and mixed at 1000 rpm

for 10 min. An important point in paint preparation is that the pH of copolymer latex should be around 8 to prevent the coagulation of latex during incorporation to the mill base.

Table 5.9. Mill base formulation.

Ingredient	Name	Amount (g)	wt%
Water		184.6	29.00
	Ammonia,	2	0.31
Thickener	Natrosol 250 HR	2	0.31
Dispersing agent	Dispex AA 4140	1.43	0.22
Defoamer	Foamaster MO 2134	2	0.31
Freeze-thaw stabilizer	Propylene glycol	10	1.57
	Butyl diglycol	10	1.57
Coalescent agent	Texanol	5	0.78
Pigment	Kronos 2190	190	29.83
Filler	Omyacarb 5 GU	180	28.25
Filler	Finntalc M15	50	7.85

Table 5.10. Waterborne paint formulation.

Ingredient	Name	Amount (g)	vol (%)
Mill base		159.25	43.91
Defoamer	Foamaster MO 2134	0.75	0.54
Rheology modifier	Rheovis PE 1330	1.00	0.62
Polymer latex		89.00	54.93
Paint weight solids (wt%)			58.01
Paint volume solids (vt%)			68.54
Pigment Volume Content (PVC) (%)			66.16

The pigment volume content (PVC) of paints is essentially the volume fraction of pigment and filler in the total volume of paint. It is calculated by Equation 5.1, where "volume of pigment and filler" accounts for the amount of pigments and fillers. The paint volume solids (vt%) is given by the ratio between volume of polymer latex binder and the volume of pigment and filler (Equation 5.2).

$$PVC\ \% = \frac{volume\ of\ (pigment+filler)}{volume\ of\ binder+\ volume\ of\ (pigment+filler)} \times 100 \qquad (5.1)$$

$$vt(\%) = \frac{volume\ of\ binder + volume\ of(\ pigment + filler)}{total\ volume} \times 100 \qquad (5.2)$$

Table 5.10 presents the PVC, paint weight and volume solids of the paints.

5.3.2.1.3. Characterization and properties of the waterborne paints

The paints were dried in both controlled environment (23 °C and 55% humidity) and at 60 °C.

The DSC scans of the paint films formulated from semicrystalline latexes in Series D are shown in Figure 5.7. It can be seen that the DSC traces contain one endothermic peak around 44 to 49 °C corresponding to crystalline domains of poly(SA), and a second order transition, which has been assigned as a glass transition. Melting temperature, heat of fusion, crystallinity degree and the glass transition temperature of the paints are summarized in Table 5.1.

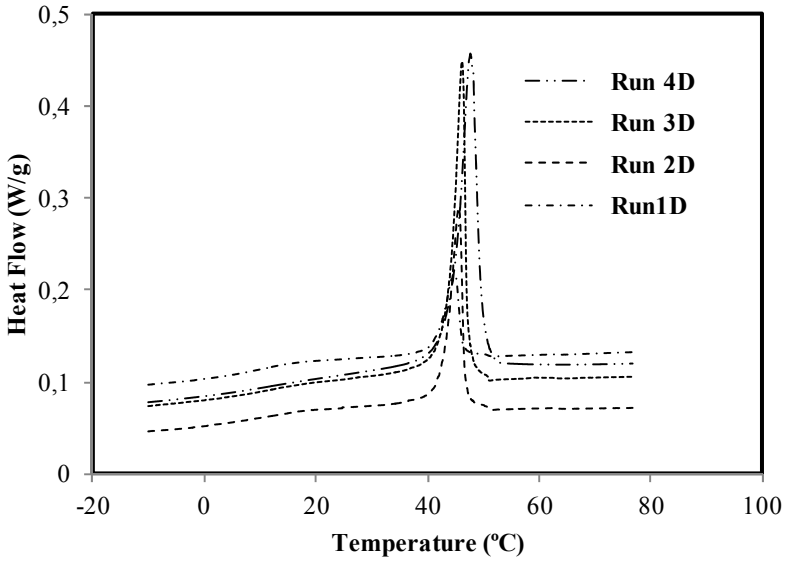

Fig. 5.7. The second heating DSC scan of the paint films formulated from Series D latexes (Runs 1D-4D, Table 5.1).

Table 5.11. Crystallinity properties and glass transition temperature of paints formulated from latexes.

Binder	Crystallinity properties			T_g (^{0}C)
	T_m (^{0}C)	ΔH_f (J/g)	Xc[a] (%)	
4D	48	8.3	3.7	12.0
3D	46	6.2	2.8	12.3
2D	46	3.8	1.7	15.3
1D	45	1.9	0.8	12.4
4C	47	4.8	2.2	13.4
2C	46	2.4	1.0	8.6
1B	----	----	----	7.0

[a] referred to the whole sample.

The tensile properties of the paints produced from Series D and Run 1B as well as from the commercial latex (paint films cast at 60 °C in silicon molds, film thickness = 500 μm) are shown in Figure 5.8(a). Moreover, the tensile properties of the paints formulated by using latexes with the same monomer composition (SA/SC(M)A =20-80 wt/wt) synthesized using different strategies (Runs 2C and 2D) and Blend 2 are presented in Figure 5.8(b). The mechanical properties of all the paint films are summarized in Table 5.12. Figure 8(a) and Table 5.12 show that the Young´s modulus, yield stress and ultimate strength increased with SA content and crystallinity in Series D. However, the elongation at break decreased. Moreover, the paint formulated with the amorphous 1B latex as well as with commercial latex had higher elongation at break than the semicrystalline paints. In addition, Figure 5.8(b) shows that the elongation at break of the paint from latex 2C with lower crystallinity is higher than for the paints of Run 2D and Blend 2. However, the Young´s modulus, yield stress and ultimate strength in Run 2C are lower. Therefore, it can be concluded that the crystalline domains of poly(SA) increase the stiffness and hardness of paint films. Conversely the amorphous domains of poly(SA) and SA/SC(M)A copolymer with low T_g decrease the stiffness and increase the flexibility of the paints.

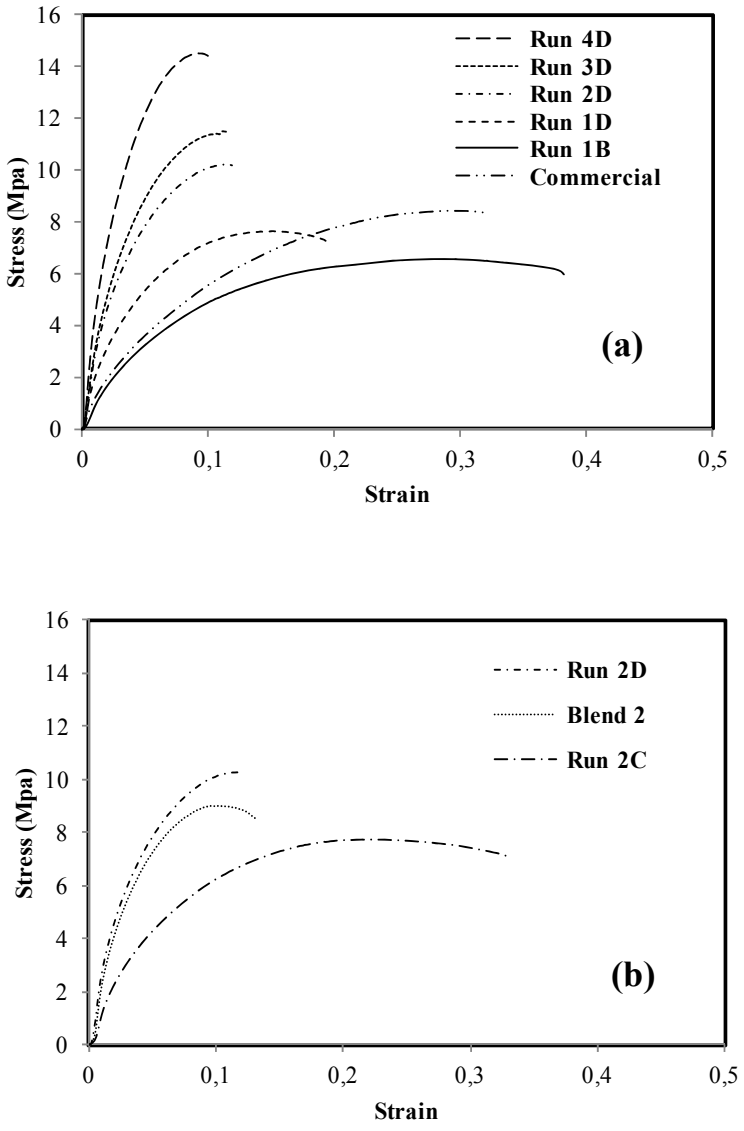

Fig. 5.8. The stress-strain behavior of paints formulated with: (a) Series D, Run 1B as well as the commercial latex; (b) Runs 2D and 2C as well as Blend 2.

Table 5.12. Mechanical properties of the paints cast at 60 °C.

Run	SA/SC(M)A[a] (wt/wt)	Young´s Modulus $\times 10^{-2}$ (MPa)	Yield Stress (MPa)	Toughness $\times 10^{-6}$ ($J \cdot m^{-3}$)	Elongation @ Break $\times 10^{-2}$ (%)	Ultimate Strength (MPa)
seeds of poly(SA) (100% conversion) + 3.5 h addition of SC(M)A pre-emulsion and KPS solution						
4D	40/60	5.89±0.30	13.92±0.45	1.06±0.05	0.10±0.01	14.43±0.60
3D	30/70	3.97±0.26	11.24±0.30	0.97±0.04	0.11±0.02	11.49±0.20
2D	20/80	3.30±0.10	9.96±0.75	0.90±0.07	0.12±0.04	10.20±0.60
1D	10/90	2.82±0.07	7.43±0.35	1.18±0.10	0.19±0.02	7.23±0.15
batch miniemulsion of SA (60% conversion) + 3.5 h addition of SC(M)A pre-emulsion and KPS solution						
4C	40/60	5.39±0.50	11.91±0.25	0.75±0.04	0.08±0.00	12.00±0.50
2C	20/80	1.95±0.25	7.18±0.45	2.08±0.12	0.33±0.03	7.10±0.40
Seeded emulsion copolymerization						
1B	0/100	0.83±0.05	5.99±0.40	2.03±0.09	0.38±0.03	5.95±0.50
Blends from Run 1A and Run 1B latexes						
Blend 4[a]	40/60	----	----	----	----	----
Blend 2	20/80	3.10±0.25	8.62±0.35	0.91±0.07	0.13±0.01	8.52±0.45
Commercial	----	1.33±0.20	8.30±0.32	2.01±0.11	0.32±0.04	8.35±0.35

[a] the film was highly brittle.

The pendulum hardnesses of the paint films cast at both 23 and 60 °C are plotted in Figure 5.9. It can be seen that for the paints prepared from the latexes in Series C and D, the hardness increased with SA content and crystallinity for both drying conditions. The hardness of the paints formulated by using blends were almost the same than for paints prepared in Series D. The presence of amorphous SA/SC(M)A copolymer with low glass transition temperature in Series C, led to lower hardness as compared with Series D and Blend 2. In addition, Figure 5.9 shows that the hardness of paints cast at 60 °C was higher than that of the films cast at 23 °C. The higher hardness of paints cast at 60 °C can be related to better coalescence of polymer particle and film quality. In addition, the hardness of the commercial paint was higher than that of the paints formulated with semicrystalline latexes and with latex 1B. The likely reason may be the composition and the T_g of the commercial latex. We had not access to the entire formulation of the commercial latex but according to the available information, the commercial latex (Acronal A754) is a dispersion with 50 wt% solids content and the minimum film formation of 17 °C. Therefore, the T_g of this polymer must be higher than that of the latexes synthesized in this study.

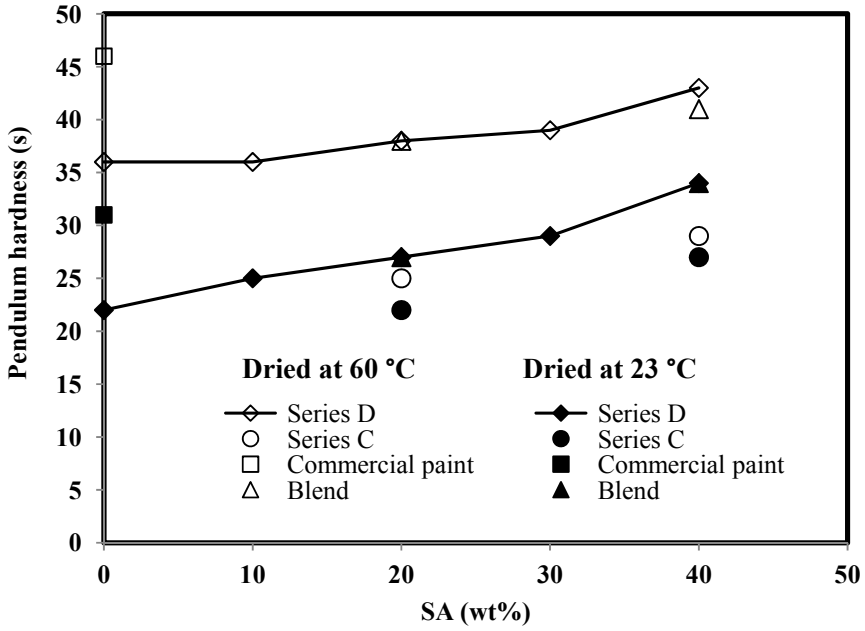

Fig. 5.9. The pendulum hardness of paints cast at both 23 and 60 ºC.

The static contact angles of the air-film interface of the paints cast at both 23 and 60 °C from latexes in Series C and D, as well as from Run 1B are given in Table 5.13. Moreover, the contact angles of commercial paint are also included. It can be seen that the contact angles increased with the content of the most hydrophobic monomer (SA) and that crystallinity had no effect on the contact angle (the contact angle values of the paints from latexes in Series C was almost the same than for

Series D and blends). On the other hand, the contact angles of the cast films at 60 °C from semicrystalline paints were slightly higher than for the paints cast at 23 °C. A possible reason for the higher hydrophobicity of the paints cast at 60 °C maybe the higher concentration of poly(SA) domains on the air-film interface. Because in the faster water evaporation rate, the time for sedimentation of larger particles containing poly(SA) was shorter. In addition, it can be seen that the hydrophobicity of the paint film formulated from commercial latex was higher than that of the paints cast from the latexes synthesized in this study. The higher hydrophobicity may due to the monomer composition and also the surfactant used in the commercial latex.

Table 5.13. Static contact angles of the air-film interface as well as gloss at 60 º of the paints cast at 23 and 60°C.

Binder	SA/SC(M)A[a] wt-wt	(AA+AM)[b] (wt %)	Contact angle		Gloss at 60 °	
			film at 23 °C	film at 60 °C	film at 23 °C	film at 60 °C
4D	40/60	1.2	91 ± 2 °	94 ± 3 °	3.2	2.8
3D	30/70	1.4	89 ± 1 °	93 ± 2 °	3.0	2.9
2D	20/80	1.6	86 ± 1 °	88 ± 1 °	3.2	2.8
1D	10/90	1.8	83 ± 2 °	84 ± 1 °	3.2	2.9
4C	40/60	1.2	90 ± 1 °	92 ± 1 °	3.1	2.9
2C	20/80	1.6	88 ± 2 °	90 ± 1 °	3.2	2.6
1B	0/100	2.0	81 ± 2 °	81 ± 1 °	3.2	2.8
Blend 4	40/60	1.2	91 ± 2 °	94 ± 1 °	3.0	2.5
Blend 2	20/80	1.6	89 ± 2 °	91 ± 1 °	3.2	3.0
Commercial	-----	-----	100 ±1°	100 ± 2 °	3.2	2.9

[a]SC(M)A: MMA/BA/AA/AM=49/49/1/1 wt%; [b]based on total monomer

Figure 5.10 shows the picture of the paints for the Run 3D latex before and after the scrub test. The scrub resistance of the paints formulated with Series D latexes as well as with latex 1B and the commercial latex cast at both 23 and 60 °C are plotted in Figure 5.11. This figure shows that the scrub resistance of the paints decreased substantially with the SA content at both 23 and 60 °C. The scrub test was performed under wet conditions, so the hydrophilicity of the latex is expected to affect the scrub results. Butler et al [11] observed that the more hydrophobic the

binder, the greater the abrasion resistance of the paints, presumably due to the reduced extent of film plasticization by water. However, this is not the case here as Table 5.13 showed that the hydrophobicity of the paints increased with the SA content, but the scrub resistance decreased. Another parameter that can affect the scrub resistance of the paints is the pigment binding ability of the latex. It is well known [12,13] that the existence of auxiliary monomers, e.g. AA and AM, in the latex formulation increases the wetting and adhesion properties of the pigment–latex system, leading to higher pigment binding ability. These monomers reduce the resistance of the paint film against water diffusion and permeation, which in turn may lower the scrub resistance of the film. These counteracting effects can be optimized by choosing an appropriate amount of auxiliary monomers to tune a desired wet scrub result. In the latexes synthesized in Series D, the concentration of auxiliary monomers (AA + AM) in the formulation decreased with the SA content (see Table 5.13). Moreover, Table 5.13 showed that the particle size of the latexes decreased with the increase of SA content. Therefore, the ratio of auxiliary monomers to the surface area of the particles decreased with increasing SA content and it may decrease the pigment binding ability of the latexes, and consequently the scrub resistance. In order to study the effect of auxiliary monomers concentration on the scrub resistance of the paints, three of the latexes in Table 5.1 (Run 1B, Run 2D and Run 4D) were synthesized with different auxiliary monomer concentrations and

the scrub resistance of the corresponding paints (cast at 60 ºC) is compared in Table 5.14. It can be seen that the scrub resistance of the paints decreases as the concentration of the auxiliary monomers increases. Therefore, the decrease of the scrub resistance of the paints with the SA content and crystallinity in Series D (Figure 5.11) was not due to the decreasing concentration of auxiliary monomers.

Fig. 5.10. Picture of the paint films from Run 3D latex before (up) and after (down) the scrub test.

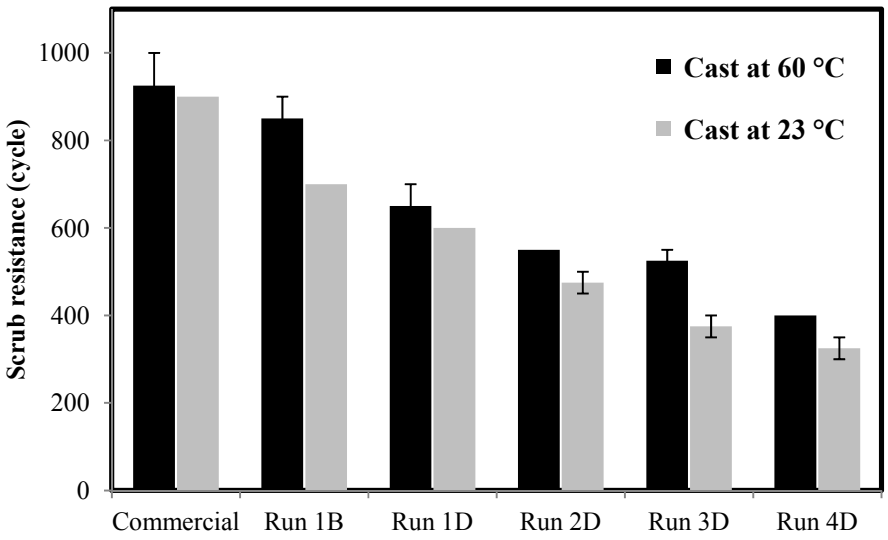

Fig. 5.11. Scrub resistance of paints films cast at both 23 and 60 ºC formulated from Series D, Run 1B and commercial latexes.

Table 5.14. Scrub resistance of paints with different auxiliary monomers concentration.

Binder	SA (wt %)	(AA+AM)[a] (wt %)	Scrub resistance (cycles)
4D	40	1.2	400 ± 0
4D-1	40	2.0	325 ± 25
2D	20	1.6	550 ± 0
2D-1	20	2	500 ± 50
1B-1	0	1.2	1200 ± 50
1B	0	2.0	850 ± 50

[a] based on total monomer

Other factors that can have an important effect on the scrub resistance of the paints include toughness and other mechanical properties [14]. But the interrelationship between these factors and the scrub resistance is not simple. The hardness, the Young´s modulus and the ultimate strength of the paints from Series D latexes increased with SA content and crystallinity but the scrub resistance decreased, perhaps because the paints lost their flexibility. On the other hand, Figure 5.11 showed that the scrub resistance of paints cast at 60 ºC was higher than the one cast at 23 ºC, likely due to better coalescence of polymer particles and film quality.

The scrub resistance of the paints formulated with the latexes with the same monomer composition (SA/SC(M)A=20/80 wt%, Run 2D, Run 2C and Blend 2) are compared in Figure 5.12. It can be seen that the scrub resistance of the paints from latexes 2C and 2D was almost the same. However, the mechanical properties of the latex 2D with higher crystallinity were different than those of latex 2C (Figure 5.5). Paint formulated with latex 2D had higher Young´s modulus, yield stress and ultimate strength than the paint obtained with latex 2C, but lower toughness and elongation at break. The lower scrub resistance of blend can be related to the phase separation between poly(SA) homopolymer and SC(M)A domains in the paints.

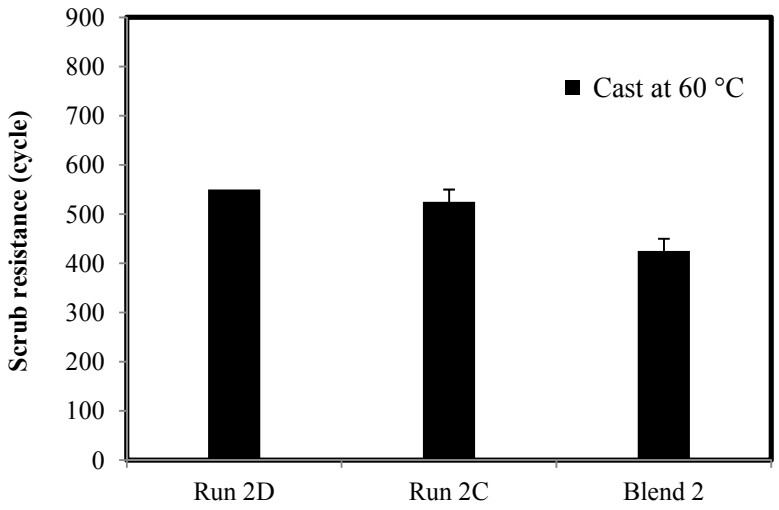

Fig. 5.12. Scrub resistance of paints cast at 60 ºC formulated from Run 2D, Run 2C and Blend 2 latexes.

Table 5.13 presents the gloss values at 60 ° of the paints cast at both 23 and 60 °C. It can be seen that they did not shown any significant effect of binder type and that they were in the range of exterior paint (< 5°). Moreover, it can be seen that the gloss of the paints cast at 23 ºC is higher than the films cast at 60 ºC, suggesting a flatter surface.

Figure 5.13(a) presents the viscosity versus shear rate for the paints formulated with Series D and Run 1B latexes as well as with the commercial latex. It is worth

mentioning that the volume solids percentage of all paints was the same (68.54 vt%). It can be seen that all the paints exhibited a pseudoplastic behavior, commonly found for waterborne paints. Moreover, it can be observed that the viscosity of the paints from Series D and Run 1B latexes increased with SA content, due to the decrease of the particle size. The viscosity of the commercial paint was substantially higher due to the smaller particle size (130 nm) and the narrower particle size distribution (obtained from seeded emulsion polymerization) of the commercial latex.

The flow behavior of the paints formulated with the latexes with the same monomer composition (SA/SC(M)A=20/80 wt%, Run 2D, Run 2C and Blend 2) is compared in Figure 5.13(b). It can be seen that the viscosity of the Blend 2 paint is lower than those of the paints from latexes 2D and 2C due to the bimodal particle size distribution of Blend (Blend of Run 1A and Run 1B latexes).

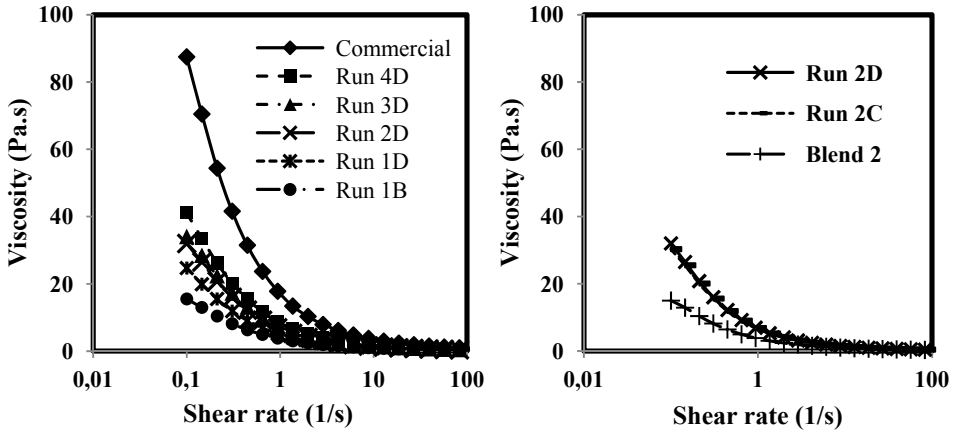

Fig. 5.13. Viscosity vs shear rate of paints formulated with: (a) Series D, Run 1B and commercial latex; (b) Runs 2D, 2C and Blend 2.

5.3.3. Characterization and performance of semicrystalline acrylic based latexes for adhesive applications

Pressure-sensitive adhesives (PSA) are viscoelastic materials that can adhere strongly to solid surfaces upon application of light contact pressures and short contact times. Considering their nature, they are classified as: hot-melt, solventborne, and waterborne. Waterborne PSAs are advantageous as they do not need any heating (unlike the hot melt adhesives) and are more environmentally friendly than the solventborne PSAs, because they do not emit volatile organic compounds during film formation. Among the different polymers used for waterborne PSAs, (meth)acrylates have enjoyed the fastest growth in commercial applications [2,16]. Their popularity

is attributable to optical clarity, UV light and oxidation stability, low toxicity, and relatively low cost. Generally, these polymers are amorphous and therefore it is interesting to explore the performance of semicrystalline PSAs.

Poly(SA) domains were used to introduce the crystalline domains to amorphous SC(M)A pressure sensitive adhesives. Two SC(M)A monomer compositions 2EHA/MAA= 99/1 wt%, and 2EHA/MMA/MAA= 84/15/1 wt% were used. Series D strategy was used to incorporate poly(SA) domains into 2EHA/MAA= 99/1 wt% (Table 5.2, Runs 1D´-4D´). On the other hand, Series C and D were used for 2EHA/MMA/MAA= 84/15/1 wt% (Table 5.3, Runs 2C″, 3C″ and Runs 1D″-4D″).

The volume average particle diameter of the poly(SA) seeds and the Z average and volume average of final latexes are given in Tables 5.15 and 5.16. Similar behaviors as for the coating latexes were observed. Briefly, secondary nucleation occurred during the second stage of polymerization in some of the experiments (see Tables 5.15 and 5.16) and the extent of this process decreased with increasing the number of seed particles at the beginning of the second stage. Moreover, the particle size decreased with increasing SA in the formulation in each series of experiments.

Table 5.15. Droplet and particle sizes of miniemulsion droplets and particles (adhesive application, Runs in Table 5.2)

Run	SA/SC(M)A[a] (wt/wt)	Disponil FES32/monomer (wt%)	Poly(SA) Particle size (HDC) (nm)	Final particle size (HDC) (nm)	Final particle size (DLS) (nm)	Theoretical Particle size[b] (nm)	Secondary Nucleation
miniemulsion batch							
1A´	100/0	2	170	170	196	----	----
seeds of poly(SA) (100% conversion) + 3.5 h addition of SC(M)A pre-emulsion and KPS solution							
4D´	40/60	2	170	220	224	231	No
3D´	30/70	2	170	236	239	254	Yes
2D´	20/80	2	170	270	245	291	Yes
1D´	10/90	2	170	317	296	366	Yes
seeded emulsion copolymerization							
1B´	0/100	2	31[c]	269	246	310	Yes

[a] SC(M)A: 2EHA/MAA=99/1 wt%. [b] without secondary nucleation and coagulations. [c] Polystyrene seeds= 0.1 wt% based on monomer.

Table 5.16. Droplet and particle sizes of miniemulsion droplets and particles (adhesive application, Runs in Table 5.3).

Run	SA/SC(M)A[a] (wt/wt)	Disponil FES32/monomer (wt%)	Poly(SA) Particle size (HDC) (nm)	Final particle size (HDC) (nm)	Final particle size (DLS) (nm)	Theoretical Particle size[b] (nm)	Secondary Nucleation
miniemulsion batch							
1A´	100/0	2	170	170	196	----	----
seeds of poly(SA) (100% conversion) + 3.5 h addition of SC(M)A pre-emulsion and KPS solution							
4D″	40/60	2	170	209	219	231	No
3D″	30/70	2	170	232	235	254	Yes
2D″	20/80	2	170	256	251	291	Yes
1D″	10/90	2	170	311	260	366	Yes
batch miniemulsion of SA (60% conversion) + 3.5 h addition of SC(M)A pre-emulsion and KPS solution							
3C″	30/70	2	170	219	228	254	Yes
2C″	20/80	2	170	253	250	291	Yes
seeded emulsion copolymerization							
1B´	0/100	2	31[c]	294	270	310	Yes

[a] SC(M)A: 2EHA/MMA/AA=84/15/1 wt%.[b] without secondary nucleation and coagulations. [c] Polystyrene seeds= 0.1 wt% based on monomer.

The gel fraction, weight-average molecular weight and the dispersity (Đ) for the soluble part, and the swelling degrees of the latexes synthesized for adhesive application (Runs in Tables 5.2 and 5.3) are presented in Tables 5.17 and 5.18. As can be seen, the gel fraction of the semicrystalline latexes increased with SA content. Moreover, the gel fractions of adhesive latexes containing MMA comonomer were lower than the latexes devoid of MMA.

Table 5.17. Gel fraction, swelling degree and sol weight-average molecular weight and the dispersity (Đ) of the latexes for Adhesive applications.

Run	SA/SC(M)A[a] (wt/wt)	Gel content (%)	Swelling degree	Mw, Soluble Part (g/mol)	Đ
batch miniemulsion					
1A´	100/0	79.1 ± 0.1	14.0 ± 0.5	392000	3.3
seeds of poly(SA) (100% conversion) + 3.5 h addition of SC(M)A pre-emulsion and KPS solution					
4D´	40/60	71.0 ± 0.1	10.3 ± 0.1	83000	3.3
3D´	30/70	69.4 ± 0.1	10.2 ± 0.1	86000	2.8
2D´	20/80	66.3 ± 0.0	10.5 ± 0.2	93000	2.8
1D´	10/90	66.5 ± 0.0	9.7 ± 0.0	100000	2.8
seeded emulsion copolymerization					
1B´	0/100	63.8 ± 0.1	10.8 ± 0.3	123000	2.7

[a] SC(M)A: 2EHA/MAA=99/1 wt%.

Table 5.18. Gel fraction, swelling degree and sol weight-average molecular weight and the dispersity (Đ) of the latexes for Adhesive applications.

Run	SA/SC(M)A[a] (wt/wt)	Gel content (%)	Swelling degree	Mw, Soluble Part (g/mol)	Đ
batch miniemulsion					
1A′	100/0	79.1 ± 0.1	14.0 ± 0.5	392000	3.3
seeds of poly(SA) (100% conversion) + 3.5 h addition of SC(M)A pre-emulsion and KPS solution					
4D″	40/60	49.0 ± 0.1	14.5 ± 0.1	170000	3.7
3D″	30/70	43.0 ± 1.0	19.4 ± 0.2	176000	3.7
2D″	20/80	41.0 ± 0.3	19.2 ± 0.5	209000	3.1
1D″	10/90	39.0 ± 1.5	22.4 ± 0.2	228000	4.0
batch miniemulsion of SA (60% conversion) + 3.5 h addition of SC(M)A pre-emulsion and KPS solution					
3C″	30/70	*	*	*	*
2C″	20/80	*	*	*	*
seeded emulsion copolymerization					
1B″	0/100	36.0 ± 0.4	22.6 ± 0.2	270000	4.0

[a] SC(M)A: 2EHA/MMA/MAA=84/15/1 wt%. * not measured.

Melting temperature, heat of fusion, crystallinity degree and the glass transition temperature of the latexes for adhesive applications (Runs in Tables 5.2 and 5.3) are given in Tables 5.19 and 5.20. The behaviors were similar to those showed by the coating latexes. Semicrystalline copolymers showed a first order transition around 51 °C which corresponds to poly(SA) crystalline domains and hence increased with SA content. Moreover, a second order transition which was associated to the glass transition of SC(M)A copolymer was observed at low temperatures. It can be seen that the Tg of the adhesive latexes containing MMA comonomer is higher than that of the adhesives devoid of MMA.

Table 5.19. Composition, crystallinity properties and glass transition temperature of the latexes for adhesive applications.

Run	SA/SC(M)A[a] (wt/wt)	Crystallinity properties			T_g (^{0}C)
		T_m (^{0}C)	ΔH_f (J/g)	Xc[b] (%)	
batch miniemulsion					
1A´	100/0	51	91.9	41.8	-116.0
seeds of poly(SA) (100% conversion) + 3.5 h addition of SC(M)A pre-emulsion and KPS solution					
4D´	40/60	51	33.7	15.3	-62.3
3D´	30/70	50	25.3	11.5	-63.0
2D´	20/80	50	15.5	7.0	-63.0
1D´	10/90	48	7.6	3.4	-65.8
Seeded emulsion copolymerization					
1B´	0/100	----	----	----	-66.0

[a]SC(M)A: 2EHA/MAA=99/1 wt%. [b]referred to the whole polymer.

Table 5.20. Composition, crystallinity properties and glass transition temperature of the latexes for adhesive applications.

Run	SA/SC(M)A[a] (wt/wt)	Crystallinity properties			T_g (^{0}C)
		T_m (^{0}C)	ΔH_f (J/g)	Xc[b] (%)	
batch miniemulsion					
1A ´	100/0	51	91.9	41.8	-116.0
seeds of poly(SA) (100% conversion) + 3.5 h addition of SC(M)A pre-emulsion and KPS solution					
4D″	40/60	51	33.0	15.0	-47.0
3D″	30/70	50	23.7	10.8	-46.4
2D″	20/80	49	14.9	6.8	-46.7
1D″	10/90	48	7.9	3.6	-46.4
batch miniemulsion of SA (60% conversion) + 3.5 h addition of SC(M)A pre-emulsion and KPS solution					
3C″	30/70	50	14.0	6.4	-47.3
2C″	20/80	49	9.0	4.1	-46.8
Seeded emulsion copolymerization					
1B″	0/100	----	----	----	-49

[a]SC(M)A: 2EHA/MMA/MAA=84/15/1 wt%. [b]referred to the whole polymer.

The adhesive films were cast both at room temperature (for 4 h) and at 90 °C (for 3 min). Figure 5.14 presents the shear resistance, peel and loop tack strengths measured at 23 °C for the adhesive films cast at room temperature from Series D

(Runs 1D′-4D′ (Table 5.2), and Runs 1D″-4D″ (Table 5.3)), Run 1B′and Run 1B″ latexes. The adhesive properties of all adhesives cast at room temperature are summarized in Tables 5.21 and 5.22. It can be seen that the shear resistance of the adhesives increased with SA content, and hence with crystallinity. It is worth mentioning that the gel content also increased with SA content in these copolymers (Tables 5.17 and 5.18). Therefore, the presence of crystalline domains and gel made the material more solid like and increases the creep resistance. Agirre et al. [16] observed that the shear resistance of the semicrystalline pressure sensitive adhesives with the same architecture (gel fraction, swelling ratio and sol molecular weight) increased with crystallinity. This might suggest that the effect of crystallinity on the shear resistance of the adhesives is more prominent than the gel fraction, but this cannot be calculated from the data obtained in this work. On the other hand, the adhesives containing MMA (even with lower gel fraction, see Table 5.16 and 5.17) showed substantially higher shear resistance than the soft adhesives devoid of MMA. Moreover, Figure 5.14 showed that the peel strength of the adhesives containing MMA increased with crystallinity and was higher than that of the adhesives with lower T_g. Conversely, the tackiness of adhesives containing MMA decreased with crystallinity and was lower than that of the adhesives with lower T_g. It is well known that the incorporation of high T_g monomers (i.e. MMA) increases the adhesive

stiffness and consequently shear and sometimes peel resistance. However, the tackiness decreases with increasing T_g [17].

The adhesion properties of these adhesives show that the presence of crystalline domains in the softer adhesive (2EHA/MAA=99/1wt%) substantially increased the shear resistance, loop tack strength and work of adhesion (Wa) of amorphous pressure sensitive adhesives. Moreover, the peel resistance of the amorphous adhesives also improved with incorporating crystalline domains. This is remarkable because adhesives showing a substantial high shear resistance usually exhibit a decrease in loop tack strength and work of adhesion (Wa). Whereas a high shear resistance requires a solid-like response (high creep resistance), loop tack strength and work of adhesion require polymer flow and energy dissipation, which is the response of a viscous material [16]. These two requirements are contradictory, but nevertheless they can be met in these semicrystalline adhesives.

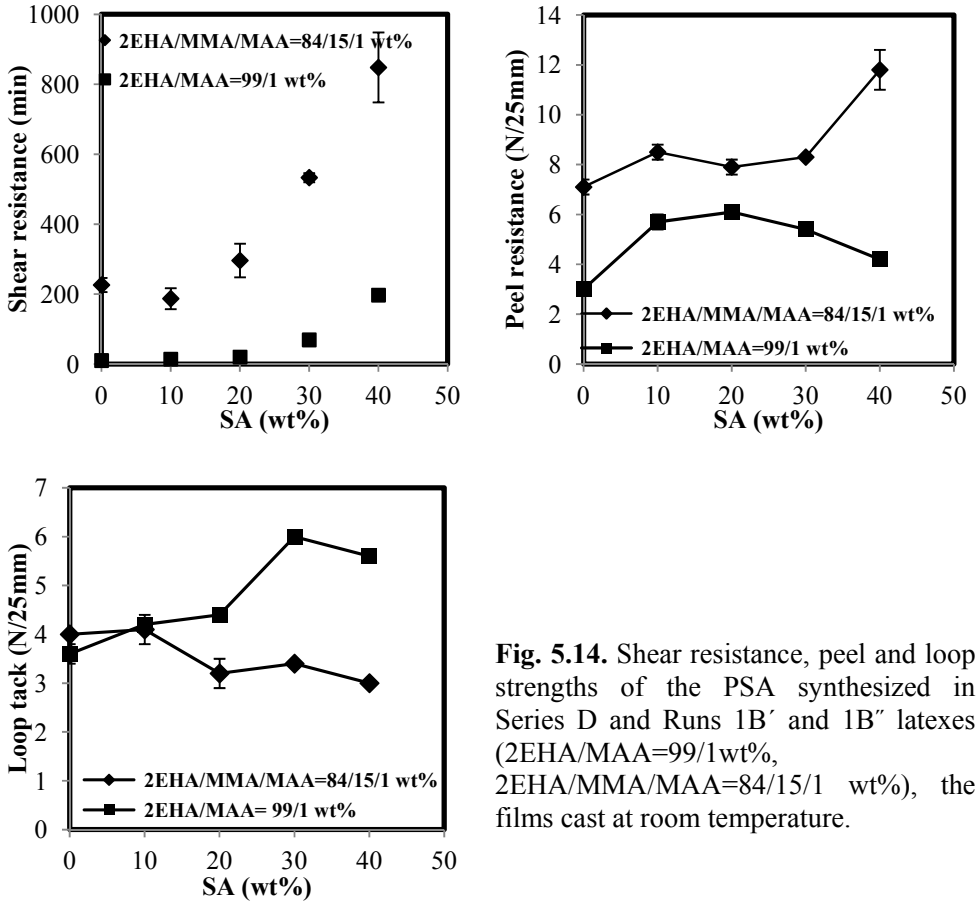

Fig. 5.14. Shear resistance, peel and loop strengths of the PSA synthesized in Series D and Runs 1B′ and 1B″ latexes (2EHA/MAA=99/1wt%, 2EHA/MMA/MAA=84/15/1 wt%), the films cast at room temperature.

The comparison of the adhesive properties of latexes with the same monomer composition obtained from different strategies (Series C and Series D, Table 5.22) showed that the shear resistance of the latex 2D″ with higher crystallinity was higher than that of the latex 2C″. However, the peel resistance was similar and the loop tack

resistance of the latex 2D″ was lower than that of latex 2C″. Latex 3D″ had higher shear resistance and work of adhesion than latex 3C″.

Table 5.21. Adhesive properties of PSA obtained for Series D and Run 1B´ (2EHA/MAA=99/1wt%), the films were cast at room temperature.

Run	SA/SC (M)A[a] (wt/wt)	Shear resistance (hours)	Peel resistance (N/25mm)	Loop tack (N/25mm)	Wa (J/m^2)
seeds of poly(SA) (100% conversion) + 3.5 h addition of SC(M)A pre-emulsion and KPS solution					
4D´	40/60	3.28 ± 0.10 (C)*	4.2 ± 0.1 (C)*	5.6 ± 0.1 (C)*	110.0 ± 4.0
3D´	30/70	1.15 ± 0.11 (C)*	5.4 ± 0.1 (C)*	6.0 ± 0.1 (SA)*	113.0 ± 1.0
2D´	20/80	0.33 ± 0.00 (C)*	6.1 ± 0.1 (C)*	4.4 ± 0.1 (A)*	75.2 ± 2.4
1D´	10/90	0.23 ± 0.01 (C)*	5.7 ± 0.3 (SC)*	4.2 ± 0.1 (A)*	74.4 ± 1.8
seeded emulsion copolymerization					
1B´	0/100	0.16 ± 0.01 (C)*	3.0 ± 0.0 (A*)	3.6 ± 0.2 (A*)	65.1 ± 1.6

[a] SC(M)A: 2EHA/MAA=99/1 wt%. * (A) Adhesive type failure. (C) Cohesive type failure. (SA) Semi-adhesive type failure. (SC) Semi-cohesive type failure.

Table 5.22. Adhesive properties of PSA obtained for Series D and Run 1B″ (2EHA/MMA/MAA=84/15/1 wt%), the films were cast at room temperature.

Run	SA/SC (M)A[a] (wt/wt)	Shear resistance (hours)	Peel resistance (N/25mm)	Loop tack (N/25mm)	Wa (J/m^2)
seeds of poly(SA) (100% conversion) + 3.5 h addition of SC(M)A pre-emulsion and KPS solution					
4D″	40/60	14.1 ± 1.67 (C)*	11.8 ± 0.8 (SA)*	3.0 ± 0.0 (A)*	59.2 ± 2.0
3D″	30/70	8.88 ± 0.22 (C)*	8.3 ± 0.0 (A)*	3.4 ± 0.0 (A)*	62.0 ± 1.4
2D″	20/80	4.93 ± 0.80 (C)*	7.9 ± 0.3 (A)*	3.2 ± 0.3 (A)*	58.2 ± 2.6
1D″	10/90	3.12 ± 0.5 (C)*	8.5 ± 0.3 (A)*	4.1 ± 0.3 (A)*	79.8 ± 4.7
batch miniemulsion of SA (60% conversion) + 3.5 h addition of SC(M)A pre-emulsion and KPS solution					
3C″	30/70	5.33 ± 0.0 (C)*	9.6 ± 0.0 (SC)*	3.0 ± 0.0 (A)*	57.2 ± 0.0
2C″	20/80	4.26 ± 0.16 (C)*	8.0 ± 0.3 (A)*	4.0 ± 0.0 (A)*	73.0 ± 2.6
copolymerization seeded emulsion					
1B″	0/100	3.76 ± 0.33 (C)*	7.1 ± 0.3 (A)*	4.0 ± 0.0 (A)*	71.8 ± 8.0

[a] SC(M)A: 2EHA/MMA/MAA=84/15/1 wt%. *(A) Adhesive type failure. (C) Cohesive type failure. (SC) Semi-cohesive type failure.

Figures 5.15 shows the adhesive properties of the films cast at both room temperature (4 hours) and 90 ºC (3 min) from latexes in Series D (Runs 1D″-4D″). The adhesive properties of amorphous SC(M)A copolymer adhesive (Latex 1B″) also is included. It can be seen that the adhesive properties were affected by the casting temperature. The shear resistance of the Series D adhesive films cast at 90 °C is higher than the one cast at room temperature, whereas the loop tack strength of the films is lower when cast at 90 °C. Moreover, the peel resistance of adhesives containing 0 - 20 wt% SA cast at both temperatures were the same, and the peel resistance of the adhesives containing SA contents higher than 20% was lower when cast at 90 °C. The effect of the casting temperatures on adhesive properties was more prominent for the adhesives with higher SA content and crystallinity.

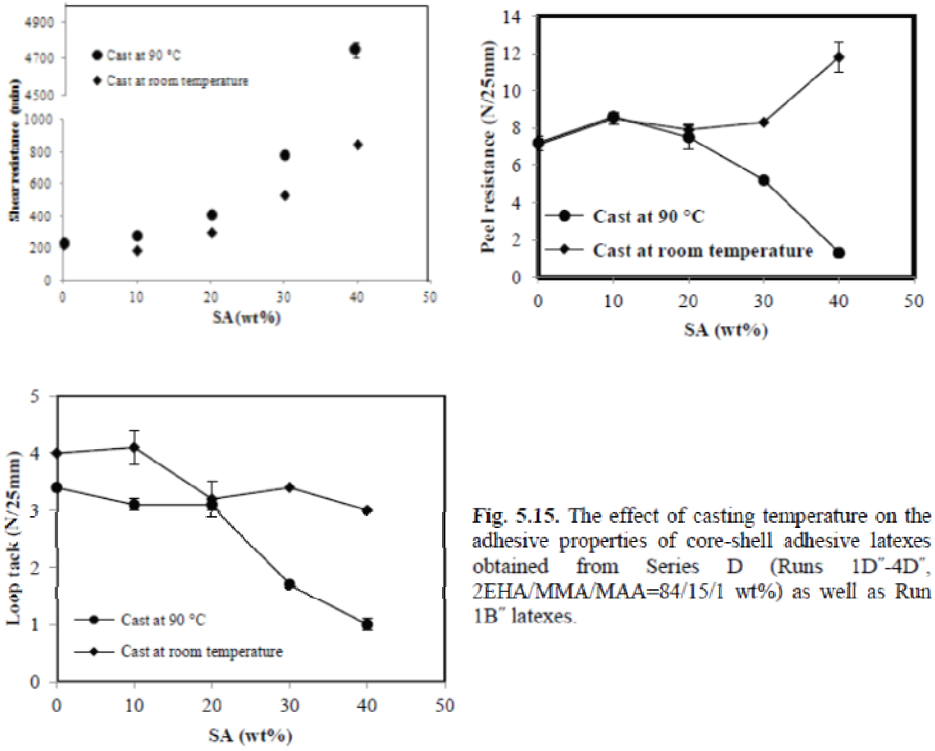

Fig. 5.15. The effect of casting temperature on the adhesive properties of core-shell adhesive latexes obtained from Series D (Runs 1D″-4D″, 2EHA/MMA/MAA=84/15/1 wt%) as well as Run 1B″ latexes.

The effect of temperature at which the test was performed on the shear resistance for the films cast at 90 °C from the semicrystalline latex 4D″ and amorphous latex 1B″ is illustrated in Figure 5.16. For both latexes the increase of temperature led to a decrease in shear resistance. The effect is more acute for the semicrystalline adhesive, perhaps due to the melting of the crystalline domains.

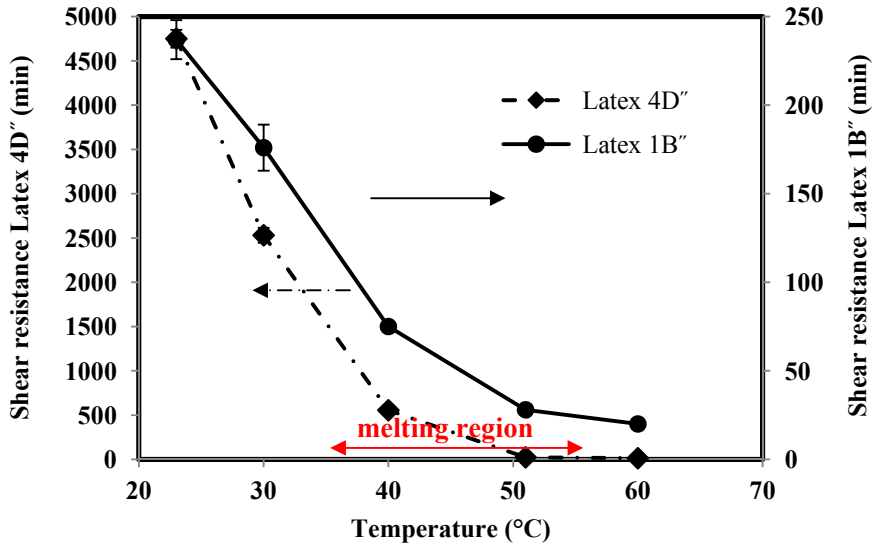

Fig. 5.16. Effect of the test temperature on the shear resistance of the latexes 4D″ and 1B″, the films cast at 90 °C.

5.4. Conclusions

In this chapter, semicrystalline polymer latexes containing poly(stearyl acrylate) crystalline domains were used in paint and adhesive formulations. Strategies C and D were used to synthesize the latexes.

In paint formulations it was found that the Young´s modulus, the yield stress and ultimate strength increased with crystallinity (poly(SA) content) but the elongation at break decreased. Toughness was higher for the completely amorphous

latex. Pendulum hardness increased and surprisingly scrub resistance decreased with crystallinity. The performance of these latexes was compared with that of a commercial latex, but the comparison was fainted by the fact that the commercial latex had an amorphous phase with a higher T_g.

For pressure sensitive adhesives it was found that shear resistance increased with crystalline content. Peel resistance increased with crystalline content for a 2EHA/MMA/MAA=84/15/1 wt% composition but showed a maximum for a 2EHA/MAA/99/1 wt% composition. Loop tack increased with SA content (crystallinity) for 2EHA/MAA/99/1 wt%, but decreased for 2EHA/MMA/MAA=84/15/1 wt%. It was found that the casting temperature affected the adhesive properties. Shear was higher when casting at 90 °C but peel resistance and loop tack were higher casting at 23 °C. Shear decreased when the testing temperature increased. The increase was more acute for the latexes containing crystalline domains.

5.5. References

[1] ASTM D 1876-95, standard test method for peel resistance of adhesives. In *Annual Book of ASTM Standards*; American Society for Testing and Materials: West Conshohocken, PA, 1996; Vol. 15.06, pp 115-117.

[2] *PSTC-7M, holding power of pressure sensitive tapes*; American Pressure Sensitive Tape Council: Naperville, IL, 1986.

[3] ASTM:D3654/D3654M-2, standard test methods for shear adhesion of pressure sensitive tapes. In *Annual Book of ASTM Standards*; American Society for Testing and Materials: West Conshohocken, PA, 1999; Vol. 15.10.

[4] FTM 9. Loop tack measurement. In *FINAT Technical Handook*, 7th ed.; FINAT: The Hague, 2005.

[5] Tag and Label Manufacturers Institute. TMLI LIB1. In *TLMI Manual of Recommended Standard Test Methods for Pressure Sensitive Labels*.

[6] [9] Aguirreurreta Z. Water-borne coatings and pressure-sensitive adhesives produced with polymerizable surfactants. PhD Thesis (under preparation), POLYMAT, The University of the Basque Country.

[7] González, I., Asua, J.M. and Leiza, J.R. *Polymer*, 2007, 48, 2542–2547.

[8] Yadav, A.K., Barandiaran, M.J. and de la Cal, J.C. *Macromol React Eng*, 2014, 8, 467-475.

[9] Arzamendi, G. and Asua, J.M. *Macromolecules*, 1995, 28, 7479-7490.

[10] Freitag, W. and Stoye, D. eds., 2008. *Paints, coatings and solvents*. John Wiley & Sons.

[11] Butler, L.N., Fellows, C.M. and Gilbert, R.G. *Prog Org Coat*. 2005, 53, 112–118.

[12] de Oliveira, M.P., Silva, C.R. and Guerrini, L.M. *J Coat Technol Res.* 2011, 8, 439-447.

[13] Khorassani, M., Afshar-Taromi, F., Mohseni, M. and Pourmahdian, S. *J Appl Polym Sci*. 2009, 113, 3264-3268.

[14] Koleske, J.V., 2006. Mechanical properties of solid coatings. *Encyclopedia of Analytical Chemistry*.

[15] Landrock, A.H. and Ebnesajjad, S., 2008. *Adhesives technology handbook*. William Andrew.

[16] Agirre, A., Heras-Alarcón, C.D.L., Wang, T., Keddie, J.L. and Asua, J.M. *ACS Appl Mater Interfaces*, 2010, 2, 443–451.

[17] Esmay, D.L. Minnesota Mining and Manufacturing Company, 1987, U. S. Patent. 4,645,711.

Chapter 6. Conclusions

In this PhD thesis, the effect of incorporating crystalline and liquid crystalline domains in the particles of waterborne polymer dispersions on the characteristic and properties of these dispersions is investigated. These dispersions were used for coating and adhesive applications. Crystalline domains were generated by homopolymerization of stearyl acrylate (SA). Liquid crystalline polymers were formed by polymerizing methacrylate side-chain crystal monomers that were synthesized in this work.

Semicrystalline, waterborne polymer latexes have been synthesized by using different strategies in 2-step miniemulsion polymerizations. The first step consisted in the homopolymerization of SA, which led to formation of crystalline domains. Homopolymerization of SA also led to the formation of very low T_g amorphous polymer. The degree of crystallinity was controlled by the conversion of SA (partially conversion (60%) (Series B and C) and full conversion (100%) (Series D)) achieved in the first step and by the way in which the short side chain (meth)acrylates

(SC(M)A) were fed in the second step (shot for Series B and semicontinuously for 3 h for Series C and D).

It was found that some secondary nucleation occurred during the second step and that the extent of this process decreased as the fraction of SA in the formulation increased. Moreover, the crystallinity of the synthesized copolymer latexes increased with SA content. For a given SA/SC(M)A monomer ratio, the maximum degree of crystallinity was achieved when all of SA is polymerized first and the SC(M)A was polymerized afterwards (Series D).

The monomer ratio and polymerization strategy affected the copolymer architecture. Gel (polymer insoluble in THF) was formed both during the homopolymerization of SA in the first step (following the classical mechanism for acrylate monomers) as well as during the copolymerization in the second stage (by grafting the second stage monomers on the amorphous part of the poly(SA)). The amount of gel produced in the second stage increased with the fraction of SA in the formulation and it was higher in Series D than in Series B and C.

The transmission electron microscopy (TEM) of the particles showed a core-shell morphology with the crystalline poly(SA) forming the dark core. Series D presented a higher proportion of dark zones in agreement with the higher crystalline

content. All the latexes yielded good films at room temperature with the crystalline domains well dispersed in the film. Scanning electron microscopy of the fractured surfaces of the films showed better compatibility between crystalline and the amorphous phases in the case of Series B and C than for Series D. TEM images showed no proof of aggregation of crystalline domains during film formation at room temperature, but substantial coalescence occurred casting the films at 60 °C (i.e. above the melting temperature of poly(SA)). Transparency of the films decreased with the size and number of crystalline domains and was the lowest for Series D cast at 60 °C.

Moreover, the performance of waterborne polymer latexes containing crystalline domains was studied. Comparison with the performance offered by regular latexes, namely latexes devoid of crystalline domains, showed that mechanical and barrier properties as well as the resistance to water improved with the incorporation of the crystalline domains. On the other hand, the performance of the latexes containing SA was affected in a complex way by the interplay between the amorphous and crystalline parts. Although in some cases, the increase of SA content led to better mechanical properties, the counteracting effect of the amorphous and crystalline fractions led in other cases to a decrease of the Young´s modulus and the yield stress.

In addition, the mechanical properties of the latexes improved with the T_g of the polymer produced in the second step that depended on the feeding strategy of short chain (meth)acrylates ($T_{g\ shot} > T_{g\ continuous\ feeding}$).

The effect of the T_g of the second step polymer was even more accused on water uptake where it overcame the effect of crystallinity.

Water vapor permeability decreased as the SA content increased and it was affected by the quality of the film that depended on the casting temperature; the higher this temperature the better film and the lower water vapor permeability. For the same overall composition, oxygen permeability decreased with the crystalline fraction.

In addition, semicrystalline polymer latexes containing poly(SA) crystalline domains were used in paint and adhesive formulations. Strategies C and D were used to synthesize the latexes.

In paint formulations it was found that the Young´s modulus, the yield stress and ultimate strength increased with crystallinity (poly(SA) content) but the elongation at break decreased. Toughness was higher for the completely amorphous latex. Pendulum hardness increased and surprisingly scrub resistance decreased with crystallinity. The performance of these latexes was compared with that of a

commercial late, but the comparison was fainted by the fact that the commercial latex had an amorphous phase with a higher T_g.

For pressure sensitive adhesives it was found that shear resistance increased with crystalline content. Peel resistance increased with crystalline content for a 2EHA/MMA/MAA=84/15/1 wt% composition but showed a maximum for a 2EHA/MAA=99/1 wt% composition. Loop tack increased with SA content (crystallinity) for 2EHA/MAA=99/1 wt%, but decreased for 2EHA/MMA/MAA=84/15/1 wt%. It was found that the casting temperature affected the adhesive properties. Shear was higher when casting at 90 °C but peel resistance and loop tack were higher casting at 23 °C. Shear decreased when the testing temperature increased. The increase was more acute for the latexes containing crystalline domains.

Another method for introducing the hard and tough domains in waterborne latex particles was using liquid crystalline polymers (LCPs). Hence, a series of methacrylate side-chain liquid crystal monomers (n-MLCMs, n=3, 4, 5, 6) containing biphenyl mesogenic group with different length of spacer and a fixed tail were synthesized and homopolymerized in aqueous media by free radical miniemulsion polymerization. Full monomer conversion and high molecular weight (M_n ~10^5 g/mol) polymers with high thermal stability were obtained. Based on differential

scanning calorimetry (DSC), polarized light microscopy (PLM) and X-ray scattering (SAXS and WAXS) studies, all polymers show mesomorphism behavior and present Smectic **E** (Smectic **E** or Smectic **C** for 4-PMLCM) ↔ Smectic **A** ↔ Isotropic Liquid transitions with increasing temperature. The results showed lower level of ordering for 4-PMLCM in comparison with other members while the maximum level of ordering obtained for 5-PMLCM. The dependence of the transition temperatures as well as the entropy changes associated with the melting and clearing transitions (expressed as the dimensionless quantity $\Delta S/R$) exhibit a distinct odd-even effect with the number of carbon atoms in the spacer, n. The odd members exhibit the higher values of these quantities.

The thermal and mesomorphic behaviors of the n-PMLCMs have also been compared to other polymers containing the same mesogenic unit but different alkyl tail. It was observed that the alkyl tail play an important role in thermal and mesomorphic properties of studied polymers. The polymers containing longer tail showed higher thermal transitions and level of ordering. Longer tails facilitate the ordering of the mesogens and allow more efficient packing around the backbones, imparting high stability to the smectic phases formed.

To introduce LCPs into the waterborne (meth)acrylate latexes, 2-step miniemulsion polymerizations have been used. In the first step the seeds of LCPs were prepared by miniemulsion homopolymerization of n-MLCMs, which led to formation of liquid crystalline domains. The SC(M)A were fed semicontinuously for 3 h in the second step and copolymerized in the presence of n-MLCM homopolymer seeds.

It was found that substantial secondary nucleation occurred during the second step of copolymerization in all experiments and the extent of this processed decreased as the fraction of n-MLCM in the formulation increased. The incorporation of LCPs in polymer particles and then in polymer films were studied by DSC, PLM and WAXS measurements. The TEM micrographs of the particles showed a core-shell morphology with the dark liquid crystalline domains of n-MLCM homopolymer in the core. The TEM micrograph of the cast film at 23 °C showed a well dispersion of liquid crystalline domains in the film, but substantial coalescence occurred when the film processed at 200 °C (i.e. above the melting temperature of poly(n-MLCM)).

It was observed that the presence of liquid crystalline domains reinforced the mechanical properties of the amorphous SC(M)A copolymer. Moreover, the spacer of n-MLCMs had plasticizing effect on the n-MLCM/SC(M)A copolymer; the longer the spacer length, the higher the plasticizing effect.

The water vapor permeability and liquid water uptake of the copolymer films containing liquid crystalline domains were substantially lower than the fully amorphous copolymer of SC(M)A.

In addition, it was observed that the film preparation conditions strongly affected the mechanical, barrier and water resistance of the films. The mechanical and barrier properties as well as the water resistance of the films processed above the melting temperature of LCPs were higher than the films cast at 23 °C.

The comparison of the (meth)acrylate polymers containing both poly(SA) and poly(6-MLCM) showed that the mechanical properties of the films were almost the same when tested at 23 ° whereas, when the test carried out at 60 °C the mechanical properties of the films containing poly(6-MLCM) at 60 °C were prominently higher than those of the films containing poly(SA). Moreover, the water uptake of the films containing poly(SA) was lower than the films containing poly(6-PMLCM).

Parts of this work have been presented will be published soon in national and international conferences, as well as in Industrial Liason Program (ILP) Meetings.

- **12th Industrial Liason Program (ILP) Meeting**

  Held in the University of the Basque Country, Donostia-San Sebastián**,** September 2012. Oral Presentation: "Comb-Like Acrylic-Based Polymer Latexes Containing Nano-Sized Crystallizable Domains".

- **5th Iberian Meeting on Colloids and Interfaces (RICI5)**

  Held in the University of the Basque Country, Donostia-San Sebastián**,** July 2013. Poster Presentation: "*Comb-Like Acrylic-Based Polymer Latexes Containing Nano-Sized Crystallizable Domains"*.

- **13th Industrial Liason Program (ILP) Meeting**

  Held in the University of the Basque Country, Donostia-San Sebastián**,** September 2013. Oral Presentation: "Comb-Like Acrylic-Based Polymer Latexes Containing Nano-Sized Crystallizable Domains".

- **BASF Research Forum Europe 2014**

  Held in BASF company, Antwerp, Belgium, March 2014. Poster Presentation: "*Comb-Like Acrylic-Based Polymer Latexes Containing Nano-Sized Crystallizable Domains"*.

- **78th PRAGUE MEETING ON MACROMOLECULES**

  Held in Prague, Czech Republic, July 2014. Oral Presentation: " Comb-Like Acrylic-Based Polymer Latexes Containing Nano-Sized Crystallizable Domains*"*.

- **14th Industrial Liason Program (ILP) Meeting**

  Held in the University of the Basque Country, Donostia-San Sebastián**,** September 2014. Oral Presentation: "Comb-Like Acrylic-Based Polymer Latexes Containing Nano-Sized Crystallizable Domains*"*.

- **15th Industrial Liason Program (ILP) Meeting**

  Held in the University of the Basque Country, Donostia-San Sebastián**,** September 2014. Oral Presentation: "Comb-Like Acrylic-Based Polymer Latexes Containing Nano-Sized Crystallizable Domains*"*.

- **European Symposium on Chemical Reaction Engineering, ESCRE 2015**

  Held in Veranstaltungsforum Fürstenfeldbruck near Munich, Germany, October 2015. Oral Presentation: "Comb-like acrylic-based polymer latexes containing nano-sized crystalline domains".

- **PhD-Workshop on Polymer Reaction Engineering**

  Held in Veranstaltungsforum Fürstenfeldbruck near Munich, Germany, October 2015. Oral Presentation: "Comb-like acrylic-based polymer latexes containing crystalline domains".

- **IUPAC World Polymer Congress (MACRO 2016)**

  Will be held in Istanbul, Turkey, July 2016: "Aacrylic-based composite latexes containing nano-sized liquid crystalline domains".

Parts of this Thesis have been published or will be published soon. The list of papers that would be issued from this work is as follows:

- E. Mehravar, J. R. Leiza, J. M. Asua. Synthesis and characterization of comb-like acrylic-based polymer latexes containing nano-sized crystallizable domains. *Polymer* **2016**, Vol. 84, 167-177.
- E. Mehravar, J. R. Leiza, J. M. Asua. Performance of Latexes Containing Nano-Sized Crystalline Domains Formed by Comb-Like Polymers. *Polymer* **2016**. doi:10.1016/j.polymer.2016.04.067.
- E. Mehravar, A. Iturrospe, A. Arbe, J. R. Leiza, J. M. Asua. Synthesis and Phase Behavior of Side-Chain Liquid-Crystalline Polymers Containing Biphenyl Mesogen with Different Lengths of Spacer. Submitted to *Polymer Chemistry*.
- E. Mehravar, J. R. Leiza, J. M. Asua. Acrylic-Based Composite Latexes Containing Liquid Crystalline Domains. (under preparation).
- E. Mehravar, J. R. Leiza, J. M. Asua. Acrylic-Based Paint Formulations Containing Crystalline Domains. (under preparation).

Conclusiones

En esta tesis, se investigó el efecto de la incorporación de dominios cristalinos y cristalinos líquidos en dispersiones de partículas de polímero en base de agua de y en las características y propiedades de estas dispersiones. Estas dispersiones tienen aplicaciones en revestimientos y en adhesivos. Los dominios cristalinos fueron generados por homopolimerización de acrilato de estearilo (SA). Los polímeros cristalinos líquidos fueron formados a través de la polimerización de monómeros metacrilato de cristal de la cadena lateral que se sintetizaron en este proyecto.

Se han sintetizado látex de polímeros semicristalinos con diferentes estrategias de polimerizacionen en miniemulsión en 2 pasos. El primer paso consistió la homopolimerización de SA, en el que que se forman los dominios cristalinos. La homopolimerización de SA también dio lugar a la formación de polímero amorfo con Tg muy baja. El grado de cristalinidad fue controlado con la conversión del SA (conversión parcial (60%) (Series B y C) y conversión completa (100%) (Series D)) alcanzado en el primer paso y con la manera en la que los (met) acrilatos (SC (M) A)

de cadena lateral corta fueron alimentados en el segundo paso (disparo en la serie B y para las series C y D fueron alimentados semicontinuamente durante 3 horas).

Se encontró que algunas nucleación secundaria ocurrió durante el segundo paso y que el alcance de este proceso se reduce cuando la fracción de SA en la formulación aumenta. Por otra parte, la cristalinidad de los látex de los polímeros sintetizados se incrementó con el contenido de SA. Para una determinada relación de SA/SC(M) monómero, se alcanzó el máximo grado de cristalinidad cuando todo el SA se polimeriza primero y el SC(M)A se polimerizó posteriormente (Serie D).

La relación de monómeros y la estrategia de polimerización afectaron a la arquitectura de copolímero. Se formó gel (polímero insoluble en THF) durante la homopolimerización del SA en el primer paso (siguiendo el mecanismo clásico de monómeros de acrilato), y también durante la copolimerización en la segunda etapa (por injerto de los segundos monómeros de la etapa en la parte amorfa del poli (SA)). La cantidad de gel producido en la segunda etapa aumenta con la fracción de SA en la formulación y era mayor en la serie D que en las series B y C.

La microscopía electrónica de transmisión (TEM) de las partículas mostró una morfología de core-shell con el poli(SA) cristalino que forma el núcleo oscuro. La serie D presenta una mayor proporción de zonas oscuras de acuerdo con el contenido

cristalino superior. Todos los látex dieron buenos filmes a temperatura ambiente con los dominios cristalinos bien dispersos en el film. La microscopía electrónica de barrido de la superficie fracturada de los filmes mostró una mejor compatibilidad entre el las fases cristalina y amorfa en el caso de las series B y C que en la serie D. Las imágenes de TEM no mostraron ninguna prueba de agregación de los dominios cristalinos durante la formación del film a temperatura ambiente, pero ocurrió una coalescencia sustancial cuando los filmes se secaron a 60 °C (es decir, por encima de la temperatura de fusión del poli(SA)). La transparencia de los filmes disminuyó con el tamaño, y el número de dominios cristalinos y fue el más bajo para la serie D secada a 60 °C.

Además, se estudió el rendimiento de los látex de polímeros que contienen dominios cristalinos. La comparación con el rendimiento ofrecido por los látex regulares, látex desprovisto de dominios cristalinos, mostró que las propiedades mecánicas y de barrera, así como la resistencia al agua mejoran con la incorporación de los dominios cristalinos. Por otra parte, el rendimiento de los látex que contienen SA se vio afectado de manera compleja por la interacción entre las partes amorfas y cristalinas. Aunque en algunos casos, el aumento del contenido de SA llevó a mejores propiedades mecánicas, el efecto de contrarresto de las fracciones amorfas y

cristalinas llevó en otros casos a una disminución del módulos de Young y del límite elástico.

Además, las propiedades mecánicas de los látex mejoraron con la T_g del polímero producido en el segundo paso que dependía de la estrategia de alimentación de (met)acrilato de cadena corta ($T_{g\ disparo} > T_{g\ alimentación\ continua}$).

El efecto de la T_g del polímero de segundo paso fue aún más acusado en la absorción del agua en el que superó el efecto de la cristalinita.

La permeabilidad al vapor de agua disminuyó a medida que aumentó el contenido SA y se ve afectada por la calidad del film que depende de la temperatura de secado; cuanto mayor sea esta temperatura, mejor es el film e inferior la permeabilidad al vapor de agua. Para la misma composición general, la permeabilidad de oxígeno disminuye con la fracción cristalina.

Además, los látex de polímero semicristalino que contienen dominios cristalinos de poli (SA) fueron utilizados en la pintura y formulaciones de adhesivo. Se utilizaron las estrategias C y D para sintetizar los látex.

En las formulaciones de pintura se encontró que el módulos de Young, el límite de elasticidad y la resistencia a la rotura aumentaron con la cristalinidad (contenido

de poli(SA)), pero la elongación en rotura disminuye. La dureza fue mayor para el látex completamente amorfo. La dureza de péndulo aumentó y la resistencia al rayado sorprendentemente disminuye con la cristalinidad. El rendimiento de estos látex se comparó con la de látex comercial, pero la comparación se desmayó por el hecho de que el látex comercial tenía una fase amorfa con una T_g superior.

Para los adhesivos sensibles a la presión se encontró que la resistencia a la cizalla (shear resistance) aumenta con contenido cristalino. La resistencia de pelado (peel resistance) aumentó con contenido cristalino para una composición de 2EHA/MMA/MAA=84/15/1 wt%, pero mostró un máximo para una composición de 2EHA/MAA=99/1 wt%. La pegajosidad de bucle (loop tack) aumenta con el contenido SA (cristalinidad) para 2EHA / MAA = 99/1 wt%, pero disminuyó por 2EHA/MMA/MAA= 84/15/1 wt%. Se encontró que la temperatura de secado afectó a las propiedades adhesivas. Cizalla fue mayor cuando se lanza a 90 ° C, pero la resistencia alpelado y pegajosidad fueron mayores de fundición a 23 ° C. Cizalla disminuyó cuando aumentó la temperatura de ensayo. El aumento fue más grave para los látex que contienen dominios cristalinos.

Otro método para la introducción de los dominios duros en partículas de látex era uso de polímeros cristalinos líquidos (LCP). Por lo tanto, una serie de monómeros metacrilato de cristal líquido de cadena lateral (n-MLCMs, n = 3, 4, 5, 6) que

contienen bifenilo mesogénico grupo con diferente longitud de espaciador y una cola fija se sintetizaron y se homopolimerizaron en medio acuoso por polimerización de radicales libres en miniemulsión. Se obtuvieron polímeros con conversión de monómero completa y de alto peso molecular (Mn ~ 10^5 g / mol) con alta estabilidad térmica. Sobre la base de estudios de calorimetría diferencial de barrido (DSC), microscopía de luz polarizada (PLM) y dispersión de rayos X (SAXS y WAXS), todos los polímeros muestran un comportamiento mesomótfico y presentan transiciones líquido esméctico E ↔ esméctica A ↔ isotrópicos con el aumento de la temperatura. La dependencia de las temperaturas de transición y los cambios de entropía de fusión asociadas a las transiciones y de compensación (expresado como la cantidad dimensional ΔS/R) exhiben un efecto impar-par distinto con el número de átomos de carbono en el espaciador, n. Los miembros impares presentan los valores más altos de estas cantidades.

Para introducir los LCP en los látex de (met)acrilato en base de agua, se han utilizado las polimerizaciones en miniemulsión de 2 pasos. En la primera etapa, las semillas de los LCP se prepararon en homopolimerización miniemulsión de n-MLCMs, lo que condujo a la formación de dominios cristalinos líquidos. El SC (M)A se alimentó semi-continuamente durante 3 h en el segundo paso y copolimerizó en presencia de semillas de homopolímero de n-MLCM.

Se encontró que se produjo una nucleación secundaria sustancial durante la segunda etapa de copolimerización en todos los experimentos y la extensión de este procesado disminuyó a medida que la fracción de n-MLCM en la formulación aumentaba. La incorporación de los LPC en partículas de polímero y luego en filmes de polímero fueron estudiados por DSC, PLM y mediciones WAXS. Las micrografías TEM de las partículas mostraban una morfología de core-shell con los dominios cristalinos líquidos oscuros de n-MLCM homopolímero en el núcleo. La micrografía TEM del film secado a 23 ° C mostró una buena dispersión de los dominios cristalinos líquidos en el film, pero se produjo coalescencia sustancial cuando el film se proceso a 200 ° C (es decir, por encima de la temperatura de fusión del poli (n-MLCM)).

Se observó que la presencia de dominios cristalinos líquidos refuerza las propiedades mecánicas del copolímero amorfo SC(M)A. Por otra parte, el espaciador de n-MLCMs tenía efecto plastificante en el copolímero de n-MLCM/SC(M)A; cuanto mayor sea la longitud del espaciador, mayor es el efecto plastificante.

La permeabilidad al vapor de agua y la absorción de agua en los filmes de copolímeros que contienen dominios cristalinos líquidos fueron sustancialmente más bajo que el copolímero totalmente amorfo de SC(M)A.

Además, se observó que las condiciones de preparación del film afectaron fuertemente la mecánica de barrera y resistencia al agua de los filmes. Las propiedades mecánicas y de barrera, así como la resistencia al agua de los filmes procesados por encima de la temperatura de fusión del LCP fueron más altas que los filmes emitidos en 23 °C.

La comparación de los polímeros de (met)acrilato que contienen los dos poli(SA) y poli(6-MLCM) mostró que las propiedades mecánicas de los filmes fueron casi las mismas cuando se ensaya a 23 ° mientras que, cuando la prueba es llevada a cabo a 60 °C las propiedades mecánicas de los filmes que contienen poli(6-MLCM) a 60 °C fueron prominentemente más altos que los de los filmes que contienen poli(SA). Por otra parte, la absorción de agua de los filmes que contienen poli(SA) fue menor que los que contienen poli(6-PLCM).

Appendix I: Thermal transitions of poly stearyl acrylate

The thermal transition processes of poly stearyl acrylate (poly(SA)) were studied by using differential scanning calorimeter (DSC), dynamic mechanical thermal analyzer (DMTA) and dielectric spectroscopy techniques.

I.1. Characterization

Calorimetric Measurements. A differential scanning calorimeter (DSC, Q1000, TA Instruments) was used to measure the thermal transitions of poly(SA) under a dry nitrogen atmosphere (sample size~11 mg). The scanning cycles consisted of first cooling to -170 °C at 5 °C min^{-1}, then heating from -170 to 80 °C at 5 °C min^{-1}, cooling again from 80 to -170 °C at 5 °C min^{-1}, and then heating to 80 °C at a rate of 5 °C min^{-1}.

Dynamic-Mechanical Thermal Analysis (DMTA). The measurement was carried out using a dynamic mechanical thermal analyzer (DMTA) (Triton 2000 DMA, Triton Technology, Ltd). The poly(SA) sample of 7×10×0.7 mm^3 was obtained from poly(SA) powder using a hydraulic hot press at 100 °C for 5 min and then cooled down to room temperature. A single cantilever tension geometry was used. The real (storage modulus, E´) and imaginary (loss modulus, E″) components of the complex shear modulus E* = E´+ iE″ and the internal fraction coefficient tan (ϕ) = E″/ E´ (mechanical loss) were measured over the temperature range -170 °C to 100 °C in constant frequency from 0.5 Hz to 50 Hz. The heating rate was 4 °C/min. During the experiment, a sinusoidal strain is applied and the response of the sample is registered, that is to say, the stress necessary to maintain the deformation.

Dielectric Measurements. Time and frequency domain dielectric techniques were used to study the dynamics of poly(SA) in a broad temperature (-150 to 100 °C) and frequency (10^{-2} - 10^{7}) range. The sample capacitor consisted of two parallel gold-plated electrodes with a diameter of 20 mm, separated by the sample (sample thickness = 0.1 mm). The plate distance of 0.1 mm was kept constant by a small Teflon spacer. The equipment consisted on a Keithley 6517A electrometer together with Novocontrol's Quatro temperature and Win thermally stimulated currents (TSC) controllers. After preparation, the sample together with Teflon spacer were placed

between the electrodes and heated up to 373 K and then cooled down to 123 K, and then reheated to 373 K while isothermal scans were made at every tenth degree. The heating rate was 5 K min^{-1}, the same rate used for DSC experiment. The experiment was performed under a dry nitrogen atmosphere**.** The complex dielectric function $\varepsilon^*(\omega)= \varepsilon'(\omega) - i\varepsilon''(\omega)$, $\omega=2\pi f$ (where f is frequency and, ε' the real part and ε'' the imaginary part of the complex dielectric constant) was then measured using a high-resolution dielectric analyzer (ALPHA Novocontrol).

I.2. Results and discussions

The second heating scan of poly(SA) is presented in Figure I.1. The DSC of poly(SA) shows an endothermic peak at 50-51 °C due to the melting of poly(SA) crystalline domains. Moreover, it can be seen that the DSC of poly(SA) detected a very weak transition at about -111 °C. Generally, the glass transition temperature (T_g) of long side chain (meth)acrylate polymers is poorly resolved and is suppressed by the side chain crystallinity, which makes it difficult to observe clearly in DSC traces [1,2].

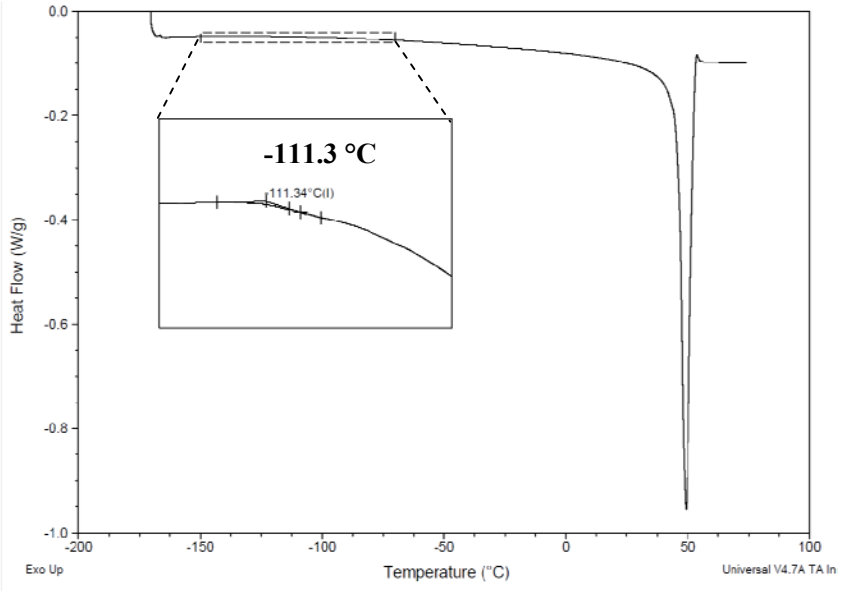

Fig. I.1. The second heating DSC scan of poly(SA)

I.2.1. Isochronal spectra

The variation with temperature of storage modulus and the internal friction coefficient tan (ϕ) obtained from mechanical spectroscopy measurements at 1 Hz from -170 °C to 100 °C for poly(SA) is shown in Figure I.2(a). This spectrum shows that the mechanical losses (tan $(\phi)_{max}$) were observed at -30 (weak transition), -80 and -137 °C (applied frequency = 1 Hz).

The loss factor tan (δ) = ε″/ε´ relaxation spectra of poly(SA) as obtained from dielectric spectroscopy is displayed on Figure I.2(b) for the measurement frequency 10 Hz. This spectrum shows 2 relaxation processes at -10 to -50 °C and -120 to -150 °C regions. The dielectric relaxational behavior is qualitatively the same as the one obtained with mechanical spectroscopy, even if the relaxation amplitudes differ prominently.

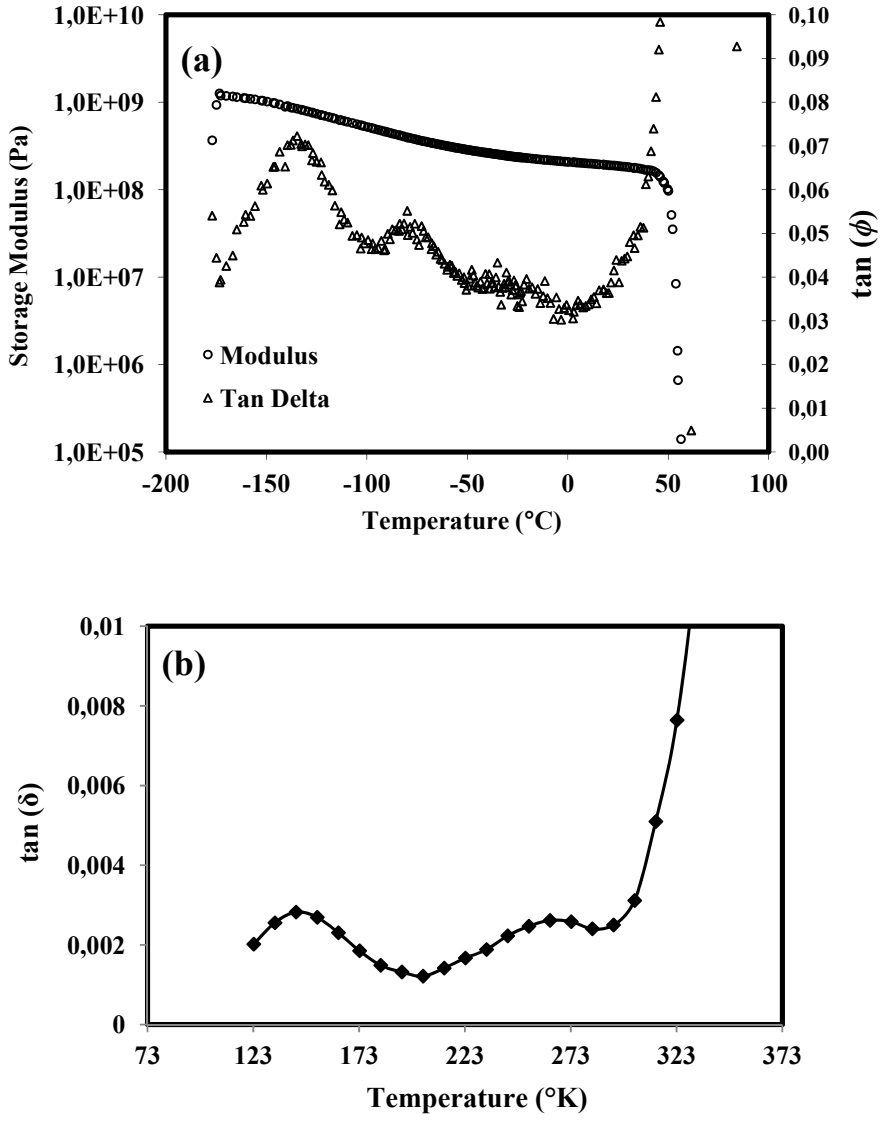

Fig. I.2. (a) Isochronal spectra obtained from mechanical spectroscopy at 1 Hz and (b) Isochronal spectra obtained from dielectric spectroscopy at 10 Hz for poly(SA).

I.2.2. Isothermal spectra

I.2.2.1. Dielectric measurements

The isothermal variations of ε'' with frequency obtained from dielectric measurement of poly(SA) are displayed in Figure I.3 between 133 K and 193 K. The ε'' curves exhibit a peak shifting towards the high frequency with increasing temperature. The same type of variation is found for the secondary relaxation processes at higher temperature region; however, the relaxation processes at higher temperature were not completely resolved in some frequencies. The coordinates of the maximum of each relaxation peak (T, f_{max}) and the corresponding characteristic times $\tau = 1/2\pi f_{max}$ can be directly evaluated. This procedure was applied for the relaxation process at lower temperature region and the values of the dielectric characteristic times derived from the relaxation peaks are displayed on an Arrhenius diagram in Figure I.4.

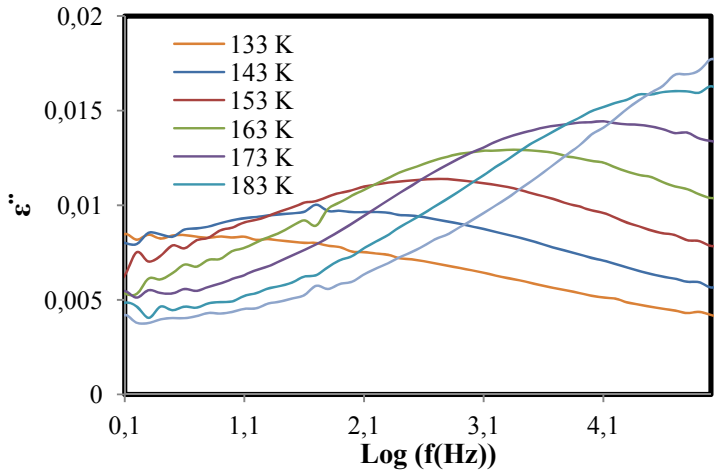

Fig. I. 3. The isothermal variations of **ε¨** with frequency obtained from dielectric measurement between 133 K and 193 K of poly(SA).

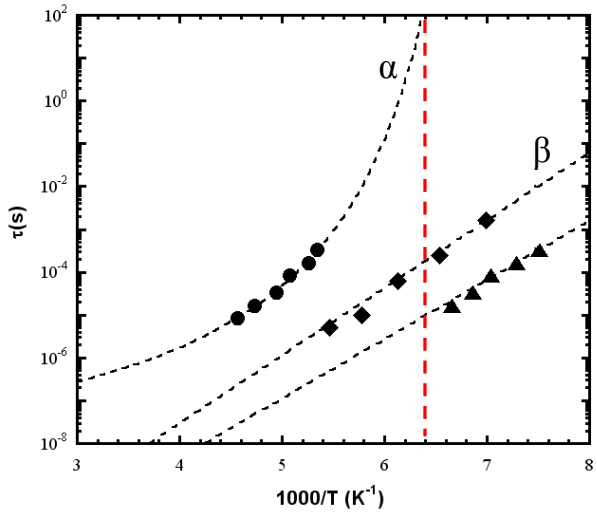

Fig. I.4. Arrhenius diagram of poly(SA) using dielectric (diamond) and mechanical spectroscopy (circle and triangle). The data fit with Arrhenius and VFT equations (dashed lines).

I.2.2.2. Mechanical measurements

The E″ and tan (ϕ) peaks of the two relaxation process obtained from dynamic mechanical measurement of poly(SA) shifted toward higher temperature with increasing frequency. In contrast to dielectric measurements, the relaxation process at higher temperature region resolved very well in dynamical mechanical measurements. The maximum of each relaxation peak (T, f_{max}) and the corresponding characteristic times $\tau = 1/2\pi f_{max}$ evaluated for both relaxation processes, and the values of characteristic times are plotted on the Arrhenius diagram in Figure I.4

I.2.3. Arrhenius diagrams

The temperature dependence of the relaxation rate for the relaxation process at lower temperature region obtained from dielectric and mechanical measurements can be described by the Arrhenius equation $\tau = \tau_0 \exp(E_a/RT)$ where E_a is the activation energy, τ_0 the pre-exponential factor, R the gas constant and T, the absolute temperature. The dashed line through the relaxation rates of this relaxation is a fit of the Arrhenius equation to the data, which yields the values of the activation energy and pre-exponential factor given in Table I.1. These values are in a good agreement with the data reported for other poly(n-alkyl acrylate)s [3,4]. This relaxation is β relaxation process. The β relaxation is attributed to the rotation, small motion and

reorientation of the side chain [4,5]. Figure I.4 and Table I.1 show that the activation energies and pre-exponential factors for the β relaxation process obtained from dielectric and mechanical measurements are almost the same.

Table I.1. Activation energies and pre-exponential factors for the β relaxation process of poly(SA) obtained from dielectric and mechanical measurements

	E_a (kJ mol^{-1})	τ_0 (s)
Dielectric spectroscopy	30.2	10^{-14}
Mechanical spectroscopy	26.6	10^{-14}

The relaxation process in a higher temperature region, which was observed in almost the same region of transition as that determined by DSC, is an α relaxation process. The α relaxation is attributed to the mobility of the side chain on the whole or to the motion of kinetically independent parts of alkyl side chains together with the polymer backbone (glass transition relaxation) [4,5]. The temperature dependence of the relaxation rate for the α relaxation obtained from mechanical measurements, is curved as a function of 1/T and can be described by a Vogel-Fulcher-Tamman (VFT) equation [6-8]:

$$\tau = \tau_0 \exp\left(B/(T-T_0)\right) \qquad \text{(I.1)}$$

Where B is the activation temperature parameter, τ_0 the pre-exponential factor, T_0 the ideal glass transition temperature. The dashed line on Figure I.4 represent the fit with VFT equation on the α process data. The VFT parameters derived from mechanical α relaxation data are B= 0.505, τ_0= 10^{-8} s and T_0 = 134 K.

The vertical dashed line in Figure I.4 indicates the level of 100 s relaxation time of α relaxation fit, which is often assumed as the relaxation time that the segmental motion can reach at the glass transition temperature [4,9,10]. The extracted T_g value of poly(SA) from α relaxation fit in Figure I.4 is 157 K (-116 ºC), which is in a very good agreement with the transition observed in DSC scan (-111 ºC) and also with the predicted T_g for the amorphous state of poly(SA), -111 °C [11].

I.3. References

[1] Alig, I., Jarek, M. and Hellmann, G.P. *Macromolecules*, 1998, 31, 2245-2251.

[2] Shang, S., Huang, S.J. and Weiss, R.A. *Polymer*, 2009, 50, 3119-3127.

[3] Hayakawa, T. and Adachi, K. *Polym J*, 2000, *32*, 845-848.

[4] Gaborieau, M., Graf, R., Kahle, S., Pakula, T. and Spiess, H.W. *Macromolecules*, 2007, *40*, 6249-6256.

[5] Plate, N.A. and Shibaev, V.P. *Macromol Rev*, 1974, 8, 117-253.

[6] Vogel, H. *Phys Z*, 1921, *22*, 645-646.

[7] Fulcher, G.S. *J Am Ceram Soc*, 1925, 8, 339-355.

[8] Tammann, G. and Hesse, W. *Z Anorg Allg Chem,* 1926,156, 245-257.

[9] Angell, C.A. *J Phys Chem Solids*, 1988, 49*,* 863-871.

[10] Saiter, J.M., Grenet, J., Dargent, E., Saiter, A. and Delbreilh, L. *Macromol Symp* 2007, 258, 152-161.

[11] Jordan, E.F. *J Polym Sci Polym Chem,* 1971, 9, 3367-3378.

Appendix II. Polarized Light Microscopy

Polarized light microscopy provides us a unique window into the internal structure of crystals and at the same time is aesthetically pleasing due to the colors and shapes of the crystals. The external view of a polarized light microscope is shown in Figure II.1. Plane polarized light is used and an analyzer is placed between the specimen stage and the eyepiece, and it is rotated to the crossed position (zero light transmission) before inserting the specimen. This equipment is useful for a quick observation. After equipping with a camera, it is convenient to record observations in high resolution. Generally, the microscope equipped with a hot stage to study the crystallography of materials.

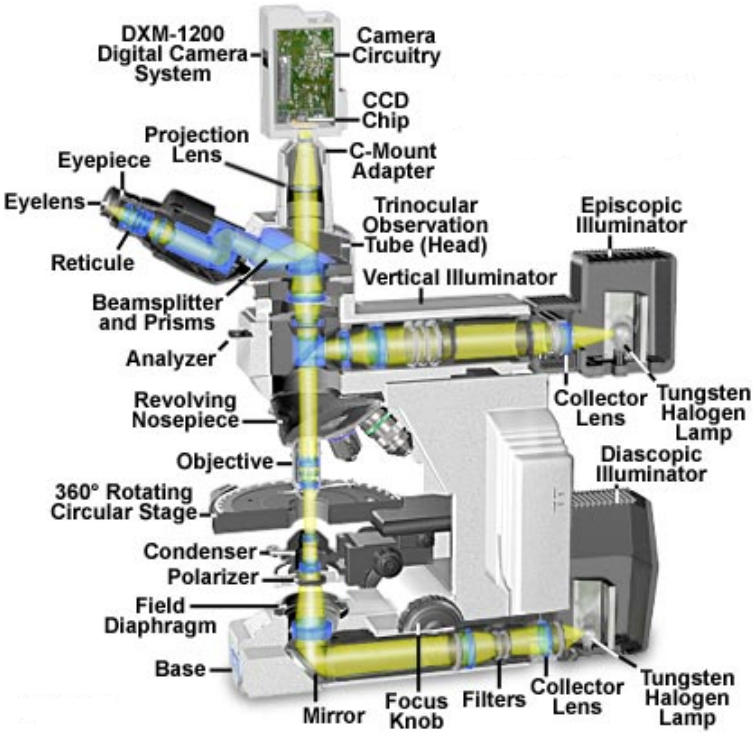

Fig. II.1. Schematic diagram of a polarized light microscope.